A kinetic theory for spin waves in yttrium-iron garnet

Dissertation
zur Erlangung des Doktorgrades
der Naturwissenschaften

vorgelegt beim Fachbereich Physik
der Johann Wolfgang Goethe - Universität
in Frankfurt am Main

von
Johannes Hick
aus Frankfurt am Main

Frankfurt (2013)
(D 30)

vom Fachbereich der Physik der
Johann Wolfgang Goethe - Universität
als Dissertation angenommen.

Dekan: Prof. Dr. Joachim Stroth

Gutachter: Prof. Dr. Peter Kopietz
             Prof. Dr. Hartmut Haug

Datum der Disputation: 05.08.2013

Abstract of the thesis

Spin waves in yttrium-iron garnet has been the subject of research for decades. Recently the report of Bose-Einstein condensation at room temperature has brought these experiments back into focus. Due to the small mass of quasi-particles compared to atoms for example, the condensation temperature can be much higher. With spin-wave quasiparticles, so-called magnons, even room temperature can be reached by externally injecting magnons. But also possible applications in information technologies are of interest. Using excitations as carriers for information instead of charges delivers a much more efficient way of processing data. Basic logical operations have already been realized. Finally the wavelength of spin waves which can be decreased to nanoscale, gives the opportunity to further miniaturize devices for receiving signals for example in smartphones.

For all of these purposes the magnon system is driven far out of equilibrium. In order to get a better fundamental understanding, we concentrate in the main part of this thesis on the nonequilibrium aspect of magnon experiments and investigate their thermalization process. In this context we develop formalisms which are of general interest and which can be adopted to many different kinds of systems.

A milestone in describing gases out of equilibrium was the Boltzmann equation discovered by Ludwig Boltzmann in 1872. In this thesis extensions to the Boltzmann equation with improved approximations are derived. For the application to yttrium-iron garnet we describe the thermalization process after magnons were excited by an external microwave field.

First we consider the Bose-Einstein condensation phenomena in chapter 2. A special property of thin films of yttrium-iron garnet is that the dispersion of magnons has its minimum at finite wave vectors which leads to an interesting behavior of the condensate. We investigate the spatial structure of the condensate using the Gross-Pitaevskii equation and find that the magnons can not condensate only at the energy minimum but that also higher Fourier modes have to be occupied macroscopically. In principle this can lead to a localization on a lattice in real space.

In chapter 3 we use functional renormalization group methods to go beyond the perturbation theory expressions in the Boltzmann equation. It is a difficult task to find a suitable cutoff scheme which fits to the constraints of nonequilibrium, namely causality and the fluctuation-dissipation theorem when approaching equilibrium. Therefore the cutoff scheme we developed for bosons in the context of our considerations is of general interest for the func-

tional renormalization group. In certain approximations we obtain a system of differential equations which have a similar transition rate structure to the Boltzmann equation. We consider a model of two kinds of free bosons of which one type of boson acts as a thermal bath to the other one. Taking a suitable initial state we can use our formalism to describe the dynamics of magnons such that an enhanced occupation of the ground state is achieved. Numerical results are in good agreement with experimental data.

Finally we extend our model to consider also the pumping process and the decrease of the magnon particle number till thermal equilibrium is reached again. Additional terms which explicitly break the $U(1)$-symmetry make it necessary to also extend the theory from which a kinetic equation can be deduced. These extensions are complicated and we therefore restrict ourselves to perturbation theory only. Because of the weak interactions in yttrium-iron garnet this provides already good results.

Inhaltsangabe

Spinwellen in Yttrium-Eisengranat sind nun über Jahrzehnte hinweg Gegenstand der Forschung. Die kürzliche Nachricht von einer Bose-Einstein- Kondensation bei Raumtemperatur hat das Interesse an diesen Systemen neu entfacht. Aufgrund ihrer im Vergleich zu beispielsweise Atomen geringer Masse kann eine höhere Kondensationstemperatur realisiert werden. Unter externer Anregung kann mit den Spinwellen-Quasiteilchen - oder auch Magnonen genannt - sogar Raumtemperatur erreicht werden. Doch auch wegen den möglichen technischen Anwendungen sind diese Systeme interessant. Die Verwendung von Vielteilchenanregungen als Informationsträger, anstatt von elektrischen Ladungen, ermöglicht eine effektivere Form der Datenverarbeitung. Grundlegende logische Operationen wurde bereits experimentell umgesetzt. Die Wellenlängen von Spinwellen mit Energien relevant zur Datenübertragung per Funk liegen in entsprechenden Systemen im Nanometerbereich. Dies eröffnet die Möglichkeit Empfangseinheiten in mobilen Geräten, wie zum Beispiel Smartphones, weiter zu verkleinern.

Für all diese Anwendungen und Experimente ist das Magnonsystem starken Nichtgleichgewichtsbedingungen ausgesetzt. Um ein besseres grundlegendes Verständnis von diesen Prozessen zu erhalten, beschäftigt sich der Hauptteil dieser Arbeit mit dem Nichtgleichgewichts-Aspekt der Magnonexperimente. In diesem Zusammenhang entwickeln wir einen Formalismus, der über die in dieser Arbeit beschriebenen Anwendungen von Interesse ist und für viele verschiedene Arten von Systemen verwendet werden kann.

Die von Ludwig Boltzmann 1872 entdeckte Boltzmann-Gleichung war ein Meilenstein in der Beschreibung von Gasen im thermischen Nichtgleichgewicht. In dieser Arbeit gehen wir über die Boltzmann-Gleichung hinaus, indem wir systematisch ihre Näherungen verbessern. Bei der Anwendung auf Yttrium-Eisengranat betrachten wir Spinwellen die zunächst durch externe Mikrowellen angeregt werden und danach frei im Material thermalisieren.

Bevor wir auf die Nichtgleichgewichtsphysik eingehen, betrachten wir in Kapitel 2 Bose-Einstein-Kondensation im thermischen Gleichgewicht. Dünnschicht-Ferromagnenten haben die besondere Eigenschaft, dass ihre Magnondispersion Minima bei endliche Wellenvektoren aufweist. Dies führt zu einem interessanten Verhalten des Kondensats. Wir untersuchen die Ortsabhängigkeit der Kondensat-Wellenfunktion mit Hilfe der Gross-Pitaevskii-Gleichung. Anders als die experimentellen Ergebnisse vermuten lassen, können die Magnonen nicht alleine beim Energieminimum kondensieren. Auch höhere Fourier-Moden müssen makroskopisch besetzt sein. Im Ortsraum bedeutet

dies, dass das Kondensat in Abhängigkeit der Wechselwirkungen auf einem Gitter lokalisiert sein kann.

In Kapitel 3 verwenden wir funktionale Renormierungsgruppen-Methoden um eine bessere Näherung für die störungstheoretischen Ausdrücke in der Boltzmann-Gleichung zu finden. Das Nichtgleichgewicht setzt zusätzliche Anforderungen an das Cutoff-Schema, wie Kausalität und die Gültigkeit des Fluktuations-Dissipations-Theorems beim Übergang zum Gleichgewicht. Hierbei ein geeignetes Schema zu entwickeln, ist eine schwierige Aufgabe. Das von uns eingeführte Cutoff-Schema für Bosonen ist daher von allgemeinem Interesse für die funktionale Renormierungsgruppe. In bestimmten Näherungen erhalten wir Differentialgleichungen, die eine ähnliche Struktur wie die Boltzmann-Gleichung aufweisen. Wir betrachten ein System bei der freie Bosonen an ein thermisches Bad aus Phononen gekoppelt sind. Mit einem geeigneten Anfangszustand sagt unser Formalismus eine erhöhte Besetzung des Grundzustands voraus, nachdem die Teilchen ins Gleichgewicht relaxiert sind. Unsere nummerischen Ergebnisse sind in guter Übereinstimmung mit dem Experiment.

Zuletzt erweitern wir unser Modell, um auch den Pumpvorgang und die Abnahme der Magnonteilchenzahl zu beschreiben. Dabei treten $U(1)$-symmetriebrechende Terme auf, die es bei der Herleitung von einer kinetischen Gleichung nötig machen von einer allgemeineren Theorie auszugehen. Da die Betrachtungen dieser Erweiterungen bereits kompliziert sind, beschränken wir uns in diesem Abschnitt auf die Verwendung der Störungstheorie. Aufgrund der schwachen Wechselwirkungen in Yttrium-Eisengranat liefert dies bereits gute Ergebnisse.

1. Basic methods

In this introductory chapter we briefly present some basic concepts needed for this thesis. In order to describe systems out of equilibrium we are using the Keldysh formalism. Although there are other equivalent nonequilibrium Green's function methods, lately the Keldysh formalism has become more popular because it is convenient for applying functional integrals. In the first section we give an overview of a functional formulation of the Keldysh formalism. Using functional integrals gives us the opportunity to obtain non-perturbative approximations for self-energies by means of functional renormalization group methods. In section 1.2 we introduce the functional renormalization group in the nonequilibrium context. Finally since the main application in this thesis is the thermalization process of spin waves in yttrium-iron garnet, we derive a spin-wave model for this system in section 1.3.

1.1. Keldysh formalism with functional integrals

The Keldysh formalism [1] is a Green's function method which is capable of describing many-body system out of equilibrium. Further description of systems far from thermal equilibrium standard methods like the linear-response theory fail and a more general formalism is required. For our purpose the Keldysh formalism is most convenient because the regularization of the functional integrals is most transparent. We are interested in one-particle properties only and central objects in our considerations are the one-particle correlation functions. For applying the functional renormalization group we have to derive the Keldysh formalism by means of functional integrals. This introduction considers only bosonic systems and mainly follows the book of A. Kamenev [2].

1.1.1. Time contour

The crucial point of describing systems out of thermal equilibrium is that we have to consider a closed loop of forward and backward time evolution. This has a big impact on the structure of the theory as we will see in section 1.1.2. Note that in nonequilibrium there is no time translational invariance and hence there is no advantage of transforming to frequencies. Therefore we consider the dynamics directly in time.

1. Basic methods

In order to see the need of the time contour let us review shortly how an expectation value of the operator $\mathcal{O}$ is calculated in equilibrium at zero temperature. Starting in the distant past $t_0 \to -\infty$ with a non-interacting Hamiltonian and the known ground state $|0\rangle$ the interactions have to be turned on adiabatically till the actual physical system is reached at the observation time t^*. Hence the expectation value expressed by the unitary time evolution operator $\hat{\mathcal{U}}(t, t') = T e^{-i \int_{t'}^{t} dt'' \, H(t'')}$ becomes

$$\langle \mathcal{O}(t) \rangle = \langle 0| \hat{\mathcal{U}}(-\infty, t^*) \hat{\mathcal{O}} \hat{\mathcal{U}}(t^*, -\infty) |0\rangle. \tag{1.1}$$

Reading the expression $\hat{\mathcal{U}}(-\infty, t^*) \hat{\mathcal{O}} \hat{\mathcal{U}}(t^*, -\infty)$ from right to the left, we can say that the system evolves at first forward in time from $-\infty$ to t^* and then backwards from t^* again to $-\infty$. This forward and backward time evolution is actually necessary but can be avoided in equilibrium. The argument is that because of the adiabatic switching of the interactions we can assume that the system stays in the ground state of the corresponding Hamiltonian at a given time. It follows that after switching off the interactions, the system will be in the same state as at the beginning of the evolution except for a possible phase factor $e^{i\alpha}$. This means that the distant past can be linked to the distant future by

$$\hat{\mathcal{U}}(\infty, -\infty) |0\rangle = e^{i\alpha} |0\rangle, \tag{1.2}$$

and with the same argument

$$\hat{\mathcal{U}}(-\infty, \infty) |0\rangle = e^{-i\alpha} |0\rangle. \tag{1.3}$$

Using these relations the expectation value can be written as

$$\begin{aligned}
\left\langle \hat{\mathcal{O}}(t) \right\rangle &= e^{-i\alpha} \langle 0| e^{i\alpha} \hat{\mathcal{U}}(-\infty, t^*) \hat{\mathcal{O}} \hat{\mathcal{U}}(t^*, -\infty) |0\rangle \\
&= e^{-i\alpha} \langle 0| \hat{\mathcal{U}}(\infty, -\infty) \hat{\mathcal{U}}(-\infty, t^*) \hat{\mathcal{O}} \hat{\mathcal{U}}(t^*, -\infty) |0\rangle \\
&= \frac{\langle 0| \hat{\mathcal{U}}(\infty, t^*) \hat{\mathcal{O}} \hat{\mathcal{U}}(t^*, -\infty) |0\rangle}{\langle 0| \hat{\mathcal{U}}(\infty, -\infty) |0\rangle},
\end{aligned} \tag{1.4}$$

where we have used the identities $\hat{\mathcal{U}}(\infty, -\infty) \hat{\mathcal{U}}(-\infty, t^*) = \hat{\mathcal{U}}(\infty, t^*)$ and

$$e^{i\alpha} = \langle 0| \hat{\mathcal{U}}(\infty, -\infty) |0\rangle. \tag{1.5}$$

Note that a single forward time evolution is left. At finite temperature the calculations can be reduced to a single forward time propagation by similar steps [2].

Out of equilibrium this procedure does not work anymore because there is no relation between the initial state and the state after switching off the interactions. For example for explicit time dependent Hamiltonians, in general, the dynamics cannot be assumed to be adiabatic and the state in the distant future will be different from the state in the distant past. Hence we cannot
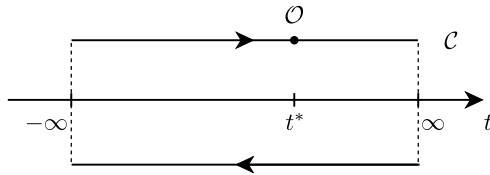
Figure 1.1.: Illustration of Eq. (1.6), operator $\mathcal{O}$ acting at $t = t^*$ on the forward time branch of the Keldysh-Schwinger closed time contour $\mathcal{C}$.

avoid the forward and backward time evolution out of equilibrium. Sometimes it is convenient to extend the forward time propagation to ∞ before going back to the initial time $-\infty$. The time evolution on such a path was first considered by Schwinger in Ref. [3] and is called the Keldysh-Schwinger closed time contour which we will label with $\mathcal{C}$. The expression of Eq. (1.1) on $\mathcal{C}$ becomes

$$\langle \mathcal{O}(t) \rangle = \langle 0| \hat{\mathcal{U}}(-\infty, \infty) \hat{\mathcal{U}}(\infty, t^*) \hat{\mathcal{O}} \hat{\mathcal{U}}(t^*, -\infty) |0\rangle \tag{1.6}$$

which is illustrated in Fig. [1.1]. Normalizing the expectation values by the phase factor Eq. (1.5) is redundant if we are working on the closed time contour, or in other words, the partition function is one in this case. That is why the Keldysh formalism has also applications for disordered system in equilibrium [2], where disorder averaging is difficult. The disadvantage is that the variables have to be doubled in order to keep track of the forward and backward time propagation. In general there is a difference between an operator acting on one or the other time branch.

1.1.2. Functional integrals

Our goal is to express expectation values as functional integrals over fields instead of taking the trace of operators. First let us demonstrate the concept of functional integrals considering a single harmonic oscillator,

$$\hat{H} = \epsilon_0 \hat{a}^\dagger \hat{a}, \tag{1.7}$$

where $\hat{a}$ and $\hat{a}^\dagger$ are the annihilation and creation operators and ϵ_0 the frequency of the oscillator. Later we can easily generalize to interacting systems of bosons. For replacing the operators by fields we are using coherent states defined as

$$|\phi\rangle = e^{\phi \hat{a}^\dagger} |0\rangle, \tag{1.8}$$

where $|0\rangle$ is the vacuum state and ϕ an arbitrary complex number. We start by calculating the partition function on the Keldysh-Schwinger closed time contour,

$$\mathcal{Z} = \text{Tr} \left[\hat{\mathcal{U}}_\mathcal{C} \hat{\rho}_0 \right], \tag{1.9}$$

where $\hat{\mathcal{U}}_\mathcal{C} = \hat{\mathcal{U}}(-\infty, \infty) \hat{\mathcal{U}}(\infty, -\infty) = \hat{1}$ is the time evolution operator along the contour $\mathcal{C}$. Without any operator acting in between, $\hat{\mathcal{U}}_\mathcal{C}$ is given by the
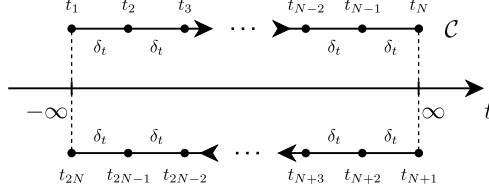
1. Basic methods

Figure 1.2.: Dividing the time contour $\mathcal{C}$ into $2\,(N-1)$ equidistant time intervals.

identity operator because the initial time is equal to the final time. For simplicity we do not consider initial correlations and assume that the initial density matrix is given by $\hat{\rho}_0 = e^{-\beta(\hat{H}-\mu\hat{N})}/\mathcal{Z}_0$, where $\mathcal{Z}_0$ is a normalization,

$$
\begin{aligned}
\mathcal{Z}_0 &= \operatorname{Tr}\left[e^{-\beta(\hat{H}-\mu\hat{N})} \right] \\
&= \sum_{n=0}^{\infty} \left[e^{-\beta(\epsilon_0-\mu)} \right]^n = \frac{1}{1 - e^{-\beta(\epsilon_0-\mu)}}.
\end{aligned}
\tag{1.10}
$$

Hence the value of the partition function $\mathcal{Z}$ is given by one,

$$
\mathcal{Z} = \operatorname{Tr}\left[\hat{\rho}_0\right] = 1.
\tag{1.11}
$$

At the moment we are just reformulating the identity in a complicated way by expressing the right hand side of Eq. (1.9) by functional integrals. Similar to the Feynman path integrals we divide the time contour $\mathcal{C}$ into $2N-1$ equidistant intervals of length δ_t, see Fig. 1.2, and insert identity operators expressed by coherent states

$$
\hat{1} = \iint \frac{d\bar{\phi}d\phi}{2\pi i} e^{-|\phi|^2} \left|\phi\right\rangle\left\langle\phi\right|,
\tag{1.12}
$$

at each time step. Expressing also the trace by coherent states we obtain

$$
\begin{aligned}
\mathcal{Z} &= \iint \frac{d\bar{\phi}_{2N}d\phi_{2N}}{2\pi i} e^{-|\phi_{2N}|^2} \left\langle\phi_{2N}\right| \hat{U}_{\mathcal{C}}\hat{\rho}_0 \left|\phi_{2N}\right\rangle \\
&= \prod_{j=1}^{2N} \left[\iint \frac{d\bar{\phi}_j d\phi_j}{2\pi i} e^{-|\phi_j|^2} \right] \left\langle\phi_{2N}\right| e^{i\delta_t\hat{H}} \left|\phi_{2N-1}\right\rangle ... \left\langle\phi_{N+2}\right| e^{i\delta_t\hat{H}} \left|\phi_{N+1}\right\rangle \\
&\quad \times \left\langle\phi_{N+1}\right| \left.\phi_N\right\rangle \left\langle\phi_N\right| e^{-i\delta_t\hat{H}} \left|\phi_{N-1}\right\rangle ... \left\langle\phi_2\right| e^{-i\delta_t\hat{H}} \left|\phi_1\right\rangle \left\langle\phi_1\right| \hat{\rho}_0 \left|\phi_{2N}\right\rangle.
\end{aligned}
\tag{1.13}
$$

From the point N to $N+1$ the forward time evolution is switching to the backward time evolution and there is no evolution operator between these points because the system is not evolving here. Up to linear order of δ_t the matrix elements of the time evolution operator can be approximated by

$$
\begin{aligned}
\left\langle\phi_j\right| e^{\pm i\delta_t\hat{H}} \left|\phi_{j-1}\right\rangle &\approx \left\langle\phi_j\right| 1 \pm i\delta_t\hat{H}\left(\hat{a}^\dagger, \hat{a}\right) \left|\phi_{j-1}\right\rangle \\
&= \left(1 \pm i\delta_t H\left(\bar{\phi}_j, \phi_{j-1}\right)\right) \left\langle\phi_j\right| \left.\phi_{j-1}\right\rangle \\
&\approx e^{\pm i\delta_t H\left(\bar{\phi}_j, \phi_{j-1}\right)} e^{\bar{\phi}_j \phi_{j-1}},
\end{aligned}
\tag{1.14}
$$

which is exact for $\delta_t \to 0$. The remaining matrix elements are given by

$$\langle \phi_{N+1} | \, \phi_N \rangle \;\; = \;\; e^{\bar{\phi}_{N+1}\phi_N}, \tag{1.15}$$

$$\langle \phi_1 | \, \hat{\rho}_0 \, | \phi_{2N} \rangle \;\; = \;\; \frac{1}{\mathcal{Z}_0} \langle \phi_1 | \, e^{-\beta\left(\hat{H}-\mu\hat{N}\right)} \, | \phi_{2N} \rangle$$

$$= \;\; \frac{1}{\mathcal{Z}_0} e^{p_0 \bar{\phi}_1 \phi_{2N}}, \tag{1.16}$$

where for the second expression we have used the identity $\langle \phi | \, p^{a^\dagger a} \, | \phi' \rangle = e^{p\bar{\phi}\phi'}$ and introduced $p_0 = e^{-\beta(\epsilon_0 - \mu)}$. Inserting the matrix elements Eqs. (1.14-1.16) into the partition function (1.13) yields

$$\mathcal{Z} = \int \mathcal{D}\left[\bar{\phi}, \phi\right] e^{iS[\bar{\phi}, \phi]}, \tag{1.17}$$

where we define the action by

$$S\left[\bar{\phi}, \phi\right] = \sum_{j=2}^{2N} \delta t_j \left[i\bar{\phi}_j \frac{\phi_j - \phi_{j-1}}{\delta t_j} - H\left(\bar{\phi}_j, \phi_{j-1}\right) \right] + i\bar{\phi}_1 \left(\phi_1 - p_0\phi_{2N}\right), \tag{1.18}$$

with

$$\delta t_j = t_j - t_{j-1} = \begin{cases} \delta_t & \text{for } 2 \leq j \leq N, \\ -\delta_t & \text{for } N + 2 \leq j \leq 2N, \\ 0 & \text{for } j = N + 1. \end{cases} \tag{1.19}$$

The measure of the integral is given by

$$\int \mathcal{D}\left[\bar{\phi}, \phi\right] = \frac{1}{\mathcal{Z}_0} \prod_{j=1}^{2N} \iint \frac{d\bar{\phi}_j \, d\phi_j}{2\pi i}. \tag{1.20}$$

Let us mention at this point that in the functional formulation the initial state is contained in the action and does not explicitly appear in the expression for the averages. The form of the action Eq. (1.18) is valid for all normal-ordered Hamiltonians but for other Hamiltonians we might have to sum or integrate over additional quantum numbers.

To make further progress we are rewriting the action in a matrix structure

$$S\left[\bar{\phi}, \phi\right] = \sum_{j,j'=1}^{2N} \bar{\phi}_j \left[\left(\hat{G}_0\right)^{-1}\right]_{jj'} \phi_{j'}, \tag{1.21}$$

where the matrix in between the fields is the inverse propagator and has the

form

$$
i\left(\hat{G}_0\right)^{-1} =
\left(
\begin{array}{ccccc|cccc}
-1 & & & & & & & & p_0 \\
1-h & -1 & & & & & & & \\
 & \ddots & \ddots & & & & \mathbf{0} & & \\
 & & 1-h & -1 & & & & & \\
\hline
 & & & 1 & -1 & & & & \\
 & & & & 1+h & -1 & & & \\
 & & \mathbf{0} & & & & \ddots & \ddots & \\
 & & & & & & & 1+h & -1
\end{array}
\right),
$$
(1.22)

where $h = i\epsilon_0\delta_t$ and all not shown components are zero. With these definitions the result of the Gaussian integral of the partition function is

$$
\mathcal{Z} = \frac{1}{\mathcal{Z}_0}\left(\det\left[-i\left(\hat{G}_0\right)^{-1}\right]\right)^{-1}.
$$
(1.23)

For calculating the determinant of the inverse propagator we expand in the first row,

$$
\det\left[-i\left(\hat{G}_0\right)^{-1}\right] = 1 \cdot \det
\left(
\begin{array}{ccccccc}
1 & & & & & & \\
h-1 & \ddots & & & & & \\
 & \ddots & \ddots & & & & \\
 & & -1 & \ddots & & & \\
 & & & \ddots & \ddots & & \\
 & & & & -h-1 & 1
\end{array}
\right)
$$

$$
+ (-1)^{2N-1}(-p_0)\det
\left(
\begin{array}{cccccc}
h-1 & 1 & & & & \\
 & \ddots & \ddots & & & \\
 & & -1 & \ddots & & \\
 & & & \ddots & 1 & \\
 & & & & -h-1 &
\end{array}
\right)
$$

$$
= 1 - p_0\left[(1-h)(1+h)\right]^{N-1} = 1 - p_0\left(1+\epsilon_0^2\delta_t^2\right)^{N-1}.
$$
(1.24)

Note that the entry p_0 in $\left(\hat{G}_0\right)^{-1}$ is crucial to get the correct expression. In the limit of infinite time steps we get the expected result for the partition function

$$
\begin{aligned}
\mathcal{Z} &= \lim_{N\to\infty}\frac{1}{\mathcal{Z}_0}\frac{1}{1-p_0\left(1+\epsilon^2\delta_t^2\right)^{N-1}} \\
&= \frac{1}{\mathcal{Z}_0}\frac{1}{1-p_0} \\
&= 1.
\end{aligned}
$$
(1.25)

To obtain a compact form it is convenient to introduce a continuum notation in the way that we replace $\phi_j \rightarrow \phi(t)$, $\sum_{j=2}^{2N} \delta t_j \rightarrow \int_{\mathcal{C}} dt$ and $(\phi_j - \phi_{j-1})/\delta t_j \rightarrow \partial \phi(t)/\partial t$. In this notation the action becomes

$$S\left[\bar{\phi}, \phi\right] = \int_{\mathcal{C}} dt\, \bar{\phi}(t)\left(i\partial_t - \epsilon_0\right)\phi(t). \tag{1.26}$$

This notation might be misleading since there does not exist such an infinitesimal mathematical limit for the discrete expression; it is just a compact notation and we have to keep in mind that the discrete version is the actual mathematical object we have to deal with. In the continuum notation we have neglected the single matrix element p_0 of the inverse propagator but as already mentioned this entry is important to get correct results. In order to work consistently with the continuum notation we have to regularize the functional integrals such that we get the correct results from the discrete version. In the next section we will find the correct regularization.

It is convenient to split the fields into the parts $\phi^+(t)$ and $\phi^-(t)$ by

$$\phi(t) \equiv \begin{cases} \phi^+(t) & \text{for } t \text{ on the forward time branch of } \mathcal{C}, \\ \phi^-(t) & \text{for } t \text{ on the backward time branch of } \mathcal{C}. \end{cases} \tag{1.27}$$

Inserting into the action yields

$$S\left[\bar{\phi}, \phi\right] = \int_{-\infty}^{\infty} dt\, \bar{\phi}^+(t)\left(i\partial_t - \epsilon_0\right)\phi^+(t) - \int_{-\infty}^{\infty} dt\, \bar{\phi}^-(t)\left(i\partial_t - \epsilon_0\right)\phi^-(t). \tag{1.28}$$

So far we only considered the partition function but actually we are interested in the expectation value of certain operators. Let us consider an operator $\hat{\mathcal{O}}\left[a^\dagger, a\right]$ given in second quantization. With functional integrals the expectation value is calculated by

$$\left\langle \mathcal{O}\left[\bar{\phi}, \phi\right]\right\rangle = \int \mathcal{D}\left[\bar{\phi}, \phi\right]\, \mathcal{O}\left[\bar{\phi}, \phi\right] e^{iS\left[\bar{\phi}, \phi\right]}, \tag{1.29}$$

where $\mathcal{O}\left[\bar{\phi}, \phi\right]$ is the operator expressed by fields. Whenever the operator $\mathcal{O}$ is given in second quantization, $\mathcal{O}\left[\bar{\phi}, \phi\right]$ can be derived in the same way we calculated the partition function. In the next section we will introduce nonequilibrium Green's functions and derive their operator and field representations.

1.1.3. Green's functions

We work with the continuum notation right from the beginning and define the Green's functions as

$$\begin{aligned} iG^<(t,t') \equiv iG^{+-}(t,t') &\equiv \left\langle \phi^+(t)\,\bar{\phi}^-(t')\right\rangle, & \text{(1.30a)} \\ iG^>(t,t') \equiv iG^{-+}(t,t') &\equiv \left\langle \phi^-(t)\,\bar{\phi}^+(t')\right\rangle, & \text{(1.30b)} \\ iG^T(t,t') \equiv iG^{++}(t,t') &\equiv \left\langle \phi^+(t)\,\bar{\phi}^+(t')\right\rangle, & \text{(1.30c)} \\ iG^{\overline{T}}(t,t') \equiv iG^{--}(t,t') &\equiv \left\langle \phi^-(t)\,\bar{\phi}^-(t')\right\rangle, & \text{(1.30d)} \end{aligned}$$

where $G^{</>}$ are the so called lesser and greater Green's function, $G^{T/\overline{T}}$ are the time-ordered and the anti-time-ordered Green's function. We will refer to this set of Green's functions as the contour basis. The definitions become more clear by transforming back to operators. For a heuristic derivation let us express the time dependence of the annihilation and creation operators using the time evolution operator for two examples:

$$
\begin{aligned}
\left\langle \hat{a}^\dagger\left(t'\right)\hat{a}\left(t\right)\right\rangle &= \left\langle \mathcal{U}\left(-\infty,t'\right)\hat{a}^\dagger\mathcal{U}\left(t',t\right)\hat{a}\mathcal{U}\left(t,-\infty\right)\right\rangle \\
&= \left\langle \mathcal{U}\left(-\infty,t'\right)\hat{a}^\dagger\mathcal{U}\left(t',\infty\right)\mathcal{U}\left(\infty,t\right)\hat{a}\mathcal{U}\left(t,-\infty\right)\right\rangle, \quad (1.31) \\
\left\langle T\left[\hat{a}\left(t\right)\hat{a}^\dagger\left(t'\right)\right]\right\rangle &= \Theta\left[t-t'\right]\left\langle \mathcal{U}\left(-\infty,\infty\right)\mathcal{U}\left(\infty,t\right)\hat{a}\mathcal{U}\left(t,t'\right)\hat{a}^\dagger\mathcal{U}\left(t',-\infty\right)\right\rangle \\
&\quad +\Theta\left[t'-t\right]\left\langle \mathcal{U}\left(-\infty,\infty\right)\mathcal{U}\left(\infty,t'\right)\hat{a}^\dagger\mathcal{U}\left(t',t\right)\hat{a}\mathcal{U}\left(t,-\infty\right)\right\rangle,
\end{aligned}
$$
$$(1.32)$$

where we introduced the time ordering T which arranges operators such that their time arguments are decreasing going from the left to the right. For later purpose we also define the anti-time ordering $\overline{T}$ which arranges operators in the opposite way such that their time arguments are increasing from left to the right. From the first example we see that the left operator can always be described by a field acting on the backward time branch and the right by a field acting on the forward branch. The second example shows that averages of time or anti-time ordered operators can be expressed by fields acting on the same time branch. From these observations we conclude that

$$
\begin{aligned}
iG^<\left(t,t'\right) &= \left\langle \hat{a}^\dagger\left(t'\right)\hat{a}\left(t\right)\right\rangle \\
&= \Theta\left(t-t'\right)\left\langle T\left[\hat{a}\left(t\right)\hat{a}^\dagger\left(t'\right)\right]\right\rangle + \Theta\left(t'-t\right)\left\langle \overline{T}\left[\hat{a}\left(t\right)\hat{a}^\dagger\left(t'\right)\right]\right\rangle,
\end{aligned}
$$
$$(1.33a)$$

$$
\begin{aligned}
iG^>\left(t,t'\right) &= \left\langle \hat{a}\left(t\right)\hat{a}^\dagger\left(t'\right)\right\rangle \\
&= \Theta\left(t-t'\right)\left\langle T\left[\hat{a}\left(t\right)\hat{a}^\dagger\left(t'\right)\right]\right\rangle + \Theta\left(t'-t\right)\left\langle \overline{T}\left[\hat{a}\left(t\right)\hat{a}^\dagger\left(t'\right)\right]\right\rangle,
\end{aligned}
$$
$$(1.33b)$$

$$
\begin{aligned}
iG^T\left(t,t'\right) &= \left\langle T\left[\hat{a}\left(t\right)\hat{a}^\dagger\left(t'\right)\right]\right\rangle \\
&= \Theta\left(t-t'\right)\left\langle \hat{a}\left(t\right)\hat{a}^\dagger\left(t'\right)\right\rangle + \Theta\left(t'-t\right)\left\langle \hat{a}^\dagger\left(t'\right)\hat{a}\left(t\right)\right\rangle, \quad (1.33c) \\
iG^{\overline{T}}\left(t,t'\right) &= \left\langle \overline{T}\left[\hat{a}\left(t\right)\hat{a}^\dagger\left(t'\right)\right]\right\rangle \\
&= \Theta\left(t'-t\right)\left\langle \hat{a}\left(t\right)\hat{a}^\dagger\left(t'\right)\right\rangle + \Theta\left(t-t'\right)\left\langle \hat{a}^\dagger\left(t'\right)\hat{a}\left(t\right)\right\rangle. \quad (1.33d)
\end{aligned}
$$

Not all of these Green's functions are independent of each other, only three of them are linearly independent since

$$G^<\left(t,t'\right) + G^>\left(t,t'\right) = G^T\left(t,t'\right) + G^{\overline{T}}\left(t,t'\right) \qquad (1.34)$$

which can be easily seen from Eqs. (1.32-1.33d). The minimum number of functions which has to be considered is two, for example all four can be expressed by $G^<$ and $G^>$.

For the regularization of the functional integrals we first have to calculate the Green's function correctly. For doing so we can either use the discrete expressions of the functional integrals or the operator formalism. Here we use the operator formalism in which the calculation is straightforward:

$$
\begin{aligned}
iG^< (t,t') &= \mathrm{Tr}\left[\hat{a}^\dagger (t') \hat{a} (t) \hat{\rho}_0\right] \\
&= \sum_{n=0}^{\infty} \langle n| e^{i\hat{H}t'} a^\dagger e^{i\hat{H}(t-t')} a e^{-i\hat{H}t} e^{-\beta(\epsilon_0-\mu)\hat{a}^\dagger\hat{a}} |n\rangle \\
&= e^{-i\epsilon_0(t-t')} \sum_{n=0}^{\infty} n p_0^n = b\left(\epsilon_0\right) e^{-i\epsilon_0(t-t')}, \quad (1.35)
\end{aligned}
$$

$$
iG^> (t,t') = \mathrm{Tr}\left[\hat{a} (t) \hat{a}^\dagger (t') \hat{\rho}_0\right] = \left[1+b\left(\epsilon_0 - \mu\right)\right] e^{-i\epsilon_0(t-t')}, \quad (1.36)
$$

where $b\left(\omega\right) = 1/\left(e^{\beta\omega}-1\right)$ is the Bose function. The time and anti-time ordered Green's function are combinations of $G^{\lessgtr}$, see Eqs. (1.33a - 1.33d).

1.1.4. Keldysh basis

In this section we want to find the correct regularization for the functional integrals. For that purpose it is more convenient to work with another set of Green's functions, which we will call the Keldysh basis. The Green's functions have easy physical interpretations and the regularization will be straightforward. Another reason for using the Keldysh formulation is that the set of Green's functions is reduced by one such that the remaining three are linearly independent.

Let us start with the introduction of the quantum field ϕ^Q and the classical field ϕ^C, which are given by

$$
\phi^C (t) = \frac{1}{\sqrt{2}}\left[\phi^+ (t) + \phi^- (t)\right], \quad (1.37a)
$$

$$
\phi^Q (t) = \frac{1}{\sqrt{2}}\left[\phi^+ (t) - \phi^- (t)\right]. \quad (1.37b)
$$

The new basis of Green's functions are now defined as

$$
\begin{aligned}
iG^R (t,t') \equiv iG^{CQ} (t,t') &\equiv \left\langle \phi^C (t) \bar{\phi}^Q (t')\right\rangle, & (1.38a) \\
iG^A (t,t') \equiv iG^{QC} (t,t') &\equiv \left\langle \phi^Q (t) \bar{\phi}^C (t')\right\rangle, & (1.38b) \\
iG^K (t,t') \equiv iG^{CC} (t,t') &\equiv \left\langle \phi^C (t) \bar{\phi}^C (t')\right\rangle, & (1.38c) \\
iG^{QQ} (t,t') &\equiv \left\langle \phi^Q (t) \bar{\phi}^Q (t')\right\rangle, & (1.38d)
\end{aligned}
$$

where R stands for "retarded", A for "advanced" and K for "Keldysh". The relation to the contour Green's functions is given by

$$
\begin{pmatrix} \hat{G}^T & \hat{G}^< \\ \hat{G}^> & \hat{G}^{\overline{T}} \end{pmatrix} = R \begin{pmatrix} \hat{G}^{CC} & \hat{G}^{CQ} \\ \hat{G}^{QC} & \hat{G}^{QQ} \end{pmatrix} R, \quad (1.39)
$$

1. Basic methods

where $R = \frac{1}{\sqrt{2}} \begin{pmatrix} 1 & 1 \\ 1 & -1 \end{pmatrix}$. Here we have introduced continuous time matrices which we label with a hat. The components of the matrix $\hat{A}$ are given by

$$\left[\hat{A}\right]_{tt'} = A\left(t, t'\right). \tag{1.40}$$

The matrix product of the times matrices $\hat{A}$ and $\hat{B}$ is defined by

$$\left[\hat{A}\hat{B}\right]_{tt'} = \int_{-\infty}^{\infty} dt A\left(t, t_1\right) B\left(t_1, t'\right). \tag{1.41}$$

This notation allows us to develop a compact formulation of the Keldyh formalism. Note that in order to avoid confusion with operators, we use this notation only in the context of functional integrals and omit the hat for the operators from now on.

From the relations Eq. (1.39) and Eq. (1.34) we obtain

$$G^{QQ} = \frac{1}{2}\left(G^T + G^{\overline{T}} - G^< - G^>\right) = 0, \tag{1.42}$$

which is due to the reduction of the linear dependence and has its origin in causality. The explicit expressions for the Green's functions in the Keldysh basis are given by

$$
\begin{align*}
G^R\left(t, t'\right) &= \frac{1}{2}\sum_{p,p'=\pm} p' G^{pp'}\left(t, t'\right) \\
&= -i\Theta\left(t - t'\right) e^{-i\epsilon_0(t-t')}, \tag{1.43a} \\
G^A\left(t, t'\right) &= \frac{1}{2}\sum_{p,p'=\pm} p G^{pp'}\left(t, t'\right), \\
&= i\Theta\left(t' - t\right) e^{-i\epsilon_0(t-t')}, \tag{1.43b} \\
G^K\left(t, t'\right) &= \frac{1}{2}\sum_{p,p'=\pm} G^{pp'}\left(t, t'\right), \\
&= -i\left[1 + 2b\left(\epsilon_0 - \mu\right)\right] e^{-i\epsilon_0(t-t')}, \tag{1.43c}
\end{align*}
$$

where $p, p' = \pm$ refer to the upper and lower contour branch, see Fig. 1.1. Here we can already see that the retarded and advanced components contain only spectral information while the Keldysh component describes also the particle distribution. Note that the Keldysh Green's function can be written as

$$\hat{G}^K = \hat{G}^R \hat{g}_0 - \hat{g}_0 \hat{G}^A, \tag{1.44}$$

where we have introduced the time matrix of the initial distribution $\hat{g}_0$ by

$$\left[\hat{g}_0\right]_{tt'} = \left[1 + 2b\left(\epsilon_0 - \mu\right)\right] \delta\left(t - t'\right). \tag{1.45}$$

In frequency space this amounts to the fluctuation-dissipation theorem in the form

$$G^K(\omega) = [1 + 2b(\epsilon_0 - \mu)] \left[G^R(\omega) - G^A(\omega)\right], \tag{1.46}$$

which is always valid in equilibrium, also for interacting systems, see appendix B. If

Expressing the averages by operators we obtain

$$iG^R(t, t') = \Theta(t - t') \left\langle \left[a(t), a^\dagger(t')\right] \right\rangle, \tag{1.47a}$$

$$iG^A(t, t') = -\Theta(t' - t) \left\langle \left[a(t), a^\dagger(t')\right] \right\rangle, \tag{1.47b}$$

$$iG^K(t, t') = \left\langle \left\{a(t), a^\dagger(t')\right\} \right\rangle, \tag{1.47c}$$

where { , } denotes the anticommutator. Usually we are interested in the occupation number $n(t) = \left\langle a^\dagger(t) a(t) \right\rangle$, which can be obtained from the Keldysh Green's function at equal times,

$$iG^K(t, t) = 1 + 2n(t). \tag{1.48}$$

For a short notation it is convenient to arrange the Green's functions in a 2×2-matrix structure,

$$\boldsymbol{G} \equiv \begin{pmatrix} \hat{G}^K & \hat{G}^R \\ \hat{G}^A & 0 \end{pmatrix}. \tag{1.49}$$

In this thesis the space of the K,R,A-components of Green's function $\boldsymbol{G}$ will be called the Keldysh space and matrices in this Keldysh space will be denoted by bold symbols. The triangular form of $\boldsymbol{G}$ is due to causality and we therefore will refer to it as having causality structure.

The action Eq. (1.28) in the new basis is usually called the Keldysh action and is given by

$$S[\bar{\phi}, \phi] = \int_{-\infty}^{\infty} dt \int_{-\infty}^{\infty} dt' \left(\begin{array}{cc} \bar{\phi}^C(t) & \bar{\phi}^Q(t) \end{array} \right) \begin{pmatrix} 0 & \hat{M}_0 \\ \hat{M}_0 & 0 \end{pmatrix}_{tt'} \begin{pmatrix} \phi^C(t') \\ \phi^Q(t') \end{pmatrix}, \tag{1.50}$$

where

$$\left[\hat{M}_0\right]_{tt'} = i\delta'(t - t') - \epsilon_0 \delta(t - t') \tag{1.51}$$

is the retarded or advanced component of the inverse Green's function without regularization. From the general formula for Gaussian integrals,

$$i\left[\hat{G}\right]_{tt'}^{\lambda\lambda'} = \int \mathcal{D}[\bar{\phi}, \phi] \, \bar{\phi}^\lambda(t) \phi^{\lambda'}(t')$$

$$\times \exp\left[i \int dt_1 \int dt_2 \sum_{\lambda_1\lambda_2} \bar{\phi}^{\lambda_1}(t_1) \left[\hat{G}^{-1}\right]_{t_1 t_2}^{\lambda_1\lambda_2} \phi^{\lambda_2}(t_2)\right], \tag{1.52}$$

we obtain the relation between the action Eq. (1.50) and the Green's functions Eqs. (1.47a-1.47c) by choosing the superscript to be C or Q and associating

the subscripts with the corresponding time components. In order to use the continuous notation in a consistent way, we have to determine the regularization of the Keldysh action Eq. (1.28) such that we obtain the correct Green's functions Eqs. (1.43a-1.43c). Therefore we have to invert the Green's functions Eqs. (1.43a-1.43c). Due to the causality structure the inverse Green's function is of the form

$$\boldsymbol{G}^{-1} = \begin{pmatrix} 0 & \left[\hat{G}^A\right]^{-1} \\ \left[\hat{G}^R\right]^{-1} & -\left[\hat{G}^R\right]^{-1} \hat{G}^K \left[\hat{G}^A\right]^{-1} \end{pmatrix}. \tag{1.53}$$

The retarded and advanced Green's function depend only on the time difference $t - t'$ and hence we perform a Fourier transformation of the inversion. Using the formula of the Fourier transformed Heaviside step function,

$$\int_{-\infty}^{\infty} dt\, e^{i\omega t} \Theta(t) = \frac{i}{\omega + i\eta}, \tag{1.54}$$

where η is an infinitesimal quantity, we obtain

$$\begin{aligned} \left[G^R(\omega)\right]^{-1} &= \left[\int_{-\infty}^{\infty} d(t - t')\, e^{i\omega(t-t')} G^R(t, t')\right]^{-1} \\ &= \left[-i \int_{-\infty}^{\infty} d(t - t')\, e^{i(\omega - \epsilon_0)(t-t')} \Theta(t - t')\right]^{-1} \\ &= \omega - \epsilon_0 + i\eta. \end{aligned} \tag{1.55}$$

Analogously we arrive at

$$\left[G^A(\omega)\right]^{-1} = \omega - \epsilon_0 - i\eta. \tag{1.56}$$

Transforming back to real time yields

$$\begin{aligned} \left[\hat{G}^R\right]^{-1}_{tt'} &= \int_{-\infty}^{\infty} \frac{d\omega}{2\pi} e^{-i\omega(t-t')} (\omega - \epsilon_0 + i\eta) \\ &= i\delta'(t - t') + \delta(t - t')(-\epsilon_0 + i\eta), \tag{1.57a} \\ \left[\hat{G}^A\right]^{-1}_{tt'} &= i\delta'(t - t') + \delta(t - t')(-\epsilon_0 - i\eta), \tag{1.57b} \end{aligned}$$

where $\delta'(t)$ is the derivative of the delta function, $d\delta(t)/dt$. The inverse propagators Eqs. (1.57a, 1.57b) are the regularized expression we were looking for. Note that these expressions yield the correct Green's functions Eqs. (1.43a, 1.43b) up to a correction of the order $\mathcal{O}(\eta)$ which can be seen from the inversion assuming η to be finite,

$$\begin{aligned} G^R_\eta(t, t') &= -i\Theta(t - t')\, e^{-i(\epsilon_0 - i\eta)(t-t')}, \tag{1.58a} \\ G^A_\eta(t, t') &= i\Theta(t' - t)\, e^{-i(\epsilon_0 + i\eta)(t-t')}. \tag{1.58b} \end{aligned}$$

Since η is infinitesimal we can usually neglect it in $G_\eta^{R/A}$ which recovers the actual Green's functions, $\lim_{\eta\to 0} G_\eta^{R/A}(t, t') = G^{R/A}(t, t')$. We have now a certain freedom in choosing the regularized Keldysh Green's function $G_\eta^K(t, t')$, only the boundary condition $\lim_{\eta\to 0} G_\eta^K(t, t') = G^K(t, t')$ has to be satisfied. The relation Eq. (1.44) implies

$$\hat{G}_\eta^K = \hat{G}_\eta^R \hat{g}_0 - \hat{g}_0 \hat{G}_\eta^A, \qquad (1.59)$$

which gives in time space

$$G_\eta^K(t, t') = -i\left[1 + 2b(\epsilon_0 - \mu)\right]\left[\Theta(t - t') e^{-i(\epsilon_0 - i\eta)(t-t')}\right.$$
$$\left. + \Theta(t' - t) e^{-i(\epsilon_0 + i\eta)(t-t')}\right]. \qquad (1.60)$$

To be consistent the regularized Green's functions Eqs. (1.58a, 1.58b, 1.60) have to be used whenever the result of a calculation is of order η, for example for calculating the nonzero diagonal element $-\left[\hat{G}^R\right]^{-1} \hat{G}_\eta^K \left[\hat{G}^A\right]^{-1}$ of the inverse Green's function Eq. (1.53):

$$-\left(\left[\hat{G}^R\right]^{-1} \hat{G}_\eta^K \left[\hat{G}^A\right]^{-1}\right)_{tt'}$$
$$= -\int_{-\infty}^{\infty} dt_1 \int_{-\infty}^{\infty} dt_2 \left[i\delta'(t - t') + \delta(t - t')(-\epsilon_0 + i\eta)\right]$$
$$\times G_\eta^K(t_1, t_2)\left[i\delta'(t - t') + \delta(t - t')(-\epsilon_0 - i\eta)\right]$$
$$= 2i\eta\left[1 + 2b(\epsilon_0 - \mu)\right]\delta(t - t'). \qquad (1.61)$$

Using the Keldysh Green's function Eq. (1.43c) instead of the regularized form $G_\eta^K(t, t')$ would not yield the correct result here.

Now we can give a regularized version of the Keldysh action Eq. (1.50),

$$S[\bar{\phi}, \phi] = \int_{-\infty}^{\infty} dt \int_{-\infty}^{\infty} dt' \left(\ \bar{\phi}^C(t), \ \ \bar{\phi}^Q(t)\ \right)$$
$$\times \begin{pmatrix} 0 & \left[\hat{G}^A\right]^{-1} \\ \left[\hat{G}^R\right]^{-1} & 2i\eta\hat{g}_0 \end{pmatrix}_{tt'} \begin{pmatrix} \phi^C(t') \\ \phi^Q(t') \end{pmatrix}. \qquad (1.62)$$

The initial distribution is contained in $-\left[\hat{G}^R\right]^{-1} \hat{G}^K \left[\hat{G}^A\right]^{-1} = 2i\eta\hat{g}_0$ and the off-diagonal components of the inverse Green's function are given by

$$\left[\hat{G}^R\right]^{-1} = \hat{M}_0 + i\eta\hat{I}, \qquad (1.63a)$$

$$\left[\hat{G}^A\right]^{-1} = \hat{M}_0 - i\eta\hat{I}, \qquad (1.63b)$$

where the identity matrix $\hat{I}$ is defined by $\left[\hat{I}\right]_{tt'} = \delta(t - t')$. The regularized action Eq. (1.62) gives the same results as the discrete one Eq. (1.18) but is

much more convenient to work with. The construction with the regularized Green's functions Eqs. (1.58a, 1.58b, 1.60) may seem to be cumbersome to use but fortunately they are rarely needed. Especially when considering interacting systems we do not need them because the self-energy leads to convergent expressions automatically. From now on we always refer to the regularized action when using the term Keldysh action. Finally let us mention that the Green's functions in the non-interacting case can also be determined by means of kinetic equations which we will use for a system of magnons coupled to a bath of phonons in section 3.3.2.

1.1.5. Interacting Bose systems

In this section we discuss the generalization from a single harmonic oscillator to interacting systems of bosons. For Hamiltonians given in second quantization and being normal ordered the procedure of introducing the functional Keldysh formalism is very similar to what we have done for the harmonic oscillator. As an example let us consider a homogeneous system with a constant two-particle interaction U_0 whose Hamiltonian is given by

$$H = \sum_{\boldsymbol{k}} \epsilon_{\boldsymbol{k}} a_{\boldsymbol{k}}^\dagger a_{\boldsymbol{k}} + \frac{U_0}{2V} \sum_{\boldsymbol{k},\boldsymbol{k}',\boldsymbol{q}} a_{\boldsymbol{k}+\boldsymbol{q}}^\dagger a_{\boldsymbol{k}'-\boldsymbol{q}}^\dagger a_{\boldsymbol{k}'} a_{\boldsymbol{k}}, \tag{1.64}$$

with dispersion $\epsilon_{\boldsymbol{k}}$ and volume V. For this system the components of the Green's function are

$$iG_{\boldsymbol{k}}^R(t,t') = \left\langle \phi_{\boldsymbol{k}}^C(t)\, \bar{\phi}_{\boldsymbol{k}}^Q(t') \right\rangle, \tag{1.65a}$$

$$iG_{\boldsymbol{k}}^A(t,t') = \left\langle \phi_{\boldsymbol{k}}^Q(t)\, \bar{\phi}_{\boldsymbol{k}}^C(t') \right\rangle, \tag{1.65b}$$

$$iG_{\boldsymbol{k}}^K(t,t') = \left\langle \phi_{\boldsymbol{k}}^C(t)\, \bar{\phi}_{\boldsymbol{k}}^C(t') \right\rangle, \tag{1.65c}$$

and the Gaussian part of the Keldysh action is given by

$$S_0\left[\bar{\phi},\phi\right] = \int_{-\infty}^{\infty} dt \int_{-\infty}^{\infty} dt' \sum_{\boldsymbol{k}} \left(\ \bar{\phi}_{\boldsymbol{k}}^C(t), \ \ \bar{\phi}_{\boldsymbol{k}}^Q(t) \ \right)$$

$$\begin{pmatrix} 0 & \left[\hat{G}_0^A\right]^{-1} \\ \left[\hat{G}_0^R\right]^{-1} & -\left[\hat{G}_0^R\right]^{-1} \hat{G}_0^K \left[\hat{G}_0^A\right]^{-1} \end{pmatrix}_{tt'} \begin{pmatrix} \phi_{\boldsymbol{k}}^C(t') \\ \phi_{\boldsymbol{k}}^Q(t') \end{pmatrix}. \tag{1.66}$$

The components of the non-interacting inverse Green's function $\boldsymbol{G}_0^{-1}$ are

$$\left[\hat{G}_0^R\right]_{\boldsymbol{k},tt'}^{-1} = i\delta'(t-t') + \delta(t-t')(-\epsilon_{\boldsymbol{k}} + i\eta), \tag{1.67a}$$

$$\left[\hat{G}_0^A\right]_{\boldsymbol{k},tt'}^{-1} = i\delta'(t-t') + \delta(t-t')(-\epsilon_{\boldsymbol{k}} - i\eta), \tag{1.67b}$$

$$-\left[\hat{G}_0^R\right]^{-1} \hat{G}_0^K \left[\hat{G}_0^A\right]^{-1} = 2i\eta\hat{g}_0. \tag{1.67c}$$
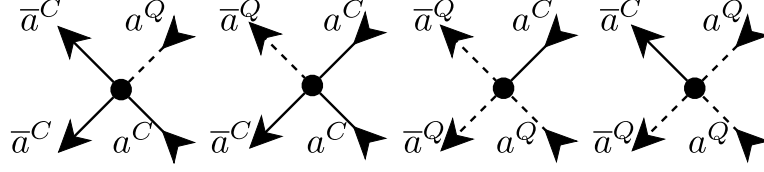
Figure 1.3.: Diagrammatic illustration of the vertices of Eq. (1.70). The solid lines represent classical fields and the dashed lines quantum fields.

We assume here that the initial distribution $\hat{g}_0$ is given by the equilibrium distribution $g_{0,\boldsymbol{k}}(t,t') = \delta(t-t')[1 + 2b(\epsilon_{\boldsymbol{k}} - \mu)]$. For the free propagators we just have to replace $\epsilon_0 \to \epsilon_{\boldsymbol{k}}$ in Eqs. (1.43a-1.43c), yielding

$$
\begin{aligned}
G^R_{0,\boldsymbol{k}}(t,t') &= -i\Theta(t-t')\,e^{-i\epsilon_{\boldsymbol{k}}(t-t')}, & \text{(1.68a)}\\
G^A_{0,\boldsymbol{k}}(t,t') &= i\Theta(t'-t)\,e^{-i\epsilon_{\boldsymbol{k}}(t-t')}, & \text{(1.68b)}\\
G^K_{0,\boldsymbol{k}}(t,t') &= -i[1 + 2b(\epsilon_{\boldsymbol{k}} - \mu)]\,e^{-i\epsilon_{\boldsymbol{k}}(t-t')}. & \text{(1.68c)}
\end{aligned}
$$

A derivation is given in section 3.3.2. Note that if the renormalization of the one-particle energy is neglected the interactions contribute to the thermalization process only and the equilibrium state is described by the non-interacting Green's functions.

The interaction part of the action is easily written down in the contour basis, we obtain from Eq. (1.18)

$$
S_I[\bar{\phi},\phi] = -\int_{-\infty}^{\infty} dt\, \frac{U_0}{2V} \sum_{\boldsymbol{k},\boldsymbol{k}',\boldsymbol{q}} \sum_{p=\pm} p\,\bar{\phi}^p_{\boldsymbol{k}+\boldsymbol{q}}(t)\,\bar{\phi}^p_{\boldsymbol{k}'-\boldsymbol{q}}(t)\,\phi^p_{\boldsymbol{k}'}(t)\,\phi^p_{\boldsymbol{k}}(t), \quad \text{(1.69)}
$$

where $p = \pm$ is a contour label. Transforming to the Keldysh basis it becomes

$$
\begin{aligned}
S_I[\bar{\phi},\phi] = &-\int_{-\infty}^{\infty} dt\, \frac{U_0}{2V}\\
&\times \sum_{\boldsymbol{k},\boldsymbol{k}',\boldsymbol{q}} \left\{ \bar{\phi}^{\mathrm{C}}_{\boldsymbol{k}+\boldsymbol{q}}(t)\,\bar{\phi}^{\mathrm{Q}}_{\boldsymbol{k}'-\boldsymbol{q}}(t)\left[\phi^{\mathrm{C}}_{\boldsymbol{k}'}(t)\,\phi^{\mathrm{C}}_{\boldsymbol{k}}(t) + \phi^{\mathrm{Q}}_{\boldsymbol{k}'}(t)\,\phi^{\mathrm{Q}}_{\boldsymbol{k}}(t)\right]\right.\\
&\left. + \left[\bar{\phi}^{\mathrm{C}}_{\boldsymbol{k}+\boldsymbol{q}}(t)\,\bar{\phi}^{\mathrm{C}}_{\boldsymbol{k}'-\boldsymbol{q}}(t) + \bar{\phi}^{\mathrm{Q}}_{\boldsymbol{k}+\boldsymbol{q}}(t)\,\bar{\phi}^{\mathrm{Q}}_{\boldsymbol{k}'-\boldsymbol{q}}(t)\right]\phi^{\mathrm{C}}_{\boldsymbol{k}'}(t)\,\phi^{\mathrm{Q}}_{\boldsymbol{k}}(t)\right\}.
\end{aligned}
$$
$$\text{(1.70)}$$

In Fig. 1.3 the vertices are shown diagrammatically. As in thermal equilibrium we parametrize the effect of the interactions on the one-particle Green's function by the matrix self-energy $\boldsymbol{\Sigma}$. In this context the Dyson equation has the form

$$
\boldsymbol{G}^{-1} = \boldsymbol{G}_0^{-1} - \boldsymbol{\Sigma}, \quad \text{(1.71)}
$$

or if we explicitly write down the matrices in the Keldysh space:

$$
\begin{pmatrix} 0 & \left[\hat{G}^A\right]^{-1} \\ \left[\hat{G}^R\right]^{-1} & -\left[\hat{G}^R\right]^{-1}\hat{G}^K\left[\hat{G}^A\right]^{-1} \end{pmatrix}
$$
$$
= \begin{pmatrix} 0 & \left[\hat{G}_0^A\right]^{-1} \\ \left[\hat{G}_0^R\right]^{-1} & -\left[\hat{G}_0^R\right]^{-1}\hat{G}_0^K\left[\hat{G}_0^A\right]^{-1} \end{pmatrix} - \begin{pmatrix} 0 & \hat{\Sigma}^A \\ \hat{\Sigma}^R & \hat{\Sigma}^K \end{pmatrix}. \quad (1.72)
$$

As it can be seen here the self-energy exhibits also the causality structure because this feature follows from the definition of the Green's function and is not affected by interactions. Also in the context of the Keldysh formalism the self-energy contains only one-particle irreducible diagrams, see for example Ref. [2].

1.1.6. Quantum kinetic equations

The introduced time dependent objects can be calculated by means of quantum kinetic equations which can be derived from the matrix Dyson equation (1.71), where the time derivative contained in the inverse free Green's function leads to differential equations. The Dyson equation can be rearranged in two different ways. Multiplying $\boldsymbol{G}$ from one or the other side yields

$$
\left(\boldsymbol{G}_0^{-1} - \boldsymbol{\Sigma}\right)\boldsymbol{G} = \boldsymbol{I}, \quad (1.73)
$$

and

$$
\boldsymbol{G}\left(\boldsymbol{G}_0^{-1} - \boldsymbol{\Sigma}\right) = \boldsymbol{I}. \quad (1.74)
$$

For the components of the Green's function we explicitly obtain from the first equation

$$
\left(\hat{G}_0^R\right)^{-1}\hat{G}^R = \hat{I} + \hat{\Sigma}^R\hat{G}^R, \quad (1.75a)
$$

$$
\left(\hat{G}_0^A\right)^{-1}\hat{G}^A = \hat{I} + \hat{\Sigma}^A\hat{G}^A, \quad (1.75b)
$$

$$
\left(\hat{G}_0^R\right)^{-1}\hat{G}^K = \hat{\Sigma}^K\hat{G}^A + \hat{\Sigma}^R\hat{G}^K, \quad (1.75c)
$$

and from the second equation

$$
\hat{G}^R\left(\hat{G}_0^R\right)^{-1} = \hat{I} + \hat{G}^R\hat{\Sigma}^R, \quad (1.76a)
$$

$$
\hat{G}^A\left(\hat{G}_0^A\right)^{-1} = \hat{I} + \hat{G}^A\hat{\Sigma}^A, \quad (1.76b)
$$

$$
\hat{G}^K\left(\hat{G}_0^A\right)^{-1} = \hat{G}^R\hat{\Sigma}^K + \hat{G}^K\hat{\Sigma}^A. \quad (1.76c)
$$

These coupled equations are exact and in principle they can be solved numerically. But we are faced with two problems: The self-energies have to be

calculated and due to the involved matrix multiplications these simple looking equations are actually partial integro-differential equations. Only for simple quantum dot systems can they be solved numerically exact, as for example in Ref. [4]. For more complex systems the system of equations have to be approximated in an appropriate way. For calculating the self-energies the most common method is perturbation theory. For going beyond usual perturbation theory for example the $1/N$ expansion [5] or functional renormalization group methods [6] can be used. In the scope of this thesis we determine the self-energy by means of perturbation theory and functional renormalization group methods. In the next section we will approximate the kinetic equations by using the Wigner transformation.

But first let us consider the equations for the Keldysh Green's function in more detail. It is convenient to introduce certain combinations of Green's functions and self-energies [7],

$$\hat{G}^M \;=\; \frac{1}{2}\left(\hat{G}^R + \hat{G}^A\right), \tag{1.77a}$$

$$\hat{G}^I \;=\; i\left(\hat{G}^R - \hat{G}^A\right), \tag{1.77b}$$

$$\hat{\Sigma}^M \;=\; \frac{1}{2}\left(\hat{\Sigma}^R + \hat{\Sigma}^A\right), \tag{1.77c}$$

$$\hat{\Sigma}^I \;=\; i\left(\hat{\Sigma}^R - \hat{\Sigma}^A\right), \tag{1.77d}$$

where M stands for "mean" and I for "imaginary". Subtracting the one form of the kinetic equation for the Keldysh Green's function Eq. (1.75c) from the other one Eq. (1.76c) and inserting the mean and imaginary Green's functions yields

$$\left[\hat{M}, \hat{G}^K\right] - \left[\hat{\Sigma}^K, \hat{G}^M\right] = \hat{C}^{\text{in}} - \hat{C}^{\text{out}}, \tag{1.78}$$

where we define the inverse free propagator without regularization but with renormalized energy as

$$\hat{M} \;=\; \hat{M}_0 - \hat{\Sigma}^M, \tag{1.79a}$$

$$\left[\hat{M}_0\right]_{\boldsymbol{k},tt'} \;=\; i\delta'\left(t - t'\right) - \epsilon_{\boldsymbol{k}}\delta\left(t - t'\right). \tag{1.79b}$$

The new introduced matrices are

$$\hat{C}^{\text{in}} \;=\; \frac{i}{2}\left\{\hat{\Sigma}^K, \hat{G}^I\right\}, \tag{1.80a}$$

$$\hat{C}^{\text{out}} \;=\; \frac{i}{2}\left\{\hat{\Sigma}^I, \hat{G}^K\right\}. \tag{1.80b}$$

The kinetic equation (1.78) is often the starting point for calculations and approximations, for example the quantum Boltzmann equation can be derived from it, where the in- and out-scattering parts of the collision integral can be traced back to $\hat{C}^{\text{in}}$ and $\hat{C}^{\text{out}}$. The terms involving $\hat{\Sigma}^M$ and $\hat{G}^M$ renormalize the energy dispersion.

Instead of considering the Keldysh Green's function itself often a distribution function is introduced via the ansatz

$$\hat{G}^K = \hat{G}^R \hat{g} - \hat{g}^\dagger \hat{G}^A. \tag{1.81}$$

Note that this ansatz is not the generalized Kadanoff-Baym ansatz [8], where the distribution function $\hat{g}^{\text{GKBA}}$ is diagonal in time,

$$\left[\hat{g}^{\text{GKBA}}\right]_{\boldsymbol{k},tt'} = \delta\left(t - t'\right) g_{\boldsymbol{k}}^{\text{GKBA}}\left(t\right). \tag{1.82}$$

In the non-interacting case it can be seen from Eqs. (1.68a-1.68c) that

$$\left[\hat{g}_0\right]_{\boldsymbol{k},tt'} = \delta\left(t - t'\right)\left[1 + 2b\left(\epsilon_{\boldsymbol{k}}\right)\right], \tag{1.83}$$

which is similar to Eqs. (1.45-1.61) for the harmonic oscillator. The easiest way of deriving the kinetic equation for $\hat{g}$ is to insert the ansatz Eq. (1.81) in the bottom right component of the Dyson equation (1.72) which yields after rearranging terms

$$-i\left(\hat{M}\hat{g} - \hat{g}^\dagger\hat{M}\right) = \hat{\Sigma}^{\text{in}} - \hat{\Sigma}^{\text{out}}, \tag{1.84}$$

where the in- and out-scattering parts are given by

$$\hat{\Sigma}^{\text{in}} = i\hat{\Sigma}^K, \tag{1.85a}$$

$$\hat{\Sigma}^{\text{out}} = \frac{1}{2}\left(\hat{\Sigma}^I\hat{g} + \hat{g}^\dagger\hat{\Sigma}^I\right). \tag{1.85b}$$

1.1.7. Wigner transformation

If the evolution of a system is determined by two different time scales, a fast microscopic and a slow macroscopic one, the kinetic equations can be simplified by means of the Wigner transformation (WT). It includes the transformation to central point $\tau = \left(t + t'\right)/2$ and difference variables $s = t - t'$ and the performance of a Fourier transformation in the fast difference variable. For a function $A\left(t, t'\right)$ the transformation is defined as

$$\text{WT}\left[A\left(t, t'\right)\right]_{(\tau;\omega)} = \int ds\, e^{i\omega s} A\left(\tau + \frac{s}{2}, \tau - \frac{s}{2}\right) \equiv A\left(\tau;\omega\right). \tag{1.86}$$

We denote the WT of a function by a semicolon between the variables in the argument. Using the fact that

$$\left[\hat{M}_0\hat{g} - \hat{g}^\dagger\hat{M}_0\right]_{(\tau;\omega)} = i\partial_\tau\text{Re}\left[g\left(\tau,\omega\right)\right] + 2i\left(\omega - \epsilon_{\boldsymbol{k}}\right)\text{Im}\left[g\left(\tau,\omega\right)\right], \tag{1.87}$$

the WT of the kinetic equation (1.84) for the distribution function is given by

$$\partial_\tau\text{Re}\left[g\left(\tau;\omega\right)\right] + 2\left(\omega - \epsilon_{\boldsymbol{k}}\right)\text{Im}\left[g\left(\tau;\omega\right)\right] + i\left(\hat{\Sigma}^M\hat{g} - \hat{g}^\dagger\hat{\Sigma}^M\right)_{(\tau;\omega)}$$

$$= i\Sigma_{\boldsymbol{k}}^K\left(\tau;\omega\right) - \frac{1}{2}\left(\hat{\Sigma}^I\hat{g} + \hat{g}^\dagger\hat{\Sigma}^I\right)_{(\tau;\omega)}. \tag{1.88}$$

For approximating this equation let us consider the FT of the matrix product

$$
\mathrm{WT}\left[\left(\hat{A}\hat{B}\right)_{tt'}\right]_{(\tau;\omega)} = \int ds \int dt'' \int \frac{d\omega_1}{2\pi} \int \frac{d\omega_2}{2\pi} e^{i\omega s} e^{i\omega_1\left(t''-\tau-\frac{s}{2}\right)} e^{-i\omega_2\left(t''-\tau+\frac{s}{2}\right)}
$$
$$
\times A\left(\frac{\tau+\frac{s}{2}+t''}{2};\omega_1\right) B\left(\frac{\tau-\frac{s}{2}+t''}{2};\omega_2\right), \quad (1.89)
$$

in more detail. We first derive a differential form of it. Therefore we transform to the variables

$$
\tau_1 = t'' - \tau + \frac{s}{2}, \tag{1.90a}
$$
$$
\tau_2 = t'' - \tau - \frac{s}{2}, \tag{1.90b}
$$
$$
\tilde{\omega}_{1/2} = \omega_{1/2} - \omega, \tag{1.90c}
$$

and rename $\tilde{\omega}_{1/2} \to \omega_{1/2}$ which yields

$$
\mathrm{WT}\left[\left(\hat{A}\hat{B}\right)_{tt'}\right]_{(\tau;\omega)} = \int d\tau_1 \int d\tau_2 \int \frac{d\omega_1}{2\pi} \int \frac{d\omega_2}{2\pi} e^{i\omega_1\tau_2 - i\omega_2\tau_1}
$$
$$
\times A\left(\tau + \frac{\tau_1}{2};\omega+\omega_1\right) B\left(\tau+\frac{\tau_2}{2};\omega+\omega_2\right). \tag{1.91}
$$

Expanding the functions in $\omega_{1/2}$ and using the relation $\int \frac{d\omega}{2\pi} e^{\pm i\omega\tau}\omega^n = (\mp i)^n \left(d^n/d\tau^n\right)\delta\left(\tau\right)$ we find that

$$
\int \frac{d\omega_1}{2\pi} e^{i\omega_1\tau_2} A\left(\tau+\frac{\tau_1}{2};\omega+\omega_1\right) = e^{-i\partial_{\tau_2}\partial_\omega} A\left(\tau+\frac{\tau_1}{2};\omega\right), \tag{1.92a}
$$
$$
\int \frac{d\omega_1}{2\pi} e^{-i\omega_2\tau_1} B\left(\tau+\frac{\tau_2}{2};\omega+\omega_2\right) = e^{i\partial_{\tau_1}\partial_\omega} B\left(\tau+\frac{\tau_2}{2};\omega\right). \tag{1.92b}
$$

Plugging into Eq. (1.91) yields

$$
\mathrm{WT}\left[\left(\hat{A}\hat{B}\right)_{tt'}\right]_{(\tau;\omega)}
$$
$$
= \int d\tau_1 \int d\tau_2 \delta\left(\tau_2\right) A\left(\tau+\frac{\tau_1}{2};\omega\right) e^{-i\overleftarrow{\partial}_{\tau_2}\overleftarrow{\partial}_\omega + i\overrightarrow{\partial}_{\tau_1}\overrightarrow{\partial}_\omega} \delta\left(\tau_1\right) B\left(\tau+\frac{\tau_2}{2};\omega\right)
$$
$$
= A\left(\tau;\omega\right) e^{-\frac{i}{2}\left(\overleftarrow{\partial}_\tau\overrightarrow{\partial}_\omega - \overrightarrow{\partial}_\tau\overleftarrow{\partial}_\omega\right)} B\left(\tau;\omega\right), \tag{1.93}
$$

where we have used integration by parts for the second line and introduced the partial derivatives $\overrightarrow{\partial}_x$ and $\overleftarrow{\partial}_x$ which are the usual derivatives but acting on functions at the left or right only. Expanding the exponential yields

$$
\mathrm{WT}\left[\left(\hat{A}\hat{B}\right)_{tt'}\right]_{(\tau;\omega)} = A\left(\tau;\omega\right) B\left(\tau;\omega\right)
$$
$$
+\frac{i}{2}\left[\partial_\tau A\left(\tau;\omega\right)\partial_\omega B\left(\tau;\omega\right) - \partial_\omega A\left(\tau;\omega\right)\partial_\tau B\left(\tau;\omega\right)\right] + \mathcal{O}\left[\left(\partial_\tau\partial_\omega\right)^2\right]. \tag{1.94}
$$

For functions varying slowly in τ and ω we may retain only the zeroth order term. In such a case the matrix product becomes just the product of the WT,

$$\mathrm{WT}\left[\left(\hat{A}\hat{B}\right)_{tt'}\right]_{(\tau;\omega)} \approx A\left(\tau;\omega\right)B\left(\tau;\omega\right). \tag{1.95}$$

For time matrices which depend only on the time difference such as the non-interacting Green's functions (1.68a-1.68c) this approximation is exact because the derivatives with respect to τ are 0. This justifies that at least in some region around thermal equilibrium the distribution function is slowly varying and the approximation (1.95) is valid also for nonequilibrium. In this approximation the kinetic equation (1.88) becomes

$$\partial_\tau \mathrm{Re}\left[g_{\boldsymbol{k}}(\tau;\omega)\right] + 2\left[\omega - \epsilon_{\boldsymbol{k}} - \Sigma_{\boldsymbol{k}}^M(\tau;\omega)\right]\mathrm{Im}\left[g_{\boldsymbol{k}}(\tau;\omega)\right]$$
$$= i\Sigma_{\boldsymbol{k}}^K(\tau;\omega) - \Sigma_{\boldsymbol{k}}^I(\tau;\omega)\mathrm{Re}\left[g_{\boldsymbol{k}}(\tau;\omega)\right]. \tag{1.96}$$

As for the WT we can argue that there is a regime where we can neglect the imaginary part of the distribution function since in equilibrium it is also real. If we do so, setting $\omega = \epsilon_{\boldsymbol{k}}$ and renaming $g_{\boldsymbol{k}}(\tau) \equiv \mathrm{Re}\left[g_{\boldsymbol{k}}(\tau, \epsilon_{\boldsymbol{k}})\right]$ yields

$$\partial_\tau g_{\boldsymbol{k}}(\tau) = i\Sigma_{\boldsymbol{k}}^K(\tau;\epsilon_{\boldsymbol{k}}) - \Sigma_{\boldsymbol{k}}^I(\tau;\epsilon_{\boldsymbol{k}})g_{\boldsymbol{k}}(\tau), \tag{1.97}$$

which we will use in chapter 3. There we will also need the WT of a product of two functions $A(t,t')$ and $B(t,t')$ both given at times t and t' which yields a convolution in frequency space,

$$\begin{aligned}
\left[A(t,t')B(t,t')\right]_{(\tau,\omega)} &= \int_{-\infty}^{\infty} ds\, e^{i\omega s} A(\tau + \frac{s}{2}, \tau - \frac{s}{2})B(\tau + \frac{s}{2}, \tau - \frac{s}{2}) \\
&= \int_{-\infty}^{\infty} \frac{d\omega'}{2\pi} A(\tau;\omega')B(\tau;\omega - \omega').
\end{aligned} \tag{1.98}$$

From the kinetic equation (1.95) we can see that using the gradient approximation (1.95) for the WT yields Markovian equations which means that the dynamics at time t does not depend on times smaller than t. Therefore we do not have to choose the initial time to be in the distant past and can consider the evolution of a system right from the time we are interested in. At the end let us mention that our considerations of the WT can also be extended to space coordinates for inhomogeneous systems.

1.2. Functional renormalization group

Correlated systems often exhibit strongly scale-dependent behavior. Going from high energies (short wavelength, microscopic scale) to low energies (long wavelength, macroscopic wavelength) new collective phenomena and effective degrees of freedom emerge. The functional renormalization group (FRG) is a convenient theory for obtaining the low energy physics from microscopical

processes by iteratively coarse-graining the system to larger scales. Moreover it is a method which permits non-perturbative approximations and the possibility to avoid divergencies arising in perturbation theory [6, 9, 10, 11, 12]. Retaining a finite number of terms in an expansion of the interaction always breaks down for sufficiently large interactions. For example the vertex expansion of the FRG [13] yields an infinte hierarchy of differential equations and as an approximation this hierarchy is truncated at some point. In contrast to perturbation theory the validity of this approximation is not directly connected to the interaction strength and hence can give good results even for strongly interacting systems. Therefore the FRG is a tool which is used for investigating such systems. It has its roots in the Wilsonian renormalization group (RG) developed by Wilson and coauthors [14, 15, 16, 17, 18, 19, 20]. The idea of the RG is to integrate out some less important modes in order to obtain a simpler effective model for the remaining modes. Whereas the RG equations are only valid for certain approximations Nicoll *et al.* [21], Weinberg [22], Nicoll and Chang [23], Wetterich [24], Bonini *et al.* [25] and Morris [13] could obtain exact equations for the effective model by means of functional methods which was the foundation of the FRG. Using a certain cutoff scheme and certain approximations, the FRG recovers the RG. In this thesis we use the FRG in order to derive a non-perturbative kinetic theory for Bose gases.

The formulation of the FRG in the book [6] is of such a general form that it can be easily adopted to nonequilibrium situations and therefore we follow this book to give a brief introduction to FRG for nonequilibrium. A nonequilibrium version of the FRG can be also found in Refs. [4, 26, 27, 28]. We will restrict ourselves to bosonic systems. In the real time context it is common to choose the normalization of the functional integrals and the Green's functions by

$$iG^{(n)}_{\alpha_1\ldots\alpha_n} \equiv \langle \Phi_{\alpha_1} \ldots \Phi_{\alpha_n} \rangle = \frac{\int \mathcal{D}\left[\Phi\right] e^{iS[\Phi]}\Phi_{\alpha_1} \ldots \Phi_{\alpha_n}}{\int \mathcal{D}\left[\Phi\right] e^{iS[\Phi]}}, \qquad (1.99)$$

as done in section 1.1. In contrast the normalization

$$G^{(n)}_{\alpha_1\ldots\alpha_n} \equiv \langle \Phi_{\alpha_1} \ldots \Phi_{\alpha_n} \rangle = \frac{\int \mathcal{D}\left[\Phi\right] e^{-S[\Phi]}\Phi_{\alpha_1} \ldots \Phi_{\alpha_n}}{\int \mathcal{D}\left[\Phi\right] e^{-S[\Phi]}}, \qquad (1.100)$$

is common for a imaginary time setup, see [29]. The measure of the functional integrals is normalized such that the partition function is given by

$$\mathcal{Z} = \int \mathcal{D}\left[\Phi\right] e^{iS[\Phi]}. \qquad (1.101)$$

Following [6] we introduce bosonic superfields Φ_α which are completely characterized by the superlabel α. The superlabel is a collection of quantum numbers specifying a field configuration of the system under consideration, for example momenta and time. We will refer to the space specified by α as the superspace. In this notation the matrix structure of the Green's functions in the

Keldysh formalism just lead to an additional label in the superlabel and thus does not change the general equations given in [6]. For the system specified by Eq. (3.1) considered in chapter 3 the superlabel is given by $\alpha = \{\sigma, X, \boldsymbol{k}, t\}$, where $\sigma = a, b$ specifies the flavor of the bosons, $X = C, Q$ the component in the Keldysh basis, $\boldsymbol{k}$ the momentum and t the time. Only the different real-time normalization will modify the FRG equations. We will first consider generating functionals for different types of Green's functions and then give the flow equations suitable for the nonequilibrium context.

1.2.1. Generating functionals for Green's functions

The complete information of all n-point Green's functions Eq. (1.99) is contained in the generating functional

$$\mathcal{G}\left[J\right] = \int \mathcal{D}\left[\Phi\right] e^{iS[\Phi]+(J,\Phi)}, \tag{1.102}$$

where we have introduced a scalar product in superspace by

$$(J, \Phi) \equiv \int_\alpha J_\alpha \Phi_\alpha. \tag{1.103}$$

We have denoted the integration over continuous quantum numbers of α and the summation over discrete ones by $\int_\alpha$. The action is assumed to have a Gaussian part $S_0\left[\Phi\right]$ and an interaction part $S_1\left[\Phi\right]$,

$$S\left[\Phi\right] = S_0\left[\Phi\right] + S_1\left[\Phi\right], \tag{1.104a}$$

$$S_0\left[\Phi\right] = \frac{1}{2}\left(\Phi, \boldsymbol{G}_0^{-1}\Phi\right), \tag{1.104b}$$

where the inverse free propagator $\boldsymbol{G}_0^{-1}$ is a matrix in superspace. Defining the free 2-point Green's function by $G_{0,\alpha\alpha'}^{(2)}$ the components of $\boldsymbol{G}_0$ are given by

$$[\boldsymbol{G}_0]_{\alpha\alpha'} = G_{0,\alpha\alpha'}^{(2)}. \tag{1.105}$$

In this section we always denote matrices in the superspace by bold symbols and will refer to them as supermatrices. The n-point Green's functions can be obtained from the generating functional Eq. (1.102) by means of functional derivatives,

$$iG_{\alpha_1\ldots\alpha_n}^{(n)} = \left.\frac{\delta^n \mathcal{G}\left[J\right]}{\delta J_{\alpha_1}\ldots\delta J_{\alpha_n}}\right|_{J=0}, \tag{1.106}$$

which implies the Taylor series

$$\mathcal{G}\left[J\right] = \sum_{n=0}^\infty \frac{1}{n!} \int_{\alpha_1}\cdots\int_{\alpha_n} iG_{\alpha_1\ldots\alpha_n}^{(n)} J_{\alpha_1}\ldots J_{\alpha_n}. \tag{1.107}$$

The n-point Green's functions Eq. (1.99) contain also disconnected diagrams and therefore depend on Green's functions of lower order than n. In

order to avoid this redundancy one has to consider so called connected Green's functions $G_{c,\alpha_1\ldots\alpha_n}^{(n)}$ which are given by retaining just the connected diagrams of Eq. (1.99). Their generating functionals are given by

$$\mathcal{G}_c\left[J\right] = \ln\frac{\int \mathcal{D}\left[\Phi\right]e^{iS[\Phi]+(J,\Phi)}}{\int \mathcal{D}\left[\Phi\right]e^{iS_0[\Phi]}}, \tag{1.108}$$

and the normalization is chosen such that

$$iG_{c,\alpha_1\ldots\alpha_n}^{(n)} = \left.\frac{\delta^n\mathcal{G}_c\left[J\right]}{\delta J_{\alpha_1}\ldots\delta J_{\alpha_n}}\right|_{J=0}. \tag{1.109}$$

The fact that $\mathcal{G}_c\left[J\right]$ indeed generates only connected diagrams can be shown by the replica trick, see Ref. [6]. In the non-interacting case we find that

$$i\left[\boldsymbol{G}_0\right]_{\alpha\alpha'} = \frac{\delta^2\mathcal{G}_{0c}\left[J\right]}{\delta J_\alpha\delta J_{\alpha'}} = \langle\Phi_\alpha\Phi_{\alpha'}\rangle_0 = iG_{0c,\alpha\alpha'}^{(2)} = iG_{0,\alpha\alpha'}^{(2)}, \tag{1.110}$$

where $\langle\ldots\rangle_0$ is the average with respect to the Gaussian part of the action only. Analogously $G_{0c,\alpha\alpha'}^{(2)}$ is the free 2-point connected Green's function and $\mathcal{G}_{0c}\left[J\right]$ is the generating functional for the free connected Green's functions. Defining the differential operator $\frac{\delta}{\delta J}\otimes\frac{\delta}{\delta J}$ by

$$\left[\frac{\delta}{\delta J}\otimes\frac{\delta}{\delta J}\right]_{\alpha\alpha'} = \frac{\delta}{\delta J_\alpha}\frac{\delta}{\delta J_{\alpha'}}, \tag{1.111}$$

we can write

$$i\boldsymbol{G}_0 = \frac{\delta}{\delta J}\otimes\frac{\delta}{\delta J}\mathcal{G}_{0c}\left[J\right]. \tag{1.112}$$

Similarly we introduce the supermatrix of the 2-point connected Green's function by

$$i\boldsymbol{G} = \left[\frac{\delta}{\delta J}\otimes\frac{\delta}{\delta J}\mathcal{G}_c\left[J\right]\right]_{J=0}. \tag{1.113}$$

Now we can define a self-energy supermatrix $\boldsymbol{\Sigma}$ by the supermatrix Dyson equation,

$$\boldsymbol{G}^{-1} = \boldsymbol{G}_0^{-1} - \boldsymbol{\Sigma}. \tag{1.114}$$

It turns out that using certain cutoff schemes yield delta functions which are not integrated over. Therefore it is more convenient to use the generating functional $\Gamma\left[\bar{\Phi}\right]$ of the n-point one-line irreducible (1PI) vertices $\Gamma_{\alpha_1\ldots\alpha_n}^{(n)}$ instead of formulating the FRG for the generating functionals Eq. (1.102) or Eq. (1.108), see Ref. [6]. In general 1PI diagrams are defined by the property that they cannot be split into two parts by cutting a single line. The generating functional $\Gamma\left[\bar{\Phi}\right]$ is defined by

$$\begin{aligned}\Gamma\left[\bar{\Phi}\right] &= \left(J\left[\bar{\Phi}\right],\bar{\Phi}\right) - \mathcal{G}_c\left[J\left[\bar{\Phi}\right]\right] + \frac{i}{2}\left(\bar{\Phi},\boldsymbol{G}_0^{-1}\bar{\Phi}\right)\\ &= \mathcal{L}\left[\bar{\Phi}\right] + iS_0\left[\bar{\Phi}\right],\end{aligned} \tag{1.115}$$

where we have denoted the functional Legendre transformation of $\mathcal{G}_c\left[J\right]$ by $\mathcal{L}\left[\bar{\Phi}\right]$. The new fields $\bar{\Phi}$ are related to the sources J by

$$\bar{\Phi}_\alpha = \left\langle \Phi_\alpha \right\rangle_J \equiv \frac{\delta \mathcal{G}_c\left[J\right]}{\delta J_\alpha}, \tag{1.116}$$

where the subscript J denotes that the sources are not set to zero in this expression. By inversion we obtain $J\left[\bar{\Phi}\right]$ from this relation. The n-point 1PI vertices are given by

$$i\Gamma^{(n)}_{\alpha_1\ldots\alpha_n} = \left.\frac{\delta^n \Gamma\left[\bar{\Phi}\right]}{\delta\bar{\Phi}_{\alpha_1}\ldots\delta\bar{\Phi}_{\alpha_n}}\right|_{\bar{\Phi}=0}, \tag{1.117}$$

and the Taylor expansion of the generating functional is

$$\Gamma\left[\bar{\Phi}\right] = \sum_{n=0}^{\infty}\int_{\alpha_1}\ldots\int_{\alpha_n} i\Gamma^{(n)}_{\alpha_1\ldots\alpha_n}\bar{\Phi}_{\alpha_1}\ldots\bar{\Phi}_{\alpha_n}. \tag{1.118}$$

The 1PI vertices contain only 1PI diagrams and describe effective interactions in a system. The connected Green's functions $G^{(n)}_{c,\alpha_1\ldots\alpha_n}$ can be decomposed in 1PI vertices, for example it can be shown that the self-energy matrix of Eq. (1.114) is equal to the 2-point 1PI vertex,

$$\Gamma^{(2)}_{\alpha\alpha'} = \left[\boldsymbol{\Sigma}\right]_{\alpha\alpha'}, \tag{1.119}$$

which determines the connected 2-point Green's function. In general we have to use the so called tree expansion of the generating functional Eq. (1.115) to obtain the relation between the n-point connected Green's functions and the 1PI vertices, for details see Ref. [6].

1.2.2. Flow equations

In order to obtain an effective description of a system, let us introduce a scale Λ in the free propagator which simplifies the problem for $\Lambda \to \infty$ and recovers the original system for $\Lambda \to 0$,

$$\boldsymbol{G}_{0,\Lambda} \sim \begin{cases} \boldsymbol{G}_0 & \text{for } \Lambda \to 0, \\ 0 & \text{for } \Lambda \to \infty. \end{cases} \tag{1.120}$$

If one uses a cutoff in momentum such that it separates modes $|\boldsymbol{k}| \gtrsim \Lambda$ which already propagate and modes $|\boldsymbol{k}| \lesssim \Lambda$ which are still neglected, the FRG corresponds to the Wilsonian renormalization group in the sense that only modes with $|\boldsymbol{k}| \gtrsim \Lambda$ contribute to the loop integrals in the Feynman diagrams. In order to achieve the condition Eq. (1.120) we add a regulator $\boldsymbol{R}_\Lambda$ to the inverse free propagator,

$$\boldsymbol{G}_{0,\Lambda}^{-1} = \boldsymbol{G}_0^{-1} - \boldsymbol{R}_\Lambda, \tag{1.121}$$

where

$$|\boldsymbol{R}_\Lambda| \sim \begin{cases} 0 & \text{for } \Lambda \to 0, \\ \infty & \text{for } \Lambda \to \infty. \end{cases} \tag{1.122}$$

In this thesis we will only use a regulator of this kind, for a different way of introducing the cutoff see Ref. [6]. Note that only the Gaussian part of the action,

$$S_{0,\Lambda}[\Phi] = \frac{1}{2}\left(\Phi, \boldsymbol{G}_{0,\Lambda}^{-1}\Phi\right), \tag{1.123}$$

becomes scale dependent and not the interacting part $S_1[\Phi]$. The change of the system when varying the scale Λ is described by differential equations which are called flow equations. In order to derive these we have to take the derivative of the generating functionals with respect to Λ. For Eqs. (1.102, 1.108) this yields

$$\partial_\Lambda \mathcal{G}_\Lambda[J] = \left[\frac{i}{2}\left(\frac{\delta}{\delta J}, \left[\partial_\Lambda \boldsymbol{G}_{0,\Lambda}^{-1}\right]\frac{\delta}{\delta J}\right) - (\partial_\Lambda \ln \mathcal{Z}_\Lambda)\right]\mathcal{G}_\Lambda[J], \tag{1.124a}$$

$$\partial_\Lambda \mathcal{G}_{c,\Lambda}[J] = \frac{i}{2}\left(\frac{\delta \mathcal{G}_{c,\Lambda}}{\delta J}, \left[\partial_\Lambda \boldsymbol{G}_{0,\Lambda}^{-1}\right]\frac{\delta \mathcal{G}_{c,\Lambda}}{\delta J}\right) + \frac{i}{2}\text{Tr}\left[\left[\partial_\Lambda \boldsymbol{G}_{0,\Lambda}^{-1}\right]\left(\frac{\delta}{\delta J} \otimes \frac{\delta}{\delta J}\mathcal{G}_{c,\Lambda}\right)\right]$$
$$-\partial_\Lambda \ln \mathcal{Z}_{0,\Lambda}, \tag{1.124b}$$

where $\text{Tr}[\dots]$ is the trace in superspace and all functions with a Λ-label are obtained by replacing $\boldsymbol{G}_0 \to \boldsymbol{G}_{0,\Lambda}$ in their definitions. In principle Eq. (1.124b) could be expanded in powers of J to derive flow equations for the connected Green's functions. But $\mathcal{G}_{c,\Lambda}$ vanishes for $\Lambda \to \infty$ which is an inconvenient boundary conditions because in this case all physics has to emerge during the flow. Instead we consider the generating functional of the 1PI vertices whose flow equation is given by

$$\partial_\Lambda \Gamma_\Lambda[\bar{\Phi}] = -\frac{1}{2}\text{Tr}\left[-i\dot{\boldsymbol{G}}_\Lambda \boldsymbol{U}_\Lambda[\bar{\Phi}]\left(1 + i\boldsymbol{G}_\Lambda \boldsymbol{U}_\Lambda[\bar{\Phi}]\right)^{-1}\right.$$
$$\left. +\dot{\boldsymbol{G}}_{0,\Lambda}\boldsymbol{\Sigma}_\Lambda\left(1 + i\boldsymbol{G}_{0,\Lambda}\boldsymbol{\Sigma}_\Lambda\right)^{-1}\right], \tag{1.125}$$

where we have introduced the new supermatrix functional

$$\boldsymbol{U}_\Lambda[\bar{\Phi}] = \left(\frac{\delta}{\delta\bar{\Phi}} \otimes \frac{\delta}{\delta\bar{\Phi}}\Gamma_\Lambda[\bar{\Phi}]\right) - i\boldsymbol{\Sigma}_\Lambda. \tag{1.126}$$

The non-interacting limit of the single-scale propagator $\dot{\boldsymbol{G}}_\Lambda = -\boldsymbol{G}_\Lambda\left[\partial_\Lambda \boldsymbol{G}_{0,\Lambda}^{-1}\right]\boldsymbol{G}_\Lambda$ is $\dot{\boldsymbol{G}}_{0,\Lambda} = \partial_\Lambda \boldsymbol{G}_{0,\Lambda}$. In the limit of $\Lambda \to \infty$ the generating functional Γ_Λ becomes $S_1[\bar{\Phi}]$, see Ref. [6], which is an appropriate boundary condition. The second line of Eq. (1.125) is field independent and has to be taken into account only for calculating corrections to the free energy. The flow equation Eq. (1.125) is the central object of the FRG and contains all the information we need. For equilibrium an equivalent formulation of the flow equation (1.125) was first
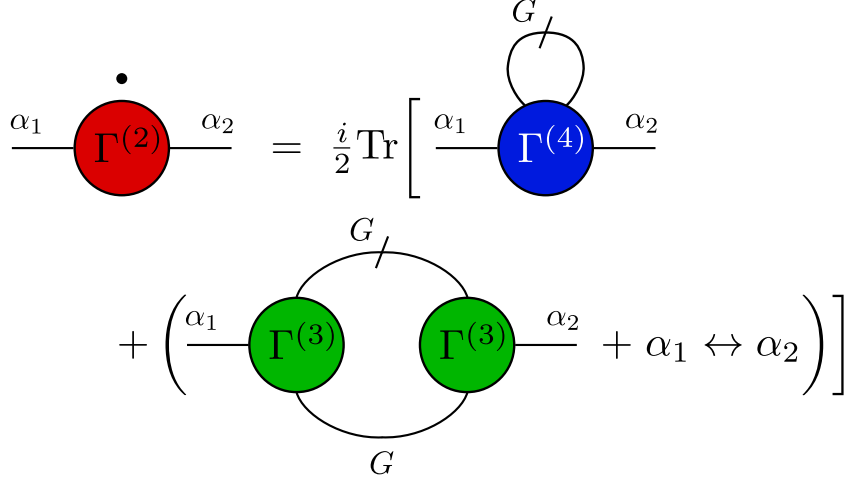
Figure 1.4.: Graphical representation of the flow equation (1.127). The filled
circles are the scale-dependent two-, three- and four-legged ver-
tices. The dot above the two-legged vertex labels the derivative
with respect to the flow parameter Λ. Solid lines starting and end-
ing at vertices denote the full propagator $\boldsymbol{G}_\Lambda$ and slashed lines the
single scale propagator $\dot{\boldsymbol{G}}_\Lambda$. The external legs are specified by the
superlabels α_1 and α_2. Interchanging α_1 with α_2 in the second
term yields the third term.

derived by Wetterich [24] and Bonini *et al.* [25]. Although it looks rather sim-
ple it is a very complicated functional integro-differential equation which can
be solved exactly for simple systems only. There are two main approximation
schemes: the derivative and the vertex expansion. In this thesis we consider
only the vertex expansion which yields a hierarchy of flow equations for the
n-point 1PI vertices, for the derivative expansion we refer to Ref. [6]. In or-
der to obtain the vertex expansion we have to expand both sides of (1.125)
in powers of $\bar{\Phi}$ and compare coefficients. For the 2-point 1PI vertex, which is
equal to the self-energy, see Eq. (1.119), we find that

$$\partial_\Lambda \Gamma^{(2)}_{\Lambda,\alpha_1\alpha_2} = \frac{i}{2}\text{Tr}\left[\dot{\boldsymbol{G}}_\Lambda \Gamma^{(4)}_{\Lambda,\alpha_1\alpha_2} + \left\{\dot{\boldsymbol{G}}_\Lambda \Gamma^{(3)}_{\Lambda,\alpha_2} \boldsymbol{G}_\Lambda \Gamma^{(3)}_{\Lambda,\alpha_1} + \alpha_1 \leftrightarrow \alpha_2\right\}\right], \quad (1.127)$$

where the components of the supermatrix $\boldsymbol{\Gamma}^{(n+2)}_{\Lambda,\alpha_1\ldots\alpha_n}$ are given by

$$\left[\boldsymbol{\Gamma}^{(n+2)}_{\Lambda,\alpha_1\ldots\alpha_n}\right]_{\alpha\alpha'} = \Gamma^{(n+2)}_{\Lambda,\alpha\alpha'\alpha_1\ldots\alpha_n}. \quad (1.128)$$

In Fig. 1.4 we illustrated the flow equation with diagrams. Since the vertex
expansion yields an infinite hierarchy of flow equations one has to truncate
the hierarchy at some point. In chapter 3 we will consider only the flow of
the self-energy and hence Eq. (1.127) is the only flow equation we need. For
a general expression of the vertex expansion we refer to [6] where one has to

do the replacements $\boldsymbol{G}_\Lambda \to -i\boldsymbol{G}_\Lambda$, $\dot{\boldsymbol{G}}_\Lambda \to -i\dot{\boldsymbol{G}}_\Lambda$ and $\Gamma^{(n)}_{\Lambda,\alpha_1\ldots\alpha_n} \to i\Gamma^{(n)}_{\Lambda,\alpha_1\ldots\alpha_n}$ in order to obtain the real-time formulation [28].

At the end let us mention that there is not a unique way of implementing the FRG since there are infinitely many cutoff schemes which fulfill the condition Eq. (1.120). Without any approximations all cutoff schemes will produce the same results for $\Lambda \to 0$. But almost all problems cannot be solved exactly and the quality of the results will crucially depend on the chosen cutoff scheme. Unfortunately there is no a priori way of choosing an appropriate cutoff.

1.3. Spin-wave theory in thin film ferromagnets

The methods presented in this thesis can be applied to general Bose gases. Here we shall focus on spin waves (magnons) in a thin film of yttrium-iron garnet (YIG). On the relevant energy scales YIG can be considered an insulating ferromagnet. In this section some basics on spin-wave theory are presented.

Magnons are elementary excitations of magnetic insulators. Spin-wave theory considers small fluctuation of the spins around their classical ground state and is very successful in describing the properties of YIG [30, 31, 32, 33]. For deriving the spin-wave theory we will bosonize the spin fluctuations by a Holstein-Primakoff transformation and perform an expansion in $1/S$ up to linear order [34, 35]. We restrict our considerations to an effective ferromagnetic description of YIG. At some points we will expand the results to leading order in powers of momentum since by Brillouin light scattering, a detection method used in the experiments [33, 36, 37, 38, 39, 40, 41, 42], only magnons with long wavelengths are accessible.

The introduction to spin-wave theory presented here follows Refs. [31, 32, 43].

1.3.1. Effective spin model for YIG

To characterize YIG realistically we use the parameters from [31, 32]: the lattice spacing a is given by

$$a = 12.376 \text{ Å}, \tag{1.129}$$

the saturation magnetization M_S is

$$4\pi M_S = 1750 \text{ G}, \tag{1.130}$$

and the exchange stiffness ρ_{ex} is determined by

$$\frac{\rho_{\text{ex}}}{\mu} = \frac{JSa^2}{\mu} \approx 5.17 \times 10^{-13} \text{ Oe m}^2, \tag{1.131}$$

where $\mu = g\mu_B$ and μ_B is the Bohr magneton. This expression for the exchange stiffness is valid for low magnon densities, see Ref. [44] for example. The unit
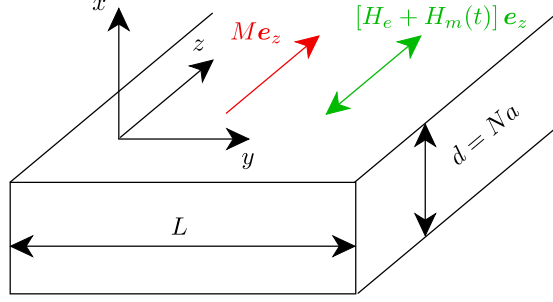
Figure 1.5.: Illustration of a thin stripe of YIG in the parallel pumping geometry. Its width is given by L and its thickness by $d = Na$, where N is the number of atomic layers and a is the lattice constant. We assume that $L \gg d$. The coordinate system is chosen such that the magnetization of the stripe M is in the z-direction. The static and the oscillating external magnetic field, H_e and H_m, are both parallel to the magnetization which is called parallel pumping.

cell of YIG has a complicated structure and YIG is actually a ferrimagnet, but for the relevant energy scales in experiments YIG can be described by a simple effective quantum Heisenberg model consisting of both exchange and dipole-dipole interactions [30, 31, 32, 45, 46, 47],

$$H = -\frac{1}{2} \sum_{ij} \sum_{\alpha\beta} \left[J_{ij}\delta^{\alpha\beta} + D_{ij}^{\alpha\beta} \right] S_i^\alpha S_j^\beta - [h_0 + h_1 \cos(\omega_0 t)] \sum_i S_i^z, \quad (1.132)$$

where the superscripts $\alpha, \beta = x, y, z$ label the three components of the spin operators S_i^α which satisfy the spin algebra. The summation indices $i, j = 1, \ldots, N$ enumerate the N sites $\boldsymbol{R}_i$ of a cubic lattice with lattice spacing a. The exchange couplings $J_{ij} = J(\boldsymbol{R}_i - \boldsymbol{R}_j)$ have the value $J \approx 1.29\mathrm{K}$ if $\boldsymbol{R}_i - \boldsymbol{R}_j$ connect nearest neighbor sites and vanish otherwise, see Refs. [31, 32, 46]. The Zeeman energy associated with a static external magnetic field H_e is denoted by $h_0 = \mu H_e$. Setting $g = 2$ we obtain an effective spin of $S \approx 14.2$ as discussed in references [31, 32, 46]. The time-dependent part of the Hamiltonian (1.132) represents the Zeeman energy $h_1 \cos(\omega_0 t) = \mu H_m(t)$ induced by an external microwave field oscillating with frequency ω_0 which is used in experiments to excite magnons. The associated energy scale h_1 is assumed to be small compared to h_0, such that both the static and the oscillating magnetic field point into the direction of the macroscopic magnetization $\boldsymbol{M} = M\boldsymbol{e}_z$, which is called parallel pumping, see Fig. 1.5. We choose the z-direction to be parallel to the magnetization. Finally, the matrix elements of the dipolar tensor $D_{ij}^{\alpha\beta} = D^{\alpha\beta}(\boldsymbol{R}_i - \boldsymbol{R}_j)$ are given by

$$D_{ij}^{\alpha\beta} = (1 - \delta_{ij}) \frac{\mu^2}{|\boldsymbol{R}_{ij}|^3} \left[3\hat{R}_{ij}^\alpha \hat{R}_{ij}^\beta - \delta^{\alpha\beta} \right], \quad (1.133)$$

where we use the abbrevations $\boldsymbol{R}_{ij} = \boldsymbol{R}_i - \boldsymbol{R}_j$ and $\hat{\boldsymbol{R}}_{ij} = \boldsymbol{R}_{ij} / |\boldsymbol{R}_{ij}|$.

1.3.2. Holstein-Primakoff transformation

Assuming that in the classical ground state all spins point in the direction of the external magnetic field, the z-direction, we can bosonize the fluctuation around the classical ground state via the Holstein-Primakoff transformation [48] in the form

$$S_i^+ = \sqrt{2S}\sqrt{1 - \frac{n_i}{2S}}b_i = \sqrt{2S}\left[b_i - \frac{n_i b_i}{4S} + \dots\right], \qquad (1.134\text{a})$$

$$S_i^- = \sqrt{2S}b_i^\dagger\sqrt{1 - \frac{n_i}{2S}} = \sqrt{2S}\left[b_i^\dagger - \frac{b_i^\dagger n_i}{4S} + \dots\right], \qquad (1.134\text{b})$$

$$S_i^z = S - n_i, \qquad (1.134\text{c})$$

where $S_i^+ = S_i^x + iS_i^y$ and $S_i^- = S_i^x - iS_i^y$, and we abbreviate $n_i = b_i^\dagger b_i$. The new operators b_i and $b_i^\dagger$ annihilate or create a magnon at the lattice site specified by $\boldsymbol{R}_i$. Retaining terms up to fourth order in the boson operators we obtain

$$H_{\text{YIG}}(t) = H_0(t) + H_2(t) + H_3 + H_4 + \mathcal{O}\left(S^{-1/2}\right), \qquad (1.135)$$

where the boson-independent term and the term quadratic in the bosons are [31, 32, 43, 45]

$$H_0(t) = -\frac{S^2}{2}\sum_{ij}\left[J_{ij} + D_{ij}^{zz}\right] - NS\left[h_0 + h_1\cos(\omega_0 t)\right], \qquad (1.136\text{a})$$

$$H_2(t) = \sum_{ij}\left[A_{ij}b_i^\dagger b_j + \frac{B_{ij}}{2}\left(b_i b_j + b_i^\dagger b_j^\dagger\right)\right] + h_1\cos(\omega_0 t)\sum_i b_i^\dagger b_i, \qquad (1.136\text{b})$$

with coefficients given by

$$A_{ij} = \delta_{ij}h_0 + S\left(\delta_{ij}\sum_n J_{in} - J_{ij}\right) + S\left[\delta_{ij}\sum_n D_{in}^{zz} - \frac{D_{ij}^{xx} + D_{ij}^{yy}}{2}\right], \qquad (1.137\text{a})$$

$$B_{ij} = -\frac{S}{2}\left[D_{ij}^{xx} - 2iD_{ij}^{xy} - D_{ij}^{yy}\right]. \qquad (1.137\text{b})$$

The cubic contribution H_3 to the boson Hamiltonian is of order $\sqrt{S}$ and involves only the dipolar tensor,

$$H_3 = \sqrt{\frac{S}{2}}\sum_{ij}\left[\left(D_{ij}^{zy} + iD_{ij}^{zx}\right)\left(b_i^\dagger b_j^\dagger b_j + \frac{1}{4}b_i^\dagger b_i^\dagger b_i\right) + h.c.\right]. \qquad (1.138)$$

1. Basic methods

The quartic part H_4 can be written as

$$
\begin{aligned}
H_4 &= -\frac{1}{2} \sum_{ij} J_{ij} \left[n_i n_j - \frac{1}{2} \left(b_i^\dagger b_j^\dagger b_j b_j + h.c. \right) \right] \\
&\quad + \frac{1}{2} \sum_{ij} \left(D_{ij}^{xx} + D_{ij}^{yy} \right) \left[n_i n_j + \frac{1}{4} \left(b_i^\dagger b_j^\dagger b_j b_j + h.c. \right) \right] \\
&\quad + \frac{1}{4} \sum_{ij} \left[\left(D_{ij}^{xx} - 2i D_{ij}^{xy} - D_{ij}^{yy} \right) b_i^\dagger b_i b_i b_j + h.c. \right].
\end{aligned} \tag{1.139}
$$

In order to describe the mentioned experiments we consider a thin stripe geometry in which we have discrete translational invariance in the yz-plane and a finite extension in the x-direction, see Fig. 1.5. Therefore we perform a partial Fourier transformation in the infinite yz-plane, setting

$$
b_i = \frac{1}{\sqrt{N_y N_z}} \sum_{\boldsymbol{k}} e^{i \boldsymbol{k} \cdot \boldsymbol{R}_i} b_{\boldsymbol{k}} \left(x_i \right), \tag{1.140}
$$

where we have introduced the wave vector $\boldsymbol{k} = (k_y, k_z)$. For our purpose it is sufficient to restrict ourselves to the lowest magnon mode which is reproduced by the uniform mode approximation rather well, as shown in [31, 32, 33]. In the uniform mode approximation the magnon operators become

$$
b_{\boldsymbol{k}} \left(x_i \right) \approx \frac{1}{N_x} \sum_j b_{\boldsymbol{k}} \left(x_j \right) \equiv \frac{1}{\sqrt{N_x}} b_{\boldsymbol{k}}, \tag{1.141}
$$

while we obtain for the quadratic part $H_2(t)$ of our bosonized Hamiltonian

$$
\begin{aligned}
H_2 &= \sum_{\boldsymbol{k}} \left[A_{\boldsymbol{k}} b_{\boldsymbol{k}}^\dagger b_{\boldsymbol{k}} + \frac{B_{\boldsymbol{k}}}{2} \left(b_{\boldsymbol{k}}^\dagger b_{-\boldsymbol{k}}^\dagger + b_{-\boldsymbol{k}} b_{\boldsymbol{k}} \right) \right] \\
&\quad + h_1 \cos(\omega_0 t) \sum_{\boldsymbol{k}} b_{\boldsymbol{k}}^\dagger b_{\boldsymbol{k}},
\end{aligned} \tag{1.142}
$$

where the time independent coefficients are given by

$$
A_{\boldsymbol{k}} = \frac{1}{N_x} \sum_{x_{ij}} \sum_{y_{ij}, z_{ij}} e^{-i \boldsymbol{k} \cdot \boldsymbol{R}_{ij}} A_{ij}, \tag{1.143}
$$

$$
B_{\boldsymbol{k}} = \frac{1}{N_x} \sum_{x_{ij}} \sum_{y_{ij}, z_{ij}} e^{-i \boldsymbol{k} \cdot \boldsymbol{R}_{ij}} B_{ij}. \tag{1.144}
$$

Note that in order to get the correct factors of N from the beginning, we have changed the normalization of the Fourier transformation in Eqs. (1.143, 1.144)

compared to Eq. (1.140). The interaction parts can be written as

$$H_3 \;=\; \frac{1}{\sqrt{N}} \sum_{\boldsymbol{k}_1 \boldsymbol{k}_2 \boldsymbol{k}_3} \delta_{\boldsymbol{k}_1+\boldsymbol{k}_2+\boldsymbol{k}_3,0} \frac{1}{2!} \left[\Gamma^{\bar{b}bb}_{1;23} b^{\dagger}_{-1} b_2 b_3 + \Gamma^{\bar{b}\bar{b}b}_{12;3} b^{\dagger}_{-1} b^{\dagger}_{-2} b_3 \right],$$

(1.145a)

$$H_4 \;=\; \frac{1}{N} \sum_{\boldsymbol{k}_1 \ldots \boldsymbol{k}_4} \delta_{\boldsymbol{k}_1+\boldsymbol{k}_2+\boldsymbol{k}_3+\boldsymbol{k}_4,0} \left[\frac{1}{(2!)^2} \Gamma^{\bar{b}\bar{b}bb}_{12;34} b^{\dagger}_{-1} b^{\dagger}_{-2} b_3 b_4 \right.$$
$$\left. + \frac{1}{3!} \Gamma^{\bar{b}bbb}_{1;234} b^{\dagger}_{-1} b_2 b_3 b_4 + \frac{1}{3!} \Gamma^{\bar{b}\bar{b}\bar{b}b}_{123;4} b^{\dagger}_{-1} b^{\dagger}_{-2} b^{\dagger}_{-3} b_4 \right],$$

(1.145b)

where the properly symmetrized three-point vertices are given by

$$\Gamma^{\bar{b}bb}_{1;23} \;=\; \sqrt{\frac{S}{2}} \left[D^{zy}_{\boldsymbol{k}_2} - i D^{zx}_{\boldsymbol{k}_2} + (\boldsymbol{k}_2 \to \boldsymbol{k}_3) + \frac{1}{2} \left(D^{zy}_{\boldsymbol{0}} - i D^{zx}_{\boldsymbol{0}} \right) \right], \text{(1.146a)}$$

$$\Gamma^{\bar{b}\bar{b}b}_{12;3} \;=\; \left(\Gamma^{\bar{b}bb}_{3;21} \right)^*, \tag{1.146b}$$

and the symmetrized four-point vertices by

$$\Gamma^{\bar{b}\bar{b}bb}_{12;34} \;=\; -\frac{1}{2} \left[J_{\boldsymbol{k}_1+\boldsymbol{k}_3} + J_{\boldsymbol{k}_2+\boldsymbol{k}_3} + J_{\boldsymbol{k}_1+\boldsymbol{k}_4} + J_{\boldsymbol{k}_2+\boldsymbol{k}_4} \right.$$
$$+ D^{zz}_{\boldsymbol{k}_1+\boldsymbol{k}_3} + D^{zz}_{\boldsymbol{k}_2+\boldsymbol{k}_3} + D^{zz}_{\boldsymbol{k}_1+\boldsymbol{k}_4} + D^{zz}_{\boldsymbol{k}_2+\boldsymbol{k}_4}$$
$$\left. - \sum_{i=1}^{4} \left(J_{\boldsymbol{k}_i} - 2 D^{zz}_{\boldsymbol{k}_i} \right) \right], \tag{1.147a}$$

$$\Gamma^{\bar{b}bbb}_{1;234} \;=\; \frac{1}{4} \left[D^{xx}_{\boldsymbol{k}_2} - 2 i D^{xy}_{\boldsymbol{k}_2} - D^{yy}_{\boldsymbol{k}_2} + (\boldsymbol{k}_2 \to \boldsymbol{k}_3) + (\boldsymbol{k}_2 \to \boldsymbol{k}_4) \right], \text{(1.147b)}$$

$$\Gamma^{\bar{b}\bar{b}\bar{b}b}_{123;4} \;=\; \left(\Gamma^{\bar{b}bbb}_{4;123} \right)^*. \tag{1.147c}$$

For simplicity we set $a_1 \equiv a_{\boldsymbol{k}_1}$ and abbreviate the interaction vertices by $\Gamma^{\bar{a}aa}_{\boldsymbol{k}_1;\boldsymbol{k}_2\boldsymbol{k}_3} \equiv \Gamma^{\bar{a}aa}_{1;23}$ etc.. The Fourier transforms of the exchange and dipolar couplings are defined by

$$J_{\boldsymbol{k}} \;=\; \frac{1}{N_x} \sum_{x_{ij}} \sum_{y_{ij}, z_{ij}} e^{-i\boldsymbol{k}\cdot\boldsymbol{R}_{ij}} J_{ij}, \tag{1.148a}$$

$$D^{\alpha\beta}_{\boldsymbol{k}} \;=\; \frac{1}{N_x} \sum_{x_{ij}} \sum_{y_{ij}, z_{ij}} e^{-i\boldsymbol{k}\cdot\boldsymbol{R}_{ij}} D^{\alpha\beta}_{ij}. \tag{1.148b}$$

For nearest neighbor coupling on a cubic lattice with spacing a, the Fourier transform of the exchange coupling becomes [31, 32]

$$J_{\boldsymbol{k}} = J \left[4 - \cos\left(k_y a \right) - \cos\left(k_z a \right) \right]. \tag{1.149}$$

The Fourier transform of the dipolar tensor is more complicated. For a YIG film with thickness $d \gg a$ we take the thermodynamic limit in which the sum

$\sum_{x_{ij}}$ is replaced by $a^{-1} \int_{-d/2}^{d/2}$. To take the factor $(1 - \delta_{ij})$ into account properly, we have to exclude a sphere around $x_{ij} = y_{ij} = z_{ij} = 0$ with infinitesimal radius from the integration area, which yields[1] [31, 32]

$$D_{\boldsymbol{k}}^{xx} = \frac{4\pi\mu^2}{a^3} \left[\frac{1}{3} - f_{\boldsymbol{k}} \right], \tag{1.150a}$$

$$D_{\boldsymbol{k}}^{yy} = \frac{4\pi\mu^2}{a^3} \left[\frac{1}{3} + \sin^2(\Theta_{\boldsymbol{k}})(f_{\boldsymbol{k}} - 1) \right], \tag{1.150b}$$

$$D_{\boldsymbol{k}}^{zz} = \frac{4\pi\mu^2}{a^3} \left[\frac{1}{3} + \cos^2(\Theta_{\boldsymbol{k}})(f_{\boldsymbol{k}} - 1) \right], \tag{1.150c}$$

$$D_{\boldsymbol{k}}^{zy} = \frac{4\pi\mu^2}{a^3} \sin(\Theta_{\boldsymbol{k}}) \cos(\Theta_{\boldsymbol{k}}) [f_{\boldsymbol{k}} - 1], \tag{1.150d}$$

$$D_{\boldsymbol{k}}^{xy} = D_{\boldsymbol{k}}^{xz} = 0, \tag{1.150e}$$

where the form factor $f_{\boldsymbol{k}}$ is given by [31, 32, 49]

$$f_{\boldsymbol{k}} = \frac{1 - e^{-|\boldsymbol{k}|d}}{|\boldsymbol{k}| \, d}. \tag{1.151}$$

Here we have parametrized the in-plane wave vector by

$$\boldsymbol{k} = |\boldsymbol{k}| \left[\cos(\Theta_{\boldsymbol{k}}) \, \boldsymbol{e}_z + \sin(\Theta_{\boldsymbol{k}}) \, \boldsymbol{e}_y \right]. \tag{1.152}$$

Now we can also determine the coefficients of the quadratic part of the Hamiltonian (1.142), which turn out to be

$$\begin{aligned} A_{\boldsymbol{k}} &= h_0 + \frac{\rho_{\text{ex}}}{a^2} \left[4 - 2\cos(k_y a) - 2\cos(k_z a) \right] \\ &\quad + \frac{\Delta}{2} \left[\frac{1}{3} + \cos^2(\Theta_{\boldsymbol{k}})(f_{\boldsymbol{k}} - 1) \right] + \frac{\Delta}{3}, \end{aligned} \tag{1.153}$$

$$B_{\boldsymbol{k}} = \frac{\Delta}{2} \left[f_{\boldsymbol{k}} + \sin^2(\Theta_{\boldsymbol{k}})(f_{\boldsymbol{k}} - 1) \right], \tag{1.154}$$

where we have introduced $\Delta = 4\pi\mu M_S$. Note that for wave-vectors parallel to the magnetic field $\boldsymbol{k} = k\boldsymbol{e}_z$ the dipole tensor component $D_{\boldsymbol{k}}^{zy}$ is zero and all cubic vertices are vanishing identically which will be important for our considerations of the Bose-Einstein condensate wave function in chapter 2.

1.3.3. Bogoliubov transformation

In order to diagonalize the time-independent part of $H_2(t)$, we perform a Bogoliubov transformation [50]. The Bogoliubov transformation is a canonical transformation for Bose systems which plays an important role in the Bogoliubov theory for BEC in weakly interacting Bose gases, see for example Ref. [50].

---

[1]Francesca Sauli, private communication.

The transformation to new operators is given by

$$
\begin{pmatrix} b_{\boldsymbol{k}} \\ b_{-\boldsymbol{k}}^{\dagger} \end{pmatrix} = \begin{pmatrix} u_{\boldsymbol{k}} & -v_{\boldsymbol{k}} \\ -v_{\boldsymbol{k}}^{*} & u_{\boldsymbol{k}} \end{pmatrix} \begin{pmatrix} a_{\boldsymbol{k}} \\ a_{-\boldsymbol{k}}^{\dagger} \end{pmatrix}, \tag{1.155}
$$

where $u_{\boldsymbol{k}}$ and $v_{\boldsymbol{k}}$ are in general complex numbers. The requirement that the new operators fulfill

$$
\left[a_{\boldsymbol{k}}, a_{\boldsymbol{k}'}^{\dagger} \right] = \delta_{\boldsymbol{k},\boldsymbol{k}'}, \qquad [a_{\boldsymbol{k}}, a_{\boldsymbol{k}'}] = 0, \tag{1.156}
$$

implies the condition

$$
|u_{\boldsymbol{k}}|^2 - |v_{\boldsymbol{k}}|^2 = 1. \tag{1.157}
$$

The phase of the transformation coefficients are arbitrary and we choose them to be real. In order to obtain a diagonal quadratic Hamiltonian the coefficients have to fulfill

$$
\frac{B_{\boldsymbol{k}}}{2} \left(u_{\boldsymbol{k}}^2 + v_{\boldsymbol{k}}^2 \right) - A_{\boldsymbol{k}} u_{\boldsymbol{k}} v_{\boldsymbol{k}} = 0. \tag{1.158}
$$

Together with the normalization condition Eq. (1.157) we get the expressions

$$
u_{\boldsymbol{k}} = \sqrt{\frac{A_{\boldsymbol{k}} + \epsilon_{\boldsymbol{k}}}{2\epsilon_{\boldsymbol{k}}}}, \qquad v_{\boldsymbol{k}} = \frac{B_{\boldsymbol{k}}}{|B_{\boldsymbol{k}}|} \sqrt{\frac{A_{\boldsymbol{k}} - \epsilon_{\boldsymbol{k}}}{2\epsilon_{\boldsymbol{k}}}}, \tag{1.159}
$$

where

$$
\epsilon_{\boldsymbol{k}} = \sqrt{A_{\boldsymbol{k}}^2 - |B_{\boldsymbol{k}}|^2} \tag{1.160}
$$

is the energy dispersion of the magnons. It turns out that for a thin YIG film the minimum of the dispersion is at $\pm\boldsymbol{q} = (0, 0, \pm k_{\min})$ which is parallel to the magnetization, see Refs. [31, 32]. Considering small wave vectors $|\boldsymbol{k}| \ll \pi/a$ we can approximate

$$
JS \left[4 - 2\cos\left(k_y a \right) - 2\cos\left(k_z a \right) \right] \approx JSa^2 \boldsymbol{k}^2 = \rho_{\mathrm{ex}} \boldsymbol{k}^2, \tag{1.161}
$$

and the dispersion simplifies to [31, 32]

$$
\epsilon_{\boldsymbol{k}} = \sqrt{\left[h + \rho_{\mathrm{ex}} \boldsymbol{k}^2 + \Delta(1 - f_{\boldsymbol{k}}) \sin^2 \Theta_{\boldsymbol{k}} \right] \left[h + \rho_{\mathrm{ex}} \boldsymbol{k}^2 + \Delta f_{\boldsymbol{k}} \right]}, \tag{1.162}
$$

which is shown in Fig. 1.6. On energy scales relevant for the experiments [36, 37, 38, 39, 40] the dispersion Eq. (1.162) is a suitable approximation, see Refs. [31, 32].

After the Bogoliubov transformation the quadratic part of the Hamiltonian becomes [45, 51]

$$
\begin{aligned}
H_2(t) =\ & \sum_{\boldsymbol{k}} \left[\epsilon_{\boldsymbol{k}} a_{\boldsymbol{k}}^{\dagger} a_{\boldsymbol{k}} + \frac{\epsilon_{\boldsymbol{k}} - A_{\boldsymbol{k}}}{2} \right] + h_1 \cos(\omega_0 t) \sum_{\boldsymbol{k}} \left[\frac{A_{\boldsymbol{k}}}{\epsilon_{\boldsymbol{k}}} a_{\boldsymbol{k}}^{\dagger} a_{\boldsymbol{k}} + \frac{A_{\boldsymbol{k}} - \epsilon_{\boldsymbol{k}}}{2\epsilon_{\boldsymbol{k}}} \right] \\
& + \sum_{\boldsymbol{k}} \left[\gamma_{\boldsymbol{k}} \cos(\omega_0 t) a_{\boldsymbol{k}}^{\dagger} a_{-\boldsymbol{k}}^{\dagger} + \gamma_{\boldsymbol{k}}^{*} \cos(\omega_0 t) a_{-\boldsymbol{k}} a_{\boldsymbol{k}} \right],
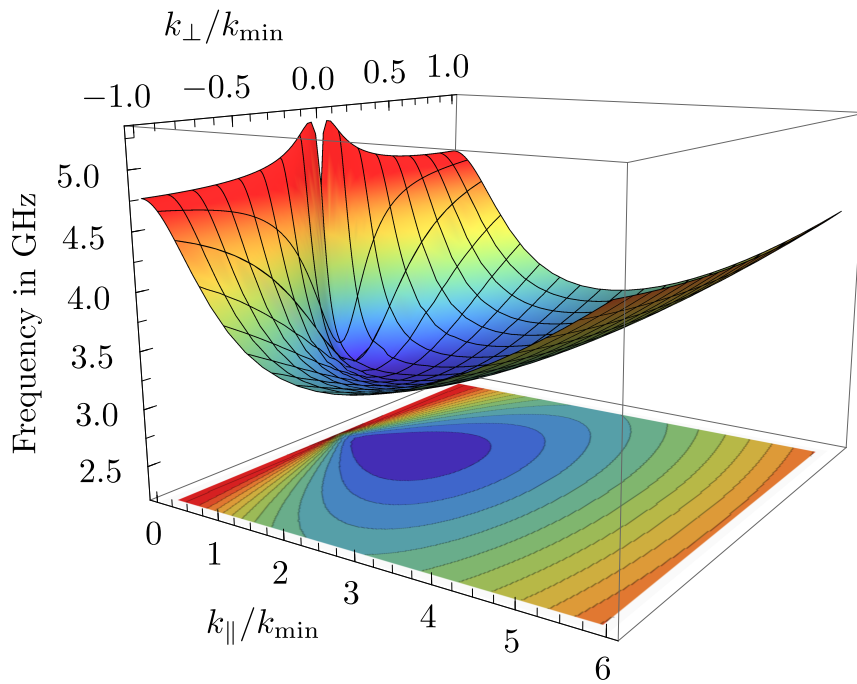\end{aligned} \tag{1.163}
$$

Figure 1.6.: Plot of the magnon dispersion Eq. (1.162) in YIG for parameters given in section 1.3.1. The static magnetic field is assumed to be $H_e = 1000$ Oe. The component $k_\perp$ is perpendicular to the static magnetic field and $k_\parallel$ parallel to it. The minimum is at $k_\perp = 0$ and $k_\parallel = \pm k_{\min}$.

where

$$\gamma_{\boldsymbol{k}} = -\frac{h_1 B_{\boldsymbol{k}}}{2\epsilon_{\boldsymbol{k}}}. \tag{1.164}$$

Applying the Bogoliubov transformation to H_3 Eq. (1.145a) yields for the cubic interactions,

$$\begin{aligned}
\Gamma^{aaa}_{123} &= -\Gamma^{\bar{b}bb}_{1;23}v_1 u_2 u_3 - \Gamma^{\bar{b}bb}_{2;13}v_2 u_1 u_3 - \Gamma^{\bar{b}bb}_{3;12}v_3 u_1 u_2 \\
&\quad + \Gamma^{\bar{b}\bar{b}b}_{12;3}v_1 v_2 u_3 + \Gamma^{\bar{b}\bar{b}b}_{23;1}v_2 v_3 u_1 + \Gamma^{\bar{b}\bar{b}b}_{13;2}v_1 v_3 u_2, &&\text{(1.165a)} \\
\Gamma^{\bar{a}aa}_{1;2,3} &= \Gamma^{\bar{b}bb}_{1;23}u_1 u_2 u_3 + \Gamma^{\bar{b}bb}_{2;13}v_1 v_2 u_3 + \Gamma^{\bar{b}bb}_{3;12}v_1 v_3 u_2 \\
&\quad - \Gamma^{\bar{b}\bar{b}b}_{32;1}v_3 v_2 v_1 - \Gamma^{\bar{b}\bar{b}b}_{12;3}v_2 u_1 u_3 - \Gamma^{\bar{b}\bar{b}b}_{13;2}v_3 u_1 u_2, &&\text{(1.165b)} \\
\Gamma^{\bar{a}\bar{a}a}_{12;3} &= \left(\Gamma^{\bar{a}aa}_{3;21}\right)^*, &&\text{(1.165c)} \\
\Gamma^{\bar{a}\bar{a}\bar{a}}_{123} &= \left(\Gamma^{aaa}_{123}\right)^*. &&\text{(1.165d)}
\end{aligned}$$

In the Bogoliubov basis the quartic vertices of H_4 Eq. (1.145b) are given by

$$\begin{aligned}
\Gamma^{aaaa}_{1234} &= \Gamma^{\bar{b}\bar{b}bb}_{12;34}u_1 u_2 v_3 v_4 + \Gamma^{\bar{b}\bar{b}bb}_{13;24}u_1 u_3 v_2 v_4 + \Gamma^{\bar{b}\bar{b}bb}_{14;23}u_1 u_4 v_2 v_3 \\
&\quad + \Gamma^{\bar{b}\bar{b}bb}_{23;14}u_2 u_3 v_1 v_4 + \Gamma^{\bar{b}\bar{b}bb}_{24;13}u_2 u_4 v_1 v_3 + \Gamma^{\bar{b}\bar{b}bb}_{34;12}u_3 u_4 v_1 v_2 \\
&\quad - \Gamma^{\bar{b}bbb}_{4;123}u_1 u_2 u_3 v_4 - \Gamma^{\bar{b}bbb}_{3;124}u_1 u_2 u_4 v_3 - \Gamma^{\bar{b}bbb}_{2;134}u_1 u_3 u_4 v_2 \\
&\quad - \Gamma^{\bar{b}bbb}_{1;234}u_2 u_3 u_4 v_1 - \Gamma^{\bar{b}\bar{b}\bar{b}b}_{234;1}u_1 v_2 v_3 v_4 - \Gamma^{\bar{b}\bar{b}\bar{b}b}_{134;2}u_2 v_1 v_3 v_4 \\
&\quad - \Gamma^{\bar{b}\bar{b}\bar{b}b}_{124;3}u_3 v_1 v_2 v_4 - \Gamma^{\bar{b}\bar{b}\bar{b}b}_{123;4}u_4 v_1 v_2 v_3, &&\text{(1.166a)} \\
\Gamma^{\bar{a}aaa}_{1;234} &= -\Gamma^{\bar{b}\bar{b}bb}_{21;34}u_2 v_1 v_3 v_4 - \Gamma^{\bar{b}\bar{b}bb}_{31;24}u_3 v_1 v_2 v_4 - \Gamma^{\bar{b}\bar{b}bb}_{41;23}u_4 v_1 v_2 v_3 \\
&\quad - \Gamma^{\bar{b}\bar{b}bb}_{34;12}u_3 u_4 u_1 v_2 - \Gamma^{\bar{b}\bar{b}bb}_{24;13}u_2 u_4 u_1 v_3 - \Gamma^{\bar{b}\bar{b}bb}_{23;14}u_2 u_3 u_1 v_4 \\
&\quad \Gamma^{\bar{b}bbb}_{1;234}u_1 u_2 u_3 u_4 + \Gamma^{\bar{b}bbb}_{4;321}u_3 u_2 v_1 v_4 + \Gamma^{\bar{b}bbb}_{3;421}u_4 u_2 v_1 v_3 \\
&\quad + \Gamma^{\bar{b}bbb}_{2;431}u_4 u_3 v_1 v_2 + \Gamma^{\bar{b}\bar{b}\bar{b}b}_{123;4}u_4 u_1 v_2 v_3 + \Gamma^{\bar{b}\bar{b}\bar{b}b}_{124;3}u_3 u_1 v_2 v_4 \\
&\quad + \Gamma^{\bar{b}\bar{b}\bar{b}b}_{134;2}u_2 u_1 v_3 v_4 + \Gamma^{\bar{b}\bar{b}\bar{b}b}_{432;1}v_4 v_2 v_3 v_1, &&\text{(1.166b)} \\
\Gamma^{\bar{a}\bar{a}aa}_{12;34} &= \Gamma^{\bar{b}\bar{b}bb}_{12;34}u_1 u_2 u_3 u_4 + \Gamma^{\bar{b}\bar{b}bb}_{13;42}u_1 u_4 v_3 v_2 + \Gamma^{\bar{b}\bar{b}bb}_{14;32}u_1 u_3 v_4 v_2 \\
&\quad + \Gamma^{\bar{b}\bar{b}bb}_{23;41}u_2 u_4 v_3 v_1 + \Gamma^{\bar{b}\bar{b}bb}_{24;31}u_2 u_3 v_4 v_1 + \Gamma^{\bar{b}\bar{b}bb}_{12;34}v_1 v_2 v_3 v_4 \\
&\quad - \Gamma^{\bar{b}bbb}_{4;321}u_3 v_2 v_1 v_4 - \Gamma^{\bar{b}bbb}_{3;421}u_4 v_2 v_1 v_3 - \Gamma^{\bar{b}bbb}_{2;341}u_2 u_3 u_4 v_1 \\
&\quad - \Gamma^{\bar{b}bbb}_{1;342}u_1 u_3 u_4 v_2 - \Gamma^{\bar{b}\bar{b}\bar{b}b}_{234;1}u_2 v_3 v_4 v_1 - \Gamma^{\bar{b}\bar{b}\bar{b}b}_{134;2}u_1 v_3 v_4 v_2 \\
&\quad - \Gamma^{\bar{b}\bar{b}\bar{b}b}_{124;3}u_1 u_2 v_3 v_4 - \Gamma^{\bar{b}\bar{b}\bar{b}b}_{123;4}u_1 u_2 u_4 v_3, &&\text{(1.166c)}
\end{aligned}$$

and

$$\begin{aligned}
\Gamma^{aaaa}_{1234} &= \Gamma^{\bar{a}\bar{a}\bar{a}\bar{a}}_{1234}, &&\text{(1.166d)} \\
\Gamma^{\bar{a}aaa}_{4;321} &= \left(\Gamma^{\bar{a}\bar{a}\bar{a}a}_{123;4}\right)^*. &&\text{(1.166e)}
\end{aligned}$$

Considering parametric resonance [49, 52, 53, 54, 55, 56, 57, 58, 59], usually the oscillating term proportional to $a^{\dagger}_{\boldsymbol{k}} a_{\boldsymbol{k}}$ is neglected and factors of the remaining oscillating terms are substituted by

$$\gamma_{\boldsymbol{k}} \cos(\omega_0 t) \rightarrow \frac{\gamma_{\boldsymbol{k}}}{2} e^{-i\omega_0 t}, \qquad \gamma_{\boldsymbol{k}}^* \cos(\omega_0 t) \rightarrow \frac{\gamma_{\boldsymbol{k}}^*}{2} e^{i\omega_0 t}, \qquad (1.167)$$

which yields

$$H_2(t) \approx \sum_{\boldsymbol{k}} \epsilon_{\boldsymbol{k}} a_{\boldsymbol{k}}^\dagger a_{\boldsymbol{k}} + \frac{1}{2} \sum_{\boldsymbol{k}} \left[\gamma_{\boldsymbol{k}} e^{-i\omega_0 t} a_{\boldsymbol{k}}^\dagger a_{-\boldsymbol{k}}^\dagger + \gamma_{\boldsymbol{k}}^* e^{i\omega_0 t} a_{-\boldsymbol{k}} a_{\boldsymbol{k}} \right], \qquad (1.168)$$

where we have dropped the constant terms. Let us mention that the approximation (1.167) is criticized in Refs. [45, 60] but here we assume that the main aspects of the YIG experiments are captured by it.

1.3.4. Rotating reference frame

The explicit time-dependence of the quadratic Hamiltonian (1.168) can be removed by a canonical transformation to the rotating reference frame [28]. The unitary time evolution operator is defined by

$$i\partial_t \mathcal{U}(t) = H(t) \mathcal{U}(t). \qquad (1.169)$$

For the transformation we make the ansatz

$$\mathcal{U}(t) = \mathcal{U}_0(t) \tilde{\mathcal{U}}(t), \qquad (1.170)$$

where

$$\mathcal{U}_0(t) = e^{-\frac{i}{2} \sum_{\boldsymbol{k}} \omega_0 t a_{\boldsymbol{k}}^\dagger a_{\boldsymbol{k}}}. \qquad (1.171)$$

The time evolution operator in the rotating reference frame satisfies

$$i\partial_t \tilde{\mathcal{U}}(t) = \tilde{H} \tilde{\mathcal{U}}(t), \qquad (1.172)$$

where the quadratic part of the transformed Hamiltonian $\tilde{H}_2$ does not depend on time [28]

$$\begin{aligned} \tilde{H}_2 &= \mathcal{U}_0^\dagger(t) \left[H_2(t) - i\partial_t \right] \mathcal{U}_0(t) \\ &= \sum_{\boldsymbol{k}} \left[\tilde{\epsilon}_{\boldsymbol{k}} a_{\boldsymbol{k}}^\dagger a_{\boldsymbol{k}} + \frac{\gamma_{\boldsymbol{k}}}{2} a_{\boldsymbol{k}}^\dagger a_{-\boldsymbol{k}}^\dagger + \frac{\gamma_{\boldsymbol{k}}^*}{2} a_{-\boldsymbol{k}} a_{\boldsymbol{k}} \right], \end{aligned} \qquad (1.173)$$

with the shifted energy dispersion $\tilde{\epsilon}_{\boldsymbol{k}} = \epsilon_{\boldsymbol{k}} - \omega_0/2$. Note that the second line can be derived for example by using the Baker-Campbell-Hausdorff lemma,

$$e^A B e^{-A} = A + [A, B] + \frac{1}{2!} [A, [A, B]] + \frac{1}{3!} [A, [A, [A, B]]] + \dots,$$

where A and B are arbitrary operators.

The Hamiltonian in the form of Eq. (1.173) will be the starting point for our calculations in chapter 2.

2. Bose-Einstein condensation in thin film ferromagnets

2.1. Introduction

In recent experiments of parametrically pumped magnons in thin films of the ferromagnetic yttrium-iron garnet (YIG) [36, 37, 38, 39, 40, 41] one can see an enhanced population of magnons in the ground state at room temperature. This phenomena has been interpreted as Bose-Einstein condensation (BEC) of magnons [61, 62], but as magnons are quasiparticles the term BEC should be interpreted differently than in the conventional sense. There is great evidence that the BEC of magnons is not accompanied by superfluidity [43, 63, 64] and that the BEC or in other words a finite expectation value of the magnon operator $\langle a_{\boldsymbol{k}} \rangle \neq 0$ is equivalent to a change in the magnetic order of the material, as argued in Refs. [63, 64, 65]. This phenomena occurring at room temperature is still very interesting. In this chapter we investigate the spatial structure of the magnon BEC.

Besides the fact that magnons are quasiparticles there is another important difference compared to a typical BEC of trapped atoms. For certain orientations of the external magnetic field the energy dispersion of magnons in a ferromagnetic thin film has two degenerate minima at finite wave vectors. This property is due to an interplay between the exchange interactions, dipole-dipole interactions and finite-size effects [31], and is crucial for the spatial structure of the condensate. A similar effect can be observed for magnon gases in quantum helimagnets in a magnetic field [66]. Already the fact that phase transitions, where the order parameter condenses on a surface in momentum space, form their own universality class [67, 68], the so-called Brazovskii universality class, suggests a different behavior for condensates at finite momenta than at zero momentum. In this chapter we use the time-independent Gross-Pitaevskii (GP) equation to investigate the spatial structure of BEC of bosons for a general class of systems. We explicitly perform calculations for the material YIG. The work presented in this chapter has been published in Ref. [43] and was done in collaboration with Francesca Sauli, Andreas Kreisel and Peter Kopietz.

2.2. Model

We consider a class of boson models on a lattice whose Hamiltonian has the form

$$H = H_2 + H_3 + H_4, \tag{2.1}$$

where H_3 and H_4 contain three- and four-point interactions respectively. The quadratic part H_2 of the Hamiltonian is given by

$$H_2 = \sum_{\boldsymbol{k}} \left[\epsilon_{\boldsymbol{k}} a_{\boldsymbol{k}}^\dagger a_{\boldsymbol{k}} + \frac{\gamma_{\boldsymbol{k}}}{2} a_{\boldsymbol{k}}^\dagger a_{-\boldsymbol{k}}^\dagger + \frac{\gamma_{\boldsymbol{k}}^*}{2} a_{-\boldsymbol{k}} a_{\boldsymbol{k}} \right], \tag{2.2}$$

where $a_{\boldsymbol{k}}$ and $a_{\boldsymbol{k}}^\dagger$ are the usual bosonic canonical annihilation and creation operators. For magnons in YIG we derived a Hamiltonian of this form in section 1.3, in particular see Eq. (1.173). As already mentioned in the introduction in the previous section the energy dispersion $\epsilon_{\boldsymbol{k}}$ is assumed to exhibit two degenerate minima at finite wave vectors $\pm\boldsymbol{q}$ which is essential for our considerations. The terms proportional to the complex parameter $\gamma_{\boldsymbol{k}}$ break the $U(1)$-symmetry such that the total particle number is not conserved. In YIG these terms correspond to an external pumping field. Without the requirement that the Hamiltonian has to be $U(1)$-symmetric, also the following interactions involving three powers of boson operators can contribute,

$$H_3 = \frac{1}{\sqrt{N}} \sum_{\boldsymbol{k}_1 \boldsymbol{k}_2 \boldsymbol{k}_3} \delta_{\boldsymbol{k}_1 + \boldsymbol{k}_2 + \boldsymbol{k}_3, 0} \left[\frac{1}{2} \Gamma_{1;23}^{\bar{a}aa} a_{-1}^\dagger a_2 a_3 + \frac{1}{2} \Gamma_{12;3}^{\bar{a}\bar{a}a} a_{-1}^\dagger a_{-2}^\dagger a_3 \right.$$
$$\left. + \frac{1}{3!} \Gamma_{123}^{aaa} a_1 a_2 a_3 + \frac{1}{3!} \Gamma_{123}^{\bar{a}\bar{a}\bar{a}} a_{-1}^\dagger a_{-2}^\dagger a_{-3}^\dagger \right], \tag{2.3}$$

where N is the total number of lattice sites. We showed in the introduction that in YIG interactions of this kind are present. As in section 1.3 we use the abbreviations $a_i \equiv a_{\boldsymbol{k}_i}$ for the magnon operators and $\Gamma_{\boldsymbol{k}_1;\boldsymbol{k}_2\boldsymbol{k}_3}^{\bar{a}aa} \equiv \Gamma_{1;23}^{\bar{a}aa}$ and so on for the vertices. Finally, the part of the Hamiltonian H_4 involving four powers of the boson operators without the restriction of $U(1)$-symmetry is given by

$$H_4 = \frac{1}{N} \sum_{\boldsymbol{k}_1 \dots \boldsymbol{k}_4} \delta_{\boldsymbol{k}_1 + \dots + \boldsymbol{k}_4, 0}$$
$$\times \left[\frac{1}{(2!)^2} \Gamma_{12;34}^{\bar{a}\bar{a}aa} a_{-1}^\dagger a_{-2}^\dagger a_3 a_4 + \frac{1}{3!} \Gamma_{1;234}^{\bar{a}aaa} a_{-1}^\dagger a_2 a_3 a_4 + \frac{1}{3!} \Gamma_{123;4}^{\bar{a}\bar{a}\bar{a}a} a_{-1}^\dagger a_{-2}^\dagger a_{-3}^\dagger a_4 \right.$$
$$\left. + \frac{1}{4!} \Gamma_{1234}^{aaaa} a_1 a_2 a_3 a_4 + \frac{1}{4!} \Gamma_{1234}^{\bar{a}\bar{a}\bar{a}\bar{a}} a_{-1}^\dagger a_{-2}^\dagger a_{-3}^\dagger a_{-4}^\dagger \right]. \tag{2.4}$$

The three- and four-point vertices are chosen to be partially symmetrized such that their value does not change if the momenta of the creation and annihilation operators in the argument are permuted seperately. In section 1.3 we showed how to obtain a boson Hamiltonian of the above form from an effective spin Hamiltonian describing the lowest magnon band of YIG in the so-called parallel pumping geometry [31, 46, 45].

2.3. Gross-Pitaevskii equation

The spatial dependence of the BEC is determined by the GP equation [69]. For the derivation of the GP equation for our model we use a functional integral approach for imaginary times in which the GP equation is obtained by the extremum condition of the Euclidean action. In order to obtain a compact notation for the interaction parts of the action, we introduce a two-component complex field $\Phi_{\boldsymbol{k}}^{\sigma}(\tau)$, where τ is the imaginary time and $\sigma = a, \bar{a}$ refers to the field corresponding to the annihilation or the creation operator,

$$a_{\boldsymbol{k}} \to \Phi_{\boldsymbol{k}}^{a}(\tau), \qquad a_{\boldsymbol{k}}^{\dagger} \to \Phi_{-\boldsymbol{k}}^{\bar{a}}(\tau). \tag{2.5}$$

The functional integral formulation can be obtained by dividing the imaginary time in small intervals and introducing complex fields for each time step through coherent states similar to the derivation of section 1.1.2, see Ref. [29]. For the quadratic part H_2 of the Hamiltonian we obtain the Gaussian action

$$
\begin{aligned}
S_2[\Phi] \;=\; & \frac{1}{2} \int_0^{\beta} d\tau \sum_{\boldsymbol{k}} \left(\Phi_{-\boldsymbol{k}}^{\bar{a}}, \Phi_{-\boldsymbol{k}}^{a} \right) \\
& \times \begin{pmatrix} \partial_\tau + \epsilon_{\boldsymbol{k}} - \mu & \gamma_{\boldsymbol{k}} \\ \gamma_{\boldsymbol{k}}^{*} & -\partial_\tau + \epsilon_{\boldsymbol{k}} - \mu \end{pmatrix} \begin{pmatrix} \Phi_{\boldsymbol{k}}^{a} \\ \Phi_{\boldsymbol{k}}^{\bar{a}} \end{pmatrix},
\end{aligned} \tag{2.6}
$$

where β is the inverse temperature and μ is the chemical potential. Introducing completely symmetrized vertices the action corresponding to the interaction parts H_3 and H_4 can be written as

$$
\begin{aligned}
S_3[\Phi] \;=\; & \int_0^{\beta} d\tau \frac{1}{\sqrt{N}} \sum_{\boldsymbol{k}_1 \boldsymbol{k}_2 \boldsymbol{k}_3} \sum_{\sigma_1 \sigma_2 \sigma_3} \delta_{\boldsymbol{k}_1 + \boldsymbol{k}_2 + \boldsymbol{k}_3, 0} \\
& \times \frac{1}{3!} \Gamma_3 \left(\boldsymbol{k}_1 \sigma_1, \boldsymbol{k}_2 \sigma_2, \boldsymbol{k}_3 \sigma_3 \right) \Phi_{\boldsymbol{k}_1}^{\sigma_1} \Phi_{\boldsymbol{k}_2}^{\sigma_2} \Phi_{\boldsymbol{k}_3}^{\sigma_3},
\end{aligned} \tag{2.7a}
$$

$$
\begin{aligned}
S_4[\Phi] \;=\; & \int_0^{\beta} d\tau \frac{1}{N} \sum_{\boldsymbol{k}_1 \ldots \boldsymbol{k}_4} \sum_{\sigma_1 \ldots \sigma_4} \delta_{\boldsymbol{k}_1 + \ldots + \boldsymbol{k}_4, 0} \\
& \times \frac{1}{4!} \Gamma_4 \left(\boldsymbol{k}_1 \sigma_1, \ldots, \boldsymbol{k}_4 \sigma_4 \right) \Phi_{\boldsymbol{k}_1}^{\sigma_1} \ldots \Phi_{\boldsymbol{k}_4}^{\sigma_4},
\end{aligned} \tag{2.7b}
$$

where the flavor indices $\sigma_i = a, \bar{a}$ refer to the two different field types as already explained above. The completely symmetrized vertices $\Gamma_3 \left(\boldsymbol{k}_1 \sigma_1, \boldsymbol{k}_2 \sigma_2, \boldsymbol{k}_3 \sigma_3 \right)$ and $\Gamma_4 \left(\boldsymbol{k}_1 \sigma_1, \ldots, \boldsymbol{k}_4 \sigma_4 \right)$ are invariant under the permutation of all momenta. With the chosen combinatorial factors [70], the completely symmetrized vertices can be directly identified with the partially symmetrized vertices used in the interaction parts of the Hamiltonian Eqs. (2.3, 2.4), for example

$$\Gamma_3 \left(\boldsymbol{k}_1 \bar{a}, \boldsymbol{k}_2 a, \boldsymbol{k}_3 a \right) = \Gamma_3 \left(\boldsymbol{k}_2 a, \boldsymbol{k}_1 \bar{a}, \boldsymbol{k}_3 a \right) = \ldots = \Gamma_{1;23}^{\bar{a}aa}. \tag{2.8}$$

As in the operator representation [50] we describe the BEC by assuming that at least one field has a finite expectation value $\phi_{\boldsymbol{k}}^{\sigma} = \langle \Phi_{\boldsymbol{k}}^{\sigma} \rangle$ which is of order $\sqrt{N}$.

Since in equilibrium the order parameter fields $\phi_{\boldsymbol{k}}^{\sigma}$ determine the ground state wave function they are independent of the imaginary time. In the GP equation any depletion of the condensate due to quantum or thermal fluctuations is neglected. In general also fluctuations can be taken into account by shifting the fields by the order parameter $\Phi_{\boldsymbol{k}}^{\sigma}(\tau) = \phi_{\boldsymbol{k}}^{\sigma} + \delta\Phi_{\boldsymbol{k}}^{\sigma}(\tau)$ and then expanding the action $S[\Phi] = S_2[\Phi] + S_3[\Phi] + S_4[\Phi]$ in powers of the fluctuations,

$$S\left[\phi + \delta\Phi\right] = S\left[\phi\right] + \int_0^{\beta} d\tau \sum_{\boldsymbol{k}\sigma} \left.\frac{\delta S\left[\Phi\right]}{\delta\Phi_{\boldsymbol{k}}^{\sigma}\left(\tau\right)}\right|_{\Phi=\phi} \delta\Phi_{\boldsymbol{k}}^{\sigma}\left(\tau\right) + \ldots. \qquad (2.9)$$

The GP equation is now given by the condition of vanishing linear terms,

$$
\begin{aligned}
0 \;=\; & \left.\frac{\delta S\left[\Phi\right]}{\delta\Phi_{\boldsymbol{k}}^{\sigma}\left(\tau\right)}\right|_{\Phi=\phi} = \left(\epsilon_{\boldsymbol{k}} - \mu\right)\phi_{-\boldsymbol{k}}^{\bar{\sigma}} + \gamma_{\boldsymbol{k}}^{\sigma}\phi_{-\boldsymbol{k}}^{\sigma} \\
& + \frac{1}{\sqrt{N}} \sum_{\boldsymbol{k}_1\boldsymbol{k}_2} \sum_{\sigma_1\sigma_2} \delta_{\boldsymbol{k}+\boldsymbol{k}_1+\boldsymbol{k}_2,0}\frac{1}{2}\Gamma_3\left(\boldsymbol{k}\sigma, \boldsymbol{k}_1\sigma_1, \boldsymbol{k}_2\sigma_2\right)\phi_{\boldsymbol{k}_1}^{\sigma_1}\phi_{\boldsymbol{k}_2}^{\sigma_2} \\
& + \frac{1}{N} \sum_{\boldsymbol{k}_1\boldsymbol{k}_2\boldsymbol{k}_3} \sum_{\sigma_1\sigma_2\sigma_3} \delta_{\boldsymbol{k}+\boldsymbol{k}_1+\boldsymbol{k}_2+\boldsymbol{k}_3,0} \\
& \times \frac{1}{3!}\Gamma_4\left(\boldsymbol{k}\sigma, \boldsymbol{k}_1\sigma_1, \boldsymbol{k}_2\sigma_2, \boldsymbol{k}_3\sigma_3\right)\phi_{\boldsymbol{k}_1}^{\sigma_1}\phi_{\boldsymbol{k}_2}^{\sigma_2}\phi_{\boldsymbol{k}_3}^{\sigma_3},
\end{aligned}
\qquad (2.10)
$$

where we have defined $\gamma_{\boldsymbol{k}}^a = \gamma_{\boldsymbol{k}}^*$ and $\gamma_{\boldsymbol{k}}^{\bar{a}} = \gamma_{\boldsymbol{k}}$. This equation amounts to the mean field approximation and has to be solved self-consistently. It is valid for dilute Bose gases at low temperatures such that depletion of the BEC can be neglected [69].

2.4. General BEC wave function

Solving the GP equation (2.10) for arbitrary fields is difficult and since in YIG experiments, occupation enhancements are observed only at the minima of the dispersion, we first assume a finite field expectation value only at the minima.

Let us start the discussion with a BEC at $\boldsymbol{k} = 0$,

$$\phi_{\boldsymbol{k}}^{\sigma} = \delta_{\boldsymbol{k},0}\sqrt{N}\psi_0^{\sigma}, \qquad (2.11)$$

which is realized in systems with a minimum at $\boldsymbol{k} = 0$. Considering only a single constant four-legged vertex $\Gamma_{00;00}^{\bar{a}\bar{a}aa} \equiv u_4$ and assuming for simplicity that $\gamma_0^{\sigma} = \gamma_0$ is real, we obtain from our general GP equation (2.10)

$$0 = r_0\psi_0^{\bar{\sigma}} + \gamma_0\psi_0^{\sigma} + \frac{1}{2}u_4\psi_0^{\bar{\sigma}}\psi_0^{\bar{\sigma}}\psi_0^{\sigma}, \qquad (2.12)$$

where

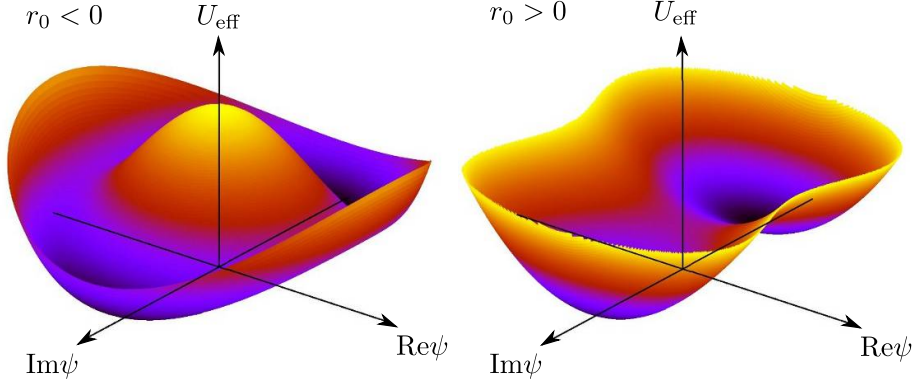$$r_0 = \epsilon_0 - \mu. \qquad (2.13)$$

Figure 2.1.: Effective Potential for a BEC at $\boldsymbol{k} = 0$ with a single four-legged interaction and with $U(1)$-symmetry breaking terms in the quadratic part, contributing to the GP equation (2.12). Both plots are for the case $\gamma_0 > r_0$ such that the potential has two degenerate minima on the imaginary axis, see Eq. (2.14). At the left the potential for $r_0 < 0$ is often referred to as the Napoleon's hat potential which has a local maximum at the origin, and at the right for $\psi = 0$ the potential has a saddle point.

Such a system is also discussed in Ref. [71].

There are two degenerate solutions for Eq. (2.12) for $\gamma_0 > r_0$,

$$\psi_0^\sigma = \pm i \sqrt{\frac{2(\gamma_0 - r_0)}{u_4}}, \tag{2.14}$$

otherwise there is only the solution $\psi_0^\sigma = 0$. Note that we obtain non-trivial solutions even for positive r_0 which is impossible for vanishing γ_0. The situation becomes clearer when plotting the effective potential

$$U_{\text{eff}}[\psi_0^{\bar{a}}, \psi_0^a] = N^{-1} S\left[\Phi_{\boldsymbol{k}}^\sigma \to \sqrt{N}\delta_{\boldsymbol{k},0}\psi_0^\sigma\right] \tag{2.15}$$

for the two cases $r_0 < 0$ and $r_0 > 0$, see Fig. 2.1.

Next we consider the more interesting problem of a system exhibiting two minima in the dispersion at finite wave-vector $\pm\boldsymbol{q}$. Naively we choose an ansatz similar to before,

$$\phi_{\boldsymbol{k}}^\sigma = \sqrt{N}\left[\delta_{\boldsymbol{k},\boldsymbol{q}}\psi_1^\sigma + \delta_{\boldsymbol{k},-\boldsymbol{q}}\psi_{-1}^\sigma\right], \tag{2.16}$$

but we will see that this is not a solution of the GP equation (2.10). Note that from $\psi_{\boldsymbol{k}}^a = \langle a_{\boldsymbol{k}}\rangle / \sqrt{N}$ and $\psi_{-\boldsymbol{k}}^{\bar{a}} = \left\langle a_{\boldsymbol{k}}^\dagger\right\rangle$ it can be seen that $\psi_1^\sigma = \left(\psi_{-1}^{\bar{\sigma}}\right)^*$. In real space such an ansatz of the condensate wave function becomes

$$\phi^\sigma(\boldsymbol{r}) = \frac{1}{\sqrt{N}}\sum_{\boldsymbol{k}} e^{i\boldsymbol{k}\cdot\boldsymbol{r}}\phi_{\boldsymbol{k}}^\sigma = e^{i\boldsymbol{q}\cdot\boldsymbol{r}}\psi_1^\sigma + e^{-i\boldsymbol{q}\cdot\boldsymbol{r}}\psi_{-1}^\sigma, \tag{2.17}$$

and if $\psi_1^\sigma = \psi_{-1}^\sigma = \psi$ the condensate density would be

$$\rho_1\left(\boldsymbol{r}\right) = \left|\phi^a\left(\boldsymbol{r}\right)\right|^2 = 4\left|\psi\right|^2\cos^2\left(\boldsymbol{q}\cdot\boldsymbol{r}\right), \tag{2.18}$$

and hence there is no localization in real space. In order to see that the ansatz Eq. (2.16) is not a solution of the GP equation we explicitly look at Eq. (2.10). For example taking the derivative with respect to $\Phi_{3\boldsymbol{q}}^a$ and inserting the ansatz yields

$$0 = \frac{1}{N}\sum_{\sigma_1\sigma_2\sigma_3}\frac{1}{3!}\Gamma_4\left(3\boldsymbol{q}a, -\boldsymbol{q}\sigma_1, -\boldsymbol{q}\sigma_2, -\boldsymbol{q}\sigma_3\right)\psi_{-1}^{\sigma_1}\psi_{-1}^{\sigma_2}\psi_{-1}^{\sigma_3}. \tag{2.19}$$

In general only by setting $\psi_{-1}^\sigma = 0$ the right hand side becomes zero which is inconsistent with our assumption that $\psi_{-1}^\sigma \neq 0$ and hence we conclude that the ansatz Eq. (2.16) is not a solution of th GP equation (2.10). Note that also the three-legged vertices are causing inconsistencies which can be seen considering for example $\boldsymbol{k} = 2\boldsymbol{q}$. We thus have to modify our ansatz to obtain a solution. From Eq. (2.19) it seems to be reasonable to assume that also higher Fourier components are finite. But considering for example $\phi_{\pm 2\boldsymbol{q}}^\sigma \neq 0$ or $\phi_{\pm 3\boldsymbol{q}}^\sigma \neq 0$ is not sufficient because then the equations for even higher Fourier modes become inconsistent. The only way we can realize that $\psi_{\pm 1}^\sigma \neq 0$ is by assuming that the components at all integer multiples of $\boldsymbol{q}$ are finite. In this case the ansatz becomes

$$\phi_{\boldsymbol{k}}^\sigma = \sqrt{N}\sum_{n=-\infty}^{\infty}\delta_{\boldsymbol{k},\boldsymbol{q}_n}\psi_n^\sigma, \tag{2.20}$$

where we define $\boldsymbol{q}_n = n\boldsymbol{q}$. Inserting this ansatz into the GP equation (2.10), setting the external wave-vector to $-\boldsymbol{q}_n$ and assuming again that $\gamma_{\boldsymbol{k}}$ is real, we obtain the discrete Gross-Pitaevskii equation,

$$
\begin{aligned}
-r_n\psi_n^{\bar\sigma} - \gamma_n\psi_n^\sigma \;=\; & \frac{1}{2}\sum_{n_1 n_2}\sum_{\sigma_1\sigma_2}\delta_{n,n_1+n_2}V_{nn_1n_2}^{\sigma\sigma_1\sigma_2}\,\psi_{n_1}^{\sigma_1}\psi_{n_2}^{\sigma_2} \\
& + \frac{1}{3!}\sum_{n_1 n_2 n_3}\sum_{\sigma_1\sigma_2\sigma_3}\delta_{n,n_1+n_2+n_3}U_{nn_1n_2n_3}^{\sigma\sigma_1\sigma_2\sigma_3}\,\psi_{n_1}^{\sigma_1}\psi_{n_2}^{\sigma_2}\psi_{n_3}^{\sigma_3},
\end{aligned}\tag{2.21}
$$

where we have introduced the abbreviations $r_n = \epsilon_{-\boldsymbol{q}_n} - \mu$, $\gamma_n = \gamma_{-\boldsymbol{q}_n}$ and for the vertices

$$
\begin{aligned}
V_{nn_1n_2}^{\sigma\sigma_1\sigma_2} \;&=\; \Gamma_3\left(\boldsymbol{q}_n\sigma, \boldsymbol{q}_{n_1}\sigma_1, \boldsymbol{q}_{n_2}\sigma_2\right), \tag{2.22a}\\
U_{nn_1n_2n_3}^{\sigma\sigma_1\sigma_2\sigma_3} \;&=\; \Gamma_4\left(\boldsymbol{q}_n\sigma, \boldsymbol{q}_{n_1}\sigma_1, \boldsymbol{q}_{n_2}\sigma_2, \boldsymbol{q}_{n_3}\sigma_3\right). \tag{2.22b}
\end{aligned}
$$

2.5. BEC wave function for YIG

In section 1.3 we gave explicit expressions for the dispersion and the interactions for magnons in a thin stripe of YIG. Here we want to use these results

γ_1/r_1	$|\psi_1|$	$|\psi_3/\psi_1|$	$|\psi_5/\psi_1|$	$|\psi_7/\psi_1|$	$|\psi_9/\psi_1|$
1.1	0.530	0.019	0.002	$\approx 10^4$	$\approx 10^5$
1.2	0.757	0.033	0.005	0.001	$\approx 10^4$
1.5	1.209	0.055	0.013	0.003	0.001
3.0	2.439	0.085	0.031	0.012	0.005

Table 2.1.: Numerical solution for $|\psi_1| \equiv |\psi_1^\sigma|$ and $|\psi_n|\,/\,|\psi_1|$ of the discrete GP equation (2.21) for different values of the dimensionless pumping parameter γ_1/r_1 for $r_1 > 0$. Note that for $r_1 > 0$ there is no condensate if $\gamma_1/r_1 < 1$. Dispersion and vertices are taken from the spin-wave calculation for YIG in section 1.3. Results for negative momenta are identical due to symmetry.

to calculate the magnon-BEC wave function. The minima of the dispersion are at $\pm\boldsymbol{q} = \pm k_{\min}\boldsymbol{e}_z$ [31, 32] and as mentioned the three-legged vertices are vanishing identically for wave vectors parallel to the magnetic field $\boldsymbol{k} = k\boldsymbol{e}_z$. Therefore due to the momentum conservation in Eq. (2.21) only Fourier modes $\psi_{\pm n}^\sigma$ where n is an odd multiple of the lowest finite Fourier component corresponding to n_1 couple to each other. Note that when using Eq. (1.173) for the quadratic part of the Hamiltonian, we neglect the time dependence of the $U(1)$-symmetry breaking vertices.

Since in the experiments [36, 37, 38, 39, 40] an enhancement of the density at $\boldsymbol{k} = \pm\boldsymbol{q}$ is observed, we are setting $n_1 = 1$ and consider a BEC wave function of the form

$$\phi_{\boldsymbol{k}}^\sigma = \sqrt{N} \sum_{n \text{ odd}} \delta_{\boldsymbol{k},\boldsymbol{q}n}\psi_n^\sigma. \tag{2.23}$$

The Fourier components ψ_n^σ can be determined by setting $n = \pm 1, \pm 3, \pm 5 \dots$ in the discrete GP equation (2.21). We calculated the Fourier components numerically for vanishing three-legged vertices $V_{nn_1n_2}^{\sigma\sigma_1\sigma_2} = 0$ and Eqs. (1.166a-1.166e) for the four-legged vertices $U_{nn_1n_2n_3}^{\sigma\sigma_1\sigma_2\sigma_3}$. Expecting that the lowest components are dominant the system of equations was truncated at a finite order such that $|n| \leq m$. The results were converging fast and in our calculation we chose $m = 9$. We found non-trivial solutions for $\gamma_1 > r_1 = \epsilon_{\boldsymbol{q}} - \mu$ if r_1 is positive and for arbitrary γ_1 if r_1 is negative. Results for certain sets of the parameter γ_1/r_1 which represent the typical behavior of the solutions are shown in Table 2.1 and are illustrated in Fig. 2.2. As it can be seen although higher modes are finite the Fourier components $\psi_{\pm 1}^\sigma$ are dominant and Eq. (2.18) is a good approximation for the condensate density, see Fig. 2.3. For increasing pumping power the contribution of the other Fourier components becomes stronger but for all considered values the fundamental modes were still dominant. Even for $\gamma_1/r_1 = 3.0$ the next component is only around $\sim 9\%$ of the lowest one, see Tab. 2.1 and Fig. 2.2. But in principle it should be possible to have vertices such that the first few Fourier components are of the same order of magnitude which would result in a strong localization on a lattice with spacing $2\pi/q$ and
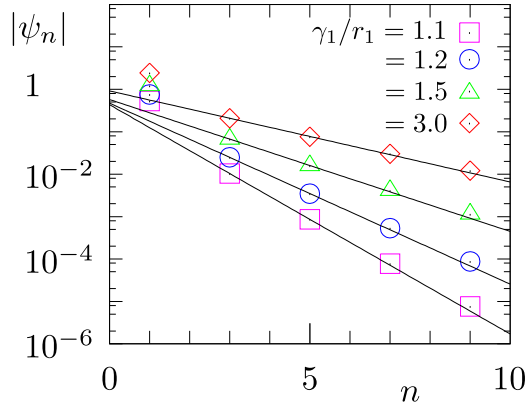
Figure 2.2.: Absolute values $|\psi_n| = |\psi_n^\sigma|$ of the Fourier components of the order parameter for BEC in YIG for different values of the dimensionless ratio $\gamma_1/r_1 = \gamma_{\boldsymbol{q}}/(\epsilon_{\boldsymbol{q}} - \mu)$ obtained from the numerical solution of the discrete GP equation (2.21) and using the parameters from spin-wave calculation shown in section 1.3. Note that the Fourier components ψ_1^σ are dominant and that the higher order Fourier components ψ_n^σ decay approximately exponentially as a function of n.

π/q for vanishing cubic vertices. In the case of YIG this is about 100 times greater than the underlying Bravais lattice, see Fig. 2.3. Then it would be justified to call the BEC a condensation phenomena in real space.

At the end let us mention that the description of the BEC by the GP equation (2.10) resembles the phenomenological Ginzburg-Landau theory of density fluctuations for the phase transition from a liquid to a crystalline solid. However the liquid-solid transition in three dimensions is more complicated since the quadratic part of the Ginzburg-Landau functional exhibits a minimum on a surface in momentum space, and three-legged vertices are also important for the crystal structure, see for example Refs. [72, 73, 74].

2.6. Summary and conclusions

We have presented a calculation for the wave function of a BEC of Bose gases whose dispersion exhibits two degenerate minima at $\pm\boldsymbol{q}$. The discussion was based on the GP equation which we derived using a functional approach. We found that for generic interactions Fourier components of the wave function at all integer multiples of the wave vector of the fundamental mode have to be macroscopically occupied in order to solve the GP equation. Due to vanishing cubic interactions only odd multiples modes are finite in YIG. In our numerical calculations using realistic vertices for YIG we found that higher Fourier modes decrease roughly exponentially and therefore retaining only the lowest
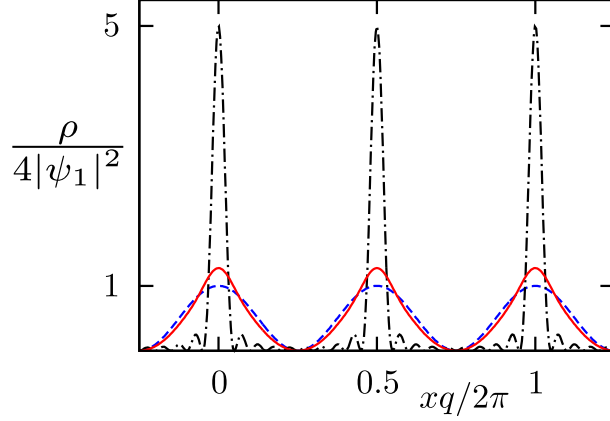
Figure 2.3.: Condensate densities for different wave functions are ploted. The first five odd Fourier components $\psi^\sigma_{\pm q_1}, \psi^\sigma_{\pm q_3}, \psi^\sigma_{\pm q_5}, \psi^\sigma_{\pm q_7}, \psi^\sigma_{\pm q_9}$ are assumed to be finite and equal for the dash-doted line. The solid line is for the results taken from the numerical calculations of YIG for γ_1/r_1, see Table 2.1. Finally for the dashed line we used Eq. (2.18) for which only the modes at $\pm q_1$ contribute. As it can be seen the wave function consisting of the lowest Fourier modes only is a good approximation for the condensate in YIG. If the first five components would be of the same order of magnitude, it would be already enough to obtain a strong localizaiotn of the wave function in real space with spacing π/q.

components of the condensate wave function is a good approximation. In previous descriptions of magnon BEC in YIG the occupation of higher Fourier modes for the condensate wave-function was not considered, see for example Refs. [46, 75]. In principle our predictions should be observable in experiments, but this seems to be a challenging task, as the relevant wave vectors for measuring these effects are not accessible in experiments so far and the small contribution of higher modes might be difficult to detect.

For certain interactions it should be possible to obtain the same order of magnitude for higher components compared to the fundamental ones. In such a case the condensate is localized in real space and there is a formal analogy to the Ginzburg-Landau theory for the liquid-solid phase transition.

3. Functional renormalization group approach to the thermalization of magnons in yttrium–iron garnet

3.1. Introduction

As in the previous chapter the considerations of this chapter are motivated by recent magnon experiments in yttrium-iron garnet (YIG) [36, 37, 38, 39, 40, 41, 76, 77]. In these experiments YIG stripes are brought to parametric resonance by applying an external microwave field in the parallel pumping geometry [31, 32, 45, 46], see Fig. 1.5. Using this phenomena magnons of certain energy and wave vectors are injected such that after turning off the pumping field the excited magnons scatter to the bottom of the dispersion and an enhanced occupation of the ground state at finite momenta $\pm\boldsymbol{q}$ is observed. In order to describe the whole process we need a formalism which is applicable to nonequilibrium conditions. Combining the Boltzmann equation with the Gross-Pitaevskii equation the dynamics of a weakly interacting Bose gas in the Bose-Einstein condensate (BEC) phase have already been successfully modeled, see for example Refs. [2, 78]. The collision integral of the Boltzmann equation is usually obtained from perturbation theory up to second order in the bare vertices. But this approximation breaks down for strong interactions or high densities and a non-perturbative approach is desirable. Berges and co-authors [79, 80, 81] showed for N-component relativistic scalar field theories that going beyond perturbation theory by means of a two-particle irreducible resummed large-N expansion qualitatively changes the scaling behavior of the momentum distribution for small momenta.

Here we go beyond perturbation theory using functional renormalization group (FRG) methods. We develop a formalism for Bose gases which in principle is not restricted to weak interactions or small densities. For the derivation we consider a model consisting of free bosons coupled to a thermal bath of phonons. For numerical calculations we will consider magnons in YIG and to avoid confusion with the phonons which are also bosons, we call the bosons magnons right from the beginning. A model similar to ours has been also considered by Bányai et $al.$ [82] for describing the kinetics of BEC of excitons. They derived a rate equation by decoupling the Heisenberg equation of mo-

tion, but in order to improve approximations systematically this approach is not suitable and we have to use another approach.

A possible generalization of our formalism including two-particle interactions is straightforward. Actually for describing BEC one needs these two-particle interactions to obtain a stable BEC. This can be seen for example by looking at the Gross-Pitaevskii equation where the non-linear terms are crucial to obtain a stable condensed ground state. These non-linear terms arise from magnon-magnon interactions which are beyond the scope of this thesis. For the thermalization of the magnons both kinds of interactions, two-particle and magnon-phonon, contribute, but for simplicity we focus on regimes where we can retain the coupling to the phonon bath only. In order to apply the FRG in section 3.4 we first re-derive the rate equation of [82] in section 3.3 using a functional version of the Keldysh formalism which can be applied to nonequilibrium conditions, see section 1.1 or Ref. [2] for example. At the end we calculate the nonequilibrium dynamics of magnons in YIG using our formalism and compare it to the experimental results of Ref. [76]. The work was done in collaboration with Thomas Kloss and Peter Kopietz and was published in [83].

3.2. Model

As mentioned in the introduction we consider a model of free bosons which are coupled to a phonon bath,

$$
\mathcal{H} = \sum_{\boldsymbol{k}} \epsilon_{\boldsymbol{k}} a_{\boldsymbol{k}}^{\dagger} a_{\boldsymbol{k}} + \sum_{\boldsymbol{q}} \omega_{\boldsymbol{q}} b_{\boldsymbol{q}}^{\dagger} b_{\boldsymbol{q}} + \frac{1}{\sqrt{V}} \sum_{\boldsymbol{k},\boldsymbol{q}} \gamma_{\boldsymbol{q}} a_{\boldsymbol{k}}^{\dagger} a_{\boldsymbol{k}-\boldsymbol{q}} \left(b_{\boldsymbol{q}} + b_{-\boldsymbol{q}}^{\dagger} \right), \qquad (3.1)
$$

where a magnon with momentum $\boldsymbol{k}$ is annihilated by $a_{\boldsymbol{k}}$ and created by $a_{\boldsymbol{k}}^{\dagger}$, and analogously a phonon with momentum $\boldsymbol{q}$ by $b_{\boldsymbol{q}}$ and $b_{\boldsymbol{q}}^{\dagger}$. The dispersion of the magnons is given by $\epsilon_{\boldsymbol{k}}$ and of the phonons by $\omega_{\boldsymbol{q}} = c \left| \boldsymbol{q} \right|$, where we assume longitudinal acoustic phonons with sound velocity c. The volume of the system is denoted by V. Based on similar arguments as in the case of electrons in a metal, the phonon operators can be traced back to the divergence of the displacement field when deriving the magnon-phonon interaction. Hence it is reasonable to consider an interaction which is proportional to $\sqrt{\omega_{\boldsymbol{q}}}$. In chapter 4 we will derive these interactions from a microscopic spin model.

3.3. Rate equation from functional Keldysh formalism

3.3.1. Keldysh action

In section 1.1 we showed how to derive the Keldysh action for a Hamiltonian like Eq. (3.1). In our case we obtain

$$
\begin{aligned}
S[\bar{a}, a, \bar{b}, b] = \int dt \int dt' \Bigg\{ \\
\sum_{\boldsymbol{k}} \left(\bar{a}^C_{\boldsymbol{k}}(t), \bar{a}^Q_{\boldsymbol{k}}(t) \right) \begin{pmatrix} 0 & (\hat{G}^A_0)^{-1} \\ (\hat{G}^R_0)^{-1} & 2i\eta \hat{g}_0 \end{pmatrix}_{tt'} \begin{pmatrix} a^C_{\boldsymbol{k}}(t') \\ a^Q_{\boldsymbol{k}}(t') \end{pmatrix} \\
+ \sum_{\boldsymbol{q}} \left(\bar{b}^C_{\boldsymbol{q}}(t), \bar{b}^Q_{\boldsymbol{q}}(t) \right) \begin{pmatrix} 0 & (\hat{F}^A_0)^{-1} \\ (\hat{F}^R_0)^{-1} & 2i\eta \hat{f}_0 \end{pmatrix}_{tt'} \begin{pmatrix} b^C_{\boldsymbol{q}}(t') \\ b^Q_{\boldsymbol{q}}(t') \end{pmatrix} \Bigg\} \\
- \int dt \frac{1}{\sqrt{V}} \sum_{\boldsymbol{k},\boldsymbol{q}} \gamma_{\boldsymbol{q}} \left[\left(\bar{a}^C_{\boldsymbol{k}+\boldsymbol{q}} a^Q_{\boldsymbol{k}} + \bar{a}^Q_{\boldsymbol{k}+\boldsymbol{q}} a^C_{\boldsymbol{k}} \right) X^C_{\boldsymbol{q}} \right. \\
\left. + \left(\bar{a}^C_{\boldsymbol{k}+\boldsymbol{q}} a^C_{\boldsymbol{k}} + \bar{a}^Q_{\boldsymbol{k}+\boldsymbol{q}} a^Q_{\boldsymbol{k}} \right) X^Q_{\boldsymbol{q}} \right],
\end{aligned} \tag{3.2}
$$

where the hat denotes a continuous time matrix as introduced in Eqs. (1.40, 1.41) and we have omitted the time argument of the fields for the interaction part since it is the same for all of them. The inverse non-interacting Green's functions for magnons are given by

$$
\left[\left(\hat{G}^R_0 \right)^{-1} \right]_{\boldsymbol{k},tt'} = i\delta'(t - t') - \epsilon_{\boldsymbol{k}}\delta(t - t') + i\eta\delta(t - t'), \tag{3.3a}
$$

$$
\left[\left(\hat{G}^A_0 \right)^{-1} \right]_{\boldsymbol{k},tt'} = i\delta'(t - t') - \epsilon_{\boldsymbol{k}}\delta(t - t') - i\eta\delta(t - t'), \tag{3.3b}
$$

and for phonons by

$$
\left[\left(\hat{F}^R_0 \right)^{-1} \right]_{\boldsymbol{q},tt'} = i\delta'(t - t') - \omega_{\boldsymbol{q}}\delta(t - t') + i\eta\delta(t - t'), \tag{3.4a}
$$

$$
\left[\left(\hat{F}^A_0 \right)^{-1} \right]_{\boldsymbol{q},tt'} = i\delta'(t - t') - \omega_{\boldsymbol{q}}\delta(t - t') - i\eta\delta(t - t'), \tag{3.4b}
$$

where η is a infinitesimal quantity which is required for a consistent continuous notation, see section 1.1.4. Graphical representations of the bare vertices of the action Eq. (3.2) are shown in Fig 3.1. The fields $\bar{a}^{C/Q}_{\boldsymbol{k}}(t)$ and $\bar{b}^{C/Q}_{\boldsymbol{q}}(t)$ correspond in the operator representation to the boson operator $a^\dagger_{\boldsymbol{k}}$ and the phonon operator $b^\dagger_{\boldsymbol{q}}$ and the upper labels C/Q keep track of the time contour
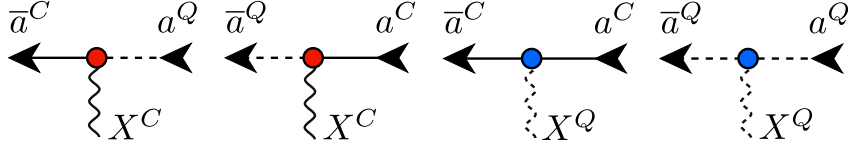
Figure 3.1.: The four different magnon-phonon interactions contained in the action Eq. (3.2). Arrows represent magnon and wavy lines phonon fields. Depending on the direction of the arrow it refers to the complex conjugated magnon field or the field itself. The quantum and the classical components of the fields are denoted by dashed or solid lines. For example a solid straight line pointing into the vertex represents the field a^C and a wavy dashed line X^Q.

branches in the Keldysh basis as introduced in Eqs. (1.37a, 1.37b),

$$a_{\boldsymbol{k}}^C(t) \;=\; \frac{1}{\sqrt{2}}\left[a_{\boldsymbol{k}}^+(t) + a_{\boldsymbol{k}}^-(t)\right], \tag{3.5a}$$

$$a_{\boldsymbol{k}}^Q(t) \;=\; \frac{1}{\sqrt{2}}\left[a_{\boldsymbol{k}}^+(t) - a_{\boldsymbol{k}}^-(t)\right], \tag{3.5b}$$

$$b_{\boldsymbol{k}}^C(t) \;=\; \frac{1}{\sqrt{2}}\left[b_{\boldsymbol{k}}^+(t) + b_{\boldsymbol{k}}^-(t)\right], \tag{3.5c}$$

$$b_{\boldsymbol{k}}^Q(t) \;=\; \frac{1}{\sqrt{2}}\left[b_{\boldsymbol{k}}^+(t) - b_{\boldsymbol{k}}^-(t)\right], \tag{3.5d}$$

where the superscripts $\pm$ refer to the upper and lower contour branch, see Fig. 1.1. The lower diagonal components of the inverse propagators are the regularizations due to the continuous notation, see section 1.1.4,

$$-\left(\hat{G}_0^R\right)^{-1}\hat{G}_0^K\left(\hat{G}_0^A\right)^{-1} \;=\; 2i\eta\hat{g}_0, \tag{3.6a}$$

$$-\left(\hat{F}_0^R\right)^{-1}\hat{F}_0^K\left(\hat{F}_0^A\right)^{-1} \;=\; 2i\eta\hat{f}_0, \tag{3.6b}$$

where η is an infinitesimal quantity and $\hat{g}_0$, $\hat{f}_0$ are diagonal time matrices which contain the initial distributions of the magnons and phonons,

$$[\hat{g}_0]_{\boldsymbol{k},tt'} \;=\; \delta(t-t')g_{0,\boldsymbol{k}} = \delta(t-t')\left[1 + 2\left\langle a_{\boldsymbol{k}}^\dagger(t_0)\,a_{\boldsymbol{k}}(t_0)\right\rangle\right], \tag{3.7a}$$

$$\left[\hat{f}_0\right]_{\boldsymbol{q},tt'} \;=\; \delta(t-t')f_{0,\boldsymbol{q}} = \delta(t-t')\left[1 + 2\left\langle b_{\boldsymbol{q}}^\dagger(t_0)\,b_{\boldsymbol{q}}(t_0)\right\rangle\right], \tag{3.7b}$$

where t_0 denotes the initial time. Since the magnons couple only to a hermitian combination of phonon operators, it is convenient to introduce real phonon fields for the components $\lambda = C, Q$ by

$$X_{\boldsymbol{q}}^\lambda(t) = \frac{1}{\sqrt{2}}\left[b_{\boldsymbol{q}}^\lambda(t) + \bar{b}_{-\boldsymbol{q}}^\lambda(t)\right], \tag{3.8}$$

corresponding to the hermitian phonon operator

$$X_{\boldsymbol{q}} = \frac{1}{\sqrt{2}} \left(b_{\boldsymbol{q}} + b_{-\boldsymbol{q}}^{\dagger} \right). \tag{3.9}$$

In the operator representation the magnon Green's functions are defined by

$$iG_{\boldsymbol{k}}^{R}(t,t') = \Theta(t-t') \left\langle \left[a_{\boldsymbol{k}}(t), a_{\boldsymbol{k}}^{\dagger}(t') \right] \right\rangle, \tag{3.10a}$$

$$iG_{\boldsymbol{k}}^{A}(t,t') = -\Theta(t'-t) \left\langle \left[a_{\boldsymbol{k}}(t), a_{\boldsymbol{k}}^{\dagger}(t') \right] \right\rangle, \tag{3.10b}$$

$$iG_{\boldsymbol{k}}^{K}(t,t') = \left\langle \left\{ a_{\boldsymbol{k}}(t), a_{\boldsymbol{k}}^{\dagger}(t') \right\} \right\rangle, \tag{3.10c}$$

and the phonon Green's functions by

$$iF_{\boldsymbol{q}}^{R}(t,t') = \Theta(t-t') \left\langle \left[b_{\boldsymbol{q}}(t), b_{\boldsymbol{q}}^{\dagger}(t') \right] \right\rangle, \tag{3.11a}$$

$$iF_{\boldsymbol{q}}^{A}(t,t') = -\Theta(t'-t) \left\langle \left[b_{\boldsymbol{q}}(t), b_{\boldsymbol{q}}^{\dagger}(t') \right] \right\rangle, \tag{3.11b}$$

$$iF_{\boldsymbol{q}}^{K}(t,t') = \left\langle \left\{ b_{\boldsymbol{q}}(t), b_{\boldsymbol{q}}^{\dagger}(t') \right\} \right\rangle, \tag{3.11c}$$

and

$$iD_{\boldsymbol{q}}^{R}(t,t') = \frac{i}{2} \left[F_{\boldsymbol{q}}^{R}(t,t') + F_{-\boldsymbol{q}}^{A}(t',t) \right]$$
$$= \Theta(t-t') \left\langle [X_{\boldsymbol{q}}(t), X_{-\boldsymbol{q}}(t')] \right\rangle, \tag{3.12a}$$

$$iD_{\boldsymbol{q}}^{A}(t,t') = \frac{i}{2} \left[F_{\boldsymbol{q}}^{A}(t,t') + F_{-\boldsymbol{q}}^{R}(t',t) \right]$$
$$= -\Theta(t'-t) \left\langle [X_{\boldsymbol{q}}(t), X_{-\boldsymbol{q}}(t')] \right\rangle, \tag{3.12b}$$

$$iD_{\boldsymbol{q}}^{K}(t,t') = \frac{i}{2} \left[F_{\boldsymbol{q}}^{K}(t,t') + F_{-\boldsymbol{q}}^{K}(t't) \right]$$
$$= \left\langle \{X_{\boldsymbol{q}}(t), X_{-\boldsymbol{q}}(t')\} \right\rangle, \tag{3.12c}$$

where [,] is the commutator and { , } is the anticommutator. In the functional approach this translates into

$$iG_{\boldsymbol{k}}^{R}(t,t') = \left\langle a_{\boldsymbol{k}}^{C}(t)\bar{a}_{\boldsymbol{k}}^{Q}(t') \right\rangle \equiv iG_{\boldsymbol{k}}^{CQ}(t,t'), \tag{3.13a}$$

$$iG_{\boldsymbol{k}}^{A}(t,t') = \left\langle a_{\boldsymbol{k}}^{Q}(t)\bar{a}_{\boldsymbol{k}}^{C}(t') \right\rangle \equiv iG_{\boldsymbol{k}}^{QC}(t,t'), \tag{3.13b}$$

$$iG_{\boldsymbol{k}}^{K}(t,t') = \left\langle a_{\boldsymbol{k}}^{C}(t)\bar{a}_{\boldsymbol{k}}^{C}(t') \right\rangle \equiv iG_{\boldsymbol{k}}^{CC}(t,t'), \tag{3.13c}$$

and similarly for the phonon Green's functions,

$$iF_{\boldsymbol{q}}^{R}(t,t') = \left\langle b_{\boldsymbol{q}}^{C}(t)\bar{b}_{\boldsymbol{q}}^{Q}(t') \right\rangle \equiv iF_{\boldsymbol{q}}^{CQ}(t,t'), \tag{3.14a}$$

$$iF_{\boldsymbol{q}}^{A}(t,t') = \left\langle b_{\boldsymbol{q}}^{Q}(t)\bar{b}_{\boldsymbol{q}}^{C}(t') \right\rangle \equiv iF_{\boldsymbol{q}}^{QC}(t,t'), \tag{3.14b}$$

$$iF_{\boldsymbol{q}}^{K}(t,t') = \left\langle b_{\boldsymbol{q}}^{C}(t)\bar{b}_{\boldsymbol{q}}^{C}(t') \right\rangle \equiv iF_{\boldsymbol{q}}^{CC}(t,t'), \tag{3.14c}$$

and finally for the real phonon fields,

$$
\begin{align}
iD_{\boldsymbol{q}}^R(t,t') &= \left\langle X_{\boldsymbol{q}}^C(t)X_{-\boldsymbol{q}}^Q(t') \right\rangle \equiv iD_{\boldsymbol{q}}^{CQ}(t,t'), \tag{3.15a}\\
iD_{\boldsymbol{q}}^A(t,t') &= \left\langle X_{\boldsymbol{q}}^Q(t)X_{-\boldsymbol{q}}^C(t') \right\rangle \equiv iD_{\boldsymbol{q}}^{QC}(t,t'), \tag{3.15b}\\
iD_{\boldsymbol{q}}^K(t,t') &= \left\langle X_{\boldsymbol{q}}^C(t)X_{-\boldsymbol{q}}^C(t') \right\rangle \equiv iD_{\boldsymbol{q}}^{CC}(t,t'). \tag{3.15c}
\end{align}
$$

In order to use a compact notation we collect the Green's functions in 2×2 matrices as indicated in the action Eq. (3.2) and similar to Eq. (1.49),

$$
\boldsymbol{G} \equiv \begin{pmatrix} \hat{G}^K & \hat{G}^R \\ \hat{G}^A & 0 \end{pmatrix}, \tag{3.16a}
$$

$$
\boldsymbol{F} \equiv \begin{pmatrix} \hat{G}^K & \hat{G}^R \\ \hat{G}^A & 0 \end{pmatrix}, \tag{3.16b}
$$

$$
\boldsymbol{D} \equiv \begin{pmatrix} \hat{D}^K & \hat{D}^R \\ \hat{D}^A & 0 \end{pmatrix}. \tag{3.16c}
$$

We are interested in the magnon particle distribution $n_{\boldsymbol{k}}(t) = \left\langle a_{\boldsymbol{k}}^\dagger(t) a_{\boldsymbol{k}}(t) \right\rangle$ which can be obtained from diagonal elements of $\hat{G}^K$,

$$
iG_{\boldsymbol{k}}^K(t,t) = 1 + 2n_{\boldsymbol{k}}(t), \tag{3.17}
$$

and therefore we derive a rate equation for the Keldysh Green's function in section 3.3.3.

For completeness let us mention that the Keldysh action (3.2) is quadratic in the phononic fields and for the consideration of magnons the phonons can be integrate out. This yields

$$
\begin{align}
S[\bar{a},a] &= \int dt \int dt' \sum_{\boldsymbol{k}} (\bar{a}_{\boldsymbol{k}}^C(t), \bar{a}_{\boldsymbol{k}}^Q(t)) \begin{pmatrix} 0 & (\hat{G}_0^A)^{-1} \\ (\hat{G}_0^R)^{-1} & 2i\eta\hat{g}_0 \end{pmatrix}_{tt'} \begin{pmatrix} a_{\boldsymbol{k}}^C(t') \\ a_{\boldsymbol{k}}^Q(t') \end{pmatrix} \\
&\quad - \int dt \int dt' \frac{1}{V} \sum_{\boldsymbol{q}} \gamma_{\boldsymbol{q}}^2 \Big\{ D_{0,\boldsymbol{q}}^R(t,t')\rho_{-\boldsymbol{q}}^{CQ}(t) \left[\rho_{\boldsymbol{q}}^{CC}(t') + \rho_{\boldsymbol{q}}^{QQ}(t') \right] \\
&\qquad\qquad + D_{0,\boldsymbol{q}}^A(t,t') \left[\rho_{-\boldsymbol{q}}^{CC}(t) + \rho_{-\boldsymbol{q}}^{QQ}(t) \right] \rho_{\boldsymbol{q}}^{QC}(t') \\
&\qquad\qquad + \frac{1}{2} D_{0,\boldsymbol{q}}^K(t,t') \left[\rho_{-\boldsymbol{q}}^{CQ}(t) + \rho_{-\boldsymbol{q}}^{QC}(t) \right] \left[\rho_{\boldsymbol{q}}^{CQ}(t') + \rho_{\boldsymbol{q}}^{QC}(t') \right] \Big\}, \tag{3.18}
\end{align}
$$

where $\rho_{\boldsymbol{q}}^{\lambda\lambda'}(t)$ for $\lambda, \lambda' = C, Q$ represent the magnon density

$$
\rho_{\boldsymbol{q}}^{\lambda\lambda'}(t) = \sum_{\boldsymbol{k}} \bar{a}_{\boldsymbol{k}}^\lambda(t) a_{\boldsymbol{k}+\boldsymbol{q}}^{\lambda'}(t). \tag{3.19}
$$

The explicit expressions for the non-interacting real phonon Green's functions $D_{0,\boldsymbol{q}}^X(t,t')$, for $X = R, A, K$ are given in the next section, Eqs. (3.32a-3.32c). Because of the time dependence of the magnon-magnon interactions in Eq. (3.18) it is for our purpose more convenient to work with the action (3.2)
.

3.3.2. Non-interacting Green's functions

Here we will derive the non-interacting Green's functions for magnons and phonons by means of kinetic equations in order to become familiar with this concept. In section 1.1.4 we calculated the Green's functions for a single harmonic oscillator directly by inverting the inverse propagator instead. The Green's functions for the action Eq. (3.2) without the interaction part are determined by the non-interacting limit of the Dyson equation (1.73),

$$
\begin{aligned}
\boldsymbol{G}_0^{-1}\boldsymbol{G}_0 &= \boldsymbol{I}, & (3.20a) \\
\boldsymbol{F}_0^{-1}\boldsymbol{F}_0 &= \boldsymbol{I}, & (3.20b)
\end{aligned}
$$

where the Green's functions with subscript 0 are defined by the non-interacting action. The unit operator $\boldsymbol{I}$ in Keldysh space is defined by

$$
\boldsymbol{I} \equiv \begin{pmatrix} \hat{I} & 0 \\ 0 & \hat{I} \end{pmatrix}, \tag{3.21}
$$

where the components of the unit operator $\hat{I}$ in momentum and time space are given by

$$
\left[\hat{I}\right]_{\boldsymbol{k},tt'} = \delta\left(t-t'\right). \tag{3.22}
$$

The inverse free propagator is given by

$$
\begin{aligned}
\boldsymbol{G}_0^{-1} &= \begin{pmatrix} 0 & (\hat{G}_0^A)^{-1} \\ (\hat{G}_0^R)^{-1} & 2i\eta\hat{g}_0 \end{pmatrix}, & (3.23a) \\[2mm]
\boldsymbol{F}_0^{-1} &= \begin{pmatrix} 0 & (\hat{F}_0^A)^{-1} \\ (\hat{F}_0^R)^{-1} & 2i\eta\hat{f}_0 \end{pmatrix}, & (3.23b)
\end{aligned}
$$

which can be seen from the action Eq. (3.2). The Green's functions also have to fulfill

$$
\begin{aligned}
\boldsymbol{G}_0\boldsymbol{G}_0^{-1} &= \boldsymbol{I}, & (3.24a) \\
\boldsymbol{F}_0\boldsymbol{F}_0^{-1} &= \boldsymbol{I}, & (3.24b) \\
\boldsymbol{D}_0\boldsymbol{D}_0^{-1} &= \boldsymbol{I}, & (3.24c)
\end{aligned}
$$

which follow from the other form of the Dyson equation (1.74). Here we need the relations for consistency only. Let us start with the calculation of the magnon Green's function $\boldsymbol{G}_0$. Using the expressions for the inverse propagators Eqs. (3.3a, 3.3b) and evaluating the matrix product in Eq. (3.20a) yields the following kinetic equations for the components of the Green's function,

$$
\begin{aligned}
(i\partial_t - \epsilon_{\boldsymbol{k}} + i\eta)\, G_{0,\eta,\boldsymbol{k}}^R\left(t,t'\right) &= \delta\left(t-t'\right), & (3.25a) \\
(i\partial_t - \epsilon_{\boldsymbol{k}} - i\eta)\, G_{0,\eta,\boldsymbol{k}}^A\left(t,t'\right) &= \delta\left(t-t'\right), & (3.25b) \\
(i\partial_t - \epsilon_{\boldsymbol{k}} + i\eta)\, G_{0,\eta,\boldsymbol{k}}^K\left(t,t'\right) &= -2i\eta g_{0,\boldsymbol{k}} G_{0,\eta,\boldsymbol{k}}^A\left(t,t'\right), & (3.25c)
\end{aligned}
$$

where we have introduced new functions $\hat{G}_{0,\eta}^{X}$, $X = R, A, Q$ for the solution of the kinetic equations with finite η. The infinitesimal quantity η comes from the regularization of the continuous notation of the functional integrals. The correct Green's functions are recovered by taking the limit $\eta \to 0$ in the solutions of the kinetic equations, $\hat{G}_{0}^{R} = \lim_{\eta \to 0} \hat{G}_{0,\eta}^{R}$ and so on, for details see section 1.1.4. In order to work consistently in the continuous notation one always has to use $\hat{G}_{0,\eta}^{X}$ when an expression is of order η or when the regularization is needed for convergence of the functional integrals.

The first two partial differential equations (3.25a, 3.25b) can easily be solved by means of Fourier transformation. When transforming Eq. (3.25a) from time difference $t - t'$ to frequency ω we obtain

$$G_{0,\eta,\boldsymbol{k}}^{R}(\omega) = \frac{1}{\omega - \epsilon_{\boldsymbol{k}} + i\eta}. \tag{3.26}$$

Transforming back to real time by using contour integration yields the desired solution,

$$G_{0,\eta,\boldsymbol{k}}^{R}(t,t') = -i\Theta(t-t')\,e^{-i(\epsilon_{\boldsymbol{k}}-i\eta)(t-t')}, \tag{3.27}$$

and similarly we find

$$G_{0,\eta,\boldsymbol{k}}^{A}(t,t') = i\Theta(t-t')\,e^{-i(\epsilon_{\boldsymbol{k}}+i\eta)(t-t')}. \tag{3.28}$$

Now Eq. (1.60) implies for the Keldysh component,

$$G_{0,\eta,\boldsymbol{k}}^{K}(t,t') = -ig_{0,\boldsymbol{k}}\left[\Theta(t-t')\,e^{-i(\epsilon_{\boldsymbol{k}}-i\eta)(t-t')} + \Theta(t'-t)\,e^{-i(\epsilon_{\boldsymbol{k}}+i\eta)(t-t')}\right], \tag{3.29}$$

which indeed solves Eq. (3.25c). The correct magnon Green's functions without any artefact from the continuous notation are given by

$$\begin{aligned}
G_{0,\boldsymbol{k}}^{R}(t,t') &= -i\Theta(t-t')\,e^{-i\epsilon_{\boldsymbol{k}}(t-t')}, & (3.30\text{a})\\
G_{0,\boldsymbol{k}}^{A}(t,t') &= i\Theta(t-t')\,e^{-i\epsilon_{\boldsymbol{k}}(t-t')}, & (3.30\text{b})\\
G_{0,\boldsymbol{k}}^{K}(t,t') &= -ig_{0,\boldsymbol{k}}e^{-i\epsilon_{\boldsymbol{k}}(t-t')}. & (3.30\text{c})
\end{aligned}$$

Note that if we neglect η in the kinetic equations (3.25a-3.25c) the Green's function Eqs. (3.30a-3.30c) are solving the resulting equations but are not unique solutions. This is why we need the construction with the regularization η.

Analogously it can be shown that the expressions for the correct phonon Green's functions are

$$\begin{aligned}
F_{0,\boldsymbol{q}}^{R}(t,t') &= -i\Theta(t-t')\,\mathrm{e}^{-i\omega_{\boldsymbol{q}}(t-t')}, & (3.31\text{a})\\
F_{0,\boldsymbol{q}}^{A}(t,t') &= i\Theta(t'-t)\,\mathrm{e}^{-i\omega_{\boldsymbol{q}}(t-t')}, & (3.31\text{b})\\
F_{0,\boldsymbol{q}}^{K}(t,t') &= -if_{0,\boldsymbol{k}}\mathrm{e}^{-i\omega_{\boldsymbol{q}}(t-t')}. & (3.31\text{c})
\end{aligned}$$

From the definitions of the real phonon Green's functions Eqs. (3.15a-3.15c) we find that

$$
\begin{aligned}
D_{0,\boldsymbol{q}}^{R}\left(t,t'\right) &= -\Theta\left(t-t'\right)\sin\left[\omega_{\boldsymbol{q}}\left(t-t'\right)\right], & \text{(3.32a)}\\
D_{0,\boldsymbol{q}}^{A}\left(t,t'\right) &= \Theta\left(t'-t\right)\sin\left[\omega_{\boldsymbol{q}}\left(t-t'\right)\right], & \text{(3.32b)}\\
D_{0,\boldsymbol{q}}^{K}\left(t,t'\right) &= -i f_{0,\boldsymbol{q}}\cos\left[\omega_{\boldsymbol{q}}\left(t-t'\right)\right]. & \text{(3.32c)}
\end{aligned}
$$

Since all non-interacting Green's functions depend only on the time difference $t-t'$ the Wigner transformation (WT) Eq. (1.86) reduces to the standard Fourier transformation. Hence the WT of the free magnon propagators are given by

$$
\begin{aligned}
G_{0,\boldsymbol{q}}^{R}(\omega) &= \frac{1}{\omega-\epsilon_{\boldsymbol{k}}+i\eta}, & \text{(3.33a)}\\[4pt]
G_{0,\boldsymbol{k}}^{A}(\omega) &= \frac{1}{\omega-\epsilon_{\boldsymbol{k}}-i\eta}, & \text{(3.33b)}\\[4pt]
G_{0,\boldsymbol{k}}^{I}(\omega) &= i\left[G_{0,\boldsymbol{k}}^{R}(\omega)-G_{0,\boldsymbol{k}}^{A}(\omega)\right]=2\pi\delta\left(\omega-\epsilon_{\boldsymbol{k}}\right), & \text{(3.33c)}\\[4pt]
iG_{0,\boldsymbol{k}}^{K}(\omega) &= g_{0,\boldsymbol{k}}G_{0,\boldsymbol{k}}^{I}(\omega). & \text{(3.33d)}
\end{aligned}
$$

Here we also give the spectral component $G_{0,\boldsymbol{k}}^{I}\left(\omega\right)$ for which we used the Dirac identity

$$
\lim_{\eta\to\infty}\frac{1}{\omega+i\eta}=\mathcal{P}\frac{1}{\omega}-i\pi\delta\left(\omega\right), \tag{3.34}
$$

where $\mathcal{P}\ldots$ denotes the principle value. For the phonons we analogously find that

$$
\begin{aligned}
F_{0,\boldsymbol{q}}^{R}(\omega) &= \frac{1}{\omega-\omega_{\boldsymbol{q}}+i\eta}, & \text{(3.35a)}\\[4pt]
F_{0,\boldsymbol{q}}^{A}(\omega) &= \frac{1}{\omega-\omega_{\boldsymbol{q}}-i\eta}, & \text{(3.35b)}\\[4pt]
F_{0,\boldsymbol{q}}^{I}(\omega) &= i\left[F_{0,\boldsymbol{q}}^{R}(\omega)-F_{0,\boldsymbol{q}}^{A}(\omega)\right]=2\pi\delta\left(\omega-\omega_{\boldsymbol{q}}\right), & \text{(3.35c)}\\[4pt]
iF_{0,\boldsymbol{q}}^{K}(\omega) &= \left[1+\frac{2}{e^{\beta\omega}-1}\right]F_{0,\boldsymbol{q}}^{I}(\omega)=f^{0}(\omega)F_{0,\boldsymbol{q}}^{I}(\omega), & \text{(3.35d)}
\end{aligned}
$$

where we have assumed that the phonons are in thermal equilibrium at the initial time t_{0},

$$
f_{0,\boldsymbol{q}}=1+\frac{2}{e^{\beta\omega_{\boldsymbol{q}}}-1}\equiv f^{0}\left(\omega_{\boldsymbol{q}}\right). \tag{3.36}
$$

For the real phonon Green's functions we arrive at

$$
\begin{aligned}
D_{0,\boldsymbol{q}}^{R}(\omega) &= \frac{\omega_{\boldsymbol{q}}}{(\omega+i\eta)^2-\omega_{\boldsymbol{q}}^2}, & \text{(3.37a)}\\
D_{0,\boldsymbol{q}}^{A}(\omega) &= \frac{\omega_{\boldsymbol{q}}}{(\omega-i\eta)^2-\omega_{\boldsymbol{q}}^2}, & \text{(3.37b)}\\
D_{0,\boldsymbol{q}}^{I}(\omega) &= i\left(D_{0,\boldsymbol{q}}^{R}(\omega)-D_{0,\boldsymbol{q}}^{A}(\omega)\right)\\
&= \frac{1}{2}\left[F_{0,\boldsymbol{q}}^{I}(\omega)-F_{0,-\boldsymbol{q}}^{I}(-\omega)\right]\\
&= \pi\mathrm{sgn}(\omega)\left[\delta\left(\omega-\omega_{\boldsymbol{q}}\right)+\delta\left(\omega+\omega_{\boldsymbol{q}}\right)\right], & \text{(3.37c)}\\
iD_{0,\boldsymbol{q}}^{K}(\omega) &= f^0(\omega)D_{0,\boldsymbol{q}}^{I}(\omega). & \text{(3.37d)}
\end{aligned}
$$

Note that the solutions Eqs. (3.30a-3.32c) also fulfill the relations from the alternative form of the Dyson equation Eqs. (3.24a-3.24c).

3.3.3. Rate equation and self-energies in perturbation theory

We use the WT to derive a rate equation for the distribution function $\hat{g}$ which is connected to the magnon particle distribution $n_{\boldsymbol{k}}(t)=\left\langle a_{\boldsymbol{k}}^{\dagger}(t)\,a_{\boldsymbol{k}}(t)\right\rangle$ by

$$
g_{\boldsymbol{k}}\left(t;\epsilon_{\boldsymbol{k}}\right)=1+2n_{\boldsymbol{k}}(t). \tag{3.38}
$$

The notation in this section is chosen such that the magnonic variables correspond to the bosonic degrees of freedom of the introduction to the Keldysh formalism in section 1.1. The exact quantum kinetic equation (1.84) for the distribution function $\hat{g}$ is too complex for solving it numerically without any further approximations. Our starting point is the kinetic equation (1.97) where we have used the gradient approximation (1.95) for the WT and neglected the imaginary part of $\hat{g}$.

Next we have to calculate the magnon self-energies contributing to the kinetic equation (1.97) in perturbation theory to second order in the magnon-phonon coupling. In the contour basis we obtain

$$
\Sigma_{\boldsymbol{k}}^{pp'}(t,t')=pp'\frac{i}{V}\sum_{\boldsymbol{q}}\gamma_{\boldsymbol{q}}^2\left[D_{\boldsymbol{q}}^{pp'}(t,t')G_{\boldsymbol{k}-\boldsymbol{q}}^{pp'}(t,t')+(\boldsymbol{q}\to-\boldsymbol{q})\right], \tag{3.39}
$$

where $p,p'=\pm$ label the corresponding contour branch, see Fig. 1.1. Due to the symmetry $\gamma_{-\boldsymbol{q}}=\gamma_{\boldsymbol{q}}$ the second term in Eq. (3.39) just gives a factor of 2.
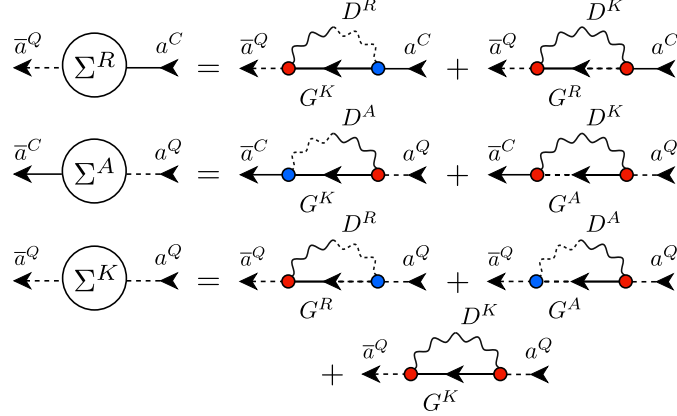
Figure 3.2.: The diagrams for the magnon self-energies up to second order in the magnon-phonon interaction. The wavy lines correspond to the phonon propagators whereas the straight lines with an arrow denote the magnon propagators. Dashed lines label the quantum component in the Keldysh basis and the solid lines the classical. See also the definitions in the caption of Fig. 3.1.

In the Keldysh basis we find that

$$
\begin{aligned}
\Sigma_{\boldsymbol{k}}^{R}(t,t') &= \Sigma_{\boldsymbol{k}}^{QC}(t,t') = \frac{i}{V} \sum_{\boldsymbol{q}} \gamma_{\boldsymbol{q}}^{2} \left[D_{\boldsymbol{q}}^{R}(t,t') G_{\boldsymbol{k}-\boldsymbol{q}}^{K}(t,t') \right. \\
&\qquad\qquad \left. + D_{\boldsymbol{q}}^{K}(t,t') G_{\boldsymbol{k}-\boldsymbol{q}}^{R}(t,t') \right] ,
\end{aligned} \tag{3.40a}
$$

$$
\begin{aligned}
\Sigma_{\boldsymbol{k}}^{A}(t,t') &= \Sigma_{\boldsymbol{k}}^{CQ}(t,t') = \frac{i}{V} \sum_{\boldsymbol{q}} \gamma_{\boldsymbol{q}}^{2} \left[D_{\boldsymbol{q}}^{A}(t,t') G_{\boldsymbol{k}-\boldsymbol{q}}^{K}(t,t') \right. \\
&\qquad\qquad \left. + D_{\boldsymbol{q}}^{K}(t,t') G_{\boldsymbol{k}-\boldsymbol{q}}^{A}(t,t') \right] ,
\end{aligned} \tag{3.40b}
$$

$$
\begin{aligned}
\Sigma_{\boldsymbol{k}}^{K}(t,t') &= \Sigma_{\boldsymbol{k}}^{QQ}(t,t') = \frac{i}{V} \sum_{\boldsymbol{q}} \gamma_{\boldsymbol{q}}^{2} \left[D_{\boldsymbol{q}}^{K}(t,t') G_{\boldsymbol{k}-\boldsymbol{q}}^{K}(t,t') \right. \\
&\qquad \left. + D_{\boldsymbol{q}}^{R}(t,t') G_{\boldsymbol{k}-\boldsymbol{q}}^{R}(t,t') + D_{\boldsymbol{q}}^{A}(t,t') G_{\boldsymbol{k}-\boldsymbol{q}}^{A}(t,t') \right] .
\end{aligned} \tag{3.40c}
$$

The diagrams representing the self-energies are shown in Fig. 3.2. In our approximations only the Keldysh and the spectral components as defined in Eqs. (1.77b, 1.77d) will contribute to the rate equation. Therefore let us give the Keldysh and spectral self-energy expressed by the Keldysh and spectral

3. FRG approach to the thermalization of magnons in YIG

Green's functions,

$$
\begin{aligned}
\Sigma_{\boldsymbol{k}}^I(t,t') &= i\left[\Sigma_{\boldsymbol{k}}^R(t,t') - \Sigma_{\boldsymbol{k}}^A(t,t')\right] \\
&= \frac{i}{V}\sum_{\boldsymbol{q}} \gamma_{\boldsymbol{q}}^2 \left[D_{\boldsymbol{q}}^I(t,t')G_{\boldsymbol{k}-\boldsymbol{q}}^K(t,t') + D_{\boldsymbol{q}}^K(t,t')G_{\boldsymbol{k}-\boldsymbol{q}}^I(t,t')\right],
\end{aligned}
$$
$$(3.41\text{a})$$
$$
\Sigma_{\boldsymbol{k}}^K(t,t') = \frac{i}{V}\sum_{\boldsymbol{q}} \gamma_{\boldsymbol{q}}^2 \left[D_{\boldsymbol{q}}^K(t,t')G_{\boldsymbol{k}-\boldsymbol{q}}^K(t,t') - D_{\boldsymbol{q}}^I(t,t')G_{\boldsymbol{k}-\boldsymbol{q}}^I(t,t')\right],
$$
$$(3.41\text{b})$$

where for the second expression we have used the fact that products of retarded and advanced functions at equal times vanish. The spectral component of the phonons and magnons are defined analogously to Eqs. (3.33c, 3.37c),

$$
G_{\boldsymbol{k}}^I(t,t') = i\left[G_{\boldsymbol{k}}^R(t,t') - G_{\boldsymbol{k}}^A(t,t')\right], \tag{3.42}
$$
$$
D_{\boldsymbol{q}}^I(t,t') = i\left[D_{\boldsymbol{q}}^R(t,t') - D_{\boldsymbol{q}}^A(t,t')\right]. \tag{3.43}
$$

Keeping in mind that the WT of a product of two functions at equal times yields a convolution in frequency space, see Eq. (1.98), we obtain for the WT of the self-energies

$$
\begin{aligned}
\Sigma_{\boldsymbol{k}}^I(\tau;\omega) &= \frac{i}{V}\sum_{\boldsymbol{q}} \int_{-\infty}^{\infty} \frac{d\omega'}{2\pi} \gamma_{\boldsymbol{q}}^2 \left[D_{\boldsymbol{q}}^I(\tau;\omega')G_{\boldsymbol{k}-\boldsymbol{q}}^K(\tau;\omega-\omega')\right. \\
&\qquad\left. + D_{\boldsymbol{q}}^K(\tau;\omega')G_{\boldsymbol{k}-\boldsymbol{q}}^I(\tau;\omega-\omega')\right],
\end{aligned}
$$
$$(3.44\text{a})$$
$$
\begin{aligned}
\Sigma_{\boldsymbol{k}}^K(\tau;\omega) &= \frac{i}{V}\sum_{\boldsymbol{q}} \int_{-\infty}^{\infty} \frac{d\omega'}{2\pi} \gamma_{\boldsymbol{q}}^2 \left[D_{\boldsymbol{q}}^K(\tau;\omega')G_{\boldsymbol{k}-\boldsymbol{q}}^K(\tau;\omega-\omega')\right. \\
&\qquad\left. - D_{\boldsymbol{q}}^I(\tau;\omega')G_{\boldsymbol{k}-\boldsymbol{q}}^I(\tau;\omega-\omega')\right].
\end{aligned}
$$
$$(3.44\text{b})$$

In order to replace the Keldysh Green's function in the self-energies we perform a WT of our parametrization Eq. (1.81) of the Keldysh Green's function and use the gradient approximation which yields

$$
iG_{\boldsymbol{k}}^K(\tau;\omega) \approx G_{\boldsymbol{k}}^I(\tau;\omega)g_{\boldsymbol{k}}(\tau;\omega). \tag{3.45}
$$

Note that this is the fluctuation-dissipation theorem which is valid in equilibrium, see Appendix B, and we can argue that there is a region around equilibrium where our approximations for Eq. (3.45) are justified, as discussed earlier in section 1.1.7.

Moreover we approximate the phonon propagators by the free ones Eqs.

(3.37c, 3.37d) and finally plugging Eq. (3.45) into Eqs. (3.44a, 3.44b) yields

$$
\begin{aligned}
\Sigma_{\boldsymbol{k}}^{\text{in}}(\tau;\omega) &= i\Sigma_{\boldsymbol{k}}^{K}(\tau;\omega) \\
&= \frac{1}{V}\sum_{\boldsymbol{q}}\gamma_{\boldsymbol{q}}^{2}\int_{-\infty}^{\infty}\frac{d\omega'}{2\pi}D_{0,\boldsymbol{q}}^{I}(\omega')G_{\boldsymbol{k}-\boldsymbol{q}}^{I}(\tau;\omega-\omega') \\
&\quad \times\left[f^{0}(\omega')g_{\boldsymbol{k}-\boldsymbol{q}}(\tau;\omega-\omega')+1\right],
\end{aligned}
\tag{3.46a}
$$

$$
\begin{aligned}
\Sigma_{\boldsymbol{k}}^{\text{out}}(\tau;\omega) &= \Sigma_{\boldsymbol{k}}^{I}(\tau;\omega)g_{\boldsymbol{k}}(\tau;\omega) \\
&= \frac{1}{V}\sum_{\boldsymbol{q}}\gamma_{\boldsymbol{q}}^{2}\int_{-\infty}^{\infty}\frac{d\omega'}{2\pi}D_{0,\boldsymbol{q}}^{I}(\omega')G_{\boldsymbol{k}-\boldsymbol{q}}^{I}(\tau;\omega-\omega') \\
&\quad \times\left[f^{0}(\omega')+g_{\boldsymbol{k}-\boldsymbol{q}}(\tau;\omega-\omega')\right]g_{\boldsymbol{k}}(\tau;\omega),
\end{aligned}
\tag{3.46b}
$$

and for the kinetic equation (1.97)

$$
\begin{aligned}
\partial_{\tau}g_{\boldsymbol{k}}(\tau;\omega) &= \frac{1}{V}\sum_{\boldsymbol{q}}\gamma_{\boldsymbol{q}}^{2}\int_{-\infty}^{\infty}\frac{d\omega'}{2\pi}D_{0,\boldsymbol{q}}^{I}(\omega')G_{\boldsymbol{k}-\boldsymbol{q}}^{I}(\tau;\omega-\omega') \\
&\quad \times\left\{f^{0}(\omega')\left[g_{\boldsymbol{k}-\boldsymbol{q}}(\tau;\omega-\omega')-g_{\boldsymbol{k}}(\tau;\omega)\right]\right. \\
&\quad\quad \left.+1-g_{\boldsymbol{k}-\boldsymbol{q}}(\tau;\omega-\omega')g_{\boldsymbol{k}}(\tau;\omega)\right\}.
\end{aligned}
\tag{3.47}
$$

The integrand in Eq. (3.47) is nullified by

$$
g_{\boldsymbol{k}}(\tau;\omega)\to\coth\left(\frac{\beta(\omega-\mu)}{2}\right)=1+\frac{2}{e^{\beta(\omega-\mu)}-1}\equiv g^{0}(\omega),
\tag{3.48}
$$

which can be seen from the relation

$$
\coth(x-y)=\frac{1-\coth x\coth y}{\coth x-\coth y},
\tag{3.49}
$$

by choosing $x=\beta(\omega-\mu)/2$ and $y=\beta\omega'/2$. In other words the thermal equilibrium distribution of the magnons is given by the Bose function

$$
b(\omega)=\frac{1}{e^{\beta\omega}-1}.
\tag{3.50}
$$

The distribution $g^{0}(\omega)$ nullifies Eq. (3.47) for arbitrary μ which can be identified as the chemical potential and is fixed by the particle number of the initial condition $g_{0,\boldsymbol{k}}$. By setting

$$
g_{\boldsymbol{k}}(\tau;\omega) = 1+2n_{\boldsymbol{k}}(\tau;\omega),
\tag{3.51a}
$$

$$
f^{0}(\omega) = 1+2b(\omega)=1+\frac{2}{e^{\beta\omega}-1},
\tag{3.51b}
$$

and shifting the phonon momentum, $\boldsymbol{q}=\boldsymbol{k}-\boldsymbol{k}'$, Eq. (3.47) can be written as

$$
\begin{aligned}
\partial_{\tau}n_{\boldsymbol{k}}(\tau;\omega) &= \frac{1}{V}\sum_{\boldsymbol{k}'}\int_{-\infty}^{\infty}\frac{d\omega'}{2\pi}2\gamma_{\boldsymbol{k}-\boldsymbol{k}'}^{2}D_{0,\boldsymbol{k}-\boldsymbol{k}'}^{I}(\omega-\omega') \\
&\quad \times G_{\boldsymbol{k}'}^{I}(\tau;\omega')\left\{[1+n_{\boldsymbol{k}}(\tau;\omega)]\,b(\omega-\omega')n_{\boldsymbol{k}'}(\tau;\omega')\right. \\
&\quad\quad \left.+[1+n_{\boldsymbol{k}'}(\tau;\omega')]\,b(\omega'-\omega)n_{\boldsymbol{k}}(\tau;\omega)\right\}.
\end{aligned}
\tag{3.52}
$$

3. FRG approach to the thermalization of magnons in YIG

Note that due to Eqs. (3.38, 3.51a) we have

$$n_{\boldsymbol{k}}(\tau; \epsilon_{\boldsymbol{k}}) = n_{\boldsymbol{k}}(\tau) = \left\langle a_{\boldsymbol{k}}^{\dagger}(\tau) a_{\boldsymbol{k}}(\tau) \right\rangle. \tag{3.53}$$

Moreover we apply the so called quasiparticle approximation to the magnons

$$G_{\boldsymbol{k}'}^{I}(\tau; \omega') \approx 2\pi\delta(\omega' - \epsilon_{\boldsymbol{k}'}), \tag{3.54}$$

where the magnonic spectral Green's function is replaced by the non-interacting which is equivalent to neglecting the damping of intermediate states. Finally setting the external frequency ω to $\epsilon_{\boldsymbol{k}}$, we obtain the kinetic equation

$$\partial_{\tau} n_{\boldsymbol{k}}(\tau) = \frac{1}{V} \sum_{\boldsymbol{k}'} \left\{ [1 + n_{\boldsymbol{k}}(\tau)] W_{\boldsymbol{k},\boldsymbol{k}'} n_{\boldsymbol{k}'}(\tau) - [1 + n_{\boldsymbol{k}'}(\tau)] W_{\boldsymbol{k}',\boldsymbol{k}} n_{\boldsymbol{k}}(\tau) \right\} \tag{3.55}$$

and the self-energies

$$i\Sigma_{\boldsymbol{k}}^{K}(\tau; \epsilon_{\boldsymbol{k}}) = \frac{1}{V} \sum_{\boldsymbol{k}'} \left\{ [1 + n_{\boldsymbol{k}'}(\tau)] W_{\boldsymbol{k}',\boldsymbol{k}} + W_{\boldsymbol{k},\boldsymbol{k}'} n_{\boldsymbol{k}'}(\tau) \right\}, \tag{3.56a}$$

$$\Sigma_{\boldsymbol{k}}^{I}(\tau; \epsilon_{\boldsymbol{k}}) = \frac{1}{V} \sum_{\boldsymbol{k}'} \left\{ [1 + n_{\boldsymbol{k}'}(\tau)] W_{\boldsymbol{k}',\boldsymbol{k}} - W_{\boldsymbol{k},\boldsymbol{k}'} n_{\boldsymbol{k}'}(\tau) \right\}, \tag{3.56b}$$

where the transition rates are given by

$$W_{\boldsymbol{k},\boldsymbol{k}'} = 2\gamma_{\boldsymbol{k}-\boldsymbol{k}'}^{2} b(\epsilon_{\boldsymbol{k}} - \epsilon_{\boldsymbol{k}'}) D_{0,\boldsymbol{k}-\boldsymbol{k}'}^{I}(\epsilon_{\boldsymbol{k}} - \epsilon_{\boldsymbol{k}'}). \tag{3.57}$$

Using the identities $D_{0,\boldsymbol{q}}^{I}(-\omega) = -D_{0,\boldsymbol{q}}^{I}(\omega)$ and $b(-\omega) = -[1 + b(\omega)] = -e^{\beta\omega} b(\omega)$ it can be seen that the transition rates satisfy the detailed balance condition

$$W_{\boldsymbol{k},\boldsymbol{k}'} e^{-\beta\epsilon_{\boldsymbol{k}'}} = W_{\boldsymbol{k}',\boldsymbol{k}} e^{-\beta\epsilon_{\boldsymbol{k}}}, \tag{3.58}$$

which agrees with the fact that the equilibrium distribution is given by the Bose function. The kinetic equation (3.55) has the form of the quantum Boltzmann equation [84]. In Ref. [82] the transition rates Eq. (3.57) have been derived by means of Fermi's golden rule.

Note that the kinetic equation (3.55) does conserve the magnon particle number since the derivative of the total particle number $N = \sum_{\boldsymbol{k}} n_{\boldsymbol{k}}(t)$ vanishes,

$$\partial_{\tau} \sum_{\boldsymbol{k}} n_{\boldsymbol{k}}(\tau) = \frac{1}{V} \sum_{\boldsymbol{k},\boldsymbol{k}'} \left\{ [1 + n_{\boldsymbol{k}}(\tau)] W_{\boldsymbol{k},\boldsymbol{k}'} n_{\boldsymbol{k}'}(\tau) - [1 + n_{\boldsymbol{k}'}(\tau)] W_{\boldsymbol{k}',\boldsymbol{k}} n_{\boldsymbol{k}}(\tau) \right\}$$

$$= 0. \tag{3.59}$$

3.3.4. Phonon renormalization

In finite systems the momentum integration in Eq. (3.55) becomes a sum and the transition rates which contain a delta function become meaningless under a summation. In Ref. [82] Banyai *et al.* use an artificial broadening in order to obtain finite results. To avoid the introduction of a phenomenological constant we use the intrinsic damping of the phonons due to the magnon-phonon interactions. Assuming that the phonons act as a thermal bath such that the phonons stay in equilibrium, the fluctuation-dissipation theorem Eq. (1.61) is still valid. This way the phononic Keldysh Green's function in the self-energies Eqs. (3.44a, 3.44b) can be replaced by

$$iD_{\boldsymbol{q}}^{K}(\tau;\omega) = \coth\left(\frac{\beta\omega}{2}\right) D_{\boldsymbol{q}}^{I}(\tau;\omega), \tag{3.60}$$

and the kinetic equation (3.57) does not change if we replace the non-interacting phononic Green's functions in the transition rates Eq. (3.57) by the renormalized ones,

$$W_{\boldsymbol{k},\boldsymbol{k}'} = 2\gamma_{\boldsymbol{k}-\boldsymbol{k}'}^{2} b(\epsilon_{\boldsymbol{k}} - \epsilon_{\boldsymbol{k}'}) D_{\boldsymbol{k}-\boldsymbol{k}'}^{I}(\epsilon_{\boldsymbol{k}} - \epsilon_{\boldsymbol{k}'}). \tag{3.61}$$

The WT of the renormalized phonon propagators can be written as

$$F_{\boldsymbol{q}}^{R}(\tau;\omega) = \frac{1}{\omega - \omega_{\boldsymbol{q}} - \Pi_{\boldsymbol{q}}^{R}(\tau;\omega)}, \tag{3.62a}$$

$$F_{\boldsymbol{q}}^{A}(\tau;\omega) = \frac{1}{\omega - \omega_{\boldsymbol{q}} - \Pi_{\boldsymbol{q}}^{A}(\tau;\omega)}, \tag{3.62b}$$

$$F_{\boldsymbol{q}}^{I}(\tau;\omega) = \frac{\Pi_{\boldsymbol{q}}^{I}(\tau;\omega)}{\left[\omega - \omega_{\boldsymbol{q}} - \Pi_{\boldsymbol{q}}^{M}(\tau;\omega)\right]^{2} + \left[\frac{1}{2}\Pi_{\boldsymbol{q}}^{I}(\tau;\omega)\right]^{2}}, \tag{3.62c}$$

$$iF_{\boldsymbol{q}}^{K}(\tau;\omega) = \coth\left(\frac{\beta\omega}{2}\right) F_{\boldsymbol{q}}^{I}(\tau;\omega), \tag{3.62d}$$

where we have introduced the phonon self-energies $\Pi_{\boldsymbol{q}}^{X}(\tau;\omega)$ for $X = R, A, I, K$ which are defined by the matrix Dyson equation

$$\boldsymbol{F}^{-1} = \boldsymbol{F}_{0}^{-1} - \boldsymbol{\Pi}, \tag{3.63}$$

with

$$\boldsymbol{\Pi} = \begin{pmatrix} 0 & \hat{\Pi}^{A} \\ \hat{\Pi}^{R} & \hat{\Pi}^{K} \end{pmatrix}. \tag{3.64}$$

For the real phonon fields we obtain

$$\begin{aligned} D_{\boldsymbol{q}}^{I}(\tau;\omega) &= \frac{1}{2}\left[F_{\boldsymbol{q}}^{I}(\tau,\omega) - F_{-\boldsymbol{q}}^{I}(\tau;-\omega)\right] \\ &= \pi\left[L_{\Pi_{\boldsymbol{q}}^{I}(\tau;\omega)/2}\left(\omega - \omega_{\boldsymbol{q}} - \Pi_{\boldsymbol{q}}^{M}(\tau;\omega)\right)\right. \\ &\quad \left. -L_{\Pi_{-\boldsymbol{q}}^{I}(\tau,-\omega)/2}\left(\omega + \omega_{\boldsymbol{q}} + \Pi_{-\boldsymbol{q}}^{M}(\tau;-\omega)\right)\right], \end{aligned} \tag{3.65}$$

3. FRG approach to the thermalization of magnons in YIG

with the Lorentzian

$$L_\Lambda\left(\omega\right) = \frac{1}{\pi}\frac{\Lambda}{\omega^2 + \Lambda^2}. \tag{3.66}$$

The other components do not contribute to the transition rates Eq. (3.3). In the contour basis the self-energies to second order in the magnon-phonon coupling are given by

$$\Pi_{\boldsymbol{q}}^{pp'}\left(t,t'\right) \;=\; pp'\frac{i}{V}\gamma_{\boldsymbol{q}}^2\sum_{\boldsymbol{k}} G_{\boldsymbol{k}}^{pp'}\left(t,t'\right) G_{\boldsymbol{k}-\boldsymbol{q}}^{p'p}\left(t',t\right), \tag{3.67}$$

where $p,p' = \pm$ label the corresponding contour branch as in Eq. (3.39). Transforming to the Keldysh basis yields

$$\Pi_{\boldsymbol{q}}^{R}\left(t,t'\right) \;=\; \frac{i}{2V}\gamma_{\boldsymbol{q}}^2\sum_{\boldsymbol{k}}\left\{G_{\boldsymbol{k}}^{R}\left(t,t'\right) G_{\boldsymbol{k}-\boldsymbol{q}}^{K}\left(t',t\right) + G_{\boldsymbol{k}}^{K}\left(t,t'\right) G_{\boldsymbol{k}-\boldsymbol{q}}^{A}\left(t',t\right)\right\}, \tag{3.68a}$$

$$\Pi_{\boldsymbol{q}}^{A}\left(t,t'\right) \;=\; \frac{i}{2V}\gamma_{\boldsymbol{q}}^2\sum_{\boldsymbol{k}}\left\{G_{\boldsymbol{k}}^{A}\left(t,t'\right) G_{\boldsymbol{k}-\boldsymbol{q}}^{K}\left(t',t\right) + G_{\boldsymbol{k}}^{K}\left(t,t'\right) G_{\boldsymbol{k}-\boldsymbol{q}}^{R}\left(t',t\right)\right\}, \tag{3.68b}$$

$$\begin{aligned}\Pi_{\boldsymbol{q}}^{I}\left(t,t'\right) \;&=\; i\left[\Pi_{\boldsymbol{q}}^{R}\left(t,t'\right) - \Pi_{\boldsymbol{q}}^{A}\left(t,t'\right)\right] \\ &=\; \frac{i}{2V}\gamma_{\boldsymbol{q}}^2\sum_{\boldsymbol{k}}\left\{G_{\boldsymbol{k}}^{I}\left(t,t'\right) G_{\boldsymbol{k}-\boldsymbol{q}}^{K}\left(t',t\right) - G_{\boldsymbol{k}}^{K}\left(t,t'\right) G_{\boldsymbol{k}-\boldsymbol{q}}^{I}\left(t',t\right)\right\},\end{aligned} \tag{3.68c}$$

$$\begin{aligned}\Pi_{\boldsymbol{q}}^{K}\left(t,t'\right) \;=\; \frac{i}{2V}\gamma_{\boldsymbol{q}}^2\sum_{\boldsymbol{k}}&\left\{G_{\boldsymbol{k}}^{R}\left(t,t'\right) G_{\boldsymbol{k}-\boldsymbol{q}}^{A}\left(t',t\right) + G_{\boldsymbol{k}}^{A}\left(t,t'\right) G_{\boldsymbol{k}-\boldsymbol{q}}^{R}\left(t',t\right)\right. \\ &\left.+ G_{\boldsymbol{k}}^{K}\left(t,t'\right) G_{\boldsymbol{k}-\boldsymbol{q}}^{K}\left(t',t\right)\right\},\end{aligned} \tag{3.68d}$$

which is shown graphically in Fig. 3.3. Here we neglect the real part $\hat{\Pi}^M$ of the phonon self-energy because it just renormalizes the phonon energy and does not contribute to the broadening of the phonon spectral function, see Eq. (3.65). The WT of the spectral component of the phonon self-energy is

$$\begin{aligned}\Pi_{\boldsymbol{q}}^{I}\left(\tau;\omega\right) \;=\; \frac{i}{2V}\gamma_{\boldsymbol{q}}^2\sum_{\boldsymbol{k}}\int\frac{\mathrm{d}\omega'}{2\pi}&\left\{G_{\boldsymbol{k}}^{I}\left(\tau;\omega+\omega'\right) G_{\boldsymbol{k}-\boldsymbol{q}}^{K}\left(\tau;\omega'\right)\right. \\ &\left.- G_{\boldsymbol{k}}^{K}\left(\tau;\omega+\omega'\right) G_{\boldsymbol{k}-\boldsymbol{q}}^{I}\left(\tau;\omega'\right)\right\}, \tag{3.69}\end{aligned}$$

and with the approximations (3.45, 3.54) which we already used for the magnons we arrive at

$$\Pi_{\boldsymbol{q}}^{I}\left(\tau;\omega\right) = \frac{2\pi}{V}\gamma_{\boldsymbol{q}}^2\sum_{\boldsymbol{k}}\delta\left(\omega + \epsilon_{\boldsymbol{k}-\boldsymbol{q}} - \epsilon_{\boldsymbol{k}}\right)\left\{n_{\boldsymbol{k}-\boldsymbol{q}}\left(\tau\right) - n_{\boldsymbol{k}}\left(\tau\right)\right\}, \tag{3.70}$$

where we use Eq. (3.53) to express the self-energy in terms of the distribution function.
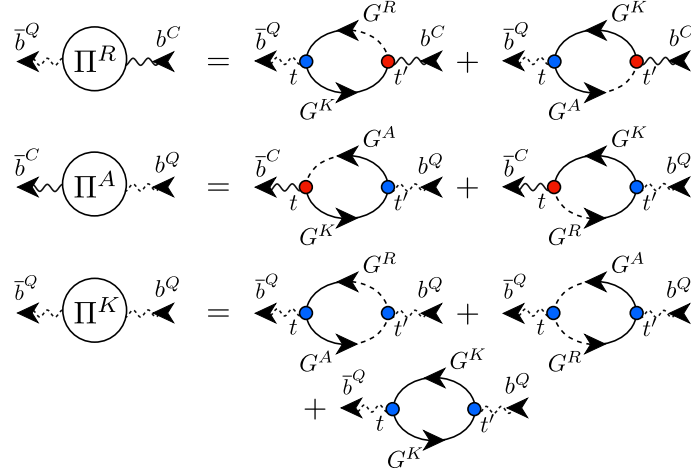
Figure 3.3.: The diagrams of the phonon self-energies. Here in contrast to Fig. 3.1 and Fig. 3.2 complex phonon fields are shown which is indicated by the arrows on the wavy phonon lines. For details of the representation see the caption of the mentioned figures.

Again the expression for the phonon damping Eq. (3.12c) becomes meaningless for finite systems where we have a summation over the momentum. Approximately we can keep the thermodynamical limit $V \to \infty$ for finite systems in the phonon damping only. Moreover in order to reduce the numerical effort for later purpose we replace the magnon particle distribution $n_{\boldsymbol{k}}(\tau)$ by its thermal equilibrium limit which is the Bose function, $n_{\boldsymbol{k}}^{\text{eq}} = b(\epsilon_{\boldsymbol{k}} - \mu)$. At least in some region around equilibrium this approximation is justified. The phonon damping then becomes

$$\Pi_{\boldsymbol{q}}^{I}(\tau;\omega) = (2\pi)^{1-D}\gamma_{\boldsymbol{q}}^{2}\int d^{D}k\,\delta\left(\omega + \epsilon_{\boldsymbol{k}-\boldsymbol{q}} - \epsilon_{\boldsymbol{k}}\right)\left\{b\left(\epsilon_{\boldsymbol{k}-\boldsymbol{q}} - \mu\right) - b\left(\epsilon_{\boldsymbol{k}}\right)\right\},$$

$$(3.71)$$

where D is the dimension of the considered system.

3.4. FRG rate equation

For setting up the FRG for our kinetic equation (3.55) we have to choose a suitable cutoff scheme. Compared to thermal equilibrium we have additional boundary conditions which should be satisfied by the cutoff scheme in the nonequilibrium context. The cutoff scheme has to be chosen such that causality and the fluctuation-dissipation theorem when approaching equilibrium are not violated for the entire flow. It turns out that for our coupled magnon-phonon system a modified hybridization cutoff scheme, which can be found in its standard version in [28, 85], is most convenient. In the standard hybridizition cutoff scheme the infinitesimal regularization η of the inverse propagator in Eqs. (1.67a-1.67c) is replaced by a finite quantity Λ which we

identify as the flow parameter of our FRG equations. Note that the similar out-scattering rate cutoff scheme from Ref. [28], where the regularization in the Keldysh component of the inverse free propagator is kept infinitesimal, violates the fluctuation dissipation theorem in equilibrium. Whereas for fermions the hybridization cutoff works fine it has to be modified for bosons because the spectral function of bosons has the same sign as its frequency argument, see Ref. [29]. Hence for bosons in frequency space we have to do the replacement $\eta \to \Lambda \text{sgn}(\omega)$ instead of $\eta \to \Lambda$ in the inverse free propagators.

The peaked form of the magnon spectral function is crucial to reduce the complexity of time matrices Eq. (1.84) to a problem involving functions of a single time Eq. (3.55). In order to keep this property we introduce the cutoff in the phonon propagators only,

$$F^R_{0,\Lambda,\boldsymbol{q}}(\tau;\omega) = \frac{1}{\omega - \omega_{\boldsymbol{q}} + i\Lambda\text{sgn}\omega}, \tag{3.72a}$$

$$F^A_{0,\Lambda,\boldsymbol{q}}(\tau;\omega) = \frac{1}{\omega - \omega_{\boldsymbol{q}} - i\Lambda\text{sgn}\omega}, \tag{3.72b}$$

$$F^I_{0,\Lambda,\boldsymbol{q}}(\tau;\omega) = \frac{2\Lambda\text{sgn}\omega}{(\omega - \omega_{\boldsymbol{q}})^2 + \left[\Lambda\text{sgn}\omega\right]^2}, \tag{3.72c}$$

$$iF^K_{0,\Lambda,\boldsymbol{q}}(\tau;\omega) = \coth\left(\frac{\beta\omega}{2}\right) F^I_{0,\Lambda,\boldsymbol{q}}(\tau;\omega). \tag{3.72d}$$

With this procedure the magnon spectral function does not smear out artificially and the flow parameter Λ can be associated with an additional damping of the phonons. Therefore the dynamics of the magnons reduces to the non-interacting case for $\Lambda \to \infty$ while the magnon self-energies vanish initially. Since we have introduced the cutoff only for the phonons the magnon propagators are finite at the initial scale and hence also the diagrams shown in Fig. 3.3 contributing to the phononic self-energies are finite initially. There is a similar situation in coupled fermion-boson systems for the bosonic momentum transfer cutoff scheme where all pure boson vertices are finite at the initial scale, see Refs. [6, 70, 86]. In our cutoff scheme the scale-dependent action becomes

$$S_\Lambda[\bar{a}, a, \bar{b}, b] =$$
$$\int dt \int dt' \left\{ \sum_{\boldsymbol{k}} (\bar{a}^C_{\boldsymbol{k}}(t), \bar{a}^Q_{\boldsymbol{k}}(t)) \begin{pmatrix} 0 & (\hat{G}^A_0)^{-1} \\ (\hat{G}^R_0)^{-1} & 2i\eta\hat{g}_0 \end{pmatrix}_{tt'} \begin{pmatrix} a^C_{\boldsymbol{k}}(t') \\ a^Q_{\boldsymbol{k}}(t') \end{pmatrix} \right.$$
$$\left. + \sum_{\boldsymbol{q}} (\bar{b}^C_{\boldsymbol{q}}(t), \bar{b}^Q_{\boldsymbol{q}}(t)) \begin{pmatrix} 0 & (\hat{F}^A_{0,\Lambda})^{-1} \\ (\hat{F}^R_{0,\Lambda})^{-1} & -(\hat{F}^R_{0,\Lambda})^{-1}\hat{F}^K_{0,\Lambda}(\hat{F}^A_{0,\Lambda})^{-1} \end{pmatrix}_{tt'} \begin{pmatrix} b^C_{\boldsymbol{q}}(t') \\ b^Q_{\boldsymbol{q}}(t') \end{pmatrix} \right\}$$
$$- \int dt \frac{1}{\sqrt{V}} \sum_{\boldsymbol{k},\boldsymbol{q}} \gamma_{\boldsymbol{q}} \left[\left(\bar{a}^C_{\boldsymbol{k}+\boldsymbol{q}}a^Q_{\boldsymbol{k}} + \bar{a}^Q_{\boldsymbol{k}+\boldsymbol{q}}a^C_{\boldsymbol{k}}\right) X^C_{\boldsymbol{q}} + \left(\bar{a}^C_{\boldsymbol{k}+\boldsymbol{q}}a^C_{\boldsymbol{k}} + \bar{a}^Q_{\boldsymbol{k}+\boldsymbol{q}}a^Q_{\boldsymbol{k}}\right) X^Q_{\boldsymbol{q}} \right],$$

$$\tag{3.73}$$

see section 1.2. The full phonon propagators are given by

$$F^R_{\Lambda,\boldsymbol{q}}(\tau;\omega) = \frac{1}{\omega - \omega_{\boldsymbol{q}} + i\Lambda\mathrm{sgn}\omega + \frac{i}{2}\Pi^I_{\Lambda,\boldsymbol{q}}(\tau;\omega)}, \tag{3.74a}$$

$$F^A_{\Lambda,\boldsymbol{q}}(\tau;\omega) = \frac{1}{\omega - \omega_{\boldsymbol{q}} - i\Lambda\mathrm{sgn}\omega - \frac{i}{2}\Pi^I_{\Lambda,\boldsymbol{q}}(\tau;\omega)}, \tag{3.74b}$$

$$F^I_{\Lambda,\boldsymbol{q}}(\tau;\omega) = \frac{2\Lambda\mathrm{sgn}\omega + \Pi^I_{\Lambda,\boldsymbol{q}}(\tau;\omega)}{(\omega - \omega_{\boldsymbol{q}})^2 + \left[\Lambda\mathrm{sgn}\omega + \frac{1}{2}\Pi^I_{\Lambda,\boldsymbol{q}}(\tau;\omega)\right]^2}, \tag{3.74c}$$

$$iF^K_{\Lambda,\boldsymbol{q}}(\tau;\omega) = \coth\left(\frac{\beta\omega}{2}\right) F^I_{\Lambda,\boldsymbol{q}}(\tau;\omega), \tag{3.74d}$$

where we have neglected the real part $\Pi^M_{\Lambda,\boldsymbol{q}}(\tau;\omega)$ of the phonon self-energy as in section 3.3.4. The phonon self-energies are still calculated in second order perturbation theory such that, similar to Eq. (3.71), we obtain for the spectral component

$$\Pi^I_{\Lambda,\boldsymbol{q}}(\tau;\omega) = \frac{2\pi}{V}\gamma^2_{\boldsymbol{q}} \sum_{\boldsymbol{k}} \delta\left(\omega + \epsilon_{\boldsymbol{k}-\boldsymbol{q}} - \epsilon_{\boldsymbol{k}}\right) \left\{n_{\Lambda,\boldsymbol{k}-\boldsymbol{q}}(\tau) - n_{\Lambda,\boldsymbol{k}}(\tau)\right\}. \tag{3.75}$$

For finite systems we use the thermodynamic limit for Eq. (3.75) to obtain finite results, see also the discussion at the end of section 3.3.4. In addition we reduce the numerical effort by replacing the magnon particle distribution by its equilibrium value which corresponds to

$$\Pi^I_{\Lambda,\boldsymbol{q}}(\tau;\omega) \to \Pi^I_{\Lambda=0,\boldsymbol{q}}(\tau = \infty;\omega). \tag{3.76}$$

We thus obtain the expression of Eq. (3.71) of the last section for the phonon spectral self-energy.

If we introduce the hybridization function

$$\Lambda_{\boldsymbol{q}}(\tau;\omega) \equiv \Lambda\mathrm{sgn}\omega + \frac{1}{2}\Pi^I_{\Lambda,\boldsymbol{q}}(\tau;\omega), \tag{3.77}$$

the expressions of the real phonon propagators become

$$D^R_{\Lambda,\boldsymbol{q}}(\omega) = \frac{\omega_{\boldsymbol{q}} - i\Lambda_{\boldsymbol{q}}(\tau;\omega)}{\omega^2 - [\omega_{\boldsymbol{q}} - i\Lambda_{\boldsymbol{q}}(\tau;\omega)]^2}, \tag{3.78a}$$

$$D^A_{\Lambda,\boldsymbol{q}}(\omega) = \frac{\omega_{\boldsymbol{q}} + i\Lambda_{\boldsymbol{q}}(\tau;\omega)}{\omega^2 - [\omega_{\boldsymbol{q}} + i\Lambda_{\boldsymbol{q}}(\tau;\omega)]^2}, \tag{3.78b}$$

$$D^I_{\Lambda,\boldsymbol{q}}(\omega) = \frac{\Lambda_{\boldsymbol{q}}(\tau;\omega)}{(\omega - \omega_{\boldsymbol{q}})^2 + \Lambda^2_{\boldsymbol{q}}(\tau;\omega)} + \frac{\Lambda_{\boldsymbol{q}}(\tau;\omega)}{(\omega + \omega_{\boldsymbol{q}})^2 + \Lambda^2_{\boldsymbol{q}}(\tau;\omega)}, \tag{3.78c}$$

$$iD^K_{\Lambda,\boldsymbol{q}}(\omega) = \coth\left(\frac{\beta\omega}{2}\right) D^I_{\Lambda,\boldsymbol{q}}(\omega). \tag{3.78d}$$

For the kinetic equation we use the same approximations as before in perturbation theory. Mainly these are:

3. FRG approach to the thermalization of magnons in YIG

1. We retain only the leading terms in the gradient expansion of the WT for products of time matrices such that they factorize, see Eq. (1.95).

2. We neglect the renormalization of the magnon energies in the kinetic equation.

3. We apply the quasiparticle approximation where the magnon spectral function $\hat{G}^I$ is replaced by the non-interacting one Eq. (3.54).

By introducing the cutoff for magnons only the derivation of the kinetic equation (1.97) does not change and we find for the distribution function that

$$2\partial_\tau n_{\Lambda,\boldsymbol{k}}(\tau) = i\Sigma^K_{\Lambda,\boldsymbol{k}}(\tau;\epsilon_{\boldsymbol{k}}) - \Sigma^I_{\Lambda,\boldsymbol{k}}(\tau;\epsilon_{\boldsymbol{k}})\left[1 + 2n_{\Lambda,\boldsymbol{k}}(\tau)\right], \qquad (3.79)$$

where the magnon particle distribution and self-energies have become cutoff-dependent. In contrast to section 3.3.3 where we calculated the self-energy in perturbation theory here the self-energies are determined by the flow equations such that we obtain a system of three coupled differential equations instead of one. Using a simple truncation where we neglect the flow of the magnon-phonon interaction we have to plug in the bare interactions into the flow equation for the self-energy Eq. (1.127). This yields

$$\partial_\Lambda i\Sigma^K_{\Lambda,\boldsymbol{k}}(\tau;\epsilon_{\boldsymbol{k}}) = \frac{1}{V}\sum_{\boldsymbol{k}'}\left\{\left[1 + n_{\Lambda,\boldsymbol{k}'}(\tau)\right]\dot{W}_{\boldsymbol{k}',\boldsymbol{k}} + \dot{W}_{\boldsymbol{k},\boldsymbol{k}'}n_{\Lambda,\boldsymbol{k}'}(\tau)\right\},$$
$$(3.80a)$$

$$\partial_\Lambda \Sigma^I_{\Lambda,\boldsymbol{k}}(\tau;\epsilon_{\boldsymbol{k}}) = \frac{1}{V}\sum_{\boldsymbol{k}'}\left\{\left[1 + n_{\Lambda,\boldsymbol{k}'}(\tau)\right]\dot{W}_{\boldsymbol{k}',\boldsymbol{k}} - \dot{W}_{\boldsymbol{k},\boldsymbol{k}'}n_{\Lambda,\boldsymbol{k}'}(\tau)\right\},$$
$$(3.80b)$$

where $\dot{W}_{\boldsymbol{k},\boldsymbol{k}'}$ is the partial derivative with respect to Λ of the scale-dependent transition rates,

$$\dot{W}_{\boldsymbol{k},\boldsymbol{k}'} = 2\gamma^2_{\boldsymbol{k}-\boldsymbol{k}'}\dot{D}^I_{\Lambda,\boldsymbol{k}-\boldsymbol{k}'}(\epsilon_{\boldsymbol{k}} - \epsilon_{\boldsymbol{k}'})b(\epsilon_{\boldsymbol{k}} - \epsilon_{\boldsymbol{k}'}). \qquad (3.81)$$

The derivative of the phonon spectral Green's function is

$$\dot{D}^I_{\Lambda,\boldsymbol{q}}(\omega) = \pi\mathrm{sgn}\omega\left[L'_{\Lambda_{\boldsymbol{q}}(\tau;\omega)}(\omega - \omega_{\boldsymbol{q}}) + L'_{\Lambda_{\boldsymbol{q}}(\tau;\omega)}(\omega + \omega_{\boldsymbol{q}})\right], \qquad (3.82)$$

where $L'_\Lambda(\omega)$ is the derivative of the Lorentzian Eq. (3.66),

$$L'_\Lambda(\omega) = \partial_\Lambda\left[\frac{1}{\pi}\frac{\Lambda}{\omega^2 + \Lambda^2}\right] = \frac{1}{\pi}\frac{\omega^2 - \Lambda^2}{(\omega^2 + \Lambda^2)^2}. \qquad (3.83)$$

The flow equations (3.80a, 3.80b) are shown diagrammatically in Fig. 3.4. We now have three coupled partial differential equations (3.79-3.80b) which determine the dynamics of the magnon distribution. Comparing the flow equations (3.80a, 3.80b) with the perturbative expressions for the self-energies Eqs. (3.56a, 3.56b) shows the similar rate structure of the FRG equations and the rate equation of section 3.3.3 except that we here have to deal with the flow-parameter derivatives of the now scale-dependent self-energies and transition rates.
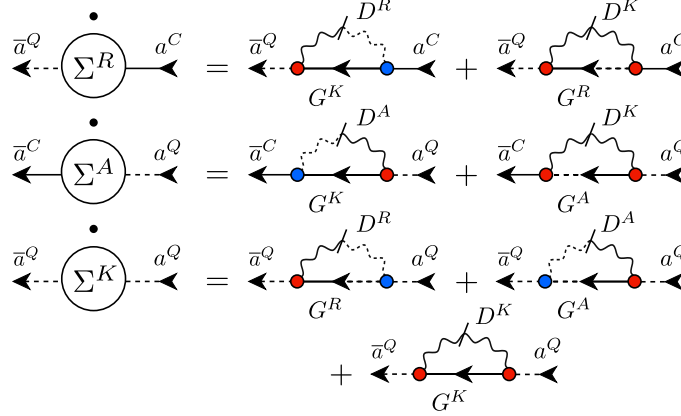
Figure 3.4.: Diagrammatic representation of the flow equations (3.80a, 3.80b). The dot above the magnon self-energies on the left hand side denotes the derivative with respect to the flow parameter Λ. The single-scale propagator is labeled by the slashes at the wavy phonon propagators. Since in our cutoff scheme we introduce the cutoff only in the phonons there are no magnon single-scale propagators. For the other definitions of the shown symbols see Fig. 3.1 and 3.2. Note that except for the flow parameter derivatives the diagrams are the same as in Fig. 3.2.

3.4.1. Particle number conservation

It turns out that the FRG equations (3.79-3.80b) do not conserve the magnon particle number in contrast to the perturbative kinetic equation (3.55), see Eq. (3.59). Since the Hamiltonian (3.1) commutes with the particle number operator $N = \sum_{\boldsymbol{k}} a_{\boldsymbol{k}}^{\dagger} a_{\boldsymbol{k}}$ the particle number indeed should be conserved. By neglecting the real part $\hat{\Sigma}^M$ of the magnon self-energy we lost the opportunity of implementing particle number conservation through varying $\hat{\Sigma}^M$. Hence we introduce a Lagrange multiplier $\mu_\Lambda(t)$ by replacing the time derivative ∂_τ in the kinetic equation (3.79) by the corresponding covariant derivative $\partial_\tau + \mu_\Lambda(t)$ [87], we then find

$$[\partial_\tau + \mu_\Lambda(\tau)]2n_{\Lambda,\boldsymbol{k}}(\tau) = i\Sigma_{\Lambda,\boldsymbol{k}}^K(\tau;\epsilon_{\boldsymbol{k}}) - \Sigma_{\Lambda,\boldsymbol{k}}^I(\tau;\epsilon_{\boldsymbol{k}})\left[1 + 2n_{\Lambda,\boldsymbol{k}}(\tau)\right]. \qquad (3.84)$$

The Lagrange multiplier is determined by the condition of particle number conservation,

$$\partial_\tau N = \sum_{\boldsymbol{k}} \partial_\tau n_{\Lambda,\boldsymbol{k}}(\tau) = 0. \qquad (3.85)$$

Inserting Eq. (3.84) and rearranging terms yields

$$\mu_\Lambda(\tau) = \frac{1}{2N} \sum_{\boldsymbol{k}} \left\{ i\Sigma_{\Lambda,\boldsymbol{k}}^K(\tau;\epsilon_{\boldsymbol{k}}) - \Sigma_{\Lambda,\boldsymbol{k}}^I(\tau;\epsilon_{\boldsymbol{k}})\left[1 + 2n_{\Lambda,\boldsymbol{k}}(\tau)\right] \right\}. \qquad (3.86)$$

Now the kinetic equation (3.84), the flow equations (3.80a,3.80b) and the Lagrange multiplier Eq. (3.86) form a closed system of FRG equations which

can be used to describe the dynamics of a Bose gas coupled to a phonon bath under the condition of particle number conservation. In the next section we apply this nonequilibrium FRG approach to the dynamics of magnons in YIG.

3.5. Application to magnons in YIG

In this section we present numerical solutions of the FRG equations from section 3.4 and compare them to the experimental results of [76]. In the experiment Demidov *et al.* prepared a highly exited initial state by parametric pumping and measured the thermalization of the magnons after turning off the pumping field. After a certain time an enhanced occupation of the ground state can be observed while the total particle number decreases during the whole process after turning off the external field. Our formalism is only capable of describing the thermalization of magnons and occupation of the ground state due to magnon-phonon scattering after the pumping. Since we have a particle number conserving model the decrease of magnons cannot be seen in the numerical results. To model the experiment we use the magnon dispersion Eq. (1.162) with parameters given in section 1.3 and start with a magnon distribution which looks similar to the excited state of the experiment, see Fig. 3.5. In agreement with the experiment we set the film thickness to $d = 5$ μm and it follows that the minima of the dispersion are located at $|k_\parallel| = 5.5 \times 10^4 \, \mathrm{cm}^{-1} \equiv k_{\min}$ and $k_\perp = 0$. For simplicity we consider a square stripe with a length of $L = 4.58 \, \mu$m and work with a truncated reciprocal space such that $|k_\parallel| \leq 41.1 \times 10^4 \, \mathrm{cm}^{-1}$ and $|k_\perp| \leq 13.7 \times 10^4 \, \mathrm{cm}^{-1}$, corresponding to 61×21 points. For solving the coupled partial differential equations (3.80a, 3.80b, 3.84) we have to discretize the time-flow parameter plane and iterate our equations in both directions simultaneously as discussed in [28]. Because of this simultaneous iteration only the simple Euler method [88] can be applied straightforwardly, for example a more advanced Runge-Kutta algorithm [88] needs sampling points inbetween the discretization but the derivatives are not known at these points. To calculate the integral over the delta function of the intrinsic phonon damping Eq. (3.71) we used a two-dimensional adaptation of the tetrahedron method of Ref. [89], see also Appendix A. The time axis was divided into 3240 equidistant steps up to a final time of 700 ns, starting at the initial time of 30 ns. The initial time is chosen to coincide with the end of the pumping pulse in the experiment. Initially the flow parameter Λ_0 was set to $404 \, \Omega_0$, where $\Omega_0 = c k_{\min}$ is the relevant energy scale for the phonon dynamics. As the flow becomes larger for small flow parameters, wherefore we divided the range of Λ into two intervals, $[0, 4\Omega_0]$ and $[4\Omega_0, \Lambda_0]$, both discretized equidistantly with 500 points. The phonon velocity was adjusted to $c = 7.15 \times 10^5 \, \mathrm{cm/s}$, taken from Ref. [90]. The numerical results of the FRG equations are shown in Fig. 3.4 and agree well with the experiment [76] although we did not consider spontaneous $U(1)$-symmetry breaking and the order parameter $\langle a_{\boldsymbol{k}}^C (t) \rangle$ vanishes in our approach. We conclude that
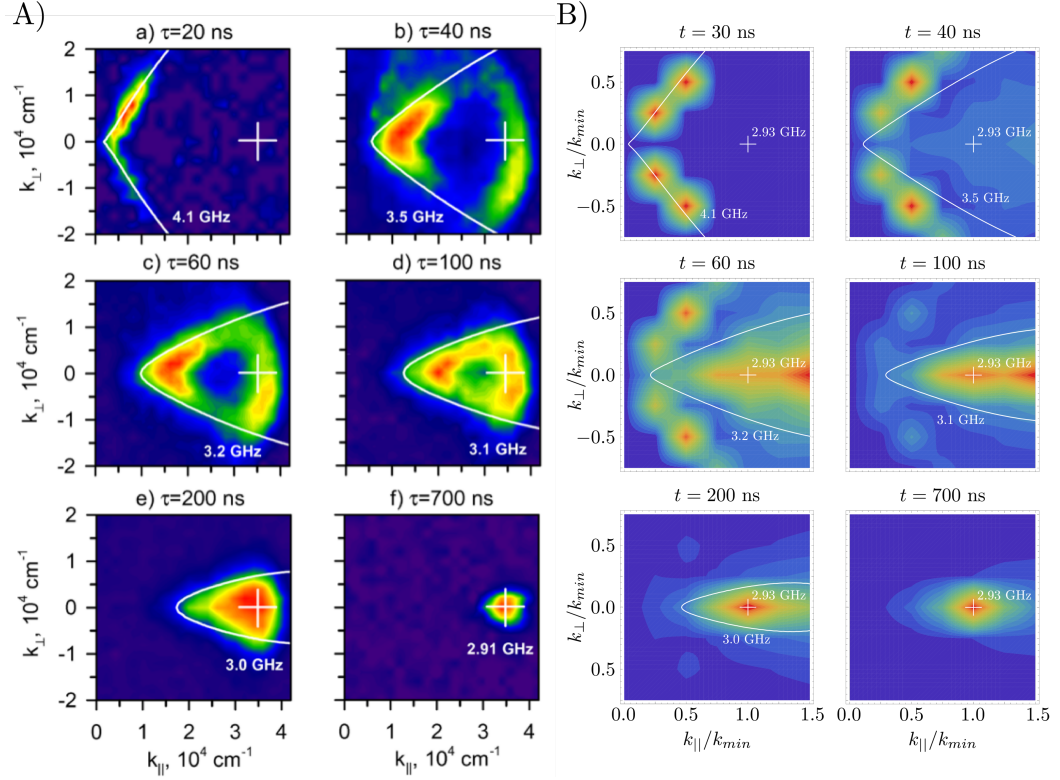
Figure 3.5.: Contour plots of the magnon distribution observed at different times. Plot A) shows experimental data and is taken from [76] (Reprinted with permission from V. E. Demidov, O. Dzyapko, M. Buchmeier, T. Stockhoff, G. Schmitz, G. A. Melkov, and S. O. Demokritov, Phys. Rev. Lett. 101, 257201 (2008). Copyright 2008 by the American Physical Society.). In B) our numerical solution of the FRG equations from section 3.4 is illustrated. The white contour lines mark the wave vectors of a certain energy and the cross refers to the minimum of the dispersion. In contrast to the experiment our calculation started with the initial state after the pumping pulse. Therefore our initial time is set to be 30 ns. Initially we have chosen a state where magnons with an energy of 4.1 GHz and $|k_\perp| < 0.5 k_{\min}$ are occupied equally. This resembles the first shown magnon distribution of the experiment in A). We assume that the asymmetry of this distribution in A) is due to some technical difficulties and is therefore ignored in our calculation. As for the experiment we set the temperature to $T = 300$ K and the static magnetic field to $H = 1000$ Oe. The magnon-phonon coupling γ and the total magnon density ρ has been chosen such that the thermalization time and the equilibrium distribution are comparable to those of Ref. [76], resulting in $\gamma = 2.0 \times 10^{-7}$ cm$\sqrt{\text{GHz}}$ and $\rho = 4.77 \times 10^6 / \mu\text{m}^2$.

the considered processes are sufficient to explain the main features of the re-distribution of magnons in YIG after preparing a highly excited initial state.

3.6. Summary and conclusion

In this chapter we have derived a kinetic equation describing the nonequilibrium dynamics of a Bose gas coupled to a thermal bath of phonons. First we re-derived the perturbative rate equation (3.55). By using the functional Keldysh formalism we could apply the FRG technique which goes beyond the simple second order perturbation theory of section 3.3.3. Our introduced modified hybridization cutoff scheme fulfills desired nonequilibrium boundary conditions and is therefore suitable for describing bosons out of equilibrium. By using certain approximations we got FRG equations (3.80a,3.80b,3.84) which have a similar structure as the perturbative equations, in particular containing the derivatives of the same transition rates Eq. (3.81). The particle number has been fixed by introducing a Lagrange multiplier which is a common procedure in statistical field theory. A similar approach has been used by Jolicoeur and Guillou in Ref. [87]. We have been able to consider finite systems without introducing a phenomenological parameter as in Ref. [82] by taking into account the intrinsic phonon damping which is straightforward in our approach.

Here we summarize the main involved approximation and justify them for the application to magnons in YIG. First of all we retained only the leading order term in the WT of the matrix product of two time matrices assuming that the functions are slowly varying in time and frequency, see Eq. (1.95). This seem to be valid for magnons in YIG since an alternative approach [91, 92] based on a phenomenological Landau-Liftshitz equation and which relies on a similar assumption is highly successful in describing such systems. Furthermore we used a delta-peaked magnon spectral function Eq. (3.54) which corresponds to an infinite lifetime of the magnons. Also this seems to be well justified since magnons behave like well-defined quasiparticle in YIG [30, 36, 61]. Finally we neglected the renormalization of the magnon dispersion by omitting the imaginary part of the magnon distribution function, see section 1.1.7. We implicitly took this effect into account by taking parameters in section 1.3 for the dispersion which were fitted to experimental data.

The numerical results in section 3.5 agree well with the experimental data of Ref. [76]. We conclude that the considered microscopic processes without taking a possible spontaneous $U(1)$-symmetry breaking into account are sufficient to describe the main features of the thermalization process which yield an enhanced occupation of the ground state of magnons in YIG. Nevertheless, in order to model also the pumping phase and the relaxation of the magnon particle number we have to extend our Hamiltonian. We shall consider this in the next chapter.

4. Dynamics of parametrically excited magnons in systems with $U(1)$-symmetry breaking interactions

In this chapter we want to extend the considerations of chapter 3 for the magnon dynamics in yttrium-iron garnet (YIG) to $U(1)$-symmetry breaking magnon-phonon interactions and parametric pumping. Including these mechanisms we can describe the excitation and relaxation of magnons as measured in experiments [36, 37, 38, 39, 40, 76, 77]. The phenomena of parametric resonance [49, 52, 53, 54, 55, 56, 57, 58, 59] is used to inject magnons into YIG and the modeling of this process in the spin-wave framework was already addressed in section 1.3. Starting from a spin model we will show explicitly in section 4.2 that anomalous magnon-phonon interactions, which break the $U(1)$-symmetry, are present in YIG. These interactions are responsible for the relaxation of the magnon particle number to an equilibrium state with zero chemical potential. With a similar model the magnon dynamics including Bose-Einstein condensation has been considered in Ref. [93]. The authors use a certain approximation scheme for the equation of motion based on a nonequilibrium statistical ensemble. At the end they introduce a kind of "two-fluid model" and give results for the condensed and the non-condensed particles only. In contrast our approach permits systematic way of improving approximations and in our numerics wave vector resolved results are accessible.

The challenge of our considerations in this chapter will be the dependence of the normal correlator on the anomalous one which requires an extension of the Keldysh formalism used in chapter 3, see Ref. [28] and section 4.3. In contrast to chapter 3 we will derive a perturbative rate equation only and will not apply the FRG. The magnon-phonon system in YIG is weakly interacting and is described by means of perturbative methods rather well, as we will see in this chapter.

In Ref. [56] a similar model, but without anomalous interactions, was considered to describe the parametric excitation of spin waves. By decoupling equations of motions using the so-called coherent-state representation the authors derived a rate equation of a similar form as the Boltzmann equation. Inspired by Ref. [56] we present a method which provides the derivation of rate equations for Hamiltonians with broken $U(1)$-symmetry via functional

methods. The approximation scheme can be improved by means of the FRG. Within the functional approach the application of the FRG is straightforward but is beyond the scope of this thesis.

In section 4.5 we will show numerical results and compare them to the experiment done by Demokritov *et al.* [40]. The work presented in this chapter is not published yet and was done in collaboration with Andreas Rückriegel and Peter Kopietz.

4.1. Model

A minimal model which includes parametric pumping and $U(1)$-symmetry breaking magnon-phonon interactions is given by

$$
\mathcal{H}(t) = \sum_{\boldsymbol{k}} \left[\epsilon_{\boldsymbol{k}} a_{\boldsymbol{k}}^{\dagger} a_{\boldsymbol{k}} + \frac{\gamma_{\boldsymbol{k}}}{2} e^{-i\omega_0 t} a_{\boldsymbol{k}}^{\dagger} a_{-\boldsymbol{k}}^{\dagger} + \frac{\gamma_{\boldsymbol{k}}^{*}}{2} e^{i\omega_0 t} a_{-\boldsymbol{k}} a_{\boldsymbol{k}} \right] + \sum_{\boldsymbol{q}} \omega_{\boldsymbol{q}} b_{\boldsymbol{q}}^{\dagger} b_{\boldsymbol{q}}
$$

$$
+ \frac{1}{\sqrt{N}} \sum_{\boldsymbol{k},\boldsymbol{q}} \left\{ \Gamma_{\boldsymbol{k},\boldsymbol{q}}^{n} a_{\boldsymbol{k}}^{\dagger} a_{\boldsymbol{k}-\boldsymbol{q}} + \Gamma_{\boldsymbol{k},\boldsymbol{q}}^{\sigma} a_{-\boldsymbol{k}} a_{\boldsymbol{k}-\boldsymbol{q}} + \left(\Gamma_{\boldsymbol{k},\boldsymbol{q}}^{\sigma} \right)^{*} a_{\boldsymbol{k}}^{\dagger} a_{-\boldsymbol{k}+\boldsymbol{q}}^{\dagger} \right\} \left(b_{\boldsymbol{q}} + b_{-\boldsymbol{q}}^{\dagger} \right),
$$

$$
\tag{4.1}
$$

where $a_{\boldsymbol{k}}$ annihilates a magnon with momentum $\boldsymbol{k}$ and $b_{\boldsymbol{q}}$ a phonon with momentum $\boldsymbol{q}$ and so on. For the quadratic magnon part we used the form and the notation of Eq. (1.168), in particular $\epsilon_{\boldsymbol{k}}$ is the magnon dispersion and $\gamma_{\boldsymbol{k}}$ and ω_0 correspond to the amplitude and the frequency of the external microwave pumping field. Pairs of magnons with opposite momenta get excited by the pumping field. In the regime of parametric resonance the energy of an excited magnon pair is close to the frequency of the microwave field ω_0. Therefore the pumping amplitude $\gamma_{\boldsymbol{k}}$ is assumed to be peaked around $\omega_0/2$ such that it is nonzero in the range $\omega_0/2 \pm \Delta$ only. We consider acoustic longitudinal phonons such that the linear dispersion is given by $\omega_{\boldsymbol{q}} = c |\boldsymbol{q}|$, where c is the speed of sound. The normal $\Gamma_{\boldsymbol{k},\boldsymbol{q}}^{n}$ and anomalous $\Gamma_{\boldsymbol{k},\boldsymbol{q}}^{\sigma}$ magnon-phonon interactions will be derived in section 4.2. In order to obtain a time-independent quadratic part of the Hamiltonian we transform to the rotating reference frame. With this transformation the dispersion gets shifted by $-\omega_0/2$ in all transformed modes which yields negative one-particle energies for modes with $\epsilon_{\boldsymbol{k}} < \omega_0/2 - \Delta$. This is an artefact of the transformation and should not be confused with the instability of parametric resonance [45, 56]. The instability occurs in noninteracting systems with parametric pumping where $\gamma_{\boldsymbol{k}} > \epsilon_{\boldsymbol{k}}$ and leads to an unbounded growth of the particle number. In principle the energy renormalization due to interactions can compensate the shift to negative energies but here we do not calculate this effect explicitly. Therefore in contrast to the transformation used in section 1.3.4 we transform the pumped magnon modes in the energy

range$\omega_0/2 \pm \Delta$ only,

$$\mathcal{U}_0\left(t\right) = \exp\left[-\frac{i}{2}\sum_{\boldsymbol{k}}\Delta_{\boldsymbol{k}}\left(\omega_0 t - \varphi_{\boldsymbol{k}}\right)a_{\boldsymbol{k}}^{\dagger}a_{\boldsymbol{k}}\right], \tag{4.2}$$

where $\Delta_{\boldsymbol{k}}$ is one for $\epsilon_{\boldsymbol{k}}$ in the range $\omega_0/2 \pm \Delta$ and zero otherwise,

$$\Delta_{\boldsymbol{k}} = \Theta\left(\epsilon_{\boldsymbol{k}} - \frac{\omega_0}{2} + \Delta\right) - \Theta\left(\epsilon_{\boldsymbol{k}} - \frac{\omega_0}{2} - \Delta\right).$$

In addition the transformation Eq. (4.2) removes the phase of the pumping amplitudes assuming that $\gamma_{\boldsymbol{k}} = |\gamma_{\boldsymbol{k}}|\,e^{i\varphi_{\boldsymbol{k}}}$. The energy renormalization of the pumped modes which compensates the instability of parametric resonance [45, 56] will be taken effectively into account by the requirement that we obtain a desired occupation number during the pumping process, see section 4.5. The transformed Hamiltonian becomes

$$\begin{aligned}
\tilde{\mathcal{H}}(t) &= \mathcal{U}_0^{\dagger}\left(t\right)\left[\mathcal{H}\left(t\right) - i\partial_t\right]\mathcal{U}_0\left(t\right) \\
&= \sum_{\boldsymbol{k}}\left[\tilde{\epsilon}_{\boldsymbol{k}}a_{\boldsymbol{k}}^{\dagger}a_{\boldsymbol{k}} + \frac{|\gamma_{\boldsymbol{k}}|}{2}a_{\boldsymbol{k}}^{\dagger}a_{-\boldsymbol{k}}^{\dagger} + \frac{|\gamma_{\boldsymbol{k}}|}{2}a_{-\boldsymbol{k}}a_{\boldsymbol{k}}\right] \\
&\quad + \sum_{\boldsymbol{q}}\omega_{\boldsymbol{q}}b_{\boldsymbol{q}}^{\dagger}b_{\boldsymbol{q}} + \frac{1}{\sqrt{N}}\sum_{\boldsymbol{k},\boldsymbol{q}}\left(b_{\boldsymbol{q}} + b_{-\boldsymbol{q}}^{\dagger}\right) \\
&\quad \times\left\{\Gamma_{\boldsymbol{k},\boldsymbol{q}}^{n}a_{\boldsymbol{k}}^{\dagger}a_{\boldsymbol{k}-\boldsymbol{q}} + \Gamma_{\boldsymbol{k},\boldsymbol{q}}^{\sigma}\left(t\right)a_{-\boldsymbol{k}}a_{\boldsymbol{k}-\boldsymbol{q}} + \left(\Gamma_{\boldsymbol{k},\boldsymbol{q}}^{\sigma}\left(t\right)\right)^{*}a_{\boldsymbol{k}}^{\dagger}a_{-\boldsymbol{k}+\boldsymbol{q}}^{\dagger}\right\}, \tag{4.3}
\end{aligned}$$

where we have assumed that $\gamma_{-\boldsymbol{k}} = \gamma_{\boldsymbol{k}}$ and define a time dependent anomalous interaction,

$$\begin{aligned}
\Gamma_{\boldsymbol{k},\boldsymbol{q}}^{\sigma}\left(t\right) &= \Gamma_{\boldsymbol{k},\boldsymbol{q}}^{\sigma}\exp\left[\frac{i}{2}\Delta_{\epsilon_{\boldsymbol{k}}}\left(-\omega_0 t + \varphi_{\boldsymbol{k}}\right)\right] \\
&\quad \times\exp\left[\frac{i}{2}\Delta_{\epsilon_{\boldsymbol{k}-\boldsymbol{q}}}\left(-\omega_0 t + \varphi_{\boldsymbol{k}-\boldsymbol{q}}\right)\right]. \tag{4.4}
\end{aligned}$$

The shifted energy is given by

$$\tilde{\epsilon}_{\boldsymbol{k}} = \epsilon_{\boldsymbol{k}} - \Delta_{\boldsymbol{k}}\frac{\omega_0}{2}.$$

In the experiments Refs. [36, 37, 38, 39, 40, 76, 77] also magnon-magnon interactions are relevant but to reduce the numerical effort we neglect these interactions here. As we will see, the essential effects of the experiments are already captured by our model.

4.2. Magnon-phonon interactions

For the derivation of the magnon-phonon interactions we start with the spin model for thin films of YIG Eq. (1.132) which includes exchange J_{ij} and

dipole-dipole interactions $D_{ij}^{\alpha\beta}$. We assume a thin film such that the system is finite in the x-direction and infinite in the y- and z-direction. The phonon degrees of freedom are modeled by

$$H^{\text{pho}} = \sum_{\boldsymbol{q},\lambda} \omega_{\boldsymbol{q},\lambda} b_{\boldsymbol{q}\lambda}^\dagger b_{\boldsymbol{q}\lambda}, \tag{4.5}$$

where we consider acoustic phonons such that for small momenta we have a linear dispersion,

$$\omega_{\boldsymbol{q},\lambda} = c_\lambda \left| \boldsymbol{q} \right|. \tag{4.6}$$

The different longitudinal and transversal phonon modes are labeled by λ and c_λ is the sound velocity. We will restrict our consideration to longitudinal phonon modes which yield the quadratic phonon part of Eq. (4.1),

$$H^{\text{pho}} = \sum_{\boldsymbol{q}} \omega_{\boldsymbol{q}} b_{\boldsymbol{q}}^\dagger b_{\boldsymbol{q}}. \tag{4.7}$$

4.2.1. Spin-phonon interactions

Phonons describe distortions in the lattice such that the actual positions of the spins are given by

$$\boldsymbol{r}_i = \boldsymbol{R}_i + \boldsymbol{X}_i, \tag{4.8}$$

where $\boldsymbol{X}_i$ is a distortion operator describing the deviation from the equilibrium position $\boldsymbol{R}_i$. The distortion operator is quantized in reciprocal space as

$$\boldsymbol{X}_i = \frac{1}{\sqrt{N}} \sum_{\boldsymbol{k}} e^{i\boldsymbol{k}\boldsymbol{R}_i} \boldsymbol{X}_{\boldsymbol{k}}, \tag{4.9a}$$

$$\boldsymbol{X}_{\boldsymbol{k}} = \boldsymbol{e}_{\boldsymbol{k}} \frac{1}{\sqrt{2M\omega_{\boldsymbol{k}}}} \left(b_{\boldsymbol{k}} + b_{-\boldsymbol{k}}^\dagger \right). \tag{4.9b}$$

Using the phase convention of Ref. [94],

$$\boldsymbol{e}_{-\boldsymbol{k}}^* = \boldsymbol{e}_{\boldsymbol{k}}, \tag{4.10}$$

yields

$$\boldsymbol{e}_{\boldsymbol{k}} = i\boldsymbol{k}/\left| \boldsymbol{k} \right|, \tag{4.11}$$

for the phonon polarization vector.

The spin model Eq. (1.132) depends on the position of the spins via the exchange and the dipole-dipole interaction and we have to express the change of the interactions by the distortion operator. Assuming that the spins are close to their equilibrium positions, we can expand the interactions around $\boldsymbol{R}_{ij}$,

$$J_{ij} \approx J\left(\boldsymbol{R}_{ij}\right) + \left(\boldsymbol{X}_{ij} \cdot \boldsymbol{\nabla}_{\boldsymbol{r}}\right) J\left(\boldsymbol{r}\right)\big|_{\boldsymbol{r}=\boldsymbol{R}_{ij}}, \tag{4.12a}$$

$$D_{ij}^{\alpha\beta} \approx D^{\alpha\beta}\left(\boldsymbol{R}_{ij}\right) + \left(\boldsymbol{X}_{ij} \cdot \boldsymbol{\nabla}_{\boldsymbol{r}}\right) D^{\alpha\beta}\left(\boldsymbol{r}\right)\big|_{\boldsymbol{r}=\boldsymbol{R}_{ij}}, \tag{4.12b}$$

where we have introduced the abbreviation $\boldsymbol{X}_{ij} = \boldsymbol{X}_i - \boldsymbol{X}_j$. We are interested in the magnon-phonon interaction where the magnon density couples to a single phonon operator. To obtain these interactions it is sufficient to expand to first order in $\boldsymbol{X}_{ij}$ because the distortion operator is linear in the phonon operators, see Eq. (4.9b). Hence we can restrict our consideration to the interaction part

$$H_{\mathrm{spin}}^{\mathrm{1pho}} = -\frac{1}{2} \sum_{ij} \sum_{\alpha,\beta} \left[J_{ij}^{(1)} \delta^{\alpha\beta} + D_{ij}^{\alpha\beta(1)} \right] S_i^\alpha S_j^\beta \qquad (4.13)$$

of the full Hamiltonian (1.132), where we define

$$J_{ij}^{(1)} = \left(\hat{\boldsymbol{X}}_{ij} \cdot \boldsymbol{\nabla}_{\boldsymbol{r}} \right) J\left(\boldsymbol{r}\right)\big|_{\boldsymbol{r}=\boldsymbol{R}_{ij}}, \qquad (4.14a)$$

$$D_{ij}^{\alpha\beta(1)} = \left(\hat{\boldsymbol{X}}_{ij} \cdot \boldsymbol{\nabla}_{\boldsymbol{r}} \right) D^{\alpha\beta}\left(\boldsymbol{r}\right)\big|_{\boldsymbol{r}=\boldsymbol{R}_{ij}}. \qquad (4.14b)$$

For example experimental data for the dispersion are reproduced rather well by retaining only the lowest magnon mode in the x-direction for the relevant energy scales of experiments, see Refs. [31, 32, 33]. Analogously we will also consider the lowest mode in the x-direction of the phonons only. To obtain the lowest mode approximation, we use the uniform mode approximation (1.141).

4.2.2. Spin-wave theory

In order to establish the spin-wave theory we assume $\hat{\boldsymbol{m}}_i$ to be a unit vector pointing in the direction of the spins in the classical ground state and $\boldsymbol{e}_i^{(1)}$, $\boldsymbol{e}_i^{(2)}$ to be arbitrary unit vectors which form an orthogonal triad with $\hat{\boldsymbol{m}}_i$. In the classical ground state the spins all point in the same direction for ferromagnetic interactions and hence $\hat{\boldsymbol{m}}_i = \hat{\boldsymbol{m}}$ and $\boldsymbol{e}_i^{(1/2)} = \boldsymbol{e}^{(1/2)}$ are independent of the spin position. We choose the coordinate system such that $\hat{\boldsymbol{m}} = \boldsymbol{e}_z$ and $\boldsymbol{e}^{(1/2)} = \boldsymbol{e}_{x/y}$. Now we can bosonize the spin operators by means of the Holstein-Primakoff transformation Eqs. (1.134a-1.134c). Retaining only the zeroth order term of the $1/S$ expansion and transforming the spin-phonon Hamiltonian $H_{\mathrm{spin}}^{\mathrm{1pho}}$ we obtain for the relevant part $H_{\mathrm{2mag}}^{\mathrm{1pho}}$ which involves one phonon and two magnons,

$$\begin{aligned} H_{\mathrm{2mag}}^{\mathrm{1pho}} = \ & -\frac{S}{2} \sum_{ij} \Bigg\{ \left(J_{ij}^{(1)} + D_{ij}^{zz(1)} \right) \left(-n_i - n_j \right) \\ & + \left(J_{ij}^{(1)} + \frac{1}{2} D_{ij}^{xx(1)} + \frac{1}{2} D_{ij}^{yy(1)} \right) \left(b_i^\dagger b_j + b_j^\dagger b_i \right) \\ & + \left(\frac{1}{2} D_{ij}^{xx(1)} - \frac{1}{2} D_{ij}^{yy(1)} \right) \left(b_i b_j + b_i^\dagger b_j^\dagger \right) \Bigg\}, \qquad (4.15) \end{aligned}$$

where we assume that the gradient of the dipole tensor is diagonal,

$$D_{ij}^{\alpha\beta(1)} = D_{ij}^{\alpha\alpha(1)} \delta^{\alpha\beta}. \qquad (4.16)$$

Later we will see that this relation is satisfied for long wavelengths.

4.2.3. Fourier transformation

Now it is convenient to perform a discrete Fourier transformation. The uniform mode approximation (1.141) is equivalent to assuming periodic boundary conditions in all directions and setting the momentum in the finite x-direction to zero, $k_x = 0$, see Refs. [31, 32, 43]. For a function f_i we define the discrete Fourier transformation by

$$f_{\boldsymbol{k}} = \frac{1}{\sqrt{N}} \sum_i e^{-i\boldsymbol{k}\cdot\boldsymbol{R}_i} f_i, \tag{4.17}$$

and the inverse transformation by

$$f_i = \frac{1}{\sqrt{N}} \sum_{\boldsymbol{k}} e^{i\boldsymbol{k}\cdot\boldsymbol{R}_i} f_{\boldsymbol{k}}, \tag{4.18}$$

where the momentum sum runs over the first Brillouin zone and the number of lattice sites is N. The Fourier transforms of the first order terms of the interaction expansions Eqs. (4.14a, 4.14b) become

$$
\begin{aligned}
J_{\boldsymbol{k},\boldsymbol{k}'}^{(1)} &= \frac{1}{N} \sum_{i,j} e^{-i\boldsymbol{k}\cdot\boldsymbol{R}_i} e^{-i\boldsymbol{k}'\cdot\boldsymbol{R}_j} J_{ij}^{(1)} \\
&= -\frac{1}{\sqrt{N}} \boldsymbol{X}_{\boldsymbol{k}+\boldsymbol{k}'} \cdot \left(\boldsymbol{J}_{\boldsymbol{k}}^{(1)} + \boldsymbol{J}_{\boldsymbol{k}'}^{(1)} \right),
\end{aligned} \tag{4.19a}
$$

$$
\begin{aligned}
D_{\boldsymbol{k},\boldsymbol{k}'}^{\alpha\beta(1)} &= \frac{1}{N} \sum_{i,j} e^{-i\boldsymbol{k}\cdot\boldsymbol{R}_i} e^{-i\boldsymbol{k}'\cdot\boldsymbol{R}_j} D_{ij}^{\alpha\beta(1)} \\
&= -\frac{1}{\sqrt{N}} \boldsymbol{X}_{\boldsymbol{k}+\boldsymbol{k}'} \left(\boldsymbol{D}_{\boldsymbol{k}}^{\alpha\beta(1)} + \boldsymbol{D}_{\boldsymbol{k}'}^{\alpha\beta(1)} \right),
\end{aligned} \tag{4.19b}
$$

where we have used the fact that the gradient of the interaction is antisymmetric in the momentum,

$$
\begin{aligned}
\boldsymbol{J}_{-\boldsymbol{k}}^{(1)} &= -\boldsymbol{J}_{\boldsymbol{k}}^{(1)}, \tag{4.20a} \\
\boldsymbol{D}_{-\boldsymbol{k}}^{\alpha\beta(1)} &= -\boldsymbol{D}_{\boldsymbol{k}}^{\alpha\beta(1)}, \tag{4.20b}
\end{aligned}
$$

which can be seen from their definitions,

$$
\begin{aligned}
\boldsymbol{J}_{\boldsymbol{k}}^{(1)} &= \sum_{\boldsymbol{R}_{ij}} e^{-i\boldsymbol{k}\cdot\boldsymbol{R}_{ij}} \left.\boldsymbol{\nabla}_{\boldsymbol{r}} J(\boldsymbol{r})\right|_{\boldsymbol{r}=\boldsymbol{R}_{ij}}, \tag{4.21a} \\
\boldsymbol{D}_{\boldsymbol{k}}^{\alpha\beta(1)} &= \sum_{\boldsymbol{R}_{ij}} e^{-i\boldsymbol{k}\cdot\boldsymbol{R}_{ij}} \left.\boldsymbol{\nabla}_{\boldsymbol{r}} D^{\alpha\beta}(\boldsymbol{r})\right|_{\boldsymbol{r}=\boldsymbol{R}_{ij}}. \tag{4.21b}
\end{aligned}
$$

As in section 1.3 we choose the normalization such that the final factors of N come out correct from the beginning. For the interaction part $H_{2\text{mag}}^{1\text{pho}}$ of the

Hamiltonian expressed by the Fourier transforms we find that

$$
\begin{aligned}
H_{2\text{mag}}^{1\text{pho}} = \frac{S}{2}\frac{1}{\sqrt{N}}\sum_{\boldsymbol{k},\boldsymbol{k}'}\boldsymbol{X}_{\boldsymbol{k}'}\cdot\Bigg\{&\Big[-2\boldsymbol{J}_0^{(1)} + 2\boldsymbol{J}_{\boldsymbol{k}}^{(1)} - 2\boldsymbol{J}_{\boldsymbol{k}'}^{(1)} + 2\boldsymbol{J}_{\boldsymbol{k}'-\boldsymbol{k}}^{(1)}\\
&+\boldsymbol{D}_{\boldsymbol{k}}^{xx(1)} + \boldsymbol{D}_{\boldsymbol{k}'-\boldsymbol{k}}^{xx(1)} + \boldsymbol{D}_{\boldsymbol{k}}^{yy(1)} + \boldsymbol{D}_{\boldsymbol{k}'-\boldsymbol{k}}^{yy(1)} - 2\boldsymbol{D}_{\boldsymbol{k}'}^{zz(1)} - 2\boldsymbol{D}_0^{zz(1)}\Big]b_{\boldsymbol{k}}^\dagger b_{\boldsymbol{k}-\boldsymbol{k}'}\\
&+\frac{1}{2}\Big[\boldsymbol{D}_{\boldsymbol{k}}^{xx(1)} + \boldsymbol{D}_{\boldsymbol{k}'-\boldsymbol{k}}^{xx(1)} - \boldsymbol{D}_{\boldsymbol{k}}^{yy(1)} - \boldsymbol{D}_{\boldsymbol{k}'-\boldsymbol{k}}^{yy(1)}\Big]\Big[b_{-\boldsymbol{k}}b_{\boldsymbol{k}-\boldsymbol{k}'} + b_{\boldsymbol{k}}^\dagger b_{-\boldsymbol{k}+\boldsymbol{k}'}^\dagger\Big]\Bigg\}.
\end{aligned}
\tag{4.22}
$$

Next we have to calculate the gradient of the interactions $\boldsymbol{J}_{\boldsymbol{k}}^{(1)}$ and $\boldsymbol{D}_{\boldsymbol{k}}^{\alpha\beta(1)}$. Note that when setting $k_x = 0$ the x-component distortion operator Eq. (4.9b) becomes zero and according to the interaction part Eq. (4.22) of the Hamiltonian we do not have to calculate the x-component of $\boldsymbol{J}_{\boldsymbol{k}}^{(1)}$ and $\boldsymbol{D}_{\boldsymbol{k}}^{\alpha\beta(1)}$. Therefore from now on we can restrict our considerations to a two-dimensional system where we neglect the x-direction.

For $\boldsymbol{J}_{\boldsymbol{k}}^{(1)}$ we have to assume some spatial dependence of the exchange interaction. According to [32] a realistic ansatz is given by $J(\boldsymbol{r}) = Je^{-\frac{\kappa}{a}(r-a)}$, with the lattice constant a and positive constants κ and J. The Fourier transform of the gradient,

$$
\boldsymbol{\nabla}J(\boldsymbol{r}) = -\frac{\kappa}{a}Je^{-\frac{\kappa}{a}(r-a)}\frac{\boldsymbol{r}}{r}
\tag{4.23}
$$

becomes [95]

$$
\begin{aligned}
\boldsymbol{J}_{\boldsymbol{k}}^{(1)} &= \frac{1}{\sqrt{N}}\sum_{\boldsymbol{R}_{ij}}e^{-i\boldsymbol{k}\cdot\boldsymbol{R}_{ij}}\boldsymbol{\nabla}J(\boldsymbol{r})\\
&= 2i\frac{1}{\sqrt{N}}\frac{\kappa}{a}J\begin{pmatrix}\sin[k_y a]\\ \sin[k_z a]\end{pmatrix}\\
&\approx 2i\frac{1}{\sqrt{N}}\kappa J\boldsymbol{k},
\end{aligned}
\tag{4.24}
$$

where we have approximated the sum to $\boldsymbol{R}_{ij} = \pm a\boldsymbol{e}_y, \pm a\boldsymbol{e}_z$ which corresponds to a next nearest neighbor exchange interaction. In the last line we assume that $|\boldsymbol{k}| \ll \pi/a$ and retain only the first order term of an expansion in $\boldsymbol{k}$. The contribution of the exchange interaction to the magnon-phonon interactions cancels in this limit which can be seen by inserting Eq. (4.24) into Eq. (4.22). It turns out that the dipole-dipole interaction is the dominant part for the magnon-phonon interactions for long wavelengths.

The dipole-dipole interaction is a long-range interaction and for the gradient of the dipole tensor $\boldsymbol{D}_{\boldsymbol{k}}^{\alpha\beta(1)}$ we can take the thermodynamic limit, $\sum_{y_{ij}} \rightarrow \frac{1}{a}\int dy$ and so on. We find that

$$
\begin{aligned}
\boldsymbol{D}_{\boldsymbol{k}}^{\alpha\beta(1)} &= \frac{1}{a^2}\int d^2 r e^{-i\boldsymbol{k}\cdot\boldsymbol{r}}\boldsymbol{\nabla}_{\boldsymbol{r}}D^{\alpha\beta}(\boldsymbol{r})\\
&= i\boldsymbol{k}D_{\boldsymbol{k}}^{\alpha\beta},
\end{aligned}
\tag{4.25}
$$

where $D_{\boldsymbol{k}}^{\alpha\beta}$ is the dipolar tensor in the uniform mode approximation Eqs. (1.150a-1.150e). In the limit $|\boldsymbol{k}| \ll \pi/a$ we can approximate the form factor Eq. (1.151) by

$$f_{\boldsymbol{k}} \approx \frac{1 - 1 + kd}{kd} = 1, \tag{4.26}$$

which yields

$$D_{\boldsymbol{k}}^{yy} = D_{\boldsymbol{k}}^{zz} = \frac{1}{\sqrt{N}} \frac{4\pi\mu^2}{3a^3} \equiv D, \tag{4.27a}$$

$$D_{\boldsymbol{k}}^{xx} = -2D, \tag{4.27b}$$

$$D_{\boldsymbol{k}}^{zy} = 0. \tag{4.27c}$$

Inserting into the interaction part $H_{2\text{mag}}^{1\text{pho}}$ of the Hamiltonian we find that

$$H_{2\text{mag}}^{1\text{pho}} = \frac{\Gamma}{\sqrt{N}} \sum_{\boldsymbol{k},\boldsymbol{q}} \sqrt{\omega_{\boldsymbol{q}}} \left\{ a_{\boldsymbol{k}}^\dagger a_{\boldsymbol{k}-\boldsymbol{q}} + \frac{1}{2} \left[a_{-\boldsymbol{k}} a_{\boldsymbol{k}-\boldsymbol{q}} + a_{\boldsymbol{k}}^\dagger a_{-\boldsymbol{k}+\boldsymbol{q}}^\dagger \right] \right\} \left(b_{\boldsymbol{q}} + b_{-\boldsymbol{q}}^\dagger \right), \tag{4.28}$$

where the interaction strength Γ is given by

$$\Gamma = \frac{3SD}{2\sqrt{2Mc}}. \tag{4.29}$$

Here we can see that the magnon-phonon interactions are of the form used in chapter 3 and that the $U(1)$-symmetry breaking interactions are of the same order of magnitude a the symmetric one.

4.2.4. Bogoliubov transformation

In order to diagonalize the quadratic time independent part of the spin-wave Hamiltonian we perform a Bogoliubov transformation Eq. (1.155). In the notation of this chapter it acquires the form

$$\begin{pmatrix} a_{\boldsymbol{k}} \\ a_{-\boldsymbol{k}}^\dagger \end{pmatrix} = \begin{pmatrix} u_{\boldsymbol{k}} & -v_{\boldsymbol{k}} \\ -v_{\boldsymbol{k}}^* & u_{\boldsymbol{k}} \end{pmatrix} \begin{pmatrix} \alpha_{\boldsymbol{k}} \\ \alpha_{-\boldsymbol{k}}^\dagger \end{pmatrix}, \tag{4.30}$$

where the transformation coefficients are given by Eqs.(1.159, 1.160). When relabeling the operators by $\alpha \to a$ we obtain for the Hamiltonian

$$\begin{aligned} H_{2\text{mag}}^{1\text{pho}} = {} & \frac{\Gamma}{\sqrt{N}} \sum_{\boldsymbol{k},\boldsymbol{q}} \sqrt{\omega_{\boldsymbol{q}}} \left(u_{\boldsymbol{k}} + v_{\boldsymbol{k}} \right) \left(u_{\boldsymbol{k}-\boldsymbol{q}} + v_{\boldsymbol{k}-\boldsymbol{q}} \right) \\ & \times \left\{ a_{\boldsymbol{k}}^\dagger a_{\boldsymbol{k}-\boldsymbol{q}} + \frac{1}{2} a_{-\boldsymbol{k}} a_{\boldsymbol{k}-\boldsymbol{q}} + \frac{1}{2} a_{\boldsymbol{k}}^\dagger a_{-\boldsymbol{k}+\boldsymbol{q}}^\dagger \right\} \left(b_{\boldsymbol{q}} + b_{-\boldsymbol{q}}^\dagger \right). \end{aligned} \tag{4.31}$$

4.3. Functional Keldysh formalism for systems with broken $U(1)$-symmetry

In the introduction to the functional Keldysh formalism in section 1.1 we considered the case in which anomalous correlations like $\left\langle a_{\boldsymbol{k}}^{\dagger}(t) a_{\boldsymbol{k}}^{\dagger}(t') \right\rangle$ were vanishing. In systems with broken $U(1)$-symmetry the anomalous correlations also become nonzero and the theory has to be extended, see Ref. [28]. For introducing this extension we mainly adapt the description of Ref. [28] to the model Eq. (4.3). Our goal is to determine the normal and the anomalous distribution functions,

$$
\begin{align}
n_{\boldsymbol{k}}(t) &= \left\langle a_{\boldsymbol{k}}^{\dagger}(t) a_{\boldsymbol{k}}(t) \right\rangle, \tag{4.32a} \\
p_{\boldsymbol{k}}(t) &= \left\langle a_{-\boldsymbol{k}}(t) a_{\boldsymbol{k}}(t) \right\rangle. \tag{4.32b}
\end{align}
$$

At the initial time t_0 these functions are given by the initial conditions and for simplicity we assume that they are symmetric under $\boldsymbol{k} \to -\boldsymbol{k}$. It follows that all correlation functions, as for example the Green's functions, also have this symmetry. We have to keep in mind this assumption when using the resulting equations for numerical calculations.

4.3.1. Keldysh action

Let us define a magnon superfield by

$$
\Phi_{\boldsymbol{k}}^{\lambda}(t) = \begin{pmatrix} a_{\boldsymbol{k}}^{\lambda}(t) \\ \bar{a}_{-\boldsymbol{k}}^{\lambda}(t) \end{pmatrix}, \tag{4.33}
$$

where the superscript $\lambda = C, Q$ refers either to the classical or the quantum component of the field. The corresponding space of the two-component vector $\Phi_{\boldsymbol{k}}^{\lambda}(t)$ we will call flavor space. The superfield allows us to write down the Gaussian part of the Keldysh action in compact form,

$$
\begin{aligned}
S_0\left[\bar{a}, a, \bar{b}, b\right] = \int \mathrm{d}t \int \mathrm{d}t' \Bigg\{ & \\
\frac{1}{2} \sum_{\boldsymbol{k}} \begin{pmatrix} \Phi_{\boldsymbol{k}}^{C}(t), & \Phi_{\boldsymbol{k}}^{Q}(t) \end{pmatrix} \begin{pmatrix} 0 & (\hat{G}_0^A)^{-1} \\ (\hat{G}_0^R)^{-1} & 2i\eta\hat{g}_0 \end{pmatrix}_{tt'} & \begin{pmatrix} \Phi_{-\boldsymbol{k}}^{C}(t') \\ \Phi_{-\boldsymbol{k}}^{Q}(t') \end{pmatrix} \\
+ \sum_{\boldsymbol{k}} \begin{pmatrix} \bar{b}_{\boldsymbol{q}}^{C}(t), & \bar{b}_{\boldsymbol{q}}^{Q}(t) \end{pmatrix} \begin{pmatrix} 0 & (F_0^A)^{-1} \\ (F_0^R)^{-1} & 2i\eta\hat{f}_0 \end{pmatrix}_{tt'} & \begin{pmatrix} b_{\boldsymbol{q}}^{C}(t') \\ b_{\boldsymbol{q}}^{Q}(t') \end{pmatrix} \Bigg\}, \tag{4.34}
\end{aligned}
$$

where the phonon part has not changed compared to the action Eq. (3.2) but where the magnon part has a more complex structure. Due to the anomalous correlations the components of the non-interacting inverse magnon propagator,

$$
\boldsymbol{G}_0^{-1} = \begin{pmatrix} 0 & (\hat{G}_0^A)^{-1} \\ (\hat{G}_0^R)^{-1} & 2i\eta\hat{g}_0 \end{pmatrix}, \tag{4.35}
$$

4. Dynamics of pumped magnons with $U(1)$-symmetry breaking interactions

have a 2×2 matrix structure themselves. In this chapter a magnon quantity labeled with a hat refers to a matrix in flavor and time space. The off-diagonal elements are given by

$$
\begin{aligned}
(\hat{G}_0^R)^{-1} &= \hat{D}_0 - i\eta\hat{Z}, & (4.36\text{a})\\
(\hat{G}_0^A)^{-1} &= \hat{D}_0 + i\eta\hat{Z}, & (4.36\text{b})
\end{aligned}
$$

where the second terms are regularizations. We have introduced the matrix $\hat{Z}$ in time and flavor space by

$$
\left[\hat{Z}\right]_{\boldsymbol{k},tt'} = \delta\left(t - t'\right) Z, \tag{4.37}
$$

and the inverse propagator without regularization by

$$
\left[\hat{D}_0\right]_{\boldsymbol{k},tt'} = Z\left[-i\delta'\left(t - t'\right) + \delta\left(t - t'\right) M_{\boldsymbol{k}}\right], \tag{4.38}
$$

where $\delta'\left(t\right) = \partial_t \delta\left(t\right)$ is the derivative of the delta function. The matrices in flavor space $M_{\boldsymbol{k}}$ and Z are given by

$$
\begin{aligned}
M_{\boldsymbol{k}} &= \begin{pmatrix} \tilde{\epsilon}_{\boldsymbol{k}} & |\gamma_{\boldsymbol{k}}| \\ -|\gamma_{\boldsymbol{k}}| & -\tilde{\epsilon}_{\boldsymbol{k}} \end{pmatrix}, & (4.39\text{a})\\
Z &= \begin{pmatrix} 0 & 1 \\ -1 & 0 \end{pmatrix}. & (4.39\text{b})
\end{aligned}
$$

The explicit expression of the bottom right diagonal element of $\boldsymbol{G}_0^{-1}$, we will determine when we calculate the free propagators in section 4.3.3. From the requirement that

$$
\boldsymbol{G}_0^{-1}\boldsymbol{G}_0 = \boldsymbol{I}, \tag{4.40}
$$

we can already see that

$$
2i\eta\hat{g}_0 = -(\hat{G}_0^R)^{-1}\hat{G}_0^K(\hat{G}_0^A)^{-1}. \tag{4.41}
$$

The identity matrix in Keldysh, flavor and time space is defined by

$$
\boldsymbol{I} = \begin{pmatrix} \hat{I} & 0 \\ 0 & \hat{I} \end{pmatrix}, \tag{4.42}
$$

with

$$
\left[\hat{I}\right]_{\boldsymbol{k},tt'} = \begin{pmatrix} \delta\left(t - t'\right) & 0 \\ 0 & \delta\left(t - t'\right) \end{pmatrix}. \tag{4.43}
$$

Taking into account the anomalous interaction $\Gamma_{\boldsymbol{k},\boldsymbol{q}}^{\sigma}$ we have six additional vertices compared to the action Eq. (3.2), see Fig. 4.1, and the interacting

88
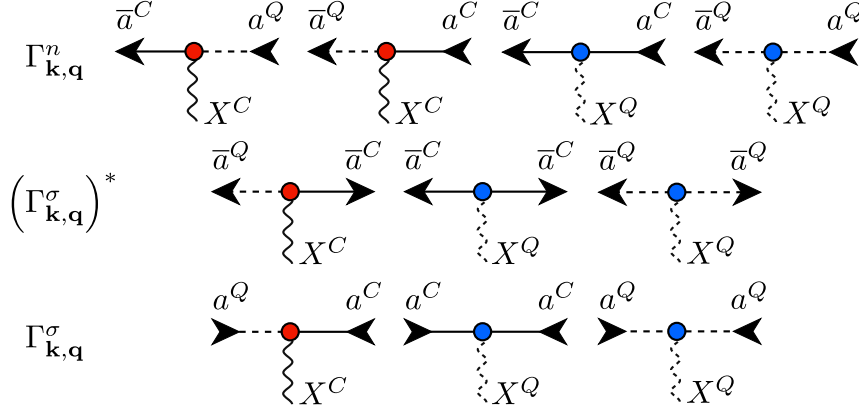
Figure 4.1.: Diagrammatic representation of the vertices of the Keldysh action Eq. (4.44). The first line corresponds to the normal interaction $\Gamma^n_{\mathbf{k,q}}$ and the last two lines to the anomalous interaction $\Gamma^\sigma_{\mathbf{k,q}}$. Pointing away from the vertex, the straight lines represent the complex conjugated magnon fields, and otherwise just the fields. The wavy lines correspond to the phonon fields. The classical components are denoted by solid lines and the quantum components by dashed lines.

part of the Keldysh action becomes

$$
S_1\left[\bar{a}, a, \bar{b}, b\right] = \int \mathrm{d}t \frac{1}{\sqrt{V}} \sum_{\mathbf{k,q}} \Gamma^n_{\mathbf{k,q}}
$$
$$
\times \left[\left(\bar{a}^{\mathrm{C}}_{\mathbf{k+q}} a^{\mathrm{Q}}_{\mathbf{k}} + \bar{a}^{\mathrm{Q}}_{\mathbf{k+q}} a^{\mathrm{C}}_{\mathbf{k}}\right) X^{\mathrm{C}}_{\mathbf{q}} + \left(\bar{a}^{\mathrm{C}}_{\mathbf{k+q}} a^{\mathrm{C}}_{\mathbf{k}} + \bar{a}^{\mathrm{Q}}_{\mathbf{k+q}} a^{\mathrm{Q}}_{\mathbf{k}}\right) X^{\mathrm{Q}}_{\mathbf{q}}\right]
$$
$$
+ \int \mathrm{d}t \frac{1}{\sqrt{V}} \sum_{\mathbf{k,q}} \left(\Gamma^\sigma_{\mathbf{k,q}}(t)\right)^* \left[2\bar{a}^{\mathrm{Q}}_{\mathbf{k}} \bar{a}^{\mathrm{C}}_{\mathbf{-k-q}} X^{\mathrm{C}}_{\mathbf{q}} + \left(\bar{a}^{\mathrm{C}}_{\mathbf{k}} \bar{a}^{\mathrm{C}}_{\mathbf{-k-q}} + \bar{a}^{\mathrm{Q}}_{\mathbf{k}} \bar{a}^{\mathrm{Q}}_{\mathbf{-k-q}}\right) X^{\mathrm{Q}}_{\mathbf{q}}\right]
$$
$$
+ \int \mathrm{d}t \frac{1}{\sqrt{V}} \sum_{\mathbf{k,q}} \Gamma^\sigma_{\mathbf{k,q}}(t) \left[2a^{\mathrm{Q}}_{\mathbf{-k}} a^{\mathrm{C}}_{\mathbf{k+q}} X^{\mathrm{C}}_{\mathbf{-q}} + \left(a^{\mathrm{C}}_{\mathbf{-k}} a^{\mathrm{C}}_{\mathbf{k+q}} + a^{\mathrm{Q}}_{\mathbf{-k}} a^{\mathrm{Q}}_{\mathbf{k+q}}\right) X^{\mathrm{Q}}_{\mathbf{-q}}\right],
$$
$$
(4.44)
$$

where the time arguments of all fields are the same and we therefore omitted them.

4.3.2. Green's functions

For convenience we define the magnon Green's functions in the way that the following the symmetry relations are fulfilled,

$$
\boldsymbol{G}^T = \boldsymbol{G}, \tag{4.45}
$$

4. Dynamics of pumped magnons with $U(1)$-symmetry breaking interactions

and

$$(\hat{G}^R)^T = \hat{G}^A, \tag{4.46a}$$

$$(\hat{G}^K)^T = \hat{G}^K, \tag{4.46b}$$

where depending on the context T denotes transposition in Keldysh, flavor and time space. The full magnon propagator is given by

$$\boldsymbol{G} = \begin{pmatrix} \hat{G}^K & \hat{G}^R \\ \hat{G}^A & 0 \end{pmatrix}, \tag{4.47}$$

and the elements in Keldysh space by

$$\hat{G}^R = \begin{pmatrix} \hat{p}^R & \hat{g}^R \\ (\hat{g}^R)^* & (\hat{p}^R)^* \end{pmatrix}, \tag{4.48a}$$

$$\hat{G}^A = \begin{pmatrix} \hat{p}^A & \hat{g}^A \\ (\hat{g}^A)^* & (\hat{p}^A)^* \end{pmatrix}, \tag{4.48b}$$

$$\hat{G}^K = \begin{pmatrix} \hat{p}^K & \hat{g}^K \\ -(\hat{g}^K)^* & -(\hat{p}^K)^* \end{pmatrix}, \tag{4.48c}$$

where we have introduced the magnon Green's functions in momentum and time space. The normal components $\hat{g}^R$, $\hat{g}^A$ and $\hat{g}^K$ correspond to the magnon Green's functions Eqs. (3.13a-3.13c) defined in chapter 3,

$$ig_{\boldsymbol{k}}^R(t,t') = \left\langle a_{\boldsymbol{k}}^C(t)\bar{a}_{\boldsymbol{k}}^Q(t') \right\rangle, \tag{4.49a}$$

$$ig_{\boldsymbol{k}}^A(t,t') = \left\langle a_{\boldsymbol{k}}^Q(t)\bar{a}_{\boldsymbol{k}}^C(t') \right\rangle, \tag{4.49b}$$

$$ig_{\boldsymbol{k}}^K(t,t') = \left\langle a_{\boldsymbol{k}}^C(t)\bar{a}_{\boldsymbol{k}}^C(t') \right\rangle. \tag{4.49c}$$

and the anomalous components are given by

$$ip_{\boldsymbol{k}}^R(t,t') = \left\langle a_{\boldsymbol{k}}^C(t)a_{\boldsymbol{k}}^Q(t') \right\rangle, \tag{4.50a}$$

$$ip_{\boldsymbol{k}}^A(t,t') = \left\langle a_{\boldsymbol{k}}^Q(t)a_{\boldsymbol{k}}^C(t') \right\rangle, \tag{4.50b}$$

$$ip_{\boldsymbol{k}}^K(t,t') = \left\langle a_{\boldsymbol{k}}^C(t)a_{\boldsymbol{k}}^C(t') \right\rangle. \tag{4.50c}$$

The equivalent definitions in operator representation of the normal components Eqs. (4.49a-4.49c) are given by the right hand sides of Eqs. (3.10a-3.10c). Analogously to the argumentation of section 1.1.4 we find for the anomalous components, that

$$ip_{\boldsymbol{k}}^R(t,t') = \Theta(t-t')\left\langle [a_{\boldsymbol{k}}(t), a_{-\boldsymbol{k}}(t')] \right\rangle, \tag{4.51a}$$

$$ip_{\boldsymbol{k}}^A(t,t') = -\Theta(t'-t)\left\langle [a_{\boldsymbol{k}}(t), a_{-\boldsymbol{k}}(t')] \right\rangle, \tag{4.51b}$$

$$ip_{\boldsymbol{k}}^K(t,t') = \left\langle \{a_{\boldsymbol{k}}(t), a_{-\boldsymbol{k}}(t')\} \right\rangle, \tag{4.51c}$$

where $a_{\boldsymbol{k}}(t)$ is the annihilation operator of a magnon with momentum $\boldsymbol{k}$ in the Heisenberg picture at time t and $[\,,\,]$ and $\{\,,\,\}$ are the commutator and anti-commutator. From Eq. (4.51c) we see that the anomalous distribution function Eq. (4.32b) is proportional to the anomalous component of the Keldysh Green's function at equal times,

$$p_{\boldsymbol{k}}(t) = \frac{i}{2} p_{\boldsymbol{k}}^{K}(t,t).$$ (4.52)

Note that the signs in Eqs. (4.48a-4.48c) are chosen such that the symmetries Eqs. (4.45-4.46b) are satisfied and that the non-interacting inverse Green's function Eq. (4.35) is consistent with these definitions. A crucial point here is that we consider an initial state which is symmetric in momentum, otherwise the Green's functions could not be defined such that the symmetries are that simple, for example in general we would have

$$[\boldsymbol{G}^{T}]_{\boldsymbol{k},tt'} = [\boldsymbol{G}]_{-\boldsymbol{k},tt'},$$ (4.53)

in contrast to Eq. (4.45).

Directly from the definitions Eqs. (4.49a-4.50c) we obtain the symmetry relations

$$\left(\hat{g}^{R}\right)^{\dagger} = \hat{g}^{A}, \qquad \left(\hat{g}^{K}\right)^{\dagger} = -\hat{g}^{K},$$ (4.54a)

$$\left(\hat{p}^{R}\right)^{T} = \hat{p}^{A}, \qquad \left(\hat{p}^{\mathrm{K}}\right)^{T} = \hat{p}^{K},$$ (4.54b)

where the dagger denotes hermitian conjugation of the time matrices. For later purpose let us define mean and spectral components equivalently to Eqs. (1.77a, 1.77b),

$$\hat{G}^{M} = \frac{1}{2}\left(\hat{G}^{R} + \hat{G}^{A}\right),$$ (4.55a)

$$\hat{G}^{I} = i\left(\hat{G}^{R} - \hat{G}^{A}\right)$$
$$= \begin{pmatrix} \hat{p}^{I} & \hat{g}^{I} \\ -(\hat{g}^{I})^{*} & -(\hat{p}^{I})^{*} \end{pmatrix},$$ (4.55b)

where the components $\hat{g}^{I} = i\left(\hat{g}^{R} - \hat{g}^{A}\right)$ and $\hat{p}^{I} = i\left(\hat{p}^{R} - \hat{p}^{A}\right)$ fulfill the symmetries

$$\left[\hat{g}^{I}\right]^{\dagger} = \hat{g}^{I}, \qquad \left[\hat{p}^{I}\right]^{T} = -\hat{p}^{I}.$$ (4.56)

For calculating the full Green's functions it is convenient to use the parametrization by the self-energy $\boldsymbol{\Sigma}$ which contain only one-particle irreducible diagrams. Due to the chosen notation the Dyson equation is equal to Eq. (1.71),

$$\boldsymbol{G}^{-1} = \boldsymbol{G}_{0}^{-1} - \boldsymbol{\Sigma},$$ (4.57)

although we have the additional structure of flavor space and hence its content has changed. The self-energy in Keldysh space is given by

$$\boldsymbol{\Sigma} = \begin{pmatrix} 0 & \hat{\Sigma}^A \\ \hat{\Sigma}^R & \hat{\Sigma}^K \end{pmatrix}, \tag{4.58}$$

and its elements by

$$\hat{\Sigma}^R = \begin{pmatrix} \hat{\pi}^R & (\hat{\sigma}^R)^* \\ \hat{\sigma}^R & (\hat{\pi}^R)^* \end{pmatrix}, \tag{4.59a}$$

$$\hat{\Sigma}^A = \begin{pmatrix} \hat{\pi}^A & (\hat{\sigma}^A)^* \\ \hat{\sigma}^A & (\hat{\pi}^A)^* \end{pmatrix}, \tag{4.59b}$$

$$\hat{\Sigma}^K = \begin{pmatrix} \hat{\pi}^K & -(\hat{\sigma}^K)^* \\ \hat{\sigma}^K & -(\hat{\pi}^K)^* \end{pmatrix}. \tag{4.59c}$$

The components in flavor space are defined such that the bottom left off-diagonal elements become the self-energies defined in Eq. (1.72) in the limit of vanishing pumping and anomalous interactions. Note that this is different for the Green's functions, where the top right component correspond to the Green's function of the $U(1)$-symmetric case, due to the fact that the self-energy is a parametrization of the inverse Green's function.

From the Dyson equation (4.57) it follows that the self-energies have the same symmetries as the Green's functions,

$$\boldsymbol{\Sigma}^T = \boldsymbol{\Sigma}, \tag{4.60a}$$

$$\left(\hat{\Sigma}^R\right)^T = \hat{\Sigma}^A, \tag{4.60b}$$

$$\left(\hat{\Sigma}^K\right)^T = \hat{\Sigma}^K, \tag{4.60c}$$

and for the components in flavor space,

$$\left(\hat{\sigma}^R\right)^\dagger = \hat{\sigma}^A, \qquad \left(\hat{\sigma}^K\right)^\dagger = -\hat{\sigma}^K, \tag{4.61a}$$

$$\left(\hat{\pi}^R\right)^T = \hat{\pi}^A, \qquad \left(\pi^K\right)^T = \pi^K. \tag{4.61b}$$

Also for the self-energies we introduce mean and spectral components,

$$\hat{\Sigma}^M = \frac{1}{2}\left(\hat{\Sigma}^R + \hat{\Sigma}^A\right), \tag{4.62a}$$

$$\hat{\Sigma}^I = i\left(\hat{\Sigma}^R - \hat{\Sigma}^A\right)$$

$$= \begin{pmatrix} \hat{\pi}^I & -(\hat{\sigma}^I)^* \\ \hat{\sigma}^I & -(\hat{\pi}^I)^* \end{pmatrix}. \tag{4.62b}$$

The spectral components in flavor space $\hat{\sigma}^I = i\left(\hat{\sigma}^R - \hat{\sigma}^A\right)$ and $\hat{\pi}^I = i\left(\hat{\pi}^R - \hat{\pi}^A\right)$ satisfy

$$\left(\hat{\sigma}^I\right)^\dagger = \hat{\sigma}^I, \qquad \left(\hat{\pi}^I\right)^T = -\hat{\pi}^I. \tag{4.63}$$

4.3.3. Non-interacting Green's functions

In this section we determine the non-interacting Green's functions from Eq. (4.40). In addition to Eq. (4.41) we obtain the relations

$$\left(\hat{G}_0^R\right)^{-1} \hat{G}_0^R = \hat{1}, \tag{4.64a}$$

$$\left(\hat{G}_0^A\right)^{-1} \hat{G}_0^A = \hat{1}, \tag{4.64b}$$

$$\left(\hat{G}_0^R\right)^{-1} \hat{G}_0^K = 0, \tag{4.64c}$$

and from the alternative form of the Dyson equation (1.74) we obtain

$$\hat{G}_0^R \left(\hat{G}_0^R\right)^{-1} = \hat{1}, \tag{4.65a}$$

$$\hat{G}_0^A \left(\hat{G}_0^A\right)^{-1} = \hat{1}, \tag{4.65b}$$

$$\hat{G}_0^K \left(\hat{G}_0^R\right)^{-1} = 0. \tag{4.65c}$$

To solve these equations we will use kinetic equations as done in section 3.3.2. Let us start with the retarded Green's function. In time and momentum we obtain explicitly from the definition of the inverse Green's function Eq. (4.36a),

$$\left[\left(\hat{G}_0^R\right)^{-1} \hat{G}_0^R\right]_{\boldsymbol{k},tt'} = Z\left[-i\partial_t + M_{\boldsymbol{k}} - i\eta\right] G_{0,\boldsymbol{k}}^R(t,t') = \delta(t-t'). \tag{4.66}$$

Using $Z^2 = -1$ it follows from this equation,

$$i\partial_t G_{0,\boldsymbol{k}}^R(t,t') = Z\delta(t-t') + M_{\boldsymbol{k}} G_{0,\boldsymbol{k}}^R(t,t'), \tag{4.67}$$

where we have neglected the regularization η. Picking the right solution analogously to section 3.3.2, yields [28]

$$G_{0,\boldsymbol{k}}^R(t,t') = -i\Theta(t-t')\,\mathrm{e}^{-iM_{\boldsymbol{k}}(t-t')}Z, \tag{4.68}$$

where the matrix exponential is given by

$$e^{-iM_{\boldsymbol{k}}t} = I\cos(\mu_{\boldsymbol{k}}t) - iM_{\boldsymbol{k}}\frac{\sin(\mu_{\boldsymbol{k}}t)}{\mu_{\boldsymbol{k}}}, \tag{4.69}$$

with $\mu_{\boldsymbol{k}} = \sqrt{\tilde{\epsilon}_{\boldsymbol{k}}^2 - |\gamma_{\boldsymbol{k}}|^2}$. Similarly we obtain for the advanced Green's function [28],

$$G_{0,\boldsymbol{k}}^A(t,t') = i\Theta(t'-t)\,\mathrm{e}^{-iM_{\boldsymbol{k}}(t-t')}Z. \tag{4.70}$$

Finally the Keldysh Green's function is determined by the conditions Eqs. (4.64c, 4.65c) which are equivalent to

$$i\partial_t G_{0,\boldsymbol{k}}^K(t,t') = M_{\boldsymbol{k}} G_{0,\boldsymbol{k}}^K(t,t'), \tag{4.71a}$$

$$i\partial_{t'} G_{0,\boldsymbol{k}}^K(t,t') = G_{0,\boldsymbol{k}}^K(t,t') M_{\boldsymbol{k}}^T, \tag{4.71b}$$

4. Dynamics of pumped magnons with $U(1)$-symmetry breaking interactions

where for the second line we have used the identity

$$ZM_{\boldsymbol{k}}Z = M_{\boldsymbol{k}}^T. \tag{4.72}$$

The solution of Eqs. (4.71a, 4.71b) is given by [28]

$$G_{0,\boldsymbol{k}}^K(t,t') = e^{-iM_{\boldsymbol{k}}t}G_{0,\boldsymbol{k}}^K(0,0)\,e^{-iM_{\boldsymbol{k}}^T t'}, \tag{4.73}$$

where for the initial condition $G_{0,\boldsymbol{k}}^K(0,0)$ we choose the initial time to be zero, $t_0 = 0$. It turns out that the Keldysh Green's function can be written as

$$\hat{G}_0^K = \hat{G}_0^R \hat{g}_0 - \hat{g}_0 \hat{G}_0^A, \tag{4.74}$$

where $\hat{g}_0$ is proportional to the bottom right diagonal element of $\boldsymbol{G}_0^{-1}$, see Eq. (4.35), which is diagonal in time,

$$g_{0,\boldsymbol{k}}(t,t') = \delta(t-t')\,g_{0,\boldsymbol{k}}(t), \tag{4.75}$$

with

$$g_{0,\boldsymbol{k}}(t) = iZG_{0,\boldsymbol{k}}^K(t,t)\,Z. \tag{4.76}$$

Taking the explicit time and momentum component of Eq. (4.74), inserting the retarded and advanced Green's functions Eqs. (4.68, 4.70), and using the identity

$$e^{-iM_{\boldsymbol{k}}(t-t')}Z = Ze^{iM_{\boldsymbol{k}}^T(t-t')}, \tag{4.77}$$

yields the expression Eq. (4.73) which proves our claim. From the Keldysh Green's function in the form Eq. (4.74) it is easy to see that the condition for the regularization Eq. (4.41) is fulfilled.

The retarded and advanced Green's functions Eqs. (4.68, 4.70) depend only on the time difference $t-t'$ and hence the Fourier transforms become [28]

$$\begin{aligned}
G_{0,\boldsymbol{k}}^R(\omega) &= (\omega - M_{\boldsymbol{k}} + i\eta)^{-1}Z, \tag{4.78a}\\
G_{0,\boldsymbol{k}}^A(\omega) &= (\omega - M_{\boldsymbol{k}} - i\eta)^{-1}Z, \tag{4.78b}
\end{aligned}$$

or explicitly in flavor space

$$G_{0,\boldsymbol{k}}^{R/A}(\omega) = \frac{1}{(\omega \pm i\eta)^2 - \tilde{\epsilon}_{\boldsymbol{k}}^2 + |\gamma_{\boldsymbol{k}}|^2}\begin{pmatrix} -|\gamma_{\boldsymbol{k}}| & \omega + \tilde{\epsilon}_{\boldsymbol{k}} \pm i\eta \\ -\omega + \tilde{\epsilon}_{\boldsymbol{k}} \mp i\eta & -|\gamma_{\boldsymbol{k}}| \end{pmatrix}. \tag{4.79}$$

Using the Dirac identity Eq. (3.34) we obtain for the spectral components $\hat{g}_0^I$ and $\hat{p}_0^I$,

$$\begin{aligned}
g_{0,\boldsymbol{k}}^I(\omega) &= 2\pi(\omega + \tilde{\epsilon}_{\boldsymbol{k}})\operatorname{sgn}(\omega)\,\delta(\omega^2 - \mu_{\boldsymbol{k}}^2), \tag{4.80a}\\
p_{0,\boldsymbol{k}}^I(\omega) &= -2\pi|\gamma_{\boldsymbol{k}}|\operatorname{sgn}(\omega)\,\delta(\omega^2 - \mu_{\boldsymbol{k}}^2), \tag{4.80b}
\end{aligned}$$

where the delta function is given by

$$\delta(\omega^2 - \mu_{\boldsymbol{k}}^2) = \frac{1}{2\mu_{\boldsymbol{k}}}[\delta(\omega - \mu_{\boldsymbol{k}}) + \delta(\omega + \mu_{\boldsymbol{k}})]. \tag{4.81}$$

After some further steps using the properties of the delta function, we obtain

$$g_{0,\boldsymbol{k}}^{I}(\omega) \;=\; \sum_{\lambda=\pm 1} \frac{2\pi}{2\mu_{\boldsymbol{k}}} \left(\lambda\mu_{\boldsymbol{k}} + \tilde{\epsilon}_{\boldsymbol{k}} \right) \lambda \delta\left(\omega - \lambda\mu_{\boldsymbol{k}} \right), \qquad (4.82a)$$

$$p_{0,\boldsymbol{k}}^{I}(\omega) \;=\; -\sum_{\lambda=\pm 1} \frac{2\pi}{2\mu_{\boldsymbol{k}}} \left| \gamma_{\boldsymbol{k}} \right| \lambda \delta\left(\omega - \lambda\mu_{\boldsymbol{k}} \right). \qquad (4.82b)$$

4.4. Rate equation

In this section we derive a rate equation for the normal correlation function Eq. (4.32a). In comparison to section 1.1 and 3.3 we have to deal with the dependence of the normal on the anomalous correlation function. A suitable approximation which reduces the problem to a rate equation similar to Eq. (3.55) is needed. At the moment this seems to be impossible by using the Wigner transformation. It is not clear why the approach of section 3.3 fails here but a rate structure could not be achieved in this way. Instead we will use a real time approach based on the generalized Kandanoff-Baym ansatz (GKBA). It turns out that in the limit of vanishing pumping and anomalous interactions, this method is equivalent to the one based on the Wigner transformation.

4.4.1. Quantum kinetic equations

The normal correlation function is related to the normal component of the Keldysh Green's function $\hat{g}^K$ at equal times. Defining

$$g_{\boldsymbol{k}}(t) \equiv 1 + 2n_{\boldsymbol{k}}(t) = ig_{\boldsymbol{k}}^K(t,t), \qquad (4.83)$$

we are looking for an equation for the time derivative

$$\partial_t g_{\boldsymbol{k}}(t) = i \left[\partial_{t_1} g_{\boldsymbol{k}}^K(t_1,t_2) + \partial_{t_2} g_{\boldsymbol{k}}^K(t_1,t_2) \right]_{t_1=t_2=t}. \qquad (4.84)$$

The two terms on the right hand side follow from the two versions of the Dyson equation Eq. (1.73) and Eq. (1.74). For the Keldysh Green's function we obtain

$$\left(\hat{G}_0^R \right)^{-1} \hat{G}^K \;=\; \hat{\Sigma}^K \hat{G}^A + \hat{\Sigma}^R \hat{G}^K, \qquad (4.85a)$$

$$\hat{G}^K \left(\hat{G}_0^A \right)^{-1} \;=\; \hat{G}^R \hat{\Sigma}^K + \hat{G}^K \hat{\Sigma}^A. \qquad (4.85b)$$

Multiplying Z from one or the other side and subtracting the second line from the first one yields

$$\left[Z\hat{D}_0\hat{G}^K - \hat{G}^K\hat{D}_0 Z \right] = Z\hat{\Sigma}^K\hat{G}^A - \hat{G}^R\hat{\Sigma}^K Z + Z\hat{\Sigma}^R\hat{G}^K - \hat{G}^K\hat{\Sigma}^A Z. \quad (4.86)$$

4. Dynamics of pumped magnons with $U(1)$-symmetry breaking interactions

Using the mean and spectral components Eqs. (4.55a, 4.55b) and Eqs. (4.62a, 4.62b) we arrive at

$$\left[Z\hat{D}\hat{G}^K - \hat{G}^K\hat{D}Z \right] - \left[Z\hat{\Sigma}^K\hat{G}^M - \hat{G}^M\hat{\Sigma}^K Z \right]$$
$$= \frac{i}{2} \left[Z\hat{\Sigma}^K\hat{G}^I + \hat{G}^I\hat{\Sigma}^K Z \right] - \frac{i}{2} \left[Z\hat{\Sigma}^I\hat{G}^K + \hat{G}^K\hat{\Sigma}^I Z \right], \qquad (4.87)$$

where we have defined

$$\hat{D} = \hat{D}_0 - \hat{\Sigma}^M. \qquad (4.88)$$

As in chapter 3 we neglect the mean components of the Green's function and the self-energy. Inserting the inverse propagator without regularization Eq. (4.38) and explicitly writing down the time dependence yields

$$i\left[\partial_t G_{\mathbf{k}}^K(t,t') + \partial_{t'} G_{\mathbf{k}}^K(t,t') \right] - \left[M_{\mathbf{k}} G_{\mathbf{k}}^K(t,t') + G_{\mathbf{k}}^K(t,t') M_{\mathbf{k}}^T \right]$$
$$= \frac{i}{2} \left[Z\hat{\Sigma}^K\hat{G}^I + \hat{G}^I\hat{\Sigma}^K Z \right]_{\mathbf{k},tt'} - \frac{i}{2} \left[Z\hat{\Sigma}^I\hat{G}^K + \hat{G}^K\hat{\Sigma}^I Z \right]_{\mathbf{k},tt'}. \qquad (4.89)$$

Performing the matrix product in flavor space and inserting the definitions of the normal and anomalous components of the Keldysh Green's function at equal times Eqs. (4.52, 4.83), we obtain for equal times,

$$\partial_t g_{\mathbf{k}}(t) + 4\left|\gamma_{\mathbf{k}}\right| \mathrm{Im}\left[p_{\mathbf{k}}(t) \right]$$
$$= \frac{i}{2} \left[\hat{\sigma}^K\hat{g}^I + \hat{g}^I\hat{\sigma}^K + \left(\hat{\pi}^K\right)^*\left(\hat{p}^I\right)^* + \hat{p}^I\hat{\pi}^K \right]_{\mathbf{k},tt}$$
$$- \frac{i}{2} \left[\left(\hat{\pi}^I\right)^*\left(\hat{p}^K\right)^* + \hat{p}^K\hat{\pi}^I + \hat{\sigma}^I\hat{g}^K + \hat{g}^K\hat{\sigma}^I \right]_{\mathbf{k},tt}, \qquad (4.90)$$
$$2\partial_t p_{\mathbf{k}}(t) + 2i\left|\gamma_{\mathbf{k}}\right| g_{\mathbf{k}}(t) + 4i\epsilon_{\mathbf{k}} p_{\mathbf{k}}(t)$$
$$= \frac{i}{2} \left[\left(\hat{\pi}^K\right)^*\left(\hat{g}^I\right)^* + \hat{g}^I\left(\hat{\pi}^K\right)^* + \hat{\sigma}^K\hat{p}^I + \hat{p}^I\left(\hat{\sigma}^K\right)^* \right]_{\mathbf{k},tt}$$
$$- \frac{i}{2} \left[\left(\hat{\pi}^I\right)^*\left(\hat{g}^K\right)^* + \hat{g}^K\left(\hat{\pi}^I\right)^* + \hat{\sigma}^I\hat{p}^K + \hat{p}^K\left(\hat{\sigma}^I\right)^* \right]_{\mathbf{k},tt}, \qquad (4.91)$$

where for the second equation we have used the fact that $g_{\mathbf{k}}(t)$ is real. The collision integrals on the right hand side of these equations can be simplified by using the symmetry relations Eqs. (4.54a, 4.54b, 4.56, 4.61a, 4.61b, 4.63), yielding

$$\partial_t g_{\mathbf{k}}(t) + 4\left|\gamma_{\mathbf{k}}\right| \mathrm{Im}\left[p_{\mathbf{k}}(t) \right]$$
$$= \mathrm{Im}\left[-\hat{g}^I\hat{\sigma}^K - \hat{p}^I\hat{\pi}^K + \hat{p}^K\hat{\pi}^I + \hat{g}^K\hat{\sigma}^I \right]_{\mathbf{k},tt}, \qquad (4.92a)$$
$$2\partial_t p_{\mathbf{k}}(t) + 2i\left|\gamma_{\mathbf{k}}\right| g_{\mathbf{k}}(t) + 4i\epsilon_{\mathbf{k}} p_{\mathbf{k}}(t)$$
$$= i\left[\hat{g}^I\left(\hat{\pi}^K\right)^* + \hat{p}^I\left(\hat{\sigma}^K\right)^* - \hat{g}^K\left(\hat{\pi}^I\right)^* - \hat{p}^K\left(\hat{\sigma}^I\right)^* \right]_{\mathbf{k},tt}. \qquad (4.92b)$$

If we write down the matrix product explicitly in time, we finally arrive at

$$\partial_t g_{\boldsymbol{k}}(t) + 4\left|\gamma_{\boldsymbol{k}}\right|\operatorname{Im}\left[p_{\boldsymbol{k}}(t)\right]$$
$$= \int_0^t dt_1 \operatorname{Im}\left[-g_{\boldsymbol{k}}^I(t,t_1)\,\sigma_{\boldsymbol{k}}^K(t_1,t) - p_{\boldsymbol{k}}^I(t,t_1)\,\pi_{\boldsymbol{k}}^K(t_1,t)\right.$$
$$\left. +p_{\boldsymbol{k}}^K(t,t_1)\,\pi_{\boldsymbol{k}}^I(t_1,t) + g_{\boldsymbol{k}}^K(t,t_1)\,\sigma_{\boldsymbol{k}}^I(t_1,t)\right], \quad (4.93\mathrm{a})$$

$$2\partial_t p_{\boldsymbol{k}}(t) + 2i\left|\gamma_{\boldsymbol{k}}\right|g_{\boldsymbol{k}}(t) + 4i\tilde{\epsilon}_{\boldsymbol{k}} p_{\boldsymbol{k}}(t)$$
$$= i\int_0^t dt_1 \left[g_{\boldsymbol{k}}^I(t,t_1)\left(\pi_{\boldsymbol{k}}^K(t_1,t)\right)^* + p_{\boldsymbol{k}}^I(t,t_1)\left(\sigma_{\boldsymbol{k}}^K(t_1,t)\right)^*\right.$$
$$\left. -g_{\boldsymbol{k}}^K(t,t_1)\left(\pi_{\boldsymbol{k}}^I(t_1,t)\right)^* - p_{\boldsymbol{k}}^K(t,t_1)\left(\sigma_{\boldsymbol{k}}^I(t_1,t)\right)^*\right], \quad (4.93\mathrm{b})$$

where the initial time has to be chosen to be zero, $t_0 = 0$, as we already did for the non-interacting Keldysh Green's function Eq. (4.73).

4.4.2. Generalized Kadanoff-Baym ansatz

Unfortunately, the kinetic equations (4.93a, 4.93b) are not a complete set of equations. The time functions $g_{\boldsymbol{k}}(t)$ and $p_{\boldsymbol{k}}(t)$ on the left hand side are related to time matrices on the right hand side where due to the matrix product also the off-diagonal time elements contribute. In order to close the set of equations we have to find approximations such that only the diagonal elements of the time matrices on the right hand side of Eqs. (4.92a, 4.92b) contribute. The two approximations we will use for this purpose are the quasiparticle approximation (3.54) and the GKBA. The latter connects the off-diagonal time elements to the diagonal ones and will be discussed in this section.

Kadanoff and Baym [96] first suggested this ansatz using the Wigner transformed representation. Later Lipavský *et al.* [8] made a generalization independent of the representation, called GKBA. The GKBA is highly successful in the field of transport in semiconductors, see Ref. [84].

In our context the GKBA assumes the identity

$$G_{\boldsymbol{k}}^K(t,t') \approx -i\left[G_{\boldsymbol{k}}^R(t,t')\,Z G_{\boldsymbol{k}}^K(t',t') - G_{\boldsymbol{k}}^K(t,t)\,Z G_{\boldsymbol{k}}^A(t,t')\right], \quad (4.94)$$

for the derivation we refer to Ref. [28]. Note that in equilibrium this relation is satisfied exactly, see Eq. (4.74). Due to the retarded and advanced functions the GKBA can be written as

$$G_{\boldsymbol{k}}^K(t,t') \approx \begin{cases} -iG_{\boldsymbol{k}}^I(t,t')\,Z G_{\boldsymbol{k}}^K(t',t') & \text{for } t > t', \\ iG_{\boldsymbol{k}}^K(t,t)\,Z G_{\boldsymbol{k}}^I(t,t') & \text{for } t < t', \end{cases} \quad (4.95)$$

where we have added a zero to obtain the spectral component $G_{\boldsymbol{k}}^I(t,t')$. Performing the matrix products in flavor space yields

$$g_{\boldsymbol{k}}^K(t,t') \approx \begin{cases} i\left[-g_{\boldsymbol{k}}^I(t,t')\,g_{\boldsymbol{k}}(t') + 2p_{\boldsymbol{k}}^I(t,t')\left(p_{\boldsymbol{k}}(t')\right)^*\right] & \text{for } t > t', \\ -i\left[g_{\boldsymbol{k}}^I(t,t')\,g_{\boldsymbol{k}}(t) + 2\left(p_{\boldsymbol{k}}^I(t,t')\right)^* p_{\boldsymbol{k}}(t)\right] & \text{for } t < t', \end{cases} \quad (4.96)$$
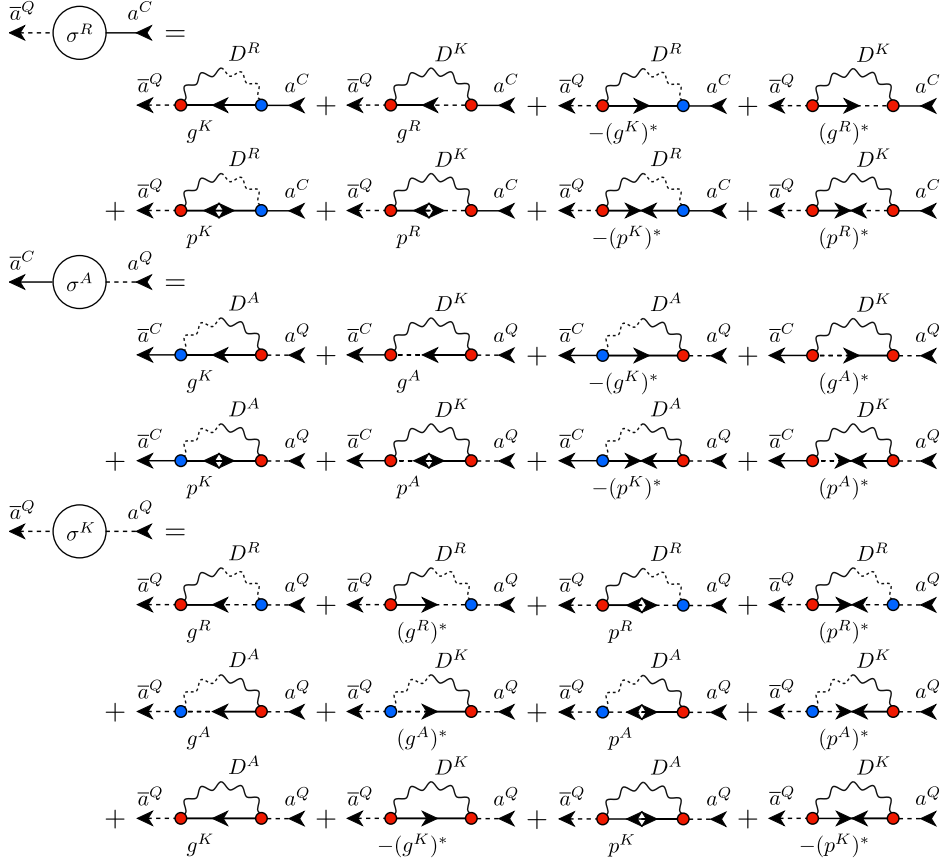
Figure 4.2.: Diagrams of the normal components of the Green's functions with the anomalous interaction $\Gamma^\sigma_{\boldsymbol{k},\boldsymbol{q}}$. The straight lines between the vertices represent magnon propagators and the wavy lines phonon propagators. The anomalous magnon propagators are denoted by two arrows whereas for the normal ones a single arrow is sufficient to be unique in the notation. For further definitions of the graph see Fig. 4.1.

and

$$
p_{\boldsymbol{k}}^K(t,t') \approx
\begin{cases}
i\left[p_{\boldsymbol{k}}^I(t,t')\,g_{\boldsymbol{k}}(t') - 2g_{\boldsymbol{k}}^I(t,t')\,p_{\boldsymbol{k}}(t')\right] & \text{for } t > t', \\
-i\left[p_{\boldsymbol{k}}^I(t,t')\,g_{\boldsymbol{k}}(t) + 2\left(g_{\boldsymbol{k}}^I(t,t')\right)^*p_{\boldsymbol{k}}(t)\right] & \text{for } t < t'.
\end{cases}
\tag{4.97}
$$

4.4.3. Self-energies in perturbation theory

In this section we determine the self-energies to second order in the magnon-phonon interactions. Compared to section 3.3.3 where we considered the normal interactions only, we have four times as many diagrams contributing, see Figs. 4.3 and 4.4. The explicit expressions for the normal components are

Figure 4.3.: In contrast to Fig. 4.4 here the anomalous self-energies are shown. Although the diagrams seem to be similar to those of the normal self-energies, the external legs and involved vertices for one diagram are different, see the explicit expressions Eqs. (4.98a-4.99b). The definitions of the diagrams are explained in the caption of Figs. 4.1 and 4.4.

given by

$$
\begin{aligned}
\sigma_{\boldsymbol{k}}^{I}\left(t, t^{\prime}\right) = & \frac{i}{V} \sum_{\boldsymbol{q}}\left\{\left(\Gamma_{\boldsymbol{k}, \boldsymbol{q}}^{n}\right)^{2}\left[g_{\boldsymbol{k}-\boldsymbol{q}}^{I} D_{\boldsymbol{q}}^{K}+g_{\boldsymbol{k}-\boldsymbol{q}}^{K} D_{\boldsymbol{q}}^{I}\right]\right. \\
& +\left(\Gamma_{\boldsymbol{k}, \boldsymbol{q}}^{\sigma}(t)\right)^{*} \Gamma_{\boldsymbol{k}, \boldsymbol{q}}^{\sigma}\left(t^{\prime}\right)\left[-\left(g_{\boldsymbol{k}-\boldsymbol{q}}^{I}\right)^{*} D_{\boldsymbol{q}}^{K}-\left(g_{\boldsymbol{k}-\boldsymbol{q}}^{K}\right)^{*} D_{\boldsymbol{q}}^{I}\right] \\
& +\Gamma_{\boldsymbol{k}, \boldsymbol{q}}^{n} \Gamma_{\boldsymbol{k}, \boldsymbol{q}}^{\sigma}\left(t^{\prime}\right)\left[p_{\boldsymbol{k}-\boldsymbol{q}}^{I} D_{\boldsymbol{q}}^{K}+p_{\boldsymbol{k}-\boldsymbol{q}}^{K} D_{\boldsymbol{q}}^{I}\right] \\
& \left.+\left(\Gamma_{\boldsymbol{k}, \boldsymbol{q}}^{\sigma}(t)\right)^{*} \Gamma_{\boldsymbol{k}, \boldsymbol{q}}^{n}\left[-\left(p_{\boldsymbol{k}-\boldsymbol{q}}^{I}\right)^{*} D_{\boldsymbol{q}}^{K}-\left(p_{\boldsymbol{k}-\boldsymbol{q}}^{K}\right)^{*} D_{\boldsymbol{q}}^{I}\right]\right\}, \quad (4.98\mathrm{a}) \\
i \sigma_{\boldsymbol{k}}^{K}\left(t, t^{\prime}\right) = & \frac{1}{V} \sum_{\boldsymbol{q}}\left\{\left(\Gamma_{\boldsymbol{k}, \boldsymbol{q}}^{n}\right)^{2}\left[-g_{\boldsymbol{k}-\boldsymbol{q}}^{K} D_{\boldsymbol{q}}^{K}+g_{\boldsymbol{k}-\boldsymbol{q}}^{I} D_{\boldsymbol{q}}^{I}\right]\right. \\
& +\left(\Gamma_{\boldsymbol{k}, \boldsymbol{q}}^{\sigma}(t)\right)^{*} \Gamma_{\boldsymbol{k}, \boldsymbol{q}}^{\sigma}\left(t^{\prime}\right)\left[\left(g_{\boldsymbol{k}-\boldsymbol{q}}^{K}\right)^{*} D_{\boldsymbol{q}}^{K}-\left(g_{\boldsymbol{k}-\boldsymbol{q}}^{I}\right)^{*} D_{\boldsymbol{q}}^{I}\right] \\
& +\Gamma_{\boldsymbol{k}, \boldsymbol{q}}^{n} \Gamma_{\boldsymbol{k}, \boldsymbol{q}}^{\sigma}\left(t^{\prime}\right)\left[-p_{\boldsymbol{k}-\boldsymbol{q}}^{K} D_{\boldsymbol{q}}^{K}+p_{\boldsymbol{k}-\boldsymbol{q}}^{I} D_{\boldsymbol{q}}^{I}\right] \\
& \left.+\left(\Gamma_{\boldsymbol{k}, \boldsymbol{q}}^{\sigma}(t)\right)^{*} \Gamma_{\boldsymbol{k}, \boldsymbol{q}}^{n}\left[\left(p_{\boldsymbol{k}-\boldsymbol{q}}^{K}\right)^{*} D_{\boldsymbol{q}}^{K}-\left(p_{\boldsymbol{k}-\boldsymbol{q}}^{I}\right)^{*} D_{\boldsymbol{q}}^{I}\right]\right\}, \quad (4.98\mathrm{b})
\end{aligned}
$$

and the anomalous components by

$$
\begin{aligned}
\pi_{\boldsymbol{k}}^{I}\left(t, t^{\prime}\right) = & \frac{i}{V} \sum_{\boldsymbol{q}}\left\{\Gamma_{\boldsymbol{k}, \boldsymbol{q}}^{\sigma}(t) \Gamma_{\boldsymbol{k}, \boldsymbol{q}}^{n}\left[g_{\boldsymbol{k}-\boldsymbol{q}}^{I} D_{\boldsymbol{q}}^{K}+g_{\boldsymbol{k}-\boldsymbol{q}}^{K} D_{\boldsymbol{q}}^{I}\right]\right. \\
& +\Gamma_{\boldsymbol{k}, \boldsymbol{q}}^{n} \Gamma_{\boldsymbol{k}, \boldsymbol{q}}^{\sigma}\left(t^{\prime}\right)\left[-\left(g_{\boldsymbol{k}-\boldsymbol{q}}^{I}\right)^{*} D_{\boldsymbol{q}}^{K}-\left(g_{\boldsymbol{k}-\boldsymbol{q}}^{K}\right)^{*} D_{\boldsymbol{q}}^{I}\right] \\
& +\Gamma_{\boldsymbol{k}, \boldsymbol{q}}^{\sigma}(t) \Gamma_{\boldsymbol{k}, \boldsymbol{q}}^{\sigma}\left(t^{\prime}\right)\left[p_{\boldsymbol{k}-\boldsymbol{q}}^{I} D_{\boldsymbol{q}}^{K}+p_{\boldsymbol{k}-\boldsymbol{q}}^{K} D_{\boldsymbol{q}}^{I}\right] \\
& \left.+\left(\Gamma_{\boldsymbol{k}, \boldsymbol{q}}^{n}\right)^{2}\left[-\left(p_{\boldsymbol{k}-\boldsymbol{q}}^{I}\right)^{*} D_{\boldsymbol{q}}^{K}-\left(p_{\boldsymbol{k}-\boldsymbol{q}}^{K}\right)^{*} D_{\boldsymbol{q}}^{I}\right]\right\}, \quad (4.99\mathrm{a}) \\
i \pi_{\boldsymbol{k}}^{K}\left(t, t^{\prime}\right) = & \frac{1}{V} \sum_{\boldsymbol{q}}\left\{\Gamma_{\boldsymbol{k}, \boldsymbol{q}}^{\sigma}(t) \Gamma_{\boldsymbol{k}, \boldsymbol{q}}^{n}\left[-g_{\boldsymbol{k}-\boldsymbol{q}}^{K} D_{\boldsymbol{q}}^{K}+g_{\boldsymbol{k}-\boldsymbol{q}}^{I} D_{\boldsymbol{q}}^{I}\right]\right. \\
& +\Gamma_{\boldsymbol{k}, \boldsymbol{q}}^{n} \Gamma_{\boldsymbol{k}, \boldsymbol{q}}^{\sigma}\left(t^{\prime}\right)\left[\left(g_{\boldsymbol{k}-\boldsymbol{q}}^{K}\right)^{*} D_{\boldsymbol{q}}^{K}-\left(g_{\boldsymbol{k}-\boldsymbol{q}}^{I}\right)^{*} D_{\boldsymbol{q}}^{I}\right] \\
& +\Gamma_{\boldsymbol{k}, \boldsymbol{q}}^{\sigma}(t) \Gamma_{\boldsymbol{k}, \boldsymbol{q}}^{\sigma}\left(t^{\prime}\right)\left[-p_{\boldsymbol{k}-\boldsymbol{q}}^{K} D_{\boldsymbol{q}}^{K}+p_{\boldsymbol{k}-\boldsymbol{q}}^{I} D_{\boldsymbol{q}}^{I}\right] \\
& \left.+\left(\Gamma_{\boldsymbol{k}, \boldsymbol{q}}^{n}\right)^{2}\left[\left(p_{\boldsymbol{k}-\boldsymbol{q}}^{K}\right)^{*} D_{\boldsymbol{q}}^{K}-\left(p_{\boldsymbol{k}-\boldsymbol{q}}^{I}\right)^{*} D_{\boldsymbol{q}}^{I}\right]\right\}, \quad (4.99\mathrm{b})
\end{aligned}
$$

where the spectral component of the phonons $D_{\boldsymbol{q}}^{I}\left(t, t^{\prime}\right)$ was introduced in Eq. (3.43). For a better overview we have omitted the time argument $t, t^{\prime}$ of all propagators. The Keldysh components we could express by spectral propagators instead of retarded and advanced ones because the product of retarded and advanced components with same time arguments is zero. We did the same for the self-energies Eqs. (3.41a, 3.41b) in the last chapter.

4.4.4. Markovian collision integrals

As in chapter 3 we assume that the phonons act like a thermal bath such that they stay in equilibrium and the feedback from the magnons can be neglected. Hence the phonon propagators are given by the non-interacting expressions Eqs. (3.32a-3.32c) and the fluctuation-dissipation theorem is valid,

$$
D_{0, \boldsymbol{q}}^{K}(\omega)=-i D_{0, \boldsymbol{q}}^{I}(\omega) f^{0}(\omega), \quad (4.100)
$$

where $f^0(\omega) = 1 + 2b(\omega) = 1 + 2/(e^{\beta\omega} - 1)$. We approximate the spectral components of the magnons $g_{\boldsymbol{k}}^I(t, t')$ and $p_{\boldsymbol{k}}^I(t, t')$ by their non-interacting expressions. The Fourier transform of these are given in Eqs. (4.82a, 4.82b). For a discussion of the validity of this approximation see section 3.6.

Instead of the gradient approximation which we used for the Wigner transformation Eq. (1.95), in real time we are applying the Markov approximation. Due to the time integration of the kinetic equations (4.93a, 4.93b), the collision integrals have memory effects and depend on all previous times. These effects are neglected in the Markov approximation. Using the GKBA the time integration will be performed over $g_{\boldsymbol{k}}(t_1)$ and $p_{\boldsymbol{k}}(t_1)$ and the Markov approximation is achieved by replacing $g_{\boldsymbol{k}}(t_1) \to g_{\boldsymbol{k}}(t)$ and $p_{\boldsymbol{k}}(t_1) \to p_{\boldsymbol{k}}(t)$, where t_1 is the integration variable. This also has to be done for the functions which are included in the self-energy.

Now we can calculate the collision integrals for the normal and anomalous distribution functions. We have to insert the GKBA Eqs. (4.96, 4.97), the self-energies Eqs. (4.98a-4.99b), the fluctuation-dissipation theorem for the phonons Eq. (4.100) and the spectral components of the magnons Eqs. (4.80a, 4.80b) into the right hand sides of the kinetic equations (4.93a, 4.93b). After performing the Markov approximation, the time integral can be done analytically. We obtain a lot of terms involving different combinations of propagators. Here we give only two generic examples. Let us start with

$$
\begin{aligned}
&\int dt_1 g_{0,\boldsymbol{k}}^I(t, t_1) g_{0,\boldsymbol{k}-\boldsymbol{q}}^I(t_1, t) D_{0,\boldsymbol{q}}^I(t_1, t) \\
&= \int dt_1 \int \frac{d\omega_1}{2\pi} \int \frac{d\omega_2}{2\pi} e^{-i\omega_1(t-t_1)} e^{i\omega_2(t-t_1)} \\
&\quad \times g_{0,\boldsymbol{k}}^I(\omega_1) g_{0,\boldsymbol{k}-\boldsymbol{q}}^I(\omega_2) \frac{1}{2} \left[e^{i\omega_{\boldsymbol{q}}(t-t_1)} - e^{-i\omega_{\boldsymbol{q}}(t-t_1)} \right] \\
&= \int \frac{d\omega_1}{2\pi} \int \frac{d\omega_2}{2\pi} \frac{1}{2} \left[2\pi\delta(\omega_1 - \omega_2 - \omega_{\boldsymbol{q}}) - 2\pi\delta(\omega_1 - \omega_2 + \omega_{\boldsymbol{q}}) \right] \\
&\quad \times g_{0,\boldsymbol{k}}^I(\omega_1) g_{0,\boldsymbol{k}-\boldsymbol{q}}^I(\omega_2) \\
&= \sum_{\lambda_1, \lambda_2 = \pm 1} D_{\boldsymbol{q}}^I(\lambda_1 \mu_{\boldsymbol{k}} - \lambda_2 \mu_{\boldsymbol{k}-\boldsymbol{q}}) \\
&\quad \times (\lambda_1 \mu_{\boldsymbol{k}} + \tilde{\epsilon}_{\boldsymbol{k}})(\lambda_2 \mu_{\boldsymbol{k}-\boldsymbol{q}} + \tilde{\epsilon}_{\boldsymbol{k}-\boldsymbol{q}}) \frac{\lambda_1}{2\mu_{\boldsymbol{k}}} \frac{\lambda_2}{2\mu_{\boldsymbol{k}-\boldsymbol{q}}},
\end{aligned}
\tag{4.101}
$$

where in the first equality we express the magnon propagators by their Fourier transform Eq. (4.82a). For the phonon propagator we first use the real time expression,

$$
D_{0,\boldsymbol{q}}^I(t, t') = i \left[D_{0,\boldsymbol{q}}^R(t, t') - D_{0,\boldsymbol{q}}^A(t, t') \right] = -i \sin\left[\omega_{\boldsymbol{q}}(t - t') \right],
\tag{4.102}
$$

see Eq. (3.32a, 3.32b), and at the end its Fourier transform Eq. (3.37c). In certain terms the time dependent interaction $\Gamma_{\boldsymbol{k},\boldsymbol{q}}^{\sigma}(t)$ is also involved in the

time integral, for example

$$\int dt_1 g_{\boldsymbol{k}}^I(t, t_1) g_{\boldsymbol{k}-\boldsymbol{q}}^I(t_1, t) D_{0,\boldsymbol{q}}^I(t_1, t) \Gamma_{\boldsymbol{k},\boldsymbol{q}}^\sigma(t_1)$$

$$= \Gamma_{\boldsymbol{k},\boldsymbol{q}}^\sigma(t) \sum_{\lambda_1,\lambda_2=\pm 1} D_{0,\boldsymbol{q}}^I \left(\lambda_1 \mu_{\boldsymbol{k}} - \lambda_2 \mu_{\boldsymbol{k}-\boldsymbol{q}} - (\Delta_{\boldsymbol{k}} + \Delta_{\boldsymbol{k}-\boldsymbol{q}}) \frac{\omega_0}{2}\right)$$

$$\times (\lambda_1 \mu_{\boldsymbol{k}} + \tilde{\epsilon}_{\boldsymbol{k}})(\lambda_2 \mu_{\boldsymbol{k}-\boldsymbol{q}} + \tilde{\epsilon}_{\boldsymbol{k}-\boldsymbol{q}}) \frac{\lambda_1}{2\mu_{\boldsymbol{k}}} \frac{\lambda_2}{2\mu_{\boldsymbol{k}-\boldsymbol{q}}}. \qquad (4.103)$$

The time integrals of the other terms can be determined analogously to our two examples.

After a tedious but straightforward calculation we arrive at expressions for the kinetic equations of $g_{\boldsymbol{k}}(t)$ and $p_{\boldsymbol{k}}(t)$ which due to their length are presented in Appendix C.

4.4.5. Bogoliubov transformed kinetic equations

We have to do a final approximation to arrive at a closed rate equation for the normal component. Instead of completely neglecting the anomalous correlations as it can be done when considering Bose-Einstein condensation [78] or considering anomalous interactions without pumping, we perform a Bogoliubov transformation and neglect the anomalous correlations in the new basis. Similar to section 1.3.3 the transformation is given by

$$\begin{pmatrix} a_{\boldsymbol{k}} \\ a_{-\boldsymbol{k}}^\dagger \end{pmatrix} = \begin{pmatrix} u_{\boldsymbol{k}} & -v_{\boldsymbol{k}} \\ -v_{\boldsymbol{k}}^* & u_{\boldsymbol{k}} \end{pmatrix} \begin{pmatrix} \alpha_{\boldsymbol{k}} \\ \alpha_{-\boldsymbol{k}}^\dagger \end{pmatrix}. \qquad (4.104)$$

In order to diagonalize the quadratic part of the Hamiltonian (4.3) we have to choose

$$u_{\boldsymbol{k}} = \frac{1}{\sqrt{2}} \sqrt{\frac{\tilde{\epsilon}_{\boldsymbol{k}}}{\mu_{\boldsymbol{k}}} + 1}, \qquad (4.105a)$$

$$v_{\boldsymbol{k}} = \frac{1}{\sqrt{2}} \sqrt{\frac{\tilde{\epsilon}_{\boldsymbol{k}}}{\mu_{\boldsymbol{k}}} - 1}. \qquad (4.105b)$$

Note that the transformation does not mix operators of different times and we therefore omitted the time arguments. Defining $n_{\boldsymbol{k}}^B(t) = \left\langle \alpha_{\boldsymbol{k}}^\dagger \alpha_{\boldsymbol{k}} \right\rangle$, the

correlation functions become

$$
\begin{aligned}
n_{\boldsymbol{k}}\left(t\right) = \left\langle a_{\boldsymbol{k}}^{\dagger} a_{\boldsymbol{k}} \right\rangle \quad &= \quad -u_{\boldsymbol{k}} v_{\boldsymbol{k}} \left(\left\langle \alpha_{-\boldsymbol{k}} \alpha_{\boldsymbol{k}} \right\rangle + \left\langle \alpha_{\boldsymbol{k}}^{\dagger} \alpha_{-\boldsymbol{k}}^{\dagger} \right\rangle \right) \\
&\quad + u_{\boldsymbol{k}}^{2} \left\langle \alpha_{\boldsymbol{k}}^{\dagger} \alpha_{\boldsymbol{k}} \right\rangle + v_{\boldsymbol{k}}^{2} \left(\left\langle \alpha_{-\boldsymbol{k}}^{\dagger} \alpha_{-\boldsymbol{k}} \right\rangle + 1 \right) \\
&\approx \quad \left(u_{\boldsymbol{k}}^{2} + v_{\boldsymbol{k}}^{2} \right) n_{\boldsymbol{k}}^{B}\left(t\right) + v_{\boldsymbol{k}}^{2}, \qquad (4.106\text{a}) \\
p_{\boldsymbol{k}}\left(t\right) = \left\langle a_{-\boldsymbol{k}} a_{\boldsymbol{k}} \right\rangle \quad &= \quad u_{\boldsymbol{k}}^{2} \left\langle \alpha_{-\boldsymbol{k}} \alpha_{\boldsymbol{k}} \right\rangle + v_{\boldsymbol{k}}^{2} \left\langle \alpha_{\boldsymbol{k}}^{\dagger} \alpha_{-\boldsymbol{k}}^{\dagger} \right\rangle \\
&\quad - u_{\boldsymbol{k}} v_{\boldsymbol{k}} \left(\left\langle \alpha_{\boldsymbol{k}}^{\dagger} \alpha_{\boldsymbol{k}} \right\rangle + \left\langle \alpha_{-\boldsymbol{k}}^{\dagger} \alpha_{-\boldsymbol{k}} \right\rangle + 1 \right) \\
&\approx \quad -u_{\boldsymbol{k}} v_{\boldsymbol{k}} \left(2 n_{\boldsymbol{k}}^{B}\left(t\right) + 1 \right), \qquad (4.106\text{b})
\end{aligned}
$$

where in the third and the last line we neglected the anomalous correlations $\left\langle \alpha_{-\boldsymbol{k}} \alpha_{\boldsymbol{k}} \right\rangle$ and used the symmetry $\boldsymbol{k} \to -\boldsymbol{k}$. Plugging in Eqs. (4.105a, 4.105b) and introducing $g_{\boldsymbol{k}}^{B}\left(t\right) = \left[2 n_{\boldsymbol{k}}^{B}\left(t\right) + 1 \right]$ yields

$$
\begin{aligned}
g_{\boldsymbol{k}}\left(t\right) &= \frac{\tilde{\epsilon}_{\boldsymbol{k}}}{\mu_{\boldsymbol{k}}} g_{\boldsymbol{k}}^{B}\left(t\right), \qquad (4.107\text{a}) \\
p_{\boldsymbol{k}}\left(t\right) &= -\frac{1}{2} \frac{\left| \gamma_{\boldsymbol{k}} \right|}{\mu_{\boldsymbol{k}}} g_{\boldsymbol{k}}^{B}\left(t\right). \qquad (4.107\text{b})
\end{aligned}
$$

As it can be seen here in this approximation $p_{\boldsymbol{k}}\left(t\right)$ is real and the normal and anomalous correlations are expressed in terms of a single function $g_{\boldsymbol{k}}^{B}\left(t\right)$.

The kinetic equations can be written as

$$
\begin{aligned}
\partial_{t} g_{\boldsymbol{k}}\left(t\right) + 2i \left| \gamma_{\boldsymbol{k}} \right| \left[\left(p_{\boldsymbol{k}}\left(t\right) \right)^{*} - p_{\boldsymbol{k}}\left(t\right) \right] &= I_{\boldsymbol{k}}^{n}\left(t\right), \qquad (4.108\text{a}) \\
2 \partial_{t} p_{\boldsymbol{k}}\left(t\right) + 2i \left[\left| \gamma_{\boldsymbol{k}} \right| g_{\boldsymbol{k}}\left(t\right) + 2 \tilde{\epsilon}_{\boldsymbol{k}} p_{\boldsymbol{k}}\left(t\right) \right] &= I_{\boldsymbol{k}}^{\sigma}\left(t\right), \qquad (4.108\text{b}) \\
2 \partial_{t} \left(p_{\boldsymbol{k}}\left(t\right) \right)^{*} - 2i \left[\left| \gamma_{\boldsymbol{k}} \right| g_{\boldsymbol{k}}\left(t\right) + 2 \tilde{\epsilon}_{\boldsymbol{k}} \left(p_{\boldsymbol{k}}\left(t\right) \right)^{*} \right] &= \left(I_{\boldsymbol{k}}^{\sigma}\left(t\right) \right)^{*}, \qquad (4.108\text{c})
\end{aligned}
$$

where the normal and anomalous collision integrals are given by

$$
\begin{aligned}
I_{\boldsymbol{k}}^{n}\left(t\right) &= \int_{0}^{t} dt_{1} \text{Im} \Bigg[-g_{\boldsymbol{k}}^{I}\left(t,t_{1}\right) \sigma_{\boldsymbol{k}}^{K}\left(t_{1},t\right) - p_{\boldsymbol{k}}^{I}\left(t,t_{1}\right) \pi_{\boldsymbol{k}}^{K}\left(t_{1},t\right) \\
&\qquad + p_{\boldsymbol{k}}^{K}\left(t,t_{1}\right) \pi_{\boldsymbol{k}}^{I}\left(t_{1},t\right) + g_{\boldsymbol{k}}^{K}\left(t,t_{1}\right) \sigma_{\boldsymbol{k}}^{I}\left(t_{1},t\right) \Bigg], \qquad (4.109\text{a}) \\
I_{\boldsymbol{k}}^{\sigma}\left(t\right) &= i \int_{0}^{t} dt_{1} \Bigg[g_{\boldsymbol{k}}^{I}\left(t,t_{1}\right) \left(\pi_{\boldsymbol{k}}^{K}\left(t_{1},t\right) \right)^{*} + p_{\boldsymbol{k}}^{I}\left(t,t_{1}\right) \left(\sigma_{\boldsymbol{k}}^{K}\left(t_{1},t\right) \right)^{*} \\
&\qquad - g_{\boldsymbol{k}}^{K}\left(t,t_{1}\right) \left(\pi_{\boldsymbol{k}}^{I}\left(t_{1},t\right) \right)^{*} - p_{\boldsymbol{k}}^{K}\left(t,t_{1}\right) \left(\sigma_{\boldsymbol{k}}^{I}\left(t_{1},t\right) \right)^{*} \Bigg]. \\
&\qquad\qquad\qquad\qquad\qquad\qquad\qquad\qquad\qquad\qquad (4.109\text{b})
\end{aligned}
$$

Replacing $p_{\boldsymbol{k}}\left(t\right)$ and $\left(p_{\boldsymbol{k}}\left(t\right) \right)^{*}$ in the first kinetic equation by using the second and third one, we obtain the self-consistency relation

$$
\tilde{\epsilon}_{\boldsymbol{k}} \partial_{t} g_{\boldsymbol{k}}\left(t\right) + \frac{1}{2} \left| \gamma_{\boldsymbol{k}} \right| \left[\partial_{t} p_{\boldsymbol{k}}\left(t\right) + \partial_{t} \left(p_{\boldsymbol{k}}\left(t\right) \right)^{*} \right] = \tilde{\epsilon}_{\boldsymbol{k}} I_{\boldsymbol{k}}^{n}\left(t\right) + \left| \gamma_{\boldsymbol{k}} \right| \left[I_{\boldsymbol{k}}^{\sigma}\left(t\right) + \left(I_{\boldsymbol{k}}^{\sigma}\left(t\right) \right)^{*} \right].
$$
$$
(4.110)
$$

4. Dynamics of pumped magnons with $U(1)$-symmetry breaking interactions

This yields the kinetic equation for $g_{\boldsymbol{k}}^B(t)$ when plugging in the transformations Eqs. (4.107a, 4.107b),

$$\partial_t g_{\boldsymbol{k}}^B(t) \;=\; \frac{|\gamma_{\boldsymbol{k}}|}{\mu_{\boldsymbol{k}}}\mathrm{Re}I_{\boldsymbol{k}}^\sigma(t) + \frac{\tilde{\epsilon}_{\boldsymbol{k}}}{\mu_{\boldsymbol{k}}}I_{\boldsymbol{k}}^n(t). \tag{4.111}$$

For the steady state, which corresponds to $\partial_t g_{\boldsymbol{k}}^B(t) = 0$, Vinikovetskii and coauthors derived this equation for another model in Ref. [56]. From now on we are working in the Bogoliubov basis only and we can rename $g_{\boldsymbol{k}}^B(t)$ to $g_{\boldsymbol{k}}(t)$. Note that for $\gamma_{\boldsymbol{k}} = 0$ the normal correlation in both basis coincide, $\left\langle a_{\boldsymbol{k}}^\dagger a_{\boldsymbol{k}}\right\rangle = \left\langle \alpha_{\boldsymbol{k}}^\dagger \alpha_{\boldsymbol{k}}\right\rangle$. The anomalous correlations are neglected completely in that limit.

Inserting the collision integrals Eqs. (C.1a, C.1b), the kinetic equation becomes surprisingly compact. If we sort the terms on the right hand side by the frequency argument of the phonon spectral function, the kinetic equation consists of three parts,

$$\partial_t g_{\boldsymbol{k}}(t) = \frac{1}{V}\sum_{\boldsymbol{q}}\sum_{\lambda_1,\lambda_2=\pm 1}\frac{\lambda_1}{2\mu_{\boldsymbol{k}}}\frac{\lambda_2}{2\mu_{\boldsymbol{k}-\boldsymbol{q}}}\left[D_{\boldsymbol{k},\boldsymbol{q},\lambda_1\lambda_2}^0(t) + D_{\boldsymbol{k},\boldsymbol{q},\lambda_1\lambda_2}^+(t) + D_{\boldsymbol{k}\boldsymbol{q},\lambda_1\lambda_2}^-(t)\right],$$

$$\tag{4.112}$$

where we have collected the terms into

$$D_{\boldsymbol{q},\lambda_1\lambda_2}^0(t) = D_{0,\boldsymbol{q}}^I\left(\lambda_1\mu_{\boldsymbol{k}} - \lambda_2\mu_{\boldsymbol{k}-\boldsymbol{q}}\right)$$

$$\times\left\{\left(\Gamma_{\boldsymbol{k},\boldsymbol{q}}^n\right)^2\left[\lambda_1\tilde{\epsilon}_{\boldsymbol{k}}\tilde{\epsilon}_{\boldsymbol{k}-\boldsymbol{q}} + \lambda_2\mu_{\boldsymbol{k}}\mu_{\boldsymbol{k}-\boldsymbol{q}} + \lambda_1|\gamma_{\boldsymbol{k}}||\gamma_{\boldsymbol{k}-\boldsymbol{q}}|\right]\right.$$

$$\left. +\Gamma_{\boldsymbol{k},\boldsymbol{q}}^n\mathrm{Re}\Gamma_{\boldsymbol{k},\boldsymbol{q}}^\sigma(t)\left[-\lambda_1\epsilon_{\boldsymbol{k}}|\gamma_{\boldsymbol{k}-\boldsymbol{q}}| - \lambda_1|\gamma_{\boldsymbol{k}}|\epsilon_{\boldsymbol{k}-\boldsymbol{q}}\right]\right\}$$

$$\times\left\{1 + f^0\left(\lambda_1\mu_{\boldsymbol{k}} - \lambda_2\mu_{\boldsymbol{k}-\boldsymbol{q}}\right)\left[\lambda_2 g_{\boldsymbol{k}-\boldsymbol{q}}(t) - \lambda_1 g_{\boldsymbol{k}}(t)\right] - \lambda_1\lambda_2 g_{\boldsymbol{k}}(t)g_{\boldsymbol{k}-\boldsymbol{q}}(t)\right\},$$

$$\tag{4.113a}$$

$$D_{\boldsymbol{k},\boldsymbol{q},\lambda_1\lambda_2}^+(t) = D_{0,\boldsymbol{q}}^I\left(\lambda_1\mu_{\boldsymbol{k}} - \lambda_2\mu_{\boldsymbol{k}-\boldsymbol{q}} + (\Delta_{\boldsymbol{k}} + \Delta_{\boldsymbol{k}-\boldsymbol{q}})\frac{\omega_0}{2}\right)$$

$$\times\left\{\Gamma_{\boldsymbol{k},\boldsymbol{q}}^n\mathrm{Re}\Gamma_{\boldsymbol{k},\boldsymbol{q}}^\sigma(t)\left[-\frac{|\gamma_{\boldsymbol{k}}|}{\mu_{\boldsymbol{k}}}\left(\lambda_1\mu_{\boldsymbol{k}} + \tilde{\epsilon}_{\boldsymbol{k}}\right)\left(-\lambda_2\mu_{\boldsymbol{k}-\boldsymbol{q}} + \tilde{\epsilon}_{\boldsymbol{k}-\boldsymbol{q}}\right)\right.\right.$$

$$\left.-\frac{\tilde{\epsilon}_{\boldsymbol{k}}}{\mu_{\boldsymbol{k}}}\left(\lambda_1\mu_{\boldsymbol{k}} + \tilde{\epsilon}_{\boldsymbol{k}}\right)|\gamma_{\boldsymbol{k}-\boldsymbol{q}}|\right]$$

$$+\left|\Gamma_{\boldsymbol{k},\boldsymbol{q}}^\sigma(t)\right|^2\frac{\tilde{\epsilon}_{\boldsymbol{k}}}{\mu_{\boldsymbol{k}}}\left(\lambda_1\mu_{\boldsymbol{k}} + \tilde{\epsilon}_{\boldsymbol{k}}\right)\left(-\lambda_2\mu_{\boldsymbol{k}-\boldsymbol{q}} + \tilde{\epsilon}_{\boldsymbol{k}-\boldsymbol{q}}\right)$$

$$\left.+\mathrm{Re}\left(\Gamma_{\boldsymbol{k},\boldsymbol{q}}^\sigma(t)\right)^{*2}\frac{|\gamma_{\boldsymbol{k}}|}{\mu_{\boldsymbol{k}}}\left(\lambda_1\mu_{\boldsymbol{k}} + \tilde{\epsilon}_{\boldsymbol{k}}\right)|\gamma_{\boldsymbol{k}-\boldsymbol{q}}|\right\}$$

$$\times\left\{1 + f^0\left(\lambda_1\mu_{\boldsymbol{k}} - \lambda_2\mu_{\boldsymbol{k}-\boldsymbol{q}} + (\Delta_{\boldsymbol{k}} + \Delta_{\boldsymbol{k}-\boldsymbol{q}})\frac{\omega_0}{2}\right)\left[\lambda_2 g_{\boldsymbol{k}-\boldsymbol{q}}(t) - \lambda_1 g_{\boldsymbol{k}}(t)\right]\right.$$

$$\left.-\lambda_1\lambda_2 g_{\boldsymbol{k}}(t)g_{\boldsymbol{k}-\boldsymbol{q}}(t)\right\}, \tag{4.113b}$$

$$D_{\boldsymbol{k},\boldsymbol{q},\lambda_1\lambda_2}^{-}(t) = D_{0,\boldsymbol{q}}^{I}\left(\lambda_1\mu_{\boldsymbol{k}} - \lambda_2\mu_{\boldsymbol{k}-\boldsymbol{q}} - (\Delta_{\boldsymbol{k}} + \Delta_{\boldsymbol{k}-\boldsymbol{q}})\frac{\omega_0}{2}\right)$$

$$\times\left\{\Gamma_{\boldsymbol{k},\boldsymbol{q}}^{n}\mathrm{Re}\Gamma_{\boldsymbol{k},\boldsymbol{q}}^{\sigma}(t)\left[-\frac{\tilde{\epsilon}_{\boldsymbol{k}}}{\mu_{\boldsymbol{k}}}|\gamma_{\boldsymbol{k}}|(\lambda_2\mu_{\boldsymbol{k}-\boldsymbol{q}} + \tilde{\epsilon}_{\boldsymbol{k}-\boldsymbol{q}}) - \frac{|\gamma_{\boldsymbol{k}}|^2}{\mu_{\boldsymbol{k}}}|\gamma_{\boldsymbol{k}-\boldsymbol{q}}|\right]\right.$$

$$\left.+\mathrm{Re}\left(\Gamma_{\boldsymbol{k},\boldsymbol{q}}^{\sigma}(t)\right)^2\frac{\tilde{\epsilon}_{\boldsymbol{k}}}{\mu_{\boldsymbol{k}}}|\gamma_{\boldsymbol{k}}||\gamma_{\boldsymbol{k}-\boldsymbol{q}}| + \left|\Gamma_{\boldsymbol{k},\boldsymbol{q}}^{\sigma}(t)\right|^2\frac{|\gamma_{\boldsymbol{k}}|^2}{\mu_{\boldsymbol{k}}}(\lambda_2\mu_{\boldsymbol{k}-\boldsymbol{q}} + \tilde{\epsilon}_{\boldsymbol{k}-\boldsymbol{q}})\right\}$$

$$\times\left\{1 + f^0\left(\lambda_1\mu_{\boldsymbol{k}} - \lambda_2\mu_{\boldsymbol{k}-\boldsymbol{q}} - (\Delta_{\boldsymbol{k}} + \Delta_{\boldsymbol{k}-\boldsymbol{q}})\frac{\omega_0}{2}\right)[\lambda_2 g_{\boldsymbol{k}-\boldsymbol{q}}(t) - \lambda_1 g_{\boldsymbol{k}}(t)]\right.$$

$$\left.-\lambda_1\lambda_2 g_{\boldsymbol{k}}(t)g_{\boldsymbol{k}-\boldsymbol{q}}(t)\right\}. \tag{4.113c}$$

Unfortunately in the argument of the phonon spectral functions the additional constant factor $\sim\omega_0$ breaks the energy conservation of the scattering processes and makes it impossible to calculate the equilibrium distribution analytically. At the moment it is not clear if Eq. (4.112) describes a relaxation into a steady state because of unstable numerical calculations. The reason for this could not be found. To work on the level of the Boltzmann equation where the energy is conserved for all scattering processes, we have to neglect the time dependence of the anomalous interactions $\Gamma_{\boldsymbol{k},\boldsymbol{q}}^{\sigma}(t)$. Obviously this is valid for small times, $t\lesssim 2/\omega_0$, where we can approximate

$$e^{i\omega_0 t/2} \approx 1. \tag{4.114}$$

In this case we obtain energy conservation for all terms and using $g_{\boldsymbol{k}}(t) = 1 + 2n_{\boldsymbol{k}}(t)$ we find

$$\partial_t n_{\boldsymbol{k}}(t) = \frac{1}{2}\frac{1}{V}\sum_{\boldsymbol{k}'}\sum_{\lambda_1,\lambda_2=\pm 1}\frac{\lambda_1}{\mu_{\boldsymbol{k}}}\frac{\lambda_2}{\mu_{\boldsymbol{k}'}}$$

$$\times\left\{\left(\Gamma_{\boldsymbol{k},\boldsymbol{k}-\boldsymbol{k}'}^{n}\right)^2\left[\lambda_1\tilde{\epsilon}_{\boldsymbol{k}}\tilde{\epsilon}_{\boldsymbol{k}'} + \lambda_1|\gamma_{\boldsymbol{k}}||\gamma_{\boldsymbol{k}'}| + \lambda_2\mu_{\boldsymbol{k}}\mu_{\boldsymbol{k}'}\right]\right.$$

$$+\left(\Gamma_{\boldsymbol{k},\boldsymbol{k}-\boldsymbol{k}'}^{\sigma}\right)^2\left[\lambda_1\tilde{\epsilon}_{\boldsymbol{k}}\tilde{\epsilon}_{\boldsymbol{k}'} + \lambda_1|\gamma_{\boldsymbol{k}}||\gamma_{\boldsymbol{k}'}| - \lambda_2\mu_{\boldsymbol{k}}\mu_{\boldsymbol{k}'}\right]$$

$$\left.+2\Gamma_{\boldsymbol{k},\boldsymbol{k}-\boldsymbol{k}'}^{n}\Gamma_{\boldsymbol{k},\boldsymbol{k}-\boldsymbol{k}'}^{\sigma}\left[-\lambda_1\tilde{\epsilon}_{\boldsymbol{k}}|\gamma_{\boldsymbol{k}'}| - \lambda_1|\gamma_{\boldsymbol{k}}|\tilde{\epsilon}_{\boldsymbol{k}'}\right]\right\}$$

$$\times\left\{W_{\boldsymbol{k},\boldsymbol{k}'}^{\lambda_1\lambda_2}\left[\lambda_2 n_{\boldsymbol{k}'}(t)[1 + \lambda_1 n_{\boldsymbol{k}}(t)] + \frac{1}{4}(\lambda_1 + 1)(\lambda_2 - 1)\right]\right.$$

$$\left.-W_{\boldsymbol{k}',\boldsymbol{k}}^{\lambda_2\lambda_1}\left[\lambda_1 n_{\boldsymbol{k}}(t)[1 + \lambda_2 n_{\boldsymbol{k}'}(t)] + \frac{1}{4}(\lambda_2 + 1)(\lambda_1 - 1)\right]\right\}, \tag{4.115}$$

where we have shifted the momentum summation index to $\boldsymbol{k}' = \boldsymbol{k} - \boldsymbol{q}$ and defined the rates as

$$W_{\boldsymbol{k},\boldsymbol{k}'}^{\lambda_1\lambda_2} = D_{0,\boldsymbol{k}-\boldsymbol{k}'}^{I}\left(\lambda_1\mu_{\boldsymbol{k}} - \lambda_2\mu_{\boldsymbol{k}'}\right)b\left(\lambda_1\mu_{\boldsymbol{k}} - \lambda_2\mu_{\boldsymbol{k}'}\right). \tag{4.116}$$

The out-scattering part can be obtained from the in-scattering part by $\boldsymbol{k} \leftrightarrow \boldsymbol{k}'$ and $\lambda_1 \leftrightarrow \lambda_2$. Hence the detailed balance condition becomes

$$W_{\boldsymbol{k},\boldsymbol{k}'}^{\lambda_1\lambda_2} e^{-\beta\lambda_2\mu_{\boldsymbol{k}'}} = W_{\boldsymbol{k}',\boldsymbol{k}}^{\lambda_2\lambda_1} e^{-\beta\lambda_1\mu_{\boldsymbol{k}}}, \tag{4.117}$$

which is fulfilled due to the identities $D_{0,\boldsymbol{q}}^I(-\omega) = -D_{0,\boldsymbol{q}}^I(\omega)$ and $b(-\omega) = -[1 + b(\omega)] = -e^{\beta\omega}b(\omega)$. The right hand side of the rate equation (4.115) is nullified for every $\boldsymbol{k}$, $\boldsymbol{k}'$ and λ_1, λ_2 separately by

$$n_{\boldsymbol{k}}(t) = b(\mu_{\boldsymbol{k}}), \tag{4.118}$$

which can be seen by using the relations

$$e^{\beta(\omega_1-\omega_2)} = \frac{b(\omega_2)[1 + b(\omega_1)]}{b(\omega_1)[1 + b(\omega_2)]}, \tag{4.119}$$

$$\lambda b(\omega) = b(\lambda\omega) - \frac{\lambda - 1}{2}. \tag{4.120}$$

In contrast to the equilibrium distribution of the kinetic equation (3.55) from last chapter, here the chemical potential has to be zero which leads to a relatively broad distribution at room temperature, see Fig. 4.4.

In the experiment of Ref. [40] it is observed that during the pumping phase the occupation of the pumped modes shoots up fast till it saturates at a certain value while all other modes increase much slower. According to Eq. (4.118) the external pumping field modifies the equilibrium occupation for the pumped modes only and hence, when the pumping field is switched on, the pumped modes thermalize to their new steady-state value whereas the other modes are not modified, see Fig. 4.4. In the pumping phase the rate equation (4.115) fails in describing any increase of modes which are not pumped. This should be fixed by taking into account the energy renormalization which is beyond the scope of this thesis.

In the setup of Ref. [40] the occupation of the not-pumped modes deviate from their equilibrium values significantly only for pumping pulses $\gtrsim 30\,\text{ns}$, see [40]. Thus we conclude that our approximations, in particular neglecting the time dependence of the anomalous interactions, are justified for pumping pulses up to roughly $30\,\text{ns}$. This is larger than the inverse frequency of the microwave field used in the experiment and thus larger than the time scale for which the approximation (4.114) should be valid. This can be justified by the fact that the magnon lifetime is much larger than this time scale. Hence the anomalous interactions themselves, which are responsible for the particle loss, are not important for such short pumping pulses, see Refs. [36, 61] for example. Even on larger scales they should not contribute much because otherwise magnons in these systems could not thermalize to a quasi-equilibrium state in which they form a BEC as claimed in Refs. [36, 37, 38, 39, 40, 61, 76, 77].

Note that the kinetic equation (4.112) could also be expressed by transition rates which fulfill the detailed balance condition Eq. (4.117). It turns

out that considering also magnon-magnon interactions our formalism yields a kinetic equation which exhibits such a transition rate structure[1]. Therefore our method is a generic tool for deriving rate equations for many different systems. In the next section we will use the rate equation (4.115) for numerical calculations.

4.5. Numerical results and comparison with experimental data

In this section we show numerical results of the rate equation (4.115) and compare it to data from experiment, in particular to Fig. 7 and Fig. 8 of Ref. [40] which we also show in Figs. 4.5 and 4.6. In the experiment magnons of certain wave vectors are injected by an external microwave field in the parallel pumping geometry [31, 45, 46]. For the data of Ref. [40] we want to compare with, the magnons were pumped for 30 ns and thus we can apply the rate equation (4.115). Due to the Markov approximation, we can also use Eq. (4.115) for calculating the thermalization after switching off the pumping by setting $\gamma_{\boldsymbol{k}} = 0$.

For the parameters of the magnon dispersion and for the sound velocity in YIG we used in our calculations the same values as in section 1.3 and 3.5. It follows that the minimum of the magnon dispersion is located at $\left|k_{\parallel}\right| = k_{\min} = 5.5 \times 10^4 \, \mathrm{cm}^{-1}$ and $k_{\perp} = 0$, where $k_{\parallel}$ is the wave vector component parallel to the static magnetic field and $k_{\perp}$ perpendicular to it. As in the last chapter we consider a square sample of length $L = 4.58 \, \mu\mathrm{m}$. With the lattice constant given by Eq. (1.129) this results in a reciprocal lattice spacing of $0.25 k_{\min}$. For finite systems the delta functions in the phonon spectral function of the transition rates Eqs. (4.116) are not well defined. To broaden the delta functions we could use the intrinsic damping of the phonons due to the feedback of the magnons like in Eq. (3.65), but for simplicity we introduce a phenomenological line width as in Ref. [82]. Note that here the self-energies of the phonons contain additional diagrams due to the anomalous interactions. Assuming a temperature of 50 K and zero magnetic field in Ref. [97] a line width of 0.7 MHz at a frequency of 10 GHz for longitudinal phonons was obtained. According to this reference the damping should not vary much when applying a magnetic field of 1000 Oe and we use this value for the damping as a rough estimate for our calculation.

Due to the fact that we have not applied functional renormalization group methods, we do not have to deal with the additional evolution in the flow parameter as in section 3.5 and the derivatives can also be calculated at intermediate points. Hence we can use the fourth-order Runge-Kutta method for solving the differential equation instead of the simple Euler method we had

---

[1]Andreas Rückriegel, private communication.

to use before. Apart from that the numerics are similar to those of the last chapter.

As mentioned in section 4.1 for parametric resonance $\gamma_{\boldsymbol{k}^*} > \tilde{\epsilon}_{\boldsymbol{k}^*}$ for all wave vectors $\boldsymbol{k}^*$ corresponding to an energy close to $\omega_0/2$. Without two-particle interactions this leads to the unphysical behavior of an unbounded growth of the particle number [45, 56]. Therefore we take the effect of magnon-magnon interactions effectively into account by fixing the pumping strength $|\gamma_{\boldsymbol{k}}|$ such that, in the steady state, a certain particle number is obtained. For simplicity we assume that the pumped modes are equally occupied by N_{pump} particles,

$$N_{\mathrm{pump}} = \frac{1}{e^{\beta\sqrt{\tilde{\epsilon}_{\boldsymbol{k}^*}^2 - |\gamma_{\boldsymbol{k}^*}|^2}} - 1}, \qquad (4.121)$$

where $\boldsymbol{k}^*$ fulfills the condition $\omega_0/2 - \Delta \leq \tilde{\epsilon}_{\boldsymbol{k}^*} \leq \omega_0/2 + \Delta$. Note that the magnon particle number N_{pump} does not necessarily have to scale linearly with the pumping power. The interaction strength Γ of Eq. (4.31) and N_{pump} are fitted to experimental results such that in particular the dynamics of the magnons at the bottom of the dispersion are similar. An interaction strength of $\Gamma = 4.74 \times 10^{-7}$ cm$\sqrt{\mathrm{GHz}}$ gives similar time scales as the experiment, see Figs. 4.5 and 4.6, and is used for our calculations. The microwave frequency is assumed to be $8.1\,\mathrm{GHz}$ and we choose $\Delta = 0.1\,\mathrm{GHz}$ such that only magnons with energies in the range $(4.1 \pm 0.1)\,\mathrm{GHz}$ get excited. However not all modes in this energy range are coupled to the external field equally. From data of Ref. [76] it can be seen that mainly wave vectors with $|k_\perp| \lesssim 0.5k_{\mathrm{min}}$ are pumped, see also the discussion in section 3.5. For our calculation we assume that all modes with energy $(4.1 \pm 0.1)\,\mathrm{GHz}$ and wave vectors $|k_\perp| < 0.5k_{\mathrm{min}}$ are equally pumped, see Fig. 4.4.

For the plots in Fig. 4.6 we assumed the magnon distribution to be continuous in momentum space and used the triangular method, see Appendix A, to perform the integrals for the occupation $n(\epsilon, t)$,

$$n(\epsilon, t) = \int \frac{d^2k}{(2\pi)^2} \delta(\mu_{\boldsymbol{k}} - \epsilon) n_{\boldsymbol{k}}(t), \qquad (4.122)$$

where ϵ is the frequency.

As it can be seen from Figs. 4.5 and 4.6 experimental data is reproduced quite well by our formalism. In particular the relaxation of the magnons at the minimum is in good agreement with experimental results. Nevertheless some differences are observable. In our calculation the magnons stay longer close the microwave frequency and the relation between the peak of the pumped magnon and the peak of the ground state is much larger than in the experimental data, see Fig. 4.6. We suspect this is due to neglecting magnon-magnon interactions. According to Ref. [40] these interactions are causing a fast redistribution of the magnons. Other deviations in time scales and in the sharpness of the peaks can be explained by the same argument. A possible consequence is that in our case the time scales are actually larger than those of the experiment

a)
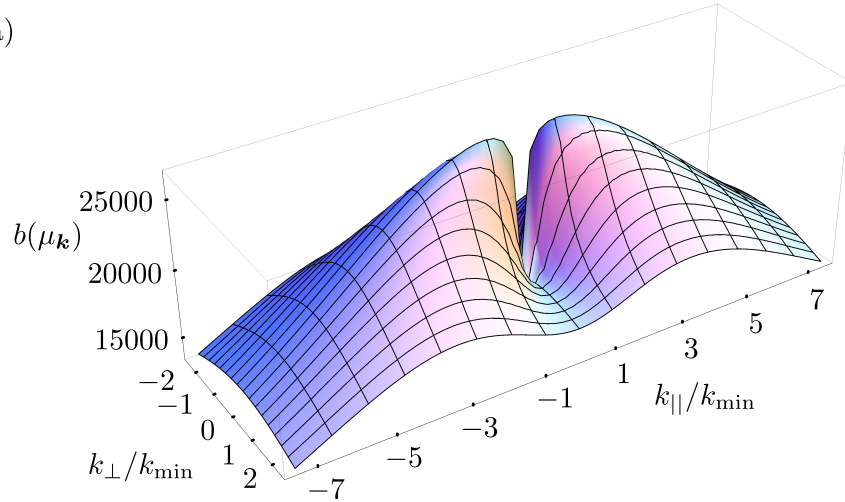
b)
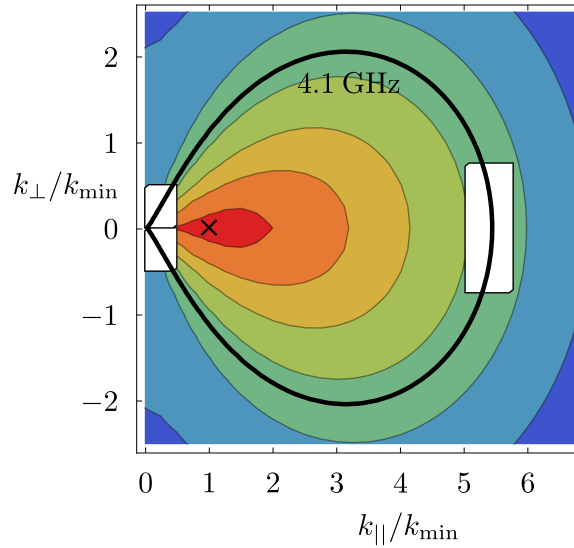
Figure 4.4.: Interpolations of the particle distributions in reciprocal space which nullify the collision integral of the kinetic equation Eq. (4.115). The component $k_\perp$ is perpendicular to the static magnetic field and $k_\parallel$ parallel to it. Plot a) is for $\gamma_{\boldsymbol{k}} = 0$ and shows the occupation number of the equilibrium distribution Eq. (4.118). The second graph is a contour plot of the steady state particle distribution with finite pumping strength. Except of the peaks of pumped magnons it shows the same distribution as a). The cross in b) marks the minimum of the dispersion and the black contour the wave vectors with energy 4.1 GHz which is half of the frequency of the microwave field. In the energy range of (4.1 ± 0.1) GHz all modes with $|k_\perp| \leq 0.5 k_{\min}$ get pumped. The white spots are peaks of same heights which are clipped in the plot.
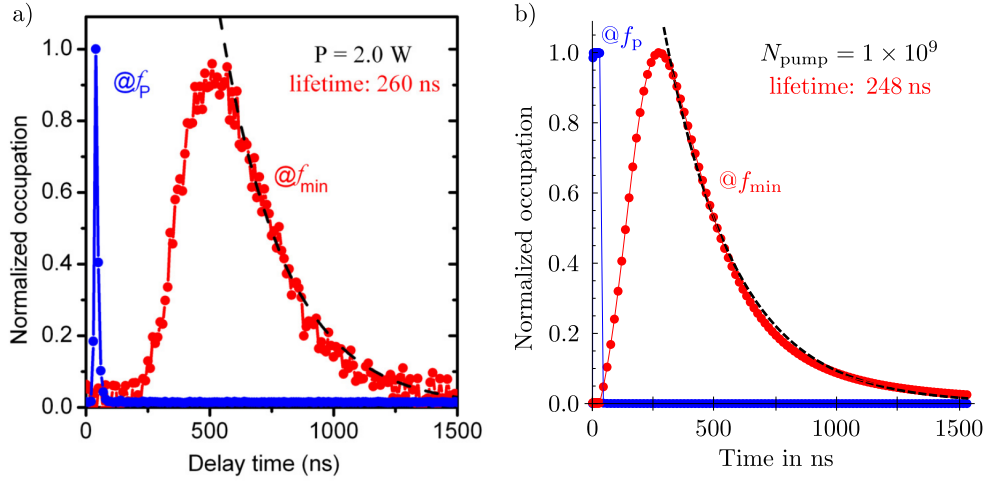
Figure 4.5.: The occupation of the pumped f_{pump} and minimal frequency f_{min} normalized to their maximum values. Plot a) is taken from Ref. [40] (©IOP Publishing Ltd and Deutsche Physikalische Gesellschaft. Published under a CC BY-NC-SA licence) and show the corresponding experimental data with a pumping power of 2.0 W to our numerical results illustrated in b). The numerical calculation was done with $N_{\mathrm{pump}} = 1 \times 10^9$. The black dashed lines are exponential fits to the occupation of f_{min}. After 248 ns the occupation of the minimum has decreased to half of its maximum value in our calculations and after 260 ns in the experiment.
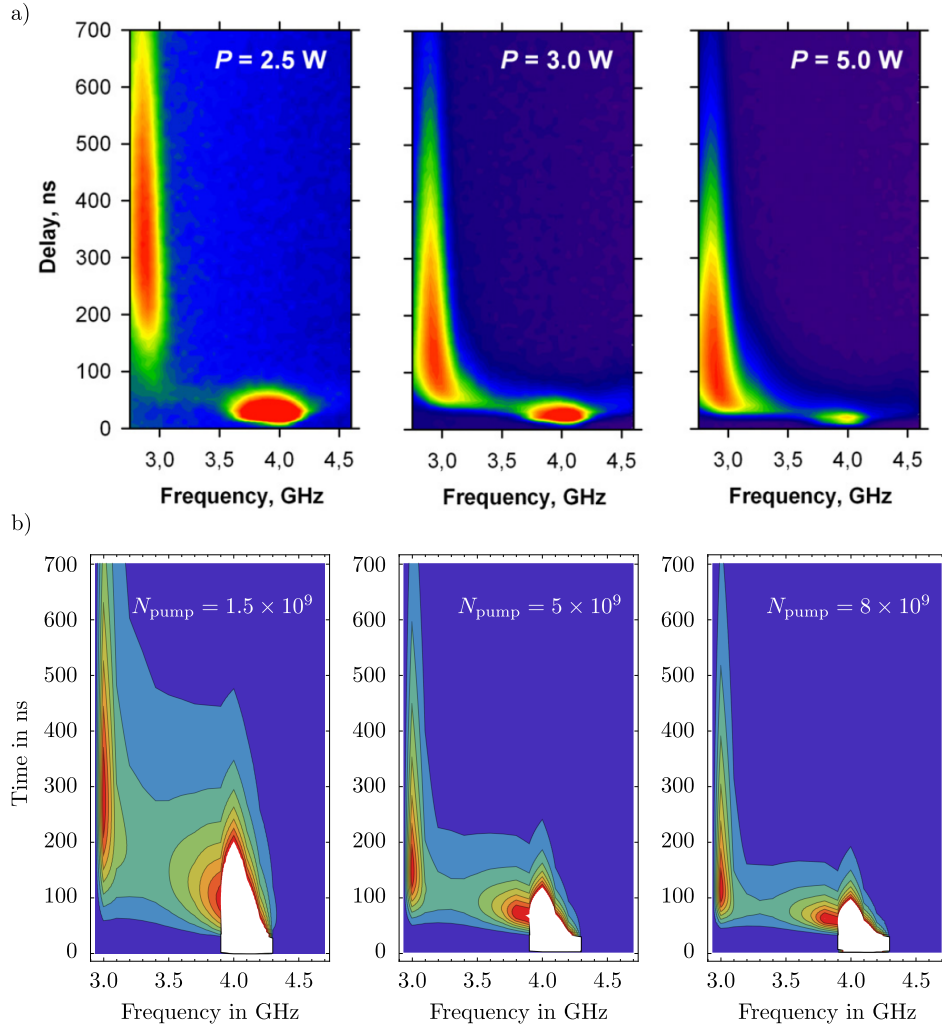
Figure 4.6.: Contour plots of the magnon occupation over frequency and time, a) is taken from Ref. [40] (©IOP Publishing Ltd and Deutsche Physikalische Gesellschaft. Published under a CC BY-NC-SA licence) and b) shows the results of our calculations. We have used an accuracy in frequency of 0.1 GHz for the numerics. The white spots in b) are peaks out of the plot range. Our chosen parameters for YIG yield a slightly higher minimum energy and hence our plots do not reach down to this lower minimal energy of experimental data. As in the experiment the pumping has been turned off after 30 ns. The particle numbers $N_{\mathrm{pump}} = 1 \times 10^8, 5 \times 10^8, 10 \times 10^8$ were chosen to yield similar dynamics around the minimum frequency compared to a) corresponding to pumping powers of $P = 2.5\,\mathrm{W}, 3.0\,\mathrm{W}, 5.0\,\mathrm{W}$. Because of the steepness of the dispersion around the origin, see Fig. 1.6, the peaks of the pumped modes would contribute also to most of the other frequencies in Eq. (4.122). In order to avoid an artificial broad peak around the pumping frequency we excluded wave vectors close to zero momentum for frequencies outside the interval 4.1 ± 0.1 GHz.

because a greater portion of magnons is lost during the observation time. Also the particle numbers might be too large compared to the experiment. If the magnons are redistributed faster, smaller occupations would be sufficient to obtain similar results as in the experiment.

4.6. Summary and conclusion

We have considered a minimal model for describing the pumping phase and the relaxation of the magnon particle number in addition to the thermalization process we covered in chapter 3. We showed in section 4.2 that the necessary anomalous interactions $\Gamma^{\sigma}_{\boldsymbol{k},\boldsymbol{q}}$ are present in YIG and can be obtained from linear spin wave theory. Due to the explicit $U(1)$-symmetry breaking the structure of the Keldysh formalism becomes more complicated which we discussed in section 4.3. We were able to derive a kinetic equation for the magnon distribution function $n_{\boldsymbol{k}}(t)$ which has a similar rate structure as the rate equation (3.55) from the previous chapter. In contrast to the case without $U(1)$-symmetry breaking we did not use the Wigner transformation but a real time approach which seems to be more general and also be applicable for systems with magnon-magnon interactions. For short pumping pulses we could neglect the time dependence of the anomalous interactions and found the expression Eq. (4.115) which has nice analytical properties, namely that the transition rate fulfill the detailed balance condition Eq. (4.117) and that the equilibrium distribution can be identified to be the Bose function with zero chemical potential. Through the comparison with the magnonic behavior during the pumping phase in experiments we could estimate the time length of pumping pulses for which our approximations are still justified. This time length is longer than the approximation (4.114) suggests. This can be explained by the fact that these interactions are not important for the dynamics on these time scales, see also the discussion at the end of section 4.4.5. In section 4.5 we compared our numerical results to the experimental data from Ref. [40]. In particular the relaxation of the occupation at the bottom of the dispersion was reproduced well. Considering also magnon-magnon interactions should further improve the results.

A. Triangular method

The triangular method is a numerical method for calculating a two dimensional integral containing a delta function as in

$$
\begin{aligned}
I &= \int\int dxdy\, f\left(\boldsymbol{r}\right)\delta\left(g\left(\boldsymbol{r}\right)-\varphi\right) \\
&= \int_{\mathcal{C}}\frac{ds}{\left|\boldsymbol{\nabla}g\left(\boldsymbol{r}\right)\right|}f\left(\boldsymbol{r}\right),
\end{aligned}
\tag{A.1}
$$

which is an integral over the contour $\mathcal{C}$ defined by $g\left(\boldsymbol{r}\right)=\varphi$ and where $\boldsymbol{r}=\left(\begin{array}{cc} x, & y \end{array}\right)^{T}$ is a two dimensional vector. The two-dimensional gradient is defined by $\boldsymbol{\nabla}=\left(\begin{array}{cc} \partial_{x}, & \partial_{y} \end{array}\right)^{T}$. The calculation of the density of states is a typical example for an application for the triangular method. In this appendix we present a two-dimensional adaptation of the tetrahedron method of Ref. [89].

We assume that the functions $f\left(\boldsymbol{r}\right)$ and $g\left(\boldsymbol{r}\right)$ are only given at the sides of a square lattice and we divide the integration area into triangles as shown in Fig. A.1. The integral then becomes

$$
I = \int_{\mathcal{C}}\frac{ds}{\left|\boldsymbol{\nabla}g\left(\boldsymbol{r}\right)\right|}f\left(\boldsymbol{r}\right) \;=\; \sum_{i}N_{i},
\tag{A.2}
$$

where N_{i} is the integral over a single triangle and the summation i runs over all triangles of the integration area.

A.1. Linearization on a triangle

Let us consider a single triangle. For the approximate calculation of N_{i} for a given triangle i we linearly extrapolate the functions $f\left(\boldsymbol{r}\right)$ and $g\left(\boldsymbol{r}\right)$,

$$
\begin{aligned}
f\left(\boldsymbol{r}\right) &= F_{0}+\boldsymbol{F}\cdot\boldsymbol{r}, & \text{(A.3a)} \\
g\left(\boldsymbol{r}\right) &= G_{0}+\boldsymbol{G}\cdot\boldsymbol{r}. & \text{(A.3b)}
\end{aligned}
$$

Note that $\boldsymbol{\nabla}g\left(\boldsymbol{r}\right)=\boldsymbol{G}$. For the integral over a single triangular we obtain that

$$
N_{i} \;=\; \frac{1}{\left|\boldsymbol{G}\right|}\left[F_{0}\int_{\triangle_{i}}ds+\boldsymbol{F}\int_{\triangle_{i}}ds\,\boldsymbol{x}\right],
\tag{A.4}
$$

where $\triangle_{i}$ indicates the integration along the contour $\mathcal{C}$ in the i'th triangle. The coefficients of the linearization can be obtained by setting the linearized

A. Triangular method
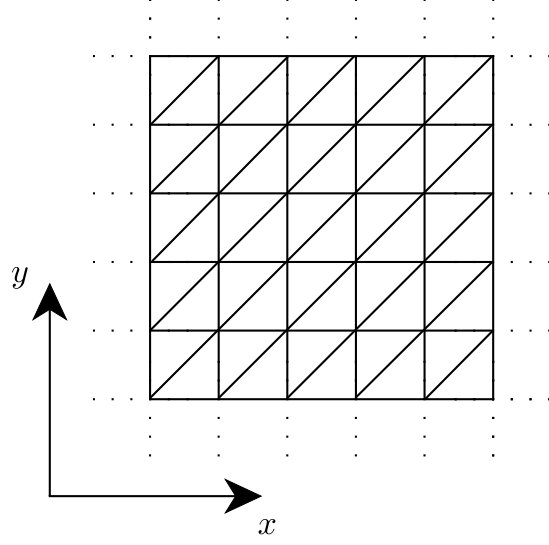
Figure A.1.: An illustration of dividing the integration area of the integral I into triangles. Here we have assumed that the functions of the integrand are given on a square lattice such that we obtain right angled triangles.

functions equal to their actual values at the lattice sides. They are determined by the following system of equations:

$$F_c = f(\boldsymbol{r}_\mathrm{c}) \stackrel{!}{=} F_0 + \boldsymbol{F} \cdot \boldsymbol{r}_\mathrm{c}, \tag{A.5a}$$

$$F_\mathrm{eqx} = f(\boldsymbol{r}_\mathrm{eqx}) \stackrel{!}{=} F_0 + \boldsymbol{F} \cdot \boldsymbol{r}_\mathrm{eqx}, \tag{A.5b}$$

$$F_\mathrm{eqy} = f(\boldsymbol{r}_\mathrm{eqy}) \stackrel{!}{=} F_0 + \boldsymbol{F} \cdot \boldsymbol{r}_\mathrm{eqy}, \tag{A.5c}$$

where we choose the coordinate system as shown in Fig. A.2 and c refers to the corner vertex at the right angle, eqx to the vertex where the x-coordinate is equal to the one at the corner and so on. The solution of this system of equations is

$$F_x = \frac{F_\mathrm{c} - F_\mathrm{eqy}}{x_\mathrm{c} - x_\mathrm{eqy}}, \tag{A.6a}$$

$$F_y = \frac{F_\mathrm{c} - F_\mathrm{eqx}}{y_\mathrm{c} - y_\mathrm{eqx}}, \tag{A.6b}$$

$$F_0 = \frac{(F_\mathrm{eqy} - F_\mathrm{c})\, x_\mathrm{c}}{x_\mathrm{c} - x_\mathrm{eqy}} + \frac{(F_\mathrm{eqx} y_\mathrm{c} - F_\mathrm{c} y_\mathrm{eqx})}{y_\mathrm{c} - y_\mathrm{eqx}}, \tag{A.6c}$$

$$\boldsymbol{r}_{\mathrm{eqx}} = \begin{pmatrix} x_{\mathrm{c}} \\ y_{\mathrm{eqx}} \end{pmatrix}$$

$$\boldsymbol{r}_{\mathrm{eqy}} = \begin{pmatrix} x_{\mathrm{eqy}} \\ y_{\mathrm{c}} \end{pmatrix} \qquad \boldsymbol{r}_{\mathrm{c}} = \begin{pmatrix} x_{\mathrm{c}} \\ y_{\mathrm{c}} \end{pmatrix}$$
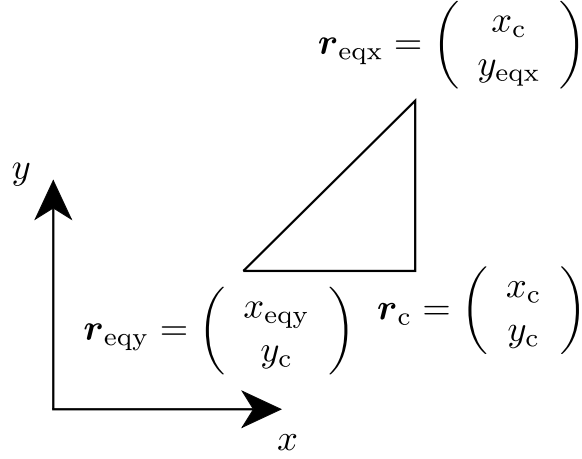
Figure A.2.: Showing the coordinates of the vertices of the considered triangle.

where F_x and F_y are the x- and y-components of $\boldsymbol{F}$. Similarly we obtain for the function $g\left(\boldsymbol{r}\right)$,

$$G_x = \frac{G_c - G_{eqy}}{x_c - x_{eqy}}, \tag{A.7a}$$

$$G_y = \frac{G_c - G_{eqx}}{y_c - y_{eqx}}, \tag{A.7b}$$

$$G_0 = \frac{\left(G_{eqy} - G_c\right) x_c}{x_c - x_{eqy}} + \frac{\left(G_{eqx} y_c - G_c y_1\right)}{y_c - y_{eqx}}, \tag{A.7c}$$

where all definitions of the coefficients are similar to those for $f\left(\boldsymbol{r}\right)$.

A.2. Integral over one triangle

Without loss of generality we define the edges of the triangle such that $G_1 \leq G_2 \leq G_3$, where we have introduced the notation $G_j = g\left(\boldsymbol{r}_j\right)$ for $j = 1, 2, 3$ and $\boldsymbol{r}_j$ refer to the vertices. There is no contribution to the integral I if $\varphi < G_1$ or $G_3 < \varphi$. First we consider the case $G_2 \leq \varphi \leq G_3$ for which the intersections of the contour and the sides of the triangle are given by

$$\boldsymbol{r}_{13} = \boldsymbol{r}_3 + \frac{G_3 - \varphi}{G_3 - G_1} \left(\boldsymbol{r}_1 - \boldsymbol{r}_3\right), \tag{A.8a}$$

$$\boldsymbol{r}_{23} = \boldsymbol{r}_3 + \frac{G_3 - \varphi}{G_3 - G_2} \left(\boldsymbol{r}_2 - \boldsymbol{r}_3\right), \tag{A.8b}$$

see Fig. A.3. Let us start with the first term of N_i Eq. (A.4). We parametrize the contour as $\boldsymbol{r}\left(t\right) = \boldsymbol{r}_{23} + t\boldsymbol{l}_{23}$, where $0 \leq t \leq 1$ and $\boldsymbol{l}_{23} = \boldsymbol{r}_{13} - \boldsymbol{r}_{23}$ is the vector pointing from one intersection to the other. The modulus of the

A. Triangular method
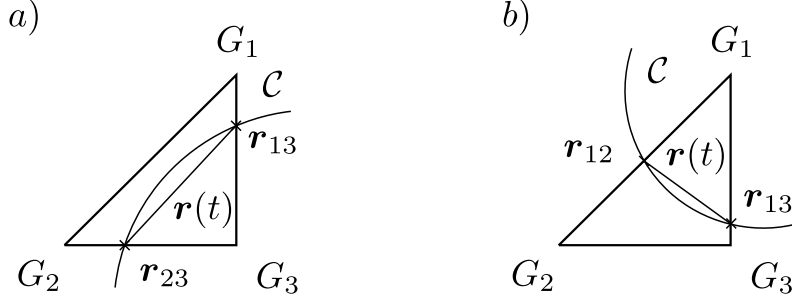
Figure A.3.: A sketch of the considered triangle with contour $\mathcal{C}$, a) for $G_1 \leq G_2 \leq \varphi \leq G_3$ and b) for $G_1 \leq \varphi \leq G_2 \leq G_3$. The parametrization of the linearized contour is denoted by $r(t)$, the coordinate r_{13} refers to the intersection of the contour and the triangle side between G_1 and G_3, and so on.

derivative of the parametrization is given by $|\dot{r}(t)| = |\partial_t r(t)| = |l_{23}|$. The contour integral becomes

$$\frac{F_0}{|\boldsymbol{G}|} \int_{\mathcal{C}} ds = \frac{F_0}{|\boldsymbol{G}|} |\boldsymbol{l}_{23}| \int_0^1 dt \tag{A.9}$$

$$= \frac{F_0}{|\boldsymbol{G}|} |\boldsymbol{l}_{23}| . \tag{A.10}$$

In the case $G_1 \leq \varphi \leq G_2 \leq G_3$, see Fig. A.3, we analogously obtain

$$\frac{F_0}{|\boldsymbol{G}|} \int_{\mathcal{C}} ds = \frac{F_0}{|\boldsymbol{G}|} |\boldsymbol{l}_{12}| , \tag{A.11}$$

where $l_{12} = r_{13} - r_{12}$.

The second term of the integral over a single triangle Eq. (A.4) is

$$\frac{\boldsymbol{F}}{|\boldsymbol{G}|} \int ds\, \boldsymbol{r} = \frac{\boldsymbol{F}}{|\boldsymbol{G}|} l_{23} \int_0^1 dt\, [\boldsymbol{r}_{23} + t\boldsymbol{l}_{23}] \tag{A.12}$$

$$= \frac{1}{2} \frac{l_{23}}{|\boldsymbol{G}|} \boldsymbol{F} \cdot [\boldsymbol{r}_{13} + \boldsymbol{r}_{23}] , \tag{A.13}$$

for $G_1 \leq G_2 \leq \varphi \leq G_3$, and

$$\frac{\boldsymbol{F}}{|\boldsymbol{G}|} \int ds\, \boldsymbol{r} = \frac{1}{2} \frac{l_{12}}{|\boldsymbol{G}|} \boldsymbol{F} \cdot [\boldsymbol{r}_{13} + \boldsymbol{r}_{12}] , \tag{A.14}$$

for $G_1 \leq \varphi \leq G_2 \leq G_3$.

Now doing this calculation for every triangle and summing them up (see Eq. (A.2)) gives the desired approximation to the integral Eq. (A.1).

116

B. Fluctuation-dissipation theorem

In this appendix we derive the fluctuation-dissipation theorem in the form as used in this thesis. We consider a system described by the Hamiltonian $\mathcal{H}$ at equilibrium conditions characterized by the inverse temperature β. We are interested in the retarded, advanced and Keldysh Greens functions,

$$iG_{nm}^{R}\left(t,t'\right) = \Theta\left(t-t'\right)\left\langle\left[a_n\left(t\right),a_m^\dagger\left(t'\right)\right]\right\rangle, \tag{B.1a}$$

$$iG_{nm}^{A}\left(t,t'\right) = -\Theta\left(t'-t\right)\left\langle\left[a_n\left(t\right),a_m^\dagger\left(t'\right)\right]\right\rangle, \tag{B.1b}$$

$$iG_{nm}^{K}\left(t,t'\right) = \left\langle\left\{a_n\left(t\right),a_m^\dagger\left(t'\right)\right\}\right\rangle, \tag{B.1c}$$

where the averages are given by $\left\langle\ldots\right\rangle = \mathrm{Tr}\left[e^{-\beta\mathcal{H}}\ldots\right]/\mathcal{Z}$ with the partition function $\mathcal{Z} = \mathrm{Tr}\left[e^{-\beta\mathcal{H}}\right]$. We denote the energy eigenvalues and the corresponding eigenstates of H by E_n and $|E_n\rangle$. The eigenstates shall form a complete orthonormalized basis such that

$$\sum_n |E_n\rangle\langle E_n| = I, \tag{B.2a}$$

$$\langle E_n|\, E_m\rangle = \delta_{nm}, \tag{B.2b}$$

where I is the identity operator in the Hilbert space of $\mathcal{H}$.

Let us first look at the retarded Green's function, using the expression for the Fourier transform of the Heaviside step function $\Theta\left(t\right)$,

$$\int \mathrm{d}t\,\Theta\left(t\right)e^{i\omega t} = \frac{i}{\omega+i\eta}, \tag{B.3}$$

we obtain the spectral representation of $G_{nm}^{R}\left(\omega\right)$,

$$\begin{aligned}
G_{nm}^{\mathrm{R}}\left(\omega\right) &= \int d\left(t-t'\right)e^{i\omega(t-t')}G_{nm}^{R}\left(t,t'\right) \\
&= \frac{1}{\mathcal{Z}}\sum_{n'm'}\int d\left(t-t'\right)e^{i\omega(t-t')}e^{-\beta E_{m'}} \\
&\quad \times \left[e^{-i\omega_{n'm'}(t-t')}\langle E_{m'}|\,a_n\,|E_{n'}\rangle\langle E_{n'}|\,a_m^\dagger\,|E_{m'}\rangle\right. \\
&\quad \left. -e^{i\omega_{n'm'}(t-t')}\langle E_{m'}|\,a_m^\dagger\,|E_{n'}\rangle\langle E_{n'}|\,a_n\,|E_{m'}\rangle\right] \tag{B.4} \\
&= \frac{1}{\mathcal{Z}}\sum_{n'm'}\frac{\langle E_{m'}|\,a_n\,|E_{n'}\rangle\langle E_{n'}|\,a_m^\dagger\,|E_{m'}\rangle}{\omega-\omega_{n'm'}+i\eta}\left[e^{-\beta E_{m'}}-e^{-\beta E_{n'}}\right], \tag{B.5}
\end{aligned}$$

B. Fluctuation-dissipation theorem

where we have introduced $\omega_{nm} = E_n - E_m$. In the second equality we have performed the trace and inserted a complete set of eigenstates. Analogously we find for the advanced Green's function that

$$G_{nm}^A(\omega) = \frac{1}{\mathcal{Z}} \sum_{n'm'} \frac{\langle E_{m'}|\, a_n \,|E_{n'}\rangle \langle E_{n'}|\, a_m^\dagger \,|E_{m'}\rangle}{\omega - \omega_{n'm'} - i\eta} \left[e^{-\beta E_{m'}} - e^{-\beta E_{n'}} \right], \quad (B.6)$$

and for the Keldysh Green's function that

$$\begin{aligned}
iG_{nm}^K(\omega) &= \frac{2\pi}{\mathcal{Z}} \sum_{n',m'} \delta(\omega - \omega_{n'm'}) \langle E_{m'}|\, a_n \,|E_{n'}\rangle \langle E_{n'}|\, a_m^\dagger \,|E_{m'}\rangle \\
&\quad \times \left[e^{-\beta E_{m'}} + e^{-\beta E_{n'}} \right].
\end{aligned} \qquad (B.7)$$

Using the Dirac identity Eq. (3.34) we obtain

$$\begin{aligned}
i\left(G_{nm}^R(\omega) - G_{nm}^A(\omega)\right) &= \frac{2\pi}{\mathcal{Z}} \sum_{n'm'} \delta(\omega - \omega_{n'm'}) \\
&\quad \times \langle E_{m'}|\, a_n \,|E_{n'}\rangle \langle E_{n'}|\, a_m^\dagger \,|E_{m'}\rangle \left[e^{-\beta E_{m'}} - e^{-\beta E_{n'}} \right],
\end{aligned} \text{(B.8)}$$

and it follows

$$\begin{aligned}
\frac{G_{nm}^K(\omega)}{G_{nm}^R(\omega) - G_{nm}^A(\omega)} &= \sum_{n'm'} \frac{\delta(\omega - \omega_{n'm'}) \left(e^{-\beta(E_{n'}-\omega)} + e^{-\beta E_{n'}} \right)}{\delta(\omega - \omega_{n'm'}) \left(e^{-\beta(E_{n'}-\omega)} - e^{-\beta E_{n'}} \right)} \\
&= \coth\left[\frac{\beta}{2}\omega \right],
\end{aligned} \qquad (B.9)$$

or alternatively

$$G_{nm}^K(\omega) = \coth\left[\frac{\beta}{2}\omega \right] \left[G_{nm}^R(\omega) - G_{nm}^A(\omega) \right], \qquad (B.10)$$

which is the fluctuation dissipation theorem, see for example Ref. [2]. For the comparison with for example Eq. (1.46), note that $\coth[\beta\omega/2] = 1 + 2b(\omega)$, where $b(\omega)$ is the Bose function Eq. (3.50). In homogeneous systems without internal degrees of freedom the quantum numbers n and m in the subscript of Eq. (B.10) become the momentum $\boldsymbol{k}$. When considering the grand canonical ensemble the replacement $\omega \to \omega - \mu$ has to be performed.

C. Collision integrals for pumped magnons

The expressions for the collision integrals $I_{\boldsymbol{k}}^n(t)$ and $I_{\boldsymbol{k}}^\sigma(t)$ for the Hamiltonian (4.3) in the approximations described in section 4.4.4 are very cumbersome without performing a Bogoliubov transformation and neglecting the anomalous correlations in the new basis. In this appendix we explicitly give these expressions. The used approximations are:

1. Generalized Kandanoff-Baym ansatz, see section 4.4.2,

2. Assuming a thermal phonon bath,

3. Neglecting damping of intermediate states,

4. Markov approximation.

Applying these to the collision integrals Eqs. (4.109a, 4.109b) yields

$$
\begin{aligned}
I_{\boldsymbol{k}}^n(t) \;=\; & \frac{1}{V} \sum_{\boldsymbol{q}} \sum_{\lambda_1,\lambda_2=\pm 1} \frac{\lambda_1}{2\mu_{\boldsymbol{k}}} \frac{\lambda_2}{2\mu_{\boldsymbol{k}-\boldsymbol{q}}} \\
& \times \Bigg\{ A_{\boldsymbol{k},\boldsymbol{q},\lambda_1\lambda_2}^{0,nn}(t) + A_{\boldsymbol{k},\boldsymbol{q},\lambda_1\lambda_2}^{0,n\sigma}(t) + A_{\boldsymbol{k},\boldsymbol{q},\lambda_1\lambda_2}^{+,n\overline{\sigma}}(t) \\
& \quad + A_{\boldsymbol{k},\boldsymbol{q},\lambda_1\lambda_2}^{+,\sigma\overline{\sigma}}(t) + A_{\boldsymbol{k},\boldsymbol{q},\lambda_1\lambda_2}^{-,n\sigma}(t) + A_{\boldsymbol{k},\boldsymbol{q},\lambda_1\lambda_2}^{-,\sigma\sigma}(t) \Bigg\}, \quad \text{(C.1a)} \\
I_{\boldsymbol{k}}^\sigma(t) \;=\; & \frac{1}{V} \sum_{\boldsymbol{q}} \sum_{\lambda_1,\lambda_2=\pm 1} \frac{\lambda_1}{2\mu_{\boldsymbol{k}}} \frac{\lambda_2}{2\mu_{\boldsymbol{k}-\boldsymbol{q}}} \\
& \times \Bigg\{ B_{\boldsymbol{k},\boldsymbol{q},\lambda_1\lambda_2}^{0,nn}(t) + B_{\boldsymbol{k},\boldsymbol{q},\lambda_1\lambda_2}^{0,n\overline{\sigma}}(t) + B_{\boldsymbol{k},\boldsymbol{q},\lambda_1\lambda_2}^{+,n\overline{\sigma}}(t) \\
& \quad + B_{\boldsymbol{k},\boldsymbol{q},\lambda_1\lambda_2}^{+,\overline{\sigma}\overline{\sigma}}(t) + B_{\boldsymbol{k},\boldsymbol{q},\lambda_1\lambda_2}^{-,n\sigma}(t) + B_{\boldsymbol{k},\boldsymbol{q},\lambda_1\lambda_2}^{-,\sigma\overline{\sigma}}(t) \Bigg\}, \quad \text{(C.1b)}
\end{aligned}
$$

where we have collected the terms on the right hand side depending on the frequency argument of the phonon spectral function and the interactions. Omit-

C. Collision integrals for pumped magnons

ting the time dependence of the functions $g_{\boldsymbol{k}}(t)$ and $p_{\boldsymbol{k}}(t)$, we obtain

$$
\begin{aligned}
A^{0,nn}_{\boldsymbol{k},\boldsymbol{q},\lambda_1\lambda_2}(t) = D^I_{\boldsymbol{q}}\left(\lambda_1\mu_{\boldsymbol{k}} - \lambda_2\mu_{\boldsymbol{k}-\boldsymbol{q}}\right)\left(\Gamma^n_{\boldsymbol{k},\boldsymbol{q}}\right)^2 \\
\times\Bigg\{ \left(\lambda_1\mu_{\boldsymbol{k}} + \epsilon_{\boldsymbol{k}}\right)\left(\lambda_2\mu_{\boldsymbol{k}-\boldsymbol{q}} + \tilde{\epsilon}_{\boldsymbol{k}-\boldsymbol{q}}\right) + |\gamma_{\boldsymbol{k}}|\,|\gamma_{\boldsymbol{k}-\boldsymbol{q}}| \\
+f^0\left(\lambda_1\mu_{\boldsymbol{k}} - \lambda_2\mu_{\boldsymbol{k}-\boldsymbol{q}}\right)\Big\{ g_{\boldsymbol{k}-\boldsymbol{q}}\big[\left(\lambda_1\mu_{\boldsymbol{k}} + \tilde{\epsilon}_{\boldsymbol{k}}\right)\left(\lambda_2\mu_{\boldsymbol{k}-\boldsymbol{q}} + \tilde{\epsilon}_{\boldsymbol{k}-\boldsymbol{q}}\right) - |\gamma_{\boldsymbol{k}}|\,|\gamma_{\boldsymbol{k}-\boldsymbol{q}}|\big] \\
-p_{\boldsymbol{k}-\boldsymbol{q}}\big[|\gamma_{\boldsymbol{k}}|\left(\lambda_2\mu_{\boldsymbol{k}-\boldsymbol{q}} + \tilde{\epsilon}_{\boldsymbol{k}-\boldsymbol{q}}\right) - \left(\lambda_1\mu_{\boldsymbol{k}} + \tilde{\epsilon}_{\boldsymbol{k}}\right)|\gamma_{\boldsymbol{k}-\boldsymbol{q}}|\big] \\
-g_{\boldsymbol{k}}\big[-|\gamma_{\boldsymbol{k}}|\,|\gamma_{\boldsymbol{k}-\boldsymbol{q}}| + \left(\lambda_1\mu_{\boldsymbol{k}} + \tilde{\epsilon}_{\boldsymbol{k}}\right)\left(\lambda_2\mu_{\boldsymbol{k}-\boldsymbol{q}} + \tilde{\epsilon}_{\boldsymbol{k}-\boldsymbol{q}}\right)\big] \\
+p_{\boldsymbol{k}}\left(\lambda_1\mu_{\boldsymbol{k}} + \tilde{\epsilon}_{\boldsymbol{k}}\right)|\gamma_{\boldsymbol{k}-\boldsymbol{q}}| - p_{\boldsymbol{k}}^*|\gamma_{\boldsymbol{k}}|\left(\lambda_2\mu_{\boldsymbol{k}-\boldsymbol{q}} + \tilde{\epsilon}_{\boldsymbol{k}-\boldsymbol{q}}\right)\Big\} \\
-g_{\boldsymbol{k}}g_{\boldsymbol{k}-\boldsymbol{q}}\big[|\gamma_{\boldsymbol{k}}|\,|\gamma_{\boldsymbol{k}-\boldsymbol{q}}| + \left(\lambda_1\mu_{\boldsymbol{k}} + \tilde{\epsilon}_{\boldsymbol{k}}\right)\left(\lambda_2\mu_{\boldsymbol{k}-\boldsymbol{q}} + \tilde{\epsilon}_{\boldsymbol{k}-\boldsymbol{q}}\right)\big] \\
-g_{\boldsymbol{k}}p_{\boldsymbol{k}-\boldsymbol{q}}\big[|\gamma_{\boldsymbol{k}}|\left(\lambda_2\mu_{\boldsymbol{k}-\boldsymbol{q}} + \tilde{\epsilon}_{\boldsymbol{k}-\boldsymbol{q}}\right) + \left(\lambda_1\mu_{\boldsymbol{k}} + \tilde{\epsilon}_{\boldsymbol{k}}\right)|\gamma_{\boldsymbol{k}-\boldsymbol{q}}|\big] \\
-p_{\boldsymbol{k}}g_{\boldsymbol{k}-\boldsymbol{q}}\left(\lambda_1\mu_{\boldsymbol{k}} + \tilde{\epsilon}_{\boldsymbol{k}}\right)|\gamma_{\boldsymbol{k}-\boldsymbol{q}}| - p_{\boldsymbol{k}}^*g_{\boldsymbol{k}-\boldsymbol{q}}|\gamma_{\boldsymbol{k}}|\left(\lambda_2\mu_{\boldsymbol{k}-\boldsymbol{q}} + \tilde{\epsilon}_{\boldsymbol{k}-\boldsymbol{q}}\right) \\
-p_{\boldsymbol{k}}p_{\boldsymbol{k}-\boldsymbol{q}}\left(\lambda_1\mu_{\boldsymbol{k}} + \tilde{\epsilon}_{\boldsymbol{k}}\right)\left(\lambda_2\mu_{\boldsymbol{k}-\boldsymbol{q}} + \tilde{\epsilon}_{\boldsymbol{k}-\boldsymbol{q}}\right) - p_{\boldsymbol{k}}^*p_{\boldsymbol{k}-\boldsymbol{q}}|\gamma_{\boldsymbol{k}}|\,|\gamma_{\boldsymbol{k}-\boldsymbol{q}}|\Bigg\},
\end{aligned}
\tag{C.2a}
$$

$$
\begin{aligned}
A^{0,n\sigma}_{\boldsymbol{k},\boldsymbol{q},\lambda_1\lambda_2}(t) = D^I_{\boldsymbol{q}}\left(\lambda_1\mu_{\boldsymbol{k}} - \lambda_2\mu_{\boldsymbol{k}-\boldsymbol{q}}\right)\Gamma^n_{\boldsymbol{k},\boldsymbol{q}}\Gamma^\sigma_{\boldsymbol{k},\boldsymbol{q}}(t) \\
\times\Bigg\{ -\left(\lambda_1\mu_{\boldsymbol{k}} + \tilde{\epsilon}_{\boldsymbol{k}}\right)|\gamma_{\boldsymbol{k}-\boldsymbol{q}}| - |\gamma_{\boldsymbol{k}}|\left(-\lambda_2\mu_{\boldsymbol{k}-\boldsymbol{q}} + \tilde{\epsilon}_{\boldsymbol{k}-\boldsymbol{q}}\right) \\
+f^0\left(\lambda_1\mu_{\boldsymbol{k}} - \lambda_2\mu_{\boldsymbol{k}-\boldsymbol{q}}\right)\Big\{ g_{\boldsymbol{k}-\boldsymbol{q}}\big[-\left(\lambda_1\mu_{\boldsymbol{k}} + \tilde{\epsilon}_{\boldsymbol{k}}\right)|\gamma_{\boldsymbol{k}-\boldsymbol{q}}| + |\gamma_{\boldsymbol{k}}|\left(-\lambda_2\mu_{\boldsymbol{k}-\boldsymbol{q}} + \tilde{\epsilon}_{\boldsymbol{k}-\boldsymbol{q}}\right)\big] \\
-p_{\boldsymbol{k}-\boldsymbol{q}}\big[\left(\lambda_1\mu_{\boldsymbol{k}} + \tilde{\epsilon}_{\boldsymbol{k}}\right)\left(-\lambda_2\mu_{\boldsymbol{k}-\boldsymbol{q}} + \tilde{\epsilon}_{\boldsymbol{k}-\boldsymbol{q}}\right) - |\gamma_{\boldsymbol{k}}|\,|\gamma_{\boldsymbol{k}-\boldsymbol{q}}|\big] \\
-g_{\boldsymbol{k}}\big[|\gamma_{\boldsymbol{k}}|\left(-\lambda_2\mu_{\boldsymbol{k}-\boldsymbol{q}} + \tilde{\epsilon}_{\boldsymbol{k}-\boldsymbol{q}}\right) - \left(\lambda_1\mu_{\boldsymbol{k}} + \tilde{\epsilon}_{\boldsymbol{k}}\right)|\gamma_{\boldsymbol{k}-\boldsymbol{q}}|\big] \\
-p_{\boldsymbol{k}}\left(\lambda_1\mu_{\boldsymbol{k}} + \tilde{\epsilon}_{\boldsymbol{k}}\right)\left(-\lambda_2\mu_{\boldsymbol{k}-\boldsymbol{q}} + \tilde{\epsilon}_{\boldsymbol{k}-\boldsymbol{q}}\right) + p_{\boldsymbol{k}}^*(t_1)|\gamma_{\boldsymbol{k}}|\,|\gamma_{\boldsymbol{k}-\boldsymbol{q}}|\Big\} \\
+g_{\boldsymbol{k}}g_{\boldsymbol{k}-\boldsymbol{q}}\big[|\gamma_{\boldsymbol{k}}|\left(-\lambda_2\mu_{\boldsymbol{k}-\boldsymbol{q}} + \tilde{\epsilon}_{\boldsymbol{k}-\boldsymbol{q}}\right) + \left(\lambda_1\mu_{\boldsymbol{k}} + \tilde{\epsilon}_{\boldsymbol{k}}\right)|\gamma_{\boldsymbol{k}-\boldsymbol{q}}|\big] \\
+g_{\boldsymbol{k}}p_{\boldsymbol{k}-\boldsymbol{q}}\big[|\gamma_{\boldsymbol{k}}|\,|\gamma_{\boldsymbol{k}-\boldsymbol{q}}| + \left(\lambda_1\mu_{\boldsymbol{k}} + \tilde{\epsilon}_{\boldsymbol{k}}\right)\left(-\lambda_2\mu_{\boldsymbol{k}-\boldsymbol{q}} + \tilde{\epsilon}_{\boldsymbol{k}-\boldsymbol{q}}\right)\big] \\
+p_{\boldsymbol{k}}g_{\boldsymbol{k}-\boldsymbol{q}}\left(\lambda_1\mu_{\boldsymbol{k}} + \tilde{\epsilon}_{\boldsymbol{k}}\right)\left(-\lambda_2\mu_{\boldsymbol{k}-\boldsymbol{q}} + \tilde{\epsilon}_{\boldsymbol{k}-\boldsymbol{q}}\right) + p_{\boldsymbol{k}}^*g_{\boldsymbol{k}-\boldsymbol{q}}|\gamma_{\boldsymbol{k}}|\,|\gamma_{\boldsymbol{k}-\boldsymbol{q}}| \\
+p_{\boldsymbol{k}}p_{\boldsymbol{k}-\boldsymbol{q}}\left(\lambda_1\mu_{\boldsymbol{k}} + \tilde{\epsilon}_{\boldsymbol{k}}\right)|\gamma_{\boldsymbol{k}-\boldsymbol{q}}| + p_{\boldsymbol{k}}^*p_{\boldsymbol{k}-\boldsymbol{q}}|\gamma_{\boldsymbol{k}}|\left(-\lambda_2\mu_{\boldsymbol{k}-\boldsymbol{q}} + \tilde{\epsilon}_{\boldsymbol{k}-\boldsymbol{q}}\right)\Bigg\},
\end{aligned}
\tag{C.2b}
$$

$$
\begin{aligned}
A^{+,n\bar\sigma}_{\boldsymbol{k},\boldsymbol{q},\lambda_1\lambda_2}(t) = D^I_{\boldsymbol{q}}\left(\lambda_1\mu_{\boldsymbol{k}} - \lambda_2\mu_{\boldsymbol{k}-\boldsymbol{q}} + \left(\Delta_{\boldsymbol{k}} + \Delta_{\boldsymbol{k}-\boldsymbol{q}}\right)\frac{\omega_0}{2}\right)\left(\Gamma^\sigma_{\boldsymbol{k},\boldsymbol{q}}(t)\right)^*\Gamma^n_{\boldsymbol{k},\boldsymbol{q}} \\
\times\Bigg\{ -\left(\lambda_1\mu_{\boldsymbol{k}} + \tilde{\epsilon}_{\boldsymbol{k}}\right)|\gamma_{\boldsymbol{k}-\boldsymbol{q}}| + f^0\left(\lambda_1\mu_{\boldsymbol{k}} - \lambda_2\mu_{\boldsymbol{k}-\boldsymbol{q}} + \left(\Delta_{\boldsymbol{k}} + \Delta_{\boldsymbol{k}-\boldsymbol{q}}\right)\frac{\omega_0}{2}\right) \\
\times\Big\{ g_{\boldsymbol{k}-\boldsymbol{q}}\left(\lambda_1\mu_{\boldsymbol{k}} + \tilde{\epsilon}_{\boldsymbol{k}}\right)|\gamma_{\boldsymbol{k}-\boldsymbol{q}}| + p_{\boldsymbol{k}-\boldsymbol{q}}\left(\lambda_1\mu_{\boldsymbol{k}} + \tilde{\epsilon}_{\boldsymbol{k}}\right)\left(\lambda_2\mu_{\boldsymbol{k}-\boldsymbol{q}} + \tilde{\epsilon}_{\boldsymbol{k}-\boldsymbol{q}}\right) \\
+g_{\boldsymbol{k}}\left(\lambda_1\mu_{\boldsymbol{k}} + \tilde{\epsilon}_{\boldsymbol{k}}\right)|\gamma_{\boldsymbol{k}-\boldsymbol{q}}| + p_{\boldsymbol{k}}^*|\gamma_{\boldsymbol{k}}|\,|\gamma_{\boldsymbol{k}-\boldsymbol{q}}|\Big\} \\
-g_{\boldsymbol{k}}g_{\boldsymbol{k}-\boldsymbol{q}}\left(\lambda_1\mu_{\boldsymbol{k}} + \tilde{\epsilon}_{\boldsymbol{k}}\right)|\gamma_{\boldsymbol{k}-\boldsymbol{q}}| - g_{\boldsymbol{k}}p_{\boldsymbol{k}-\boldsymbol{q}}\left(\lambda_1\mu_{\boldsymbol{k}} + \tilde{\epsilon}_{\boldsymbol{k}}\right)\left(\lambda_2\mu_{\boldsymbol{k}-\boldsymbol{q}} + \tilde{\epsilon}_{\boldsymbol{k}-\boldsymbol{q}}\right) \\
-p_{\boldsymbol{k}}^*g_{\boldsymbol{k}-\boldsymbol{q}}|\gamma_{\boldsymbol{k}}|\,|\gamma_{\boldsymbol{k}-\boldsymbol{q}}| - p_{\boldsymbol{k}}^*p_{\boldsymbol{k}-\boldsymbol{q}}|\gamma_{\boldsymbol{k}}|\left(\lambda_2\mu_{\boldsymbol{k}-\boldsymbol{q}} + \tilde{\epsilon}_{\boldsymbol{k}-\boldsymbol{q}}\right)\Bigg\},
\end{aligned}
\tag{C.2c}
$$

$$A^{+,\sigma\bar{\sigma}}_{\boldsymbol{k},\boldsymbol{q},\lambda_1\lambda_2}(t) = D^I_{\boldsymbol{q}}\left(\lambda_1\mu_{\boldsymbol{k}} - \lambda_2\mu_{\boldsymbol{k}-\boldsymbol{q}} + (\Delta_{\boldsymbol{k}} + \Delta_{\boldsymbol{k}-\boldsymbol{q}})\frac{\omega_0}{2}\right)\left|\Gamma^\sigma_{\boldsymbol{k},\boldsymbol{q}}(t)\right|^2$$

$$\times\Bigg\{ (\lambda_1\mu_{\boldsymbol{k}} + \tilde{\epsilon}_{\boldsymbol{k}})(-\lambda_2\mu_{\boldsymbol{k}-\boldsymbol{q}} + \tilde{\epsilon}_{\boldsymbol{k}-\boldsymbol{q}}) + f^0\left(\lambda_1\mu_{\boldsymbol{k}} - \lambda_2\mu_{\boldsymbol{k}-\boldsymbol{q}} + (\Delta_{\boldsymbol{k}} + \Delta_{\boldsymbol{k}-\boldsymbol{q}})\frac{\omega_0}{2}\right)$$

$$\times\Big\{ -g_{\boldsymbol{k}-\boldsymbol{q}}(\lambda_1\mu_{\boldsymbol{k}} + \tilde{\epsilon}_{\boldsymbol{k}})(-\lambda_2\mu_{\boldsymbol{k}-\boldsymbol{q}} + \tilde{\epsilon}_{\boldsymbol{k}-\boldsymbol{q}}) - p_{\boldsymbol{k}-\boldsymbol{q}}(\lambda_1\mu_{\boldsymbol{k}} + \tilde{\epsilon}_{\boldsymbol{k}})|\gamma_{\boldsymbol{k}-\boldsymbol{q}}|$$

$$-g_{\boldsymbol{k}}(\lambda_1\mu_{\boldsymbol{k}} + \tilde{\epsilon}_{\boldsymbol{k}})(-\lambda_2\mu_{\boldsymbol{k}-\boldsymbol{q}} + \tilde{\epsilon}_{\boldsymbol{k}-\boldsymbol{q}}) - p^*_{\boldsymbol{k}}|\gamma_{\boldsymbol{k}}|(-\lambda_2\mu_{\boldsymbol{k}-\boldsymbol{q}} + \tilde{\epsilon}_{\boldsymbol{k}-\boldsymbol{q}})\Big\}$$

$$+g_{\boldsymbol{k}}g_{\boldsymbol{k}-\boldsymbol{q}}(\lambda_1\mu_{\boldsymbol{k}} + \tilde{\epsilon}_{\boldsymbol{k}})(-\lambda_2\mu_{\boldsymbol{k}-\boldsymbol{q}} + \tilde{\epsilon}_{\boldsymbol{k}-\boldsymbol{q}}) + g_{\boldsymbol{k}}p_{\boldsymbol{k}-\boldsymbol{q}}(\lambda_1\mu_{\boldsymbol{k}} + \tilde{\epsilon}_{\boldsymbol{k}})|\gamma_{\boldsymbol{k}-\boldsymbol{q}}|$$

$$+p^*_{\boldsymbol{k}}g_{\boldsymbol{k}-\boldsymbol{q}}|\gamma_{\boldsymbol{k}}|(-\lambda_2\mu_{\boldsymbol{k}-\boldsymbol{q}} + \tilde{\epsilon}_{\boldsymbol{k}-\boldsymbol{q}}) + p^*_{\boldsymbol{k}}p_{\boldsymbol{k}-\boldsymbol{q}}|\gamma_{\boldsymbol{k}}||\gamma_{\boldsymbol{k}-\boldsymbol{q}}|\Bigg\}, \tag{C.2d}$$

$$A^{-,n\sigma}_{\boldsymbol{k},\boldsymbol{q},\lambda_1\lambda_2}(t) = D^I_{\boldsymbol{q}}\left(\lambda_1\mu_{\boldsymbol{k}} - \lambda_2\mu_{\boldsymbol{k}-\boldsymbol{q}} - (\Delta_{\boldsymbol{k}} + \Delta_{\boldsymbol{k}-\boldsymbol{q}})\frac{\omega_0}{2}\right)\Gamma^n_{\boldsymbol{k},\boldsymbol{q}}\Gamma^\sigma_{\boldsymbol{k},\boldsymbol{q}}(t)$$

$$\times\Bigg\{ -|\gamma_{\boldsymbol{k}}|(\lambda_2\mu_{\boldsymbol{k}-\boldsymbol{q}} + \tilde{\epsilon}_{\boldsymbol{k}-\boldsymbol{q}}) + f^0\left(\lambda_1\mu_{\boldsymbol{k}} - \lambda_2\mu_{\boldsymbol{k}-\boldsymbol{q}} - (\Delta_{\boldsymbol{k}} + \Delta_{\boldsymbol{k}-\boldsymbol{q}})\frac{\omega_0}{2}\right)$$

$$\times\Big\{ -g_{\boldsymbol{k}-\boldsymbol{q}}|\gamma_{\boldsymbol{k}}|(\lambda_2\mu_{\boldsymbol{k}-\boldsymbol{q}} + \tilde{\epsilon}_{\boldsymbol{k}-\boldsymbol{q}}) - p_{\boldsymbol{k}-\boldsymbol{q}}|\gamma_{\boldsymbol{k}}||\gamma_{\boldsymbol{k}-\boldsymbol{q}}|$$

$$-g_{\boldsymbol{k}}|\gamma_{\boldsymbol{k}}|(\lambda_2\mu_{\boldsymbol{k}-\boldsymbol{q}} + \tilde{\epsilon}_{\boldsymbol{k}-\boldsymbol{q}}) - p_{\boldsymbol{k}}(\lambda_1\mu_{\boldsymbol{k}} + \tilde{\epsilon}_{\boldsymbol{k}})(\lambda_2\mu_{\boldsymbol{k}-\boldsymbol{q}} + \tilde{\epsilon}_{\boldsymbol{k}-\boldsymbol{q}})\Big\}$$

$$-g_{\boldsymbol{k}}g_{\boldsymbol{k}-\boldsymbol{q}}|\gamma_{\boldsymbol{k}}|(\lambda_2\mu_{\boldsymbol{k}-\boldsymbol{q}} + \tilde{\epsilon}_{\boldsymbol{k}-\boldsymbol{q}}) - g_{\boldsymbol{k}}p_{\boldsymbol{k}-\boldsymbol{q}}|\gamma_{\boldsymbol{k}}||\gamma_{\boldsymbol{k}-\boldsymbol{q}}|$$

$$-p_{\boldsymbol{k}}g_{\boldsymbol{k}-\boldsymbol{q}}(\lambda_1\mu_{\boldsymbol{k}} + \tilde{\epsilon}_{\boldsymbol{k}})(\lambda_2\mu_{\boldsymbol{k}-\boldsymbol{q}} + \tilde{\epsilon}_{\boldsymbol{k}-\boldsymbol{q}}) - p_{\boldsymbol{k}}p_{\boldsymbol{k}-\boldsymbol{q}}(\lambda_1\mu_{\boldsymbol{k}} + \tilde{\epsilon}_{\boldsymbol{k}})|\gamma_{\boldsymbol{k}-\boldsymbol{q}}|\Bigg\}, \tag{C.2e}$$

$$A^{-,\sigma\sigma}_{\boldsymbol{k},\boldsymbol{q},\lambda_1\lambda_2}(t) = D^I_{\boldsymbol{q}}\left(\lambda_1\mu_{\boldsymbol{k}} - \lambda_2\mu_{\boldsymbol{k}-\boldsymbol{q}} - (\Delta_{\boldsymbol{k}} + \Delta_{\boldsymbol{k}-\boldsymbol{q}})\frac{\omega_0}{2}\right)\left(\Gamma^\sigma_{\boldsymbol{k},\boldsymbol{q}}(t)\right)^2$$

$$\times\Bigg\{ |\gamma_{\boldsymbol{k}}||\gamma_{\boldsymbol{k}-\boldsymbol{q}}| + f^0\left(\lambda_1\mu_{\boldsymbol{k}} - \lambda_2\mu_{\boldsymbol{k}-\boldsymbol{q}} - (\Delta_{\boldsymbol{k}} + \Delta_{\boldsymbol{k}-\boldsymbol{q}})\frac{\omega_0}{2}\right)$$

$$\times\Big\{ g_{\boldsymbol{k}-\boldsymbol{q}}|\gamma_{\boldsymbol{k}}||\gamma_{\boldsymbol{k}-\boldsymbol{q}}| + p_{\boldsymbol{k}-\boldsymbol{q}}|\gamma_{\boldsymbol{k}}|(-\lambda_2\mu_{\boldsymbol{k}-\boldsymbol{q}} + \tilde{\epsilon}_{\boldsymbol{k}-\boldsymbol{q}})$$

$$+g_{\boldsymbol{k}}|\gamma_{\boldsymbol{k}}||\gamma_{\boldsymbol{k}-\boldsymbol{q}}| + p_{\boldsymbol{k}}(\lambda_1\mu_{\boldsymbol{k}} + \tilde{\epsilon}_{\boldsymbol{k}})|\gamma_{\boldsymbol{k}-\boldsymbol{q}}|\Big\}$$

$$+g_{\boldsymbol{k}}g_{\boldsymbol{k}-\boldsymbol{q}}|\gamma_{\boldsymbol{k}}||\gamma_{\boldsymbol{k}-\boldsymbol{q}}| + g_{\boldsymbol{k}}p_{\boldsymbol{k}-\boldsymbol{q}}|\gamma_{\boldsymbol{k}}|(-\lambda_2\mu_{\boldsymbol{k}-\boldsymbol{q}} + \tilde{\epsilon}_{\boldsymbol{k}-\boldsymbol{q}})$$

$$+p_{\boldsymbol{k}}g_{\boldsymbol{k}-\boldsymbol{q}}(\lambda_1\mu_{\boldsymbol{k}} + \tilde{\epsilon}_{\boldsymbol{k}})|\gamma_{\boldsymbol{k}-\boldsymbol{q}}| + p_{\boldsymbol{k}}p_{\boldsymbol{k}-\boldsymbol{q}}(\lambda_1\mu_{\boldsymbol{k}} + \tilde{\epsilon}_{\boldsymbol{k}})(-\lambda_2\mu_{\boldsymbol{k}-\boldsymbol{q}} + \tilde{\epsilon}_{\boldsymbol{k}-\boldsymbol{q}})\Bigg\}, \tag{C.2f}$$

C. Collision integrals for pumped magnons

and for the anomalous collision integral

$$B^{0,nn}_{\boldsymbol{k},\boldsymbol{q},\lambda_1\lambda_2}(t) = \left(\Gamma^n_{\boldsymbol{k},\boldsymbol{q}}\right)^2 D^I_{\boldsymbol{q}}\left(\lambda_1\mu_{\boldsymbol{k}} - \lambda_2\mu_{\boldsymbol{k}-\boldsymbol{q}}\right)$$

$$\times\Bigg\{ |\gamma_{\boldsymbol{k}}|\left(-\lambda_2\mu_{\boldsymbol{k}-\boldsymbol{q}} + \tilde{\epsilon}_{\boldsymbol{k}-\boldsymbol{q}}\right) + \left(\lambda_1\mu_{\boldsymbol{k}} + \tilde{\epsilon}_{\boldsymbol{k}}\right)|\gamma_{\boldsymbol{k}-\boldsymbol{q}}|$$

$$+ f^0\left(\lambda_1\mu_{\boldsymbol{k}} - \lambda_2\mu_{\boldsymbol{k}-\boldsymbol{q}}\right)\Big\{ g_{\boldsymbol{k}-\boldsymbol{q}}\big[-|\gamma_{\boldsymbol{k}}|\left(-\lambda_2\mu_{\boldsymbol{k}-\boldsymbol{q}} + \tilde{\epsilon}_{\boldsymbol{k}-\boldsymbol{q}}\right) + \left(\lambda_1\mu_{\boldsymbol{k}} + \tilde{\epsilon}_{\boldsymbol{k}}\right)|\gamma_{\boldsymbol{k}-\boldsymbol{q}}|\big]$$

$$- p_{\boldsymbol{k}-\boldsymbol{q}}\big[|\gamma_{\boldsymbol{k}}||\gamma_{\boldsymbol{k}-\boldsymbol{q}}| - \left(\lambda_1\mu_{\boldsymbol{k}} + \tilde{\epsilon}_{\boldsymbol{k}}\right)\left(-\lambda_2\mu_{\boldsymbol{k}-\boldsymbol{q}} + \tilde{\epsilon}_{\boldsymbol{k}-\boldsymbol{q}}\right)\big]$$

$$- g_{\boldsymbol{k}}\big[\left(\lambda_1\mu_{\boldsymbol{k}} + \tilde{\epsilon}_{\boldsymbol{k}}\right)|\gamma_{\boldsymbol{k}-\boldsymbol{q}}| - |\gamma_{\boldsymbol{k}}|\left(-\lambda_2\mu_{\boldsymbol{k}-\boldsymbol{q}} + \tilde{\epsilon}_{\boldsymbol{k}-\boldsymbol{q}}\right)\big]$$

$$- p^*_{\boldsymbol{k}}|\gamma_{\boldsymbol{k}}||\gamma_{\boldsymbol{k}-\boldsymbol{q}}| + p_{\boldsymbol{k}}\left(\lambda_1\mu_{\boldsymbol{k}} + \tilde{\epsilon}_{\boldsymbol{k}}\right)\left(-\lambda_2\mu_{\boldsymbol{k}-\boldsymbol{q}} + \tilde{\epsilon}_{\boldsymbol{k}-\boldsymbol{q}}\right)\Big\}$$

$$- g_{\boldsymbol{k}}g_{\boldsymbol{k}-\boldsymbol{q}}\left(\lambda_1\mu_{\boldsymbol{k}} + \tilde{\epsilon}_{\boldsymbol{k}}\right)|\gamma_{\boldsymbol{k}-\boldsymbol{q}}| - g_{\boldsymbol{k}}g_{\boldsymbol{k}-\boldsymbol{q}}|\gamma_{\boldsymbol{k}}|\left(-\lambda_2\mu_{\boldsymbol{k}-\boldsymbol{q}} + \tilde{\epsilon}_{\boldsymbol{k}-\boldsymbol{q}}\right)$$

$$- g_{\boldsymbol{k}}p_{\boldsymbol{k}-\boldsymbol{q}}\left(\lambda_1\mu_{\boldsymbol{k}} + \tilde{\epsilon}_{\boldsymbol{k}}\right)\left(-\lambda_2\mu_{\boldsymbol{k}-\boldsymbol{q}} + \tilde{\epsilon}_{\boldsymbol{k}-\boldsymbol{q}}\right) - g_{\boldsymbol{k}}p_{\boldsymbol{k}-\boldsymbol{q}}|\gamma_{\boldsymbol{k}}||\gamma_{\boldsymbol{k}-\boldsymbol{q}}|$$

$$- p^*_{\boldsymbol{k}}g_{\boldsymbol{k}-\boldsymbol{q}}|\gamma_{\boldsymbol{k}}||\gamma_{\boldsymbol{k}-\boldsymbol{q}}| - p_{\boldsymbol{k}}g_{\boldsymbol{k}-\boldsymbol{q}}\left(\lambda_1\mu_{\boldsymbol{k}} + \tilde{\epsilon}_{\boldsymbol{k}}\right)\left(-\lambda_2\mu_{\boldsymbol{k}-\boldsymbol{q}} + \tilde{\epsilon}_{\boldsymbol{k}-\boldsymbol{q}}\right)$$

$$- p^*_{\boldsymbol{k}}p_{\boldsymbol{k}-\boldsymbol{q}}|\gamma_{\boldsymbol{k}}|\left(-\lambda_2\mu_{\boldsymbol{k}-\boldsymbol{q}} + \tilde{\epsilon}_{\boldsymbol{k}-\boldsymbol{q}}\right) - p_{\boldsymbol{k}}p_{\boldsymbol{k}-\boldsymbol{q}}\left(\lambda_1\mu_{\boldsymbol{k}} + \tilde{\epsilon}_{\boldsymbol{k}}\right)|\gamma_{\boldsymbol{k}-\boldsymbol{q}}|\Bigg\}, \qquad (C.3a)$$

$$B^{0,n\bar{\sigma}}_{\boldsymbol{k},\boldsymbol{q},\lambda_1\lambda_2}(t) = \Gamma^n_{\boldsymbol{k},\boldsymbol{q}}\left(\Gamma^\sigma_{\boldsymbol{k},\boldsymbol{q}}(t)\right)^* D^I_{\boldsymbol{q}}\left(\lambda_1\mu_{\boldsymbol{k}} - \lambda_2\mu_{\boldsymbol{k}-\boldsymbol{q}}\right)$$

$$\times\Bigg\{ |\gamma_{\boldsymbol{k}}||\gamma_{\boldsymbol{k}-\boldsymbol{q}}| - \left(\lambda_1\mu_{\boldsymbol{k}} + \tilde{\epsilon}_{\boldsymbol{k}}\right)\left(\lambda_2\mu_{\boldsymbol{k}-\boldsymbol{q}} + \tilde{\epsilon}_{\boldsymbol{k}-\boldsymbol{q}}\right)$$

$$+ f^0\left(\lambda_1\mu_{\boldsymbol{k}} - \lambda_2\mu_{\boldsymbol{k}-\boldsymbol{q}}\right)\Big\{ g_{\boldsymbol{k}-\boldsymbol{q}}\big[|\gamma_{\boldsymbol{k}}||\gamma_{\boldsymbol{k}-\boldsymbol{q}}| - \left(\lambda_1\mu_{\boldsymbol{k}} + \tilde{\epsilon}_{\boldsymbol{k}}\right)\left(\lambda_2\mu_{\boldsymbol{k}-\boldsymbol{q}} + \tilde{\epsilon}_{\boldsymbol{k}-\boldsymbol{q}}\right)\big]$$

$$- p_{\boldsymbol{k}-\boldsymbol{q}}\big[-|\gamma_{\boldsymbol{k}}|\left(\lambda_2\mu_{\boldsymbol{k}-\boldsymbol{q}} + \tilde{\epsilon}_{\boldsymbol{k}-\boldsymbol{q}}\right) + \left(\lambda_1\mu_{\boldsymbol{k}} + \tilde{\epsilon}_{\boldsymbol{k}}\right)|\gamma_{\boldsymbol{k}-\boldsymbol{q}}|\big]$$

$$- g_{\boldsymbol{k}}\big[-\left(\lambda_1\mu_{\boldsymbol{k}} + \tilde{\epsilon}_{\boldsymbol{k}}\right)\left(\lambda_2\mu_{\boldsymbol{k}-\boldsymbol{q}} + \tilde{\epsilon}_{\boldsymbol{k}-\boldsymbol{q}}\right) + |\gamma_{\boldsymbol{k}}||\gamma_{\boldsymbol{k}-\boldsymbol{q}}|\big]$$

$$+ p^*_{\boldsymbol{k}}|\gamma_{\boldsymbol{k}}|\left(\lambda_2\mu_{\boldsymbol{k}-\boldsymbol{q}} + \tilde{\epsilon}_{\boldsymbol{k}-\boldsymbol{q}}\right) - p_{\boldsymbol{k}}\left(\lambda_1\mu_{\boldsymbol{k}} + \tilde{\epsilon}_{\boldsymbol{k}}\right)|\gamma_{\boldsymbol{k}-\boldsymbol{q}}|\Big\}$$

$$- g_{\boldsymbol{k}}g_{\boldsymbol{k}-\boldsymbol{q}}\big[-\left(\lambda_1\mu_{\boldsymbol{k}} + \tilde{\epsilon}_{\boldsymbol{k}}\right)\left(\lambda_2\mu_{\boldsymbol{k}-\boldsymbol{q}} + \tilde{\epsilon}_{\boldsymbol{k}-\boldsymbol{q}}\right) - |\gamma_{\boldsymbol{k}}||\gamma_{\boldsymbol{k}-\boldsymbol{q}}|\big]$$

$$+ g_{\boldsymbol{k}}p_{\boldsymbol{k}-\boldsymbol{q}}\big[\left(\lambda_1\mu_{\boldsymbol{k}} + \tilde{\epsilon}_{\boldsymbol{k}}\right)|\gamma_{\boldsymbol{k}-\boldsymbol{q}}| + |\gamma_{\boldsymbol{k}}|\left(\lambda_2\mu_{\boldsymbol{k}-\boldsymbol{q}} + \tilde{\epsilon}_{\boldsymbol{k}-\boldsymbol{q}}\right)\big]$$

$$+ p^*_{\boldsymbol{k}}g_{\boldsymbol{k}-\boldsymbol{q}}|\gamma_{\boldsymbol{k}}|\left(\lambda_2\mu_{\boldsymbol{k}-\boldsymbol{q}} + \tilde{\epsilon}_{\boldsymbol{k}-\boldsymbol{q}}\right) + p_{\boldsymbol{k}}g_{\boldsymbol{k}-\boldsymbol{q}}\left(\lambda_1\mu_{\boldsymbol{k}} + \tilde{\epsilon}_{\boldsymbol{k}}\right)|\gamma_{\boldsymbol{k}-\boldsymbol{q}}|$$

$$+ p^*_{\boldsymbol{k}}p_{\boldsymbol{k}-\boldsymbol{q}}|\gamma_{\boldsymbol{k}}||\gamma_{\boldsymbol{k}-\boldsymbol{q}}| + p_{\boldsymbol{k}}p_{\boldsymbol{k}-\boldsymbol{q}}\left(\lambda_1\mu_{\boldsymbol{k}} + \tilde{\epsilon}_{\boldsymbol{k}}\right)\left(\lambda_2\mu_{\boldsymbol{k}-\boldsymbol{q}} + \tilde{\epsilon}_{\boldsymbol{k}-\boldsymbol{q}}\right)\Bigg\}, \qquad (C.3b)$$

$$B^{+,n\bar{\sigma}}_{\boldsymbol{k},\boldsymbol{q},\lambda_1\lambda_2}(t) = \left(\Gamma^\sigma_{\boldsymbol{k},\boldsymbol{q}}(t)\right)^* \Gamma^n_{\boldsymbol{k},\boldsymbol{q}} D^I_{\boldsymbol{q}}\left(\lambda_1\mu_{\boldsymbol{k}} - \lambda_2\mu_{\boldsymbol{k}-\boldsymbol{q}} + \left(\Delta_{\boldsymbol{k}} + \Delta_{\boldsymbol{k}-\boldsymbol{q}}\right)\frac{\omega_0}{2}\right)$$

$$\times\Bigg\{ -\left(\lambda_1\mu_{\boldsymbol{k}} + \tilde{\epsilon}_{\boldsymbol{k}}\right)\left(-\lambda_2\mu_{\boldsymbol{k}-\boldsymbol{q}} + \tilde{\epsilon}_{\boldsymbol{k}-\boldsymbol{q}}\right) + f^0\left(\lambda_1\mu_{\boldsymbol{k}} - \lambda_2\mu_{\boldsymbol{k}-\boldsymbol{q}} + \left(\Delta_{\boldsymbol{k}} + \Delta_{\boldsymbol{k}-\boldsymbol{q}}\right)\frac{\omega_0}{2}\right)$$

$$\times\Big\{ g_{\boldsymbol{k}-\boldsymbol{q}}\left(\lambda_1\mu_{\boldsymbol{k}} + \tilde{\epsilon}_{\boldsymbol{k}}\right)\left(-\lambda_2\mu_{\boldsymbol{k}-\boldsymbol{q}} + \tilde{\epsilon}_{\boldsymbol{k}-\boldsymbol{q}}\right) + p_{\boldsymbol{k}-\boldsymbol{q}}\left(\lambda_1\mu_{\boldsymbol{k}} + \tilde{\epsilon}_{\boldsymbol{k}}\right)|\gamma_{\boldsymbol{k}-\boldsymbol{q}}|$$

$$+ g_{\boldsymbol{k}}\left(\lambda_1\mu_{\boldsymbol{k}} + \tilde{\epsilon}_{\boldsymbol{k}}\right)\left(-\lambda_2\mu_{\boldsymbol{k}-\boldsymbol{q}} + \tilde{\epsilon}_{\boldsymbol{k}-\boldsymbol{q}}\right) + p^*_{\boldsymbol{k}}|\gamma_{\boldsymbol{k}}|\left(-\lambda_2\mu_{\boldsymbol{k}-\boldsymbol{q}} + \tilde{\epsilon}_{\boldsymbol{k}-\boldsymbol{q}}\right)\Big\}$$

$$- g_{\boldsymbol{k}}g_{\boldsymbol{k}-\boldsymbol{q}}\left(\lambda_1\mu_{\boldsymbol{k}} + \tilde{\epsilon}_{\boldsymbol{k}}\right)\left(-\lambda_2\mu_{\boldsymbol{k}-\boldsymbol{q}} + \tilde{\epsilon}_{\boldsymbol{k}-\boldsymbol{q}}\right) - g_{\boldsymbol{k}}p_{\boldsymbol{k}-\boldsymbol{q}}\left(\lambda_1\mu_{\boldsymbol{k}} + \tilde{\epsilon}_{\boldsymbol{k}}\right)|\gamma_{\boldsymbol{k}-\boldsymbol{q}}|$$

$$- p^*_{\boldsymbol{k}}g_{\boldsymbol{k}-\boldsymbol{q}}|\gamma_{\boldsymbol{k}}|\left(-\lambda_2\mu_{\boldsymbol{k}-\boldsymbol{q}} + \tilde{\epsilon}_{\boldsymbol{k}-\boldsymbol{q}}\right) - p^*_{\boldsymbol{k}}p_{\boldsymbol{k}-\boldsymbol{q}}|\gamma_{\boldsymbol{k}}||\gamma_{\boldsymbol{k}-\boldsymbol{q}}|\Bigg\}, \qquad (C.3c)$$

$$B^{+,\overline{\sigma\sigma}}_{\bm{k},\bm{q},\lambda_1\lambda_2}(t) = \left(\Gamma^\sigma_{\bm{k},\bm{q}}(t)\right)^{*2} D^I_{\bm{q}}\left(\lambda_1\mu_{\bm{k}} - \lambda_2\mu_{\bm{k}-\bm{q}} + (\Delta_{\bm{k}} + \Delta_{\bm{k}-\bm{q}})\frac{\omega_0}{2}\right)$$

$$\times\Bigg\{ (\lambda_1\mu_{\bm{k}} + \tilde{\epsilon}_{\bm{k}})\,|\gamma_{\bm{k}-\bm{q}}| + f^0\left(\lambda_1\mu_{\bm{k}} - \lambda_2\mu_{\bm{k}-\bm{q}} + (\Delta_{\bm{k}} + \Delta_{\bm{k}-\bm{q}})\frac{\omega_0}{2}\right)$$

$$\times\Big\{ -g_{\bm{k}-\bm{q}}\left(\lambda_1\mu_{\bm{k}} + \tilde{\epsilon}_{\bm{k}}\right)|\gamma_{\bm{k}-\bm{q}}| - p_{\bm{k}-\bm{q}}\left(\lambda_1\mu_{\bm{k}} + \tilde{\epsilon}_{\bm{k}}\right)\left(\lambda_2\mu_{\bm{k}-\bm{q}} + \tilde{\epsilon}_{\bm{k}-\bm{q}}\right)$$

$$-g_{\bm{k}}\left(\lambda_1\mu_{\bm{k}} + \tilde{\epsilon}_{\bm{k}}\right)|\gamma_{\bm{k}-\bm{q}}| - p^*_{\bm{k}}\,|\gamma_{\bm{k}}|\,|\gamma_{\bm{k}-\bm{q}}|\Big\}$$

$$+g_{\bm{k}}g_{\bm{k}-\bm{q}}\left(\lambda_1\mu_{\bm{k}} + \tilde{\epsilon}_{\bm{k}}\right)|\gamma_{\bm{k}-\bm{q}}| + g_{\bm{k}}p_{\bm{k}-\bm{q}}\left(\lambda_1\mu_{\bm{k}} + \tilde{\epsilon}_{\bm{k}}\right)\left(\lambda_2\mu_{\bm{k}-\bm{q}} + \tilde{\epsilon}_{\bm{k}-\bm{q}}\right)$$

$$+p^*_{\bm{k}}g_{\bm{k}-\bm{q}}\,|\gamma_{\bm{k}}|\,|\gamma_{\bm{k}-\bm{q}}| + p^*_{\bm{k}}p_{\bm{k}-\bm{q}}\,|\gamma_{\bm{k}}|\left(\lambda_2\mu_{\bm{k}-\bm{q}} + \tilde{\epsilon}_{\bm{k}-\bm{q}}\right)\Bigg\}, \tag{C.3d}$$

$$B^{-,n\sigma}_{\bm{k},\bm{q},\lambda_1\lambda_2}(t) = \Gamma^n_{\bm{k},\bm{q}}\Gamma^\sigma_{\bm{k},\bm{q}}(t)\, D^I_{\bm{q}}\left(\lambda_1\mu_{\bm{k}} - \lambda_2\mu_{\bm{k}-\bm{q}} - (\Delta_{\bm{k}} + \Delta_{\bm{k}-\bm{q}})\frac{\omega_0}{2}\right)$$

$$\times\Bigg\{ -|\gamma_{\bm{k}}|\,|\gamma_{\bm{k}-\bm{q}}| + f^0\left(\lambda_1\mu_{\bm{k}} - \lambda_2\mu_{\bm{k}-\bm{q}} - (\Delta_{\bm{k}} + \Delta_{\bm{k}-\bm{q}})\frac{\omega_0}{2}\right)$$

$$\times\Big\{ -g_{\bm{k}-\bm{q}}\,|\gamma_{\bm{k}}|\,|\gamma_{\bm{k}-\bm{q}}| - p_{\bm{k}-\bm{q}}\,|\gamma_{\bm{k}}|\left(-\lambda_2\mu_{\bm{k}-\bm{q}} + \tilde{\epsilon}_{\bm{k}-\bm{q}}\right)$$

$$-g_{\bm{k}}\,|\gamma_{\bm{k}}|\,|\gamma_{\bm{k}-\bm{q}}| - p_{\bm{k}}\left(\lambda_1\mu_{\bm{k}} + \tilde{\epsilon}_{\bm{k}}\right)|\gamma_{\bm{k}-\bm{q}}|\Big\}$$

$$-g_{\bm{k}}g_{\bm{k}-\bm{q}}\,|\gamma_{\bm{k}}|\,|\gamma_{\bm{k}-\bm{q}}| - g_{\bm{k}}p_{\bm{k}-\bm{q}}\,|\gamma_{\bm{k}}|\left(-\lambda_2\mu_{\bm{k}-\bm{q}} + \tilde{\epsilon}_{\bm{k}-\bm{q}}\right)$$

$$-p_{\bm{k}}g_{\bm{k}-\bm{q}}\left(\lambda_1\mu_{\bm{k}} + \tilde{\epsilon}_{\bm{k}}\right)|\gamma_{\bm{k}-\bm{q}}| - p_{\bm{k}}p_{\bm{k}-\bm{q}}\left(\lambda_1\mu_{\bm{k}} + \tilde{\epsilon}_{\bm{k}}\right)\left(-\lambda_2\mu_{\bm{k}-\bm{q}} + \tilde{\epsilon}_{\bm{k}-\bm{q}}\right)\Bigg\}, \tag{C.3e}$$

$$B^{-,\sigma\overline{\sigma}}_{\bm{k},\bm{q},\lambda_1\lambda_2}(t) = \left|\Gamma^\sigma_{\bm{k},\bm{q}}(t)\right|^2 D^I_{\bm{q}}\left(\lambda_1\mu_{\bm{k}} - \lambda_2\mu_{\bm{k}-\bm{q}} - (\Delta_{\bm{k}} + \Delta_{\bm{k}-\bm{q}})\frac{\omega_0}{2}\right)$$

$$\times\Bigg\{ |\gamma_{\bm{k}}|\left(\lambda_2\mu_{\bm{k}-\bm{q}} + \tilde{\epsilon}_{\bm{k}-\bm{q}}\right) + f^0\left(\lambda_1\mu_{\bm{k}} - \lambda_2\mu_{\bm{k}-\bm{q}} - (\Delta_{\bm{k}} + \Delta_{\bm{k}-\bm{q}})\frac{\omega_0}{2}\right)$$

$$\times\Big\{ g_{\bm{k}-\bm{q}}\,|\gamma_{\bm{k}}|\left(\lambda_2\mu_{\bm{k}-\bm{q}} + \tilde{\epsilon}_{\bm{k}-\bm{q}}\right) + p_{\bm{k}-\bm{q}}\,|\gamma_{\bm{k}}|\,|\gamma_{\bm{k}-\bm{q}}|$$

$$+g_{\bm{k}}\,|\gamma_{\bm{k}}|\left(\lambda_2\mu_{\bm{k}-\bm{q}} + \tilde{\epsilon}_{\bm{k}-\bm{q}}\right) + p_{\bm{k}}\left(\lambda_1\mu_{\bm{k}} + \tilde{\epsilon}_{\bm{k}}\right)\left(\lambda_2\mu_{\bm{k}-\bm{q}} + \tilde{\epsilon}_{\bm{k}-\bm{q}}\right)\Big\}$$

$$+g_{\bm{k}}g_{\bm{k}-\bm{q}}\,|\gamma_{\bm{k}}|\left(\lambda_2\mu_{\bm{k}-\bm{q}} + \tilde{\epsilon}_{\bm{k}-\bm{q}}\right) + g_{\bm{k}}p_{\bm{k}-\bm{q}}\,|\gamma_{\bm{k}}|\,|\gamma_{\bm{k}-\bm{q}}|$$

$$+p_{\bm{k}}g_{\bm{k}-\bm{q}}\left(\lambda_1\mu_{\bm{k}} + \tilde{\epsilon}_{\bm{k}}\right)\left(\lambda_2\mu_{\bm{k}-\bm{q}} + \tilde{\epsilon}_{\bm{k}-\bm{q}}\right) + p_{\bm{k}}p_{\bm{k}-\bm{q}}\left(\lambda_1\mu_{\bm{k}} + \tilde{\epsilon}_{\bm{k}}\right)|\gamma_{\bm{k}-\bm{q}}|\Bigg\}. \tag{C.3f}$$

See chapter 4 for the definitions of the functions used here.

D. Deutsche Zusammenfassung

In dieser Arbeit wird eine kinetische Theorie zur Beschreibung der Dynamik von Spinwellen in dünnen Filmen aus dem ferromagnetischen Material Yttrium-Eisengranat (YIG) vorgestellt. Ferromagnetismus ist ein seit Jahrhunderten bekannter Effekt, der große Relevanz für unseren Alltag gewonnen hat. Eine theoretische Erklärung für diesen Effekt wurde erst Anfang des 20. Jahrhunderts durch die Quantenmechanik erbracht. Auch wenn die prinzipielle Ursache verstanden wurde, ist das Feld des Magnetismus aufgrund seiner Komplexität heute noch immer ein großes Feld der experimentellen und theoretischen Forschung. Die Schwierigkeit ist darin begründet, dass Ferromagnetismus, oder auch Antiferromagnetismus, ein Vielteilcheneffekt ist, der erst durch Wechselwirkungen zwischen Teilchen erklärt werden kann. Da in einem Festkörper $\sim 10^{23}$ Teilchen enthalten sind, gestaltet es sich als unmöglich dieses System exakt zu beschreiben. Deshalb muss in der Praxis auf Modellsysteme zurückgegriffen werden, welche die wesentlichen Eigenschaften der exakten Theorie beinhalten. Für den Ferromagnetismus und Antiferromagnetismus ist dies das Heisenberg-Modell. Für quantenmechanische Systeme ist es gegeben durch

$$H = -\sum_{ij} J_{ij} \boldsymbol{S}_i \cdot \boldsymbol{S}_j,$$

wobei $\boldsymbol{S}_i$ der Spinvektoroperator am Gitterplatz i ist und die sogenannte Austauschwechselwirkung zwischen den Spins durch J_{ij} beschrieben wird. Wir wollen uns bei dieser Arbeit auf ferromagnetische Systeme beschränken, das heißt, dass die Wechselwirkungen in unserer gewählten Normierung positiv sind und sich für $T \to 0$ alle Spins parallel ausrichten. Während der Grundzustand von Ferromagneten leicht bestimmt werden kann, liegt die Herausforderung in der Beschreibung des Systems bei endlichen Temperaturen. Bei niedrigen Temperaturen kann hierzu die Spinwellentheorie genutzt werden. Spinwellen sind Anregungen mit kleiner Energie, die Abweichungen vom Grundzustand beschreiben. Aufgrund von kürzlich durchgeführten Experimenten [36, 37, 38, 39, 40, 76, 77], sind wir bestrebt, dünne Filme aus YIG zu beschreiben. In dünnen ferromagnetischen Schichten wird die Dipol-Dipol-Wechselwirkung relevant und das entsprechende Spinmodell ist gegeben durch

$$H = -\frac{1}{2} \sum_{ij} \sum_{\alpha\beta} \left[J_{ij} \delta^{\alpha\beta} + D_{ij}^{\alpha\beta} \right] S_i^\alpha S_j^\beta - [h_0 + h_1 \cos(\omega_0 t)] \sum_i S_i^z, \quad \text{(D.1)}$$

wobei der Dipol-Dipol-Tensor definiert ist als

$$D_{ij}^{\alpha\beta} = (1 - \delta_{ij}) \frac{\mu^2}{|\boldsymbol{r}_{ij}|^3} \left[3\hat{r}_{ij}^{\alpha}\hat{r}_{ij}^{\beta} - \delta^{\alpha\beta} \right] . \tag{D.2}$$

Die vorliegende Arbeit baut auf diesem Modell auf. Der Vektor $\boldsymbol{r}_{ij} = \boldsymbol{r}_i - \boldsymbol{r}_j$ zeigt vom Gitterplatz i zum Gitterplatz j und normiert ist dieser Vektor gegeben durch $\hat{\boldsymbol{r}}_{ij}$. Auf die Ortsraumkomponenten x, y, z der Vektoren und Vektoroperatoren wird mit den hochstehenden Indices α und β verwiesen. Zusätzlich zur Dipol-Dipol-Wechselwirkung haben wir angenommen, dass ein statisches und ein oszillierendes externes magnetisches Feld mit der entsprechenden Zeeman-Energie h_0 beziehungsweise h_1 und der Frequenz ω_0 angelegt sind. Obwohl Spinwellen keine exakten Eigenzustände des Hamilton-Operator (D.1) sind, ist die Spinwellentheorie trotzdem ein geeigneter Formalismus um solche Systeme bei niedrigen Energien zu beschreiben. Durch sie kann die unhandliche Spin-Algebra durch Erzeugungs- und Vernichtungsoperatoren von Quasiteilchen, den sogenannten Magnonen, ersetzt werden.

Aufgrund der besonderen Eigenschaften funktioniert dieser Ansatz bei YIG besonders gut. Obwohl YIG eigentlich ein ferrimagnetisches Material mit komplizierter Einheitszelle ist, verhält es sich für die relevanten Energien effektiv als Ferromagnet mit Spins auf einem kubischen Gitter. Der Betrag S des effektiven Spins ist ~ 14.2 [31, 32, 46] und bei der Abbildung auf ein Quasiteilchen-System mit Hilfe der Holsten-Primakoff-Transformation können deshalb Terme der Ordnung $1/S$ ohne großen Fehler vernachlässigt werden. Dies äußert sich darin, dass die charakteristische Zeit für Magnon-Magnon-Streuprozesse sehr viel kleiner als die Magnonlebenszeit von $\sim 1\,\mu$s ist und Spinwellen ein ausgeprägtes Teilchenverhalten aufweisen. Zuletzt ist YIG für sichtbares Licht transparent und mit der Brillouin-Lichtstreuung [33, 36, 39, 42, 76] können die Energien und Impulse der Magnonen sehr genau gemessen werden.

Im Rahmen dieser Arbeit betrachten wir Experimente, bei denen zunächst durch den Effekt der ferromagnetischen Resonanz [31, 46, 45] Spinwellen in YIG angeregt werden und dann die Dynamik des freien Systems beobachtet wird. Auf diese Weise konnte bei [36] eine Art Bose-Einstein-Kondensation (BEC) von Quasiteilchen bei Raumtemperatur erreicht werden. Diese Veröffentlichung hat einiges Aufsehen erregt und eine Diskussion darüber hervorgerufen, ob es sich dabei um ein BEC im engeren Sinne handelt [61]. Ein Diskussionspunkt ist zum Beispiel der Widerspruch, dass die Magnonen im Experiment starken Nichtgleichgewichtsbedingungen ausgesetzt sind, während BEC ein Gleichgewichtsphänomen ist. Auch wenn hier argumentiert werden kann, dass die Magnonen im Experiment sich in einem Quasigleichgewicht befinden, muss für eine ganzheitliche Beschreibung des Experiments die Dynamik der Magnonen berücksichtigt werden. Dies war die Hauptmotivation um im Rahmen dieser Arbeit eine Nichtgleichgewichtstheorie für die Magnonen-experimente in YIG zu entwickeln. Die Nichtgleichgewichtsdynamik ist auch in vielen anderen Bereichen von Interesse [?], unter anderem bei ultrakalten Atomen [98], bei Kollisionsexperimenten mit schweren Kernen [99], bei

Exciton-Polariton-Systemen in Halbleiter-Mikrokavitäten [100] und in dissipativen Quantensystemen [101].

Obwohl der Alltag hauptsächlich durch Nichtgleichgewichtsprozesse bestimmt wird, beschäftigt sich ein Großteil der Physik mit dem thermischen Gleichgewicht und Systemen nahe dem thermischen Gleichgewicht. Unter anderem liegt das an der Komplexität von Nichtgleichgewichtsproblemen. Während man in der Thermodynamik eine einheitliche Sprache für das thermische Gleichgewicht gefunden hat, kann man selbst hier nur eine sehr kleine Zahl an wechselwirkenden Modellsystemen exakt lösen. Im Nichtgleichgewicht wächst die Komplexität auf Grund des zusätzlichen Freiheitsgrads der Zeit noch einmal deutlich an. Für näherungsweise Lösungen müssen mehr Annahmen als im Gleichgewicht gemacht werden. Hierbei allgemeine Zugänge zu finden gestaltet sich als äußerst schwierig. Als ein Meilenstein auf diesem Gebiet gilt die Boltzmann-Gleichung, von Ludwig Boltzmann 1872 hergeleitet. Durch sie wird eine Verbindung zwischen Nichtgleichgewicht und Gleichgewicht hergestellt. Die Lösung der Boltzmann-Gleichung läuft unabhängig vom Anfangszustand für große Zeiten immer ins Gleichgewicht. Ihre Gültigkeit beschränkt sich vor allem auf Gase mit geringer Dichte. Um die Näherungen der Boltzmann-Gleichung systematisch zu verbessern, ist der Keldysh-Formalismus - eine exakte Theorie für Greensche Funktionen - ein geeigneter Startpunkt. Wie wir in Kapitel 3 zeigen, kann aus ihr mit geeigneten Näherungen die Boltzmann-Gleichung hergeleitet werden. Unter anderem müssen wir dazu annehmen, dass die Wechselwirkungsstärke klein ist. An diesem Punkt haben wir angesetzt, um mit der funktionalen Renomierungsgruppe (FRG) über diese Einschränkung hinauszugehen. Es wurde ein System von Differentialgleichungen hergeleitet, welches eine ähnliche Struktur wie die Boltzmann-Gleichung aufweist, aber nicht grundsätzlich auf schwache Wechselwirkungen beschränkt ist.

Üblicherweise werden für die Beschreibung von BEC endliche Vakuumserwartungswerte angenommen. Bei der Betrachtung der Dynamik von Magnonen haben wir diese einfachheitshalber vernachlässigt. Trotzdem konnte eine gute Übereinstimmung mit dem Experiment erreicht werden. Prinzipiell können endliche Vakuumserwartungswerte in unsere kinetische Theorie miteingebaut werden.

Im ersten Teil der Arbeit sind wir genauer auf die Wellenfunktion eines möglichen BEC eingegangen, haben dafür aber thermisches Gleichgewicht angenommen. Interessant wird dieses Problem durch die speziellen Eigenschaften von Dünnschicht-Ferromagneten. Das Zusammenspiel von endlicher Systemgröße, Austausch- und Dipol-Dipol-Wechselwirkung führt zu einem Minimum in der Dispersion bei endlichen Wellenvektoren. Dies hat wesentlichen Einfluss auf die Form der Wellenfunktion.

Zuletzt wollen wir anmerken, dass die betrachteten Magnonsysteme auch interessant für technische Anwendungen sind. Typische Wellenlängen von Signalen in WLAN- oder Mobilfunknetzen betragen einige Zentimeter. Um die Empfangsmodule in mobilen Geräten wie Handys möglichst klein zu halten,

werden diese Signale an Anregungen in Festkörpern gekoppelt, welche bei gleicher Frequenz eine geringere Wellenlänge aufweisen. Mit Spinwellen in magnetischen Materialien könnte diese Wellenlänge von derzeit einigen Mikrometern auf den Nanometerbereich reduziert werden. Damit wäre eine weitere Miniatisierung möglich.

Ein zweites größeres Anwendungsgebiet könnte in der Informationsverarbeitung liegen. Anstelle von elektrischen Ladungen, können Spinwellen als Informationsträger dienen. Durch ihre deutlich geringere effektive Masse sollte es möglich sein, die Datenverarbeitungsprozesse effektiver zu gestalten. Grundlegende logische Operationen wurden bereits in Spinsystemen, zum Beispiel in der Gruppe von Hillebrands in Kaiserslautern [102, 103, 104], realisiert.

Die Forschung zu dieser Arbeit wurde in Zusammenarbeit mit diversen Kollegen durchgeführt. Für den ersten Abschnitt waren dies Francesca Sauli, Andreas Kreisel und Peter Kopietz, beim zweiten Thomas Kloss und Peter Kopietz, und beim letzten Andreas Rückriegel und Peter Kopietz.

D.1. Bose-Einstein-Kondensation in Dünnschicht-Ferromagneten

Bevor wir genauer auf den Nichtgleichgewichts Aspekt in den YIG-Experimenten eingehen, wollen wir zunächst die Wellenfunktion eines möglichen BEC untersuchen. Dazu nehmen wir an, dass das System sich nach dem parametrischen Pumpprozess im Gleichgewicht befände und entsprechend viele Teilchen vorhanden sind, sodass es zur BEC kommt. Das Besondere an dem betrachteten Fall ist, dass die Dispersion der Magnonen bei endlichem Wellenvektor $\pm\boldsymbol{q}$ ihr Minimum hat [31, 32]. In Kapitel 2 haben wir die Gross-Pitaevskii (GP)-Gleichung benutzt, um die Ortsabhängigkeit der BEC-Wellenfunktion zu berechnen. Anders als die Ergebnisse von den Experimenten vermuten lassen, konnten wir zeigen, dass eine Wellenfunktion bei der nur die Fourier-Komponenten bei $\pm\boldsymbol{q}$ ungleich Null sind, keine Lösung der GP-Gleichung ist. Dies sieht man bereits an der diskretisierten GP-Gleichung,

$$
\begin{aligned}
-r_n\psi_n^{\bar{\sigma}} - \gamma_n\psi_n^{\sigma} = \; & \frac{1}{2}\sum_{n_1 n_2}\sum_{\sigma_1\sigma_2}\delta_{n,n_1+n_2}V_{nn_1n_2}^{\sigma\sigma_1\sigma_2}\,\psi_{n_1}^{\sigma_1}\psi_{n_2}^{\sigma_2} \\
& + \frac{1}{3!}\sum_{n_1 n_2 n_3}\sum_{\sigma_1\sigma_2\sigma_3}\delta_{n,n_1+n_2+n_3}U_{nn_1n_2n_3}^{\sigma\sigma_1\sigma_2\sigma_3}\,\psi_{n_1}^{\sigma_1}\psi_{n_2}^{\sigma_2}\psi_{n_3}^{\sigma_3},
\end{aligned} \tag{D.3}
$$

wobei die tiefgestellten Indices n_i das n_i-te Vielfache vom Impuls $\boldsymbol{q}$ angibt und n_i eine ganze Zahl ist. Die Fourier-Transformierte der Wellenfunktion ist gegeben durch,

$$
\phi_{\boldsymbol{k}}^{\sigma} = \sqrt{N}\sum_{n=-\infty}^{\infty}\delta_{\boldsymbol{k},n\boldsymbol{q}}\psi_n^{\sigma}, \tag{D.4}
$$

wobei $\sigma = a, \bar{a}$ ebenso wie die Indices σ_1, σ_2 und σ_3 im obigen Ausdruck auf die Funktion selbst, beziehungsweise auf die komplex konjugierte Funktion verweist. Für die Größe $\epsilon_n - \mu$ wurde die Abkürzung r_n eingeführt und γ_n ist die Amplitude des externen Pumpfeldes. Die Dreipunkts- und Vierpunktswechselwirkungen sind $V_{nn_1n_2}^{\sigma\sigma_1\sigma_2}$ und $U_{nn_1n_2n_3}^{\sigma\sigma_1\sigma_2\sigma_3}$. Wenn man nun $n = 3$ setzt, sieht man, dass auch ψ_3^σ ungleich Null sein muss, wenn $\psi_{\pm 1}^\sigma$ endlich sein soll. Die einzige Möglichkeit eine Lösung zu konstruieren, ist anzunehmen, dass alle Komponenten mit einem ganzzahligen Vielfachen von q von Null verschieden sind. Prinzipiell kann dies zu einer Lokalisierung der BEC-Wellenfunktion im Ortsraum führen. Bei YIG sind allerdings die Wechselwirkungen derart, dass der Wert der Fourier-Komponenten mit steigendem Wellenvektor in etwa exponentiell abnimmt und die erste Fourier-Komponenten bereits eine gute Näherung der Wellenfunktion ergibt, dazu siehe Abbildungen 2.2 und 2.3. Wir wollen darauf hinweisen, dass für Vielfache von q die Dreipunktswechselwirkungen $V_{nn_1n_2}^{\sigma\sigma_1\sigma_2}$ in YIG verschwinden und deshalb nur Komponenten mit ungeraden Vielfachen endlich sind. Im Experiment konnte die Besetzung der höheren Komponenten nicht nachgewiesen werden, da mit der verwendeten Brillouin-Lichtstreuungsmethode entsprechende Wellenvektoren nicht gemessen werden konnten. Zusätzlich wäre es aufgrund der starken Abnahme bei höheren Moden schwierig, dies experimentell zu erfassen.

D.2. Funktionaler Renormierungsgruppen-Ansatz für die Thermalisierung von Magnonen in Yttrium-Eisengranat

Nun kommen wir zu der Nichtgleichgewichtsdynamik von Magnonen. Hierzu betrachteten wir in Kapitel 3 ein Modell, dass freie Magnonen mit einem thermischen Bad aus Phononen koppelt. Die Wechselwirkung ist derart, dass die Teilchenzahl der Magnonen erhalten bleibt. Dies ist ein minimales Modell um die Thermalisierung von Magnonen beschreiben zu können.

Damit wir die FRG nutzen konnten, wurde zunächst die Boltzmann-Gleichung mit funktionalen Methoden hergeleitet. Mit der Wigner-Transformation konnten wir die relevante Zeitskala im Problem absondern und haben dadurch ein Equivalent zur Verteilungsfunktion in der Boltzmann-Gleichung erhalten. Bei der Herleitung mussten einige Näherungen gemacht werden. Die Summe aus retardierter und avancierter Selbstenergie führt zur Renormalisierung der Magnondispersion. Durch die Verwendung der an experimentelle Daten angepasste Dispersion haben wir die Renormalisierung der Energien indirekt bereits enthalten, und diese Kombination der Selbstenergien konnte vernachlässigt werden. Dadurch entsprechen die freien Greenschen Funktionen der Gleichgewichts-Greenschen Funktionen.

D. Deutsche Zusammenfassung

Für langsam veränderliche Funktionen in Zeit und Frequenz lässt sich eine einfache Näherung für die Wigner-Transformation von Zeitmatrixprodukten herleiten. In dieser Näherung wird das Matrixprodukt zu einem einfachen Produkt der Wigner-Transformierten. Für die freien Greenschen Funktionen ist dies exakt und wir können annehmen, dass um das Gleichgewicht ein Bereich existiert, in dem diese Näherung gerechtfertigt ist.

Zuletzt wird bei der Quasiteilchennäherung die Spektralfunktion der Magnonen durch die freie ersetzt. Dies ergibt eine unendliche Quasiteilchenlebenszeit und kann für YIG gut begründet werden, da hier die Magnonen besonders langlebig sind.

Nach der Herleitung mit funktionalen Methoden konnte die FRG verwendet werden, um die Näherung der störungstheoretischen Ausdrücke der Selbstenergien zu verbessern. Die FRG ist eine exakte Theorie mit der zum Beispiel Selbstenergien berechnet werden können. Allerdings müssen in der Praxis Näherungen gemacht werden, damit die sich ergebenden Gleichungen gelöst werden können. Das besondere an der FRG ist, dass sie Näherungen ermöglicht, bei denen kein kleiner Parameter so wie die Störungstheorie benötigt wird. Deshalb kann sie auch auf Systeme mit starken Wechselwirkungen angewendet werden. In der sogenannten Vertexentwicklung ergibt die FRG eine unendliche Hierarchie an gekoppelten Flussgleichungen für Einteilchen-irreduziblen Vertices. Um den nummerischen Aufwand zu begrenzen, muss diese Hierarchie an einer geeigneten Stelle trunkiert werden. In unserem Fall haben wir nur den Fluss der Selbstenergien betrachtet und die Magnon-Phonon-Wechselwirkung als konstant angenommen. Das schwierige an der FRG ist es, das richtige Cutoff-Schema zu wählen. Dabei wird ein Flussparameter Λ derart in das System eingeführt, dass die Beschreibung für $\Lambda \to \infty$ sehr einfach wird und für $\Lambda \to 0$ das ursprüngliche System wiederhergestellt wird. Bis auf diese Bedingung kann das Cutoff-Schema aber beliebig gewählt werden. Aufgrund der Exaktheit der Theorie erhält man prinzipiell in allen Fällen die gleichen Ergebnisse, wenn das System nach $\Lambda \to 0$ entwickelt wird. Erst wenn Näherungen gemacht werden, ergeben sich Unterschiede und das Cutoff-Schema muss entsprechend der Näherungen gewählt werden. Dies ist der entscheidende Punkt für die Qualität der Ergebnisse, aber leider gibt es hierfür keine feste Vorschrift. Im Nichtgleichgewicht kommt hinzu, dass das Cutoff-Schema gewisse Eigenschaften erhalten lassen sollte. In der Struktur des Keldysh-Formalismus erkennt man bereits die Kausalitätsbedingung. Diese sollte durch den Cutoff nicht verletzt werden. Zudem ist es für die Annäherung ans Gleichgewicht wichtig, dass das Fluktuation-Dissipations-Theorem im Gleichgewicht für alle Flussparameter gültig bleibt. Es hat sich herausgestellt, dass eine Modifikation des Ansatzes aus [28, 85], dem sogenannten Hybridisierungscutoff, die gewünschten Eigenschaften erfüllt. Die Modifikation betrifft die Tatsache, dass wir Bosonen statt Fermionen betrachten. Daraus ergibt sich, dass die Spektralfunktion zusammen mit der Frequenz im Argument sein Vorzeichen wechselt und deshalb der Flussparameter Λ in den Wigner-Transformierten durch $\Lambda \mathrm{sgn}\omega$ ersetzt werden

muss. Zuletzt sei noch erwähnt, dass wir den Cutoff nur für die Phononen eingeführt haben. Dies verhindert eine künstliche Verbreiterung der Magnonspektralfunktion und ergibt eine einfache Struktur der Gleichungen.

Das Ergebnis unseres Formalismus ist ein System aus Differentialgleichungen bestehend aus einer kinetischen Gleichung für die Verteilungsfunktion $n_{\Lambda,\boldsymbol{k}}(\tau)$,

$$\partial_\tau + \mu_\Lambda(\tau)] 2 n_{\Lambda,\boldsymbol{k}}(\tau) = i\Sigma_{\Lambda,\boldsymbol{k}}^K(\tau;\epsilon_{\boldsymbol{k}}) - \Sigma_{\Lambda,\boldsymbol{k}}^I(\tau;\epsilon_{\boldsymbol{k}})\left[1 + 2n_{\Lambda,\boldsymbol{k}}(\tau)\right]. \tag{D.5}$$

und zwei Flussgleichungen für die Wigner-transformierte Keldysh- $\Sigma_{\Lambda,\boldsymbol{k}}^K(\tau;\epsilon_{\boldsymbol{k}})$ und spektrale Selbstenergie $\Sigma_{\Lambda,\boldsymbol{k}}^I(\tau;\epsilon_{\boldsymbol{k}})$,

$$\partial_\Lambda i\Sigma_{\Lambda,\boldsymbol{k}}^K(\tau;\epsilon_{\boldsymbol{k}}) = \frac{1}{V}\sum_{\boldsymbol{k}'}\left\{\left[1 + n_{\Lambda,\boldsymbol{k}'}(\tau)\right]\dot{W}_{\boldsymbol{k}',\boldsymbol{k}} + \dot{W}_{\boldsymbol{k},\boldsymbol{k}'}n_{\Lambda,\boldsymbol{k}'}(\tau)\right\}, \tag{D.6a}$$

$$\partial_\Lambda \Sigma_{\Lambda,\boldsymbol{k}}^I(\tau;\epsilon_{\boldsymbol{k}}) = \frac{1}{V}\sum_{\boldsymbol{k}'}\left\{\left[1 + n_{\Lambda,\boldsymbol{k}'}(\tau)\right]\dot{W}_{\boldsymbol{k}',\boldsymbol{k}} - \dot{W}_{\boldsymbol{k},\boldsymbol{k}'}n_{\Lambda,\boldsymbol{k}'}(\tau)\right\}. \tag{D.6b}$$

Die Ableitung der Übergangsrate nach dem Flussparameter Λ ist gegeben durch

$$\dot{W}_{\boldsymbol{k},\boldsymbol{k}'} = 2\gamma_{\boldsymbol{k}-\boldsymbol{k}'}^2\dot{D}_{\Lambda,\boldsymbol{k}-\boldsymbol{k}'}^I(\epsilon_{\boldsymbol{k}} - \epsilon_{\boldsymbol{k}'})b(\epsilon_{\boldsymbol{k}} - \epsilon_{\boldsymbol{k}'}), \tag{D.7}$$

wobei $\dot{D}_{\Lambda,\boldsymbol{q}}^I(\omega)$ die Ableitung der Phononspektralfunktion ist,

$$\dot{D}_{\Lambda,\boldsymbol{q}}^I(\omega) = \pi\operatorname{sgn}\omega\left[L_{\Lambda_{\boldsymbol{q}}(\tau;\omega)}'(\omega - \omega_{\boldsymbol{q}}) + L_{\Lambda_{\boldsymbol{q}}(\tau;\omega)}'(\omega + \omega_{\boldsymbol{q}})\right], \tag{D.8}$$

mit der Ableitung der Lorenzkurve

$$L_\Lambda'(\omega) = \partial_\Lambda\left[\frac{1}{\pi}\frac{\Lambda}{\omega^2 + \Lambda^2}\right] = \frac{1}{\pi}\frac{\omega^2 - \Lambda^2}{(\omega^2 + \Lambda^2)^2}. \tag{D.9}$$

Zu den Übergangsraten trägt noch die Magnon-Phonon-Kopplung $\gamma_{\boldsymbol{q}}$ und die Bose-Funktion $b(\omega)$ bei. Die Breite der Lorentzkurven im Ausdruck für die Phononspektralfunktion ist definiert durch

$$\Lambda_{\boldsymbol{q}}(\tau;\omega) \equiv \Lambda\operatorname{sgn}\omega + \frac{1}{2}\Pi_{\Lambda,\boldsymbol{q}}^I(\tau;\omega). \tag{D.10}$$

Mit der Wigner-transformierten spektralen Phononselbstenergie $\Pi_{\Lambda,\boldsymbol{q}}^I(\tau;\omega)$ in D.10 berücksichtigen wir die intrinsische Phonondämpfung. Dies ist notwendig damit sich für $\Lambda \to 0$ keine Deltafunktionen in den Übergangsraten ergeben, welche für endliche Systeme, bei denen über den Impuls summiert wird, mathematisch nicht definiert sind. Auf diese Weise haben wir in unserem Zugang eine elegante Möglichkeit zur Lösung dieses Problems gefunden.

Das skalenabhängige chemische Potential in D.5,

$$\mu_\Lambda(\tau) = \frac{1}{2N}\sum_{\boldsymbol{k}}\left\{i\Sigma_{\Lambda,\boldsymbol{k}}^K(\tau;\epsilon_{\boldsymbol{k}}) - \Sigma_{\Lambda,\boldsymbol{k}}^I(\tau;\epsilon_{\boldsymbol{k}})\left[1 + 2n_{\Lambda,\boldsymbol{k}}(\tau)\right]\right\}, \tag{D.11}$$

fungiert als Lagrange-Multiplikator, der dafür sorgt, dass die Teilchenzahl der Magnonen erhalten bleibt. Obwohl der Hamilton-Operator des betrachteten Systems mit dem Teilchenzahloperator vertauscht, wurde dies nötig, weil die Näherungen für die Selbstenergien die Teilchenzahl nicht konstant hält. Einen Lagrange-Multiplikator für diesen Zweck einzuführen ist eine übliche Vorgehensweise.

Für den Vergleich der numerischen Ergebnisse unseres Gleichungssystems mit dem Experiment von [76] haben wir eine Verteilung ähnlich der Daten, die kurz vor Ende des Pumpprozesses gemessen wurden, als Anfangswert präpariert. Der Pumpprozess an sich und die Abnahme der Teilchenzahl kann mit unserem Modell nicht beschrieben werden. Wie man aber anhand von Abbildung 3.5 erkennen kann, erhalten wir mit dem Experiment qualitativ gut übereinstimmende Ergebnisse für den Thermalisierungsprozess der Magnonen. Insbesondere die Ausbildung einer erhöhten Besetzung des Grundzustandes wird durch unsere Simulation gut wiedergegeben. Erstaunlich ist, dass sich eine solche Übereinstimmung trotz Vernachlässigung der für diesen Prozess als wichtig erachteten Magnon-Magnon-Wechselwirkungen ergeben hat. In unseren Berechnungen haben wir die unbekannte Kopplungsstärke zwischen Magnonen und Phononen so angepasst, dass wir für eine dem Experiment entsprechenden Zeit den stationären Zustand erreichen. Wir vermuten, dass wir dadurch Differenzen aufgrund der Vernachlässigung der Magnon-Magnon-Wechselwirkungen kompensiert haben. Wenn wir zusätzlich die Abnahme der Teilchenzahl betrachten, ist dies nicht mehr möglich und es ergeben sich Unterschiede in den Zeitskalen von Berechnung und Experiment. Siehe dazu das nächste Kapitel, in dem wir ein erweitertes Modell betrachten.

D.3. Dynamik von parametrisch erzeugten Magnonen in Systemen mit $U(1)$-symmetriebrechenden Wechselwirkungen

Als Nächstes betrachten wir ein Modell, dass im Vergleich zum letzten Abschnitt auch den Pumpprozess und die Abnahme der Magnonteilchenzahl beschreibt. Hierfür werden im Hamilton-Operator Terme mit gebrochener $U(1)$-Symmetrie benötigt, da die Teilchenzahl bei beiden Prozessen nicht erhalten bleibt. Das Mikrowellenfeld, dass zur Anregung von Magnonen benutzt wird, ergibt Nichtdiagonalelemente im quadratischen Magnonteil. Dreipunktswechselwirkungen, die einen einzelnen Phonon-Vernichtungs- oder Erzeugeroperator an zwei Vernichtungs- oder Erzeugeroperatoren der Magnonen koppelt, führen zur zusätzlichen Thermalisierung der Magnonteilchenzahl. Zunächst haben wir in Kapitel 4 gezeigt, dass solche Wechselwirkungen sich in YIG durch die Dipol-Dipol-Wechselwirkung ergeben. Das Spinwellenmodell für Systeme

mit Pumpfeld haben wir bereits in der Einleitung in Kapitel 1 vorgestellt. Anders als bei der vorherigen Betrachtung kann die explizite Zeitabhängigkeit des Hamilton-Operators durch eine Transformation zum rotierenden Referenzsystem nicht gänzlich beseitigt werden. Es bleibt eine Zeitabhängigkeit der anormalen Wechselwirkungen.

Durch die explizite $U(1)$-Symmetriebrechung im Hamilton-Operator koppeln auch anormale Korrelationen $\langle a_{\boldsymbol{k}}(t) a_{\boldsymbol{k}}(t) \rangle$ an die normalen Korrelationen $\left\langle a_{\boldsymbol{k}}^{\dagger}(t) a_{\boldsymbol{k}}(t) \right\rangle$. Der Keldysh-Formalismus muss für diesen Fall erweitert werden. Es ergibt sich eine komplexere Struktur, bei der zum Beispiel die Keldysh-Greensche-Funktion selbst eine 2×2 Matrixstruktur aus normalen und anormalen Komponenten aufweist. In Abschnitt 4.3 haben wir die Diskussion eines solchen Keldysh-Formalismus aus [28] an unser Modell angepasst. Aus einem nicht bekannten Grund ergab ein vergleichbarer Ansatz wie für das Modell aus dem letzten Abschnitt keine einfache Übergangsratenstruktur in der kinetischen Gleichung, welche die Boltzmann-Gleichung aufweist. Allerdings konnte zusammen mit Andreas Rückriegel und Peter Kopietz ein Verfahren entwickelt werden, welches solch eine Ratengleichung ergibt. Bei diesem Verfahren werden nur Realzeiten betrachtet und keine Wigner-Transformation angewendet. Trotzdem ist es für Modelle ohne explizite $U(1)$-Symmetriebrechung äquivalent zu dem vorherigen Verfahren.

Die verwendeten Näherungen beinhalten wie zuvor die Vernachlässigung der Energierenormalisierung und die Quasiteilchennäherung. Anstatt die Wigner-Transformation von Matrixprodukten in der Zeit zu nähern, muss nun die Markov-Näherung benutzt werden. Dabei wird die Verteilungsfunktion vor das Zeitintegral gezogen und Gedächtniseffekte vernachlässigt. Damit hängt die Zeitentwicklung des System wie beim vorherigen Abschnitt nur von der Konfiguration zum Zeitpunkt der Betrachtung ab. In dem wir die Pumpstärke Null setzen, können wir deshalb das System für Zeiten, bei denen das Pumpfeld abgeschaltet ist, mit der gleichen kinetischen Gleichung beschreiben. Ohne Markov-Näherung müssten wir hierzu eine Heaviside-Funktion in den Hamilton-Operator einfügen.

Aufgrund der hohen Komplexität des betrachteten Systems und da Magnonen in YIG als schwach wechselwirkende Teilchen gelten - dies haben auch unsere Ergebnisse bestätigt - wenden wir hier keine FRG an und beschränken uns auf die Störungstheorie. Die Herleitung der Ratengleichung stellt sich als sehr langwierig heraus. Wenn die Zeitabhängigkeit der anormalen Wechselwirkungen berücksichtigt wird, ergeben sich zusätzliche Terme in den Übergangsraten, die dafür sorgen, dass die Energie bei den Stoßprozessen zwischen Magnonen und Phononen nicht erhalten bleibt. Dies sorgt dafür, dass die Gleichgewichtsverteilung nicht analytisch bestimmt werden kann. Aufgrund instabiler nummerischer Berechnungen ist es unklar, ob diese Ratengleichung die Relaxation ins Gleichgewicht beschreibt. Deshalb wurde eine weitere Näherung gemacht und die Zeitabhängigkeit der Wechselwirkungen vernachlässigt. Dies ist nur für den Pumpprozess nötig und für kurze Zeiten gerechtfertigt. Eine weitere

Begründung für diese Näherung ist, dass die anormalen Wechselwirkungen generell keinen großen Einfluss auf die Dynamik während des Pumpens haben. Nach dieser Näherung ergibt sich eine Ratengleichung, die zwar immer noch sehr komplex ist, aber auf einfache Weise die Annäherung an stationäre Zustände beschreibt. Ohne äußeres Mikrowellenfeld ist die Gleichgewichtsverteilung eine Bose-Funktion mit verschwindendem chemischen Potential. An der stationären Lösung für den Fall mit äußerem Mikrowellenfeld kann man erkennen, dass sich die Gleichgewichtsverteilung nur für die gepumpten Moden ändert. Bei diesen stellt sich abhängig von der Pumpstärke eine neue Besetzung ein. Im Experiment [40] wird beobachtet, dass für Pumppulse mit einer Dauer von $\lesssim 30\,\mathrm{ns}$ die Besetzung der anderen Moden annähernd unverändert bleibt. Erst für längere Pulse steigen auch diese stärker an. Daraus schließen wir, dass wir das Experiment [40] für Pulse mit einer Dauer von bis zu 30 ns mit unseren Näherungen beschreiben können.

Die Wechselwirkungs- und die Pumpstärke haben wir derart gewählt, dass die numerischen Ergebnisse möglichst gut mit den experimentellen Daten übereinstimmen. Anders als im Experiment ist der Peak in der Besetzung der gepumpten Moden etwa zwei Größenordnungen größer als der beim Minimum der Dispersion, siehe Abbildung 4.6. Wir vermuten, dass dies daran liegt, dass wir die Teilchen-Teilchen-Wechselwirkungen vernachlässigt haben und dadurch bereits viele Magnonen verloren gehen, bis der Grundzustand besetzt wird. Die Betrachtung dieser Wechselwirkungen sollte die größten Abweichungen zum Experiment beheben. Doch davon abgesehen ergibt unser Modell bereits eine gute Übereinstimmung mit den experimentellen Daten, siehe Abbildung 4.5 und 4.6. Insbesondere die Dynamik der Besetzung beim Minimum der Dispersion wird gut wiedergegeben.

Bibliography

[1] L. V. Keldysh, Diagram technique for nonequilibrium processes, Sov. Phys. JETP **20**, 1018 (1965).

[2] A. Kamenev, *Field Theory of Non-Equilibrium Systems*, Cambridge University Press, Cambridge, 2011.

[3] J. Schwinger, Brownian Motion of a Quantum Oscillator, J. Math. Phys. **2**(3), 407 (1961).

[4] D. M. Kennes, S. G. Jakobs, C. Karrasch, and V. Meden, A renormalization group approach to time dependent transport through correlated quantum dots, Phys. Rev. B **85**, 085113 (2012).

[5] J. Berges, Introduction to nonequilibrium quantum field theory, AIP Conf. Proc. **739**, 3 (2005).

[6] P. Kopietz, L. Bartosch, and F. Schütz, *Introduction to the Functional Renormalization Group*, Springer, 2010.

[7] J. Rammer, *Quantum Field Theory of Nonequilibrium States*, Cambridge University Press, Cambridge, 2007.

[8] P. Lipavský, V. Špička, and B. Velický, Generalized Kadanoff-Baym ansatz for deriving quantum transport equations, Phys. Rev. B **34**, 6933 (1986).

[9] C. Bagnuls and C. Bervillier, Exact renormalization group equations: an introductory review, Phys. Rep. **348**(1-2), 91 (2001).

[10] J. Berges, N. Tetradis, and C. Wetterich, Non-perturbative renormalization flow in quantum field theory and statistical physics, Phys. Rep. **363**(4-6), 223 (2002).

[11] O. J. Rosten, Fundamentals of the exact renormalization group, Phys. Rep. **511**(4), 177 (2012).

[12] W. Metzner, M. Salmhofer, C. Honerkamp, V. Meden, and K. Schönhammer, Functional renormalization group approach to correlated fermion systems, Rev. Mod. Phys. **84**, 299 (2012).

[13] T. R. Morris, The Exact Renormalization Group and Approximate Solutions, Int. J. Mod. Phys. A **9**, 2411 (1994).

[14] K. G. Wilson, Non-Lagrangian Models of Current Algebra, Phys. Rev. **179**, 1499 (1969).

[15] K. G. Wilson, Renormalization Group and Critical Phenomena. I. Renormalization Group and the Kadanoff Scaling Picture, Phys. Rev. B **4**, 3174 (1971).

[16] K. G. Wilson, Renormalization Group and Critical Phenomena. II. Phase-Space Cell Analysis of Critical Behavior, Phys. Rev. B **4**, 3184 (1971).

[17] K. G. Wilson, Feynman-Graph Expansion for Critical Exponents, Phys. Rev. Lett. **28**, 548 (1972).

[18] K. G. Wilson and M. E. Fisher, Critical Exponents in 3.99 Dimensions, Phys. Rev. Lett. **28**, 240 (1972).

[19] K. G. Wilson and J. Kogut, The renormalization group and the ϵ expansion, Physics Reports **12**(2), 75 (1974).

[20] K. G. Wilson, The renormalization group: Critical phenomena and the Kondo problem, Rev. Mod. Phys. **47**, 773 (1975).

[21] J. F. Nicoll, T. S. Chang, and H. E. Stanley, Approximate Renormalization Group Based on the Wegner-Houghton Differential Generator, Phys. Rev. Lett. **33**, 540 (1974).

[22] S. Weinberg, Critical Phenomena for Field Theorists, in *Proc. Int. School of Subnuclear Physics*, edited by A. Zichichi, page 1, Plenum, New York, 1976.

[23] J. Nicoll and T. Chang, An exact one-particle-irreducible renormalization-group generator for critical phenomena, Phys. Lett. A **62**(5), 287 (1977).

[24] C. Wetterich, Exact evolution equation for the effective potential, Phys. Lett. B **301**(1), 90 (1993).

[25] M. Bonini, M. D'Attanasio, and G. Marchesini, Perturbative renormalization and infrared finiteness in the Wilson renormalization group: the massless scalar case, Nucl. Phys. B **409**(2), 441 (1993).

[26] T. Gasenzer and J. M. Pawlowski, Towards far-from-equilibrium quantum field dynamics: A functional renormalisation-group approach, Physics Letters B **670**(2), 135 (2008).

[27] T. Gasenzer, S. Keßler, and J. M. Pawlowski, Far-from-equilibrium quantum many-body dynamics, Eur. Phys. J. C **70**(1-2), 423 (2010).

[28] T. Kloss and P. Kopietz, Nonequilibrium time evolution of bosons from the functional renormalization group, Phys. Rev. B **83**, 205118 (2011).

[29] J. W. Negele and H. Orland, *Quantum Many-Particle Systems*, Westview Press, 1998.

[30] V. Cherepanov, I. Kolokolov, and V. L'vov, The saga of YIG: spectra, thermodynamics, interaction and relaxation of magnons in a complex magnet, Physics Reports **229**, 81 (1993).

[31] A. Kreisel, F. Sauli, L. Bartosch, and P. Kopietz, Microscopic spin-wave theory for yttrium-iron garnet films, Eur. Phys. J. B **71**, 59 (2009).

[32] A. Kreisel, *Spin-wave calculations for Heisenberg magnets with reduced symmetry*, PhD thesis, J. W. Goethe-Universität Frankfurt am Main, 2011.

[33] A. A. Serga, C. W. Sandweg, V. I. Vasyuchka, M. B. Jungfleisch, B. Hillebrands, A. Kreisel, P. Kopietz, and M. P. Kostylev, Brillouin light scattering spectroscopy of parametrically excited dipole-exchange magnons, Phys. Rev. B **86**, 134403 (2012).

[34] A. I. Akhiezer, V. G. Bar'yakhtar, and S. V. Peletminskii, *Spin Waves*, North Holland, Amsterdam, 1968.

[35] D. C. Mattis, *The theory of magnetism made simple*, World Scientific, Singapore, 2006.

[36] S. O. Demokritov, V. E. Demidov, O. Dzyapko, G. A. Melkov, A. A. Serga, B. Hillebrands, and A. N. Slavin, Bose-Einstein condensation of quasi-equilibrium magnons at room temperature under pumping, Nature **443**, 430 (2006).

[37] V. E. Demidov, O. Dzyapko, S. O. Demokritov, G. A. Melkov, and A. N. Slavin, Thermalization of a Parametrically Driven Magnon Gas Leading to Bose-Einstein Condensation, Phys. Rev. Lett. **99**, 037205 (2007).

[38] O. Dzyapko, V. E. Demidov, S. O. Demokritov, G. A. Melkov, and A. N. Slavin, Direct observation of Bose-Einstein condensation in a parametically driven gas of magnons, New J. Phys. **9**, 64 (2007).

[39] V. E. Demidov, O. Dzyapko, S. O. Demokritov, G. A. Melkov, and A. N. Slavin, Observation of Spontaneous Coherence in Bose-Einstein Condensate of Magnons, Phys. Rev. Lett. **100**, 047205 (2008).

[40] S. O. Demokritov, V. E. Demidov, O. Dzyapko, G. A. Melkov, and A. N. Slavin, Quantum coherence due to Bose-Einstein condensation of parametically driven magnons, New J. Phys. **10**, 045029 (2008).

[41] A. V. Chumak, G. A. Melkov, V. E. Demidov, O. Dzyapko, V. L. Safonov, and S. O. Demokritov, Bose-Einstein Condensation of Magnons under Incoherent Pumping, Phys. Rev. Lett. **102**, 187205 (2009).

[42] C. W. Sandweg, M. B. Jungfleisch, V. I. Vasyuchka, A. A. Serga, P. Clausen, H. Schultheiss, B. Hillebrands, A. Kreisel, and P. Kopietz, Wide-range wavevector selectivity of magnon gases in Brillouin light scattering spectroscopy, Rev. Sci. Instrum. **81**(7), 073902 (2010).

[43] J. Hick, F. Sauli, A. Kreisel, and P. Kopietz, Bose-Einstein condensation at finite momentum and magnon condensation in thin film ferromagnets, Eur. Phys. J. B **78**, 429 (2010).

[44] A. G. Gurevich and G. A. Melkov, *Magnetization Oscillations and Waves*, CRC Press, 1996.

[45] T. Kloss, A. Kreisel, and P. Kopietz, Parametric pumping and kinetics of magnons in dipolar ferromagnets, Phys. Rev. B **81**, 104308 (2010).

[46] I. S. Tupitsyn, P. C. E. Stamp, and A. L. Burin, Stability of Bose-Einstein Condensates of Hot Magnons in Yttrium Iron Garnet Films, Phys. Rev. Lett. **100**, 257202 (2008).

[47] S. M. Rezende, F. M. de Aguiar, and A. Azevedo, Magnon excitation by spin-polarized direct currents in magnetic nanostructures, Phys. Rev. B **73**, 094402 (2006).

[48] T. Holstein and H. Primakoff, Field Dependence of the Intrinsic Domain Magnetization of a Ferromagnet, Phys. Rev. **58**, 1098 (1940).

[49] S. M. Rezende, Theory of coherence in Bose-Einstein condensation phenomena in a microwave-driven interacting magnon gas, Phys. Rev. B **79**, 174411 (2009).

[50] C. J. Pethick and H. Smith, *Bose-Einstein Condensation in Dilute Gases*, Cambridge University Press, 2002.

[51] V. S. L'vov, *Wave Turbulence Under Parametric Excitations*, Springer, Berlin, 1994.

[52] S. M. Rezende, Theory of microwave superradiance from a Bose-Einstein condensate of magnons, Phys. Rev. B **79**, 060410 (2009).

[53] V. E. Zakharov, V. S. L'vov, and S. S. Starobinets, Stationary nonlinear theory of parametric excitation of waves, Sov. Phys. JETP **32**, 656 (1971).

[54] V. E. Zakharov, V. S. L'vov, and S. S. Starobinets, Spin-wave turbulence beyond the parametric excitation threshold, Sov. Phys. Usp. **17**, 896 (1975).

[55] V. M. Tsukernik and R. P. Yankelevich, Stationary distribution of magnons following parametric excitation in ferromagnetic substances, Sov. Phys. JETP **41**, 1059 (1976).

[56] I. A. Vinikovetskii, A. M. Frishman, and V. M. Tsukernik, Kinetic equation for a system of parametically excited spin waves, Sov. Phys. JETP **49**, 1067 (1979).

[57] S. P. Lim and D. L. Huber, Microscopic theory of spin-wave instabilities in parallel-pumped easy-plane ferromagnets, Phys. Rev. B **37**, 5426 (1988).

[58] Y. D. Kalafati and V. L. Safanov, Thermodynamic approach in the theory of paramagnetic resonance of magnons, Sov. Phys. JETP **68**, 1162 (1989).

[59] S. P. Lim and D. L. Huber, Possible mechanism for limiting the number of modes in spin-wave instabilities in parallel pumping, Phys. Rev. B **41**, 9283 (1990).

[60] A. Zvyagin, V. Serebryannii, A. Frishman, and V. Tsukernik, Dynamics of spin-waves under parametric-excitation by a stepped periodic magnetic field of arbitrary amplitude, Sov. J. Low Temp. Phys. **8**, 612 (1982).

[61] D. Snoke, Coherent questions, Nature **443**, 403 (2006).

[62] A. I. Bugrij and V. M. Loktev, On the theory of Bose-Einstein condensation of quasiparticles: On the possibility of condensation of ferromagnons at high temperatures, Low Temp. Phys. **33**, 37 (2007).

[63] A. Rückriegel, A. Kreisel, and P. Kopietz, Time-dependent spin-wave theory, Phys. Rev. B **85**, 054422 (2012).

[64] W. Kohn and D. Sherrington, Two Kinds of Bosons and Bose Condensates, Rev. Mod. Phys. **42**, 1 (1970).

[65] M. Wouters and I. Carusotto, Superfluidity and Critical Velocities in Nonequilibrium Bose-Einstein Condensates, Phys. Rev. Lett. **105**, 020602 (2010).

[66] H. T. Ueda and K. Totsuka, Magnon Bose-Einstein condensation and various phases of three-dimensonal quantum helimagnets under high magnetic field, Phys. Rev. B **80**, 014417 (2009).

[67] S. A. Brazovskii, Phase transition of an isotropic system to a nonuniform state, Sov. Phys. JETP **41**, 85 (1975).

[68] P. C. Hohenberg and J. B. Swift, Metastability in fluctuation-driven first-order transitions: Nucleation of lamellar phases, Phys. Rev. E **52**, 1828 (1995).

[69] L. P. Pitaevskii and S. Stringari, *Bose-Einstein Condensation*, Oxford University Press, 2003.

[70] F. Schütz, L. Bartosch, and P. Kopietz, Collective fields in the functional renormalization group for fermions, Ward identities, and the exact solution of the Tomonaga-Luttinger model, Phys. Rev. B **72**, 035107 (2005).

[71] R. Dell'Amore, A. Schilling, and K. Krämer, $U(1)$ symmetry breaking and violated axial symmetry in TlCuCl$_3$ and other insulating spin systems, Phys. Rev. B **79**, 014438 (2009).

[72] S. Alexander and J. McTague, Should All Crystals Be bcc? Landau Theory of Solidification and Crystal Nucleation, Phys. Rev. Lett. **41**, 702 (1978).

[73] P. W. Anderson, *Basic Notions Of Condensed Matter Physics*, Westview Press, 1997.

[74] P. M. Chaikin and T. C. Lubensky, *Principles of condensed matter physics*, Cambridge University Press, 1995.

[75] B. A. Malomed, O. Dzyapko, V. E. Demidov, and S. O. Demokritov, Ginzburg-Landau model of Bose-Einstein condensation of magnons, Phys. Rev. B **81**, 024418 (2010).

[76] V. E. Demidov, O. Dzyapko, M. Buchmeier, T. Stockhoff, G. Schmitz, G. A. Melkov, and S. O. Demokritov, Magnon Kinetics and Bose-Einstein Condensation Studied in Phase Space, Phys. Rev. Lett. **101**, 257201 (2008).

[77] O. Dzyapko, V. E. Demidov, G. A. Melkov, and S. O. Demokritov, Bose-Einstein condensation of spin wave quanta at room temperature, Phil. Trans. R. Soc. A **369**, 3575 (2011).

[78] A. Griffin, T. Nikuni, and E. Zaremba, *Bose-Condensed Gases at Finite Temperature*, Cambridge University Press, Cambridge, 2009.

[79] J. Berges and G. Hoffmeister, Nonthermal fixed points and the functional renormalization group, Nucl. Phys. B **813**(3), 383 (2009).

[80] J. Berges and D. Sexty, Strong versus weak wave-turbulence in relativistic field theory, Phys. Rev. D **83**, 085004 (2011).

[81] J. Berges and D. Sexty, Bose-Einstein Condensation in Relativistic Field Theories Far from Equilibrium, Phys. Rev. Lett. **108**, 161601 (2012).

[82] L. Bányai, P. Gartner, O. M. Schmitt, and H. Haug, Condensation kinetics for bosonic excitons interacting with a thermal phonon bath, Phys. Rev. B **61**, 8823 (2000).

[83] J. Hick, T. Kloss, and P. Kopietz, Thermalization of magnons in yttrium-iron garnet: Nonequilibrium functional renormalization group approach, Phys. Rev. B **86**, 184417 (2012).

[84] H. Haug and A. Jauho, *Quantum Kinetics in Transport and Optics of Semiconductors*, Springer, Berlin, 2008.

[85] S. G. Jakobs, M. Pletyukhov, and H. Schoeller, Nonequilibrium functional renormalization group with frequency-dependent vertex function: A study of the single-impurity Anderson model, Phys. Rev. B **81**, 195109 (2010).

[86] F. Schütz and P. Kopietz, Functional renormalization group with vacuum expectation values and spontaneous symmetry breaking, J Phys A: Math. Gen. **39**(25), 8205 (2006).

[87] T. Jolicoeur and J. C. Le Guillou, Fluctuations beyond the Gutzwiller approximation in the slave-boson approach, Phys. Rev. B **44**, 2403 (1991).

[88] W. H. Press, S. A. Teukolsky, W. T. Vetterling, and B. P. Flannery, *Numerical Recipes*, Cambridge University Press, 2007.

[89] O. Jepsen, J. Madsen, and O. K. Andersen, Band structure of thin films by the linear augmented-plane-wave method, Phys. Rev. B **18**, 605 (1978).

[90] G. G. Siu, C. M. Lee, and Y. Liu, Magnons and acoustic phonons in $Y_{3-x}Bi_xFe_5O_{12}$, Phys. Rev. B **64**, 094421 (2001).

[91] B. A. Kalinikos and A. N. Slavin, Theory of dipole-exchange spin wave spectrum for ferromagnetic films with mixed exchange boundary conditions, J. Phys. C **19**(35), 7013 (1986).

[92] B. A. Kalinikos, M. P. Kostylev, N. V. Kozhus, and A. N. Slavin, The dipole-exchange spin wave spectrum for anisotropic ferromagnetic films with mixed exchange boundary conditions, J. Phys. Condens. Matter **2**(49), 9861 (1990).

[93] F. S. Vannucchi, Á. R. Vasconcellos, and R. Luzzi, Dynamics of a Bose-Einstein Condensate of Excited Magnons, arXiv:1302.1765 [cond-mat.quant-gas] (2013).

[94] L. D. Landau and E. M. Lifshitz, *Statistical Physics Part 1*, Butterworth-Heinemann, 1980.

[95] L. M. Woods, Magnon-phonon effects in ferromagnetic manganites, Phys. Rev. B **65**, 014409 (2001).

[96] L. P. Kadanoff and G. A. Baym, *Quantum Statistical Mechanics*, Benjamin, New York, 1962.

[97] A. E. Lord, Jr., Sound wave attenuation due to the magnon-phonon interaction, Phys. kondens. Materie **7**(3), 232 (1968).

[98] A. Polkovnikov, K. Sengupta, A. Silva, and M. Vengalattore, *Colloquium*: Nonequilibrium dynamics of closed interacting quantum systems, Rev. Mod. Phys. **83**, 863 (2011).

[99] W. Cassing, From Kadanoff-Baym dynamics to off-shell parton transport, Eur. Phys. J. Special Topics **168**, 3 (2009).

[100] H. Deng, H. Haug, and Y. Yamamoto, Exciton-polariton Bose-Einstein condensation, Rev. Mod. Phys. **82**, 1489 (2010).

[101] H. Schoeller, A perturbative nonequilibrium renormalizationgroup method for dissipative quantum mechanics, Eur. Phys. J. Special Topics **168**, 179 (2009).

[102] M. P. Kostylev, A. A. Serga, T. Schneider, B. Leven, and B. Hillebrands, Spin-wave logical gates, Appl. Phys. Lett. **87**(15), 153501 (2005).

[103] T. Schneider, A. A. Serga, B. Leven, B. Hillebrands, R. L. Stamps, and M. P. Kostylev, Realization of spin-wave logic gates, Appl. Phys. Lett. **92**(2), 022505 (2008).

[104] A. D. Karenowska, J. F. Gregg, A. V. Chumak, A. A. Serga, and B. Hillebrands, Spin information transfer and transport in hybrid spinmechatronic structures, Journal of Physics: Conference Series **303**(1), 012018 (2011).

Lebenslauf

Angaben zur Person

Name: Johannes Hick

Gerburtsdatum: 24. Januar 1984

Geburtsort: Frankfurt am Main

Familienstand: Verheiratet

Staatsangehörigkeit: Deutsch

Bildung und beruflicher Werdegang

08/2013   Promotion

10/2009 - 2013   Doktorand am Institut für Theoretische Physik
                      an der Goethe-Universität Frankfurt am Main
                      Betreuer: Prof. Dr. Peter Kopietz

09/2008   Master of Science in Physik, Note: 1.0
                      Masterarbeit: Bell Experiments with Entangled Atoms and
                      Photons
                      Betreuer: Prof. Dr. Gernot Alber

02/2007   Bachelor of Science in Physik, Note: 1.7
                      Bachelorarbeit: Diffraktive optische Elemente zur Laser-
                      lötanwendung
                      Betreuer: Prof. Dr. Theo Tschudi

10/2003 - 09/2008   Studium der Physik an der Technischen Universität Darm-
                      stadt

06/2003   Abitur an der Freien Christlichen Schule Frankfurt am
                      Main

Danksagung

Während meiner Promotion haben einige Personen für mich eine große Rolle gespielt. Zum Abschluss möchte ich mich herzlich für sämtlich erhaltene Unterstützung bedanken.

Anfangen möchte ich dabei bei meinem Betreuer Prof. Dr. Peter Kopietz. Ihm verdanke ich die Möglichkeit interessante Forschung betreiben zu können. Es gab eine intensive Zusammenarbeit, bei der er mir immer wieder bei schwierigen Problemen helfen konnte. Durch seine Erfahrung und sein Wissen war er eine große Inspiration und ich durfte viel von ihm lernen. Seine sympathische und unkomplizierte Art der Arbeitsgruppenführung, haben maßgeblich zu einer sehr angenehmen und produktiven Arbeitsatmosphäre beigetragen.

Für die reibungslose und produktive Zusammenarbeit bei den Projekten danke ich Francesca Sauli, Dr. Andreas Kreisel, Dr. Thomas Kloss und Andreas Rückriegel. Inhaltliche Ergänzungen durch Francesca Sauli und Dr. Andreas Kreisel haben mein erstes Projekt vervollständigt. Wichtige Beiträge zum zweiten und dritten Projekt haben Dr. Thomas Kloss und Andreas Rückriegel erbracht. Mir ist bewusst, dass eine so wohlwollende Zusammenarbeit nicht immer selbstverständlich ist und bin deshalb meinen Kollegen sehr dankbar für die gemeinsame Arbeit.

Sämtliche Mitglieder der Arbeitsgruppe Kopietz waren eine große Unterstützung. Meinen momentanen und ehemaligen Bürokollegen Dr. Thomas Kloss, Francesca Sauli, Kira Riedl und Casper Drukier bin ich für fachliche und persönliche Gespräche dankbar. Durch sie wurde der gewöhnliche Arbeitsalltag zu einer schönen Zeit. Insbesondere hat mir der intensive Austausch mit Casper Drukier und Dr. Thomas Kloss immer wieder große Freude bereitet. Darüber hinaus danke ich Casper Drukier für das Korrekturlesen dieser Arbeit. JProf. Dr. Lorenz Bartosch, Dr. Aldo Isidori und Dr. Andreas Kreisel danke ich für ihr offenes Ohr. Bei häufigen Fragen hat mir ihre fachliche Expertise weitergeholfen. Dr. Andreas Kreisel möchte ich zudem für die regelmäßige Hilfe bei Problemen mit dem Computer und die Organisation der Student Workshops im Rahmen des SFB TRR 49 danken. Dr. Mathieu Tailefumier danke ich für die Tipps beim Programmieren der nummerischen Programme.

Im Rahmen des SFB TRR 49 gab es immer wieder Verknüpfungen zum Experiment und einen fachlichen Austausch über das eigene Projekt hinaus. Den Kollegen möchte ich dafür danken. Vor allem durch Dr. Alexander Serga habe ich einige Erläuterungen zum Experiment erhalten.

Bei Prof. Dr. Hartmut Haug bedanke ich mich für die Anfertigung eines Gutachtens. Seine Arbeiten auf dem Gebiet der kinetischen Theorie waren

lehrreiche Lektüren.

Zu guter Letzt möchte ich mich bei meinen Freunden, meinen Eltern und meiner Frau bedanken. Meine Eltern haben mich auf meinem gesamten bisherigen Lebensweg unterstützt und so auch bei dieser Arbeit. Meinen Freunden und meiner Frau danke ich für die Ermutigungen und das regelmäßige Nachfragen nach dem Stand der Arbeit und meinem Befinden. Zuletzt danke ich Gott für diese Gelegenheit in meinem Leben.